第58回 フラーレン・ナノチューブ・グラフェン 総合シンポジウム講演要旨集

令和2年3月15日～18日

FNTG Research Society

第 58 回
フラーレン・ナノチューブ・グラフェン
総合シンポジウム

The 58th Fullerenes-Nanotubes-Graphene General Symposium

講演要旨集
Abstracts

2020 年 3 月 15 日（日） ～ 18 日（水）
東京大学　伊藤国際学術研究センター
The University of Tokyo, ITO INTERNATIONAL RESEARCH CENTER

主催　フラーレン・ナノチューブ・グラフェン学会
The Fullerenes, Nanotubes and Graphene Research Society

共催 ・ 後援
日本化学会　The Chemical Society of Japan
東京大学大学院工学系研究科　School of Engineering, The University of Tokyo
東京大学 CIAiS　Consortium for Innovation of Advanced Integrated Science (UTokyo)
東京大学 GMSI　Graduate Program for Mechanical Systems Innovation (UTokyo)
JST-CREST ([Thermal Control]Creation of Innovative Core Technologies for Nano-enabled Thermal Management)

協賛
日本物理学会　The Physical Society of Japan
応用物理学会　The Japan Society of Applied Physics
高分子学会　The Society of Polymer Science, Japan
電気化学会　The Electrochemical Society of Japan

グラフェンの量産化に向けて…

Neutron

▾概要▾
Roll-to-Roll (R2R)
ロール状に巻いた金属ホイルを、巻き取りながら連続的にグラフェンを成長可能な量産用装置

◆特徴◆
- 連続成長
- 生産能力 20,000 m^2 / year
- Cuホイル及びSteelホイルの両方に対応
- 大気環境で成長可能で、真空チャンバ不要
- 生産コストの大幅削減

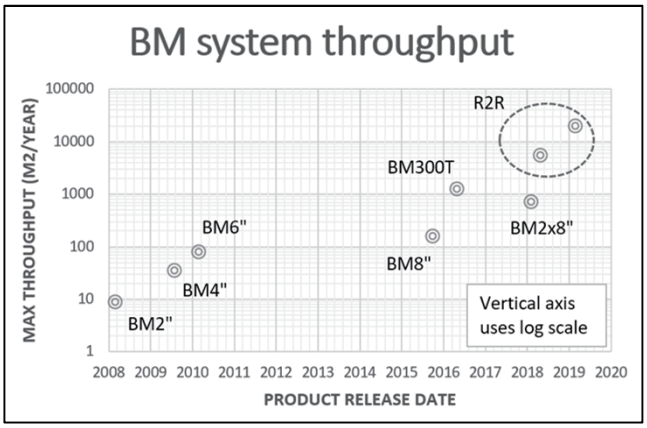

CCS 2D & NOVO

▾概要▾
2D材料及びグラフェンの成長装置

◆特徴◆
- Closed Coupled Showerhead(CCS) 技術を適用
- 成長温度は1400℃まで昇温可能
- 基板に直接2D材料またはグラフェンを成長可能
- プラズマ機能装備
- 多種原料を搭載可能(hBN, MoS2, WSe2)

BM300T

▾概要▾
ウェハ基板上CNT及びグラフェン成長装置

◆特徴◆
- 12”及び8” wafer 自動搬送対応
- プラズマ機能装備
- High 2D/G > 2.5の高品質を達成

アイクストロン株式会社 www.aixtron.com
〒140-0001 東京都品川区北品川1-8-11 Daiwa品川Northビル9F
E-mail: japaninfo@aixtron.com Phone: 03-5781-0931 Fax: 03-5781-0940

AIXTRON
Our technology. YOUR FUTURE

Abstract of
The 58th Fullerenes-Nanotubes-Graphene General Symposium

Sponsored by : The Fullerenes, Nanotubes and Graphene Research Society

Co-Sponsored by : The Chemical Society of Japan
School of Engineering, The University of Tokyo
Consortium for Innovation of Advanced Integrated Science (UTokyo)
Graduate Program for Mechanical Systems Innovation (UTokyo)
JST-CREST ([Thermal Control]Creation of Innovative Core Technologies for Nano-enabled Thermal Management)

Supported by : The Physical Society of Japan
The Japan Society of Applied Physics
The Society of Polymer Science, Japan
The Electrochemical Society of Japan

Date : March 15th(Sun.) – March 18th(Wed.), 2020

Place : The University of Tokyo, ITO INTERNATIONAL RESEARCH CENTER
7-3-1 Hongo, Bunkyo-ku, Tokyo 113-8656

Presentation Time : Special Lecture (25 min presentation + 5min discussion)
Invited Lecture (10 min presentation + 5min discussion)
General Lecture (10 min presentation + 5min discussion)
Poster Preview (1 min presentation without discussion)

第 58 回フラーレン・ナノチューブ・グラフェン総合シンポジウム
講演要旨集

主催 : フラーレン・ナノチューブ・グラフェン学会

共催・後援 : 日本化学会
東京大学大学院工学系研究科
東京大学 CIAiS
東京大学 GMSI
JST-CREST（「熱制御」ナノスケール・サーマルマネージメント基盤技術の創出）

協賛 : 日本物理学会、応用物理学会、高分子学会、電気化学会

日時 : 令和 2 年 3 月 15 日（日）～3 月 18 日（水）

場所 : 東京大学　伊藤国際学術研究センター　伊藤謝恩ホール
〒113-8656　東京都文京区本郷 7-3-1

発表時間 : 特別講演　（発表　25 分 + 質疑応答　5 分）
招待講演　（発表　10 分 + 質疑応答　5 分）
一般講演　（発表　10 分 + 質疑応答　5 分）
ポスタープレビュー（発表 1 分・質疑応答　なし）

展示団体御芳名 （五十音順、 敬称略）

（株）島津製作所

（株）セントラル科学貿易

テレダイン・ジャパン(株）

日本シノプシス（同）

（株）日本レーザー

フィルジェン（株）

（株）名城ナノカーボン

広告掲載団体御芳名 （五十音順、 敬称略）

アイクストロン(株）

エクセルソフト（株）

（株）コロナ社

（株）セントラル科学貿易

ソーラボジャパン（株）

テレダイン・ジャパン(株）

日本電子（株）

（株）日本レーザー

Contents

Time Table ・・・・・・・・・・・・・・・・・・・・ i
Chairperson ・・・・・・・・・・・・・・・・・・・iii
Program Japanese ・・・・・・・・・・・・・・ iv
English ・・・・・・・・・・・・・・xviii
Abstracts Special Lecture ・・・・・・・・・・ 1
Invited Lecture ・・・・・・・・・ 9
Commemorative Session ・・・・・・ 11
General Lecture ・・・・・・・・・ 17
Poster Preview ・・・・・・・・・・ 45
Author Index ・・・・・・・・・・・・・・・・・137

目次

早見表 ・・・・・・・・・・・・・・・・・・・・ i
座長一覧・・・・・・・・・・・・・・・・・・・・iii
プログラム 和文・・・・・・・・・・・・・・・・iv
英文・・・・・・・・・・・・・・・xviii
講演予稿 特別講演・・・・・・・・・・・・・・ 1
招待講演・・・・・・・・・・・・・・ 9
記念セッション・・・・・・・・・・・・11
一般講演・・・・・・・・・・・・・・・17
ポスター発表・・・・・・・・・・・・・45
発表索引・・・・・・・・・・・・・・・・・・・ 137

プログラム早見表

3月15日 （日）

	受付開始 8:30～ 講演開始 9:30～
9:30	招待講演（Esko I. Kauppinen）9:30–9:45
9:45	一般講演 3件 （ナノチューブの生成と精製・ ナノチューブの応用）9:45–10:30
10:30	休憩 10:30–10:45
10:45	一般講演 3件 （ナノチューブの応用） 10:45–11:30
11:30	ポスタープレビュー （ 1P–1 ～ 1P–31 ） 11:30–12:15
12:15	昼食 （幹事会） 12:15–13:30
13:30	ポスターセッション 【 多目的スペース 】 13:30–15:15 13:30–14:00 若手奨励賞候補審査優先時間
15:15	特別講演 （中野 匡規） 15:15–15:45
15:45	一般講演 3件 （グラフェン生成・原子層・ グラフェンの物性）15:45–16:30
16:30	特別講演 （窪田 芳之） 16:30–17:00
17:00	一般講演 4件 （内包ナノチューブ・ 金属内包フラーレン・その他） 17:00–18:00
18:00	休憩 18:00–18:15
18:15	チュートリアル 講師：（松田 一成） 京都大学 【 伊藤謝恩ホール 】 18:15–19:45
19:45	

3月16日 （月）

	受付開始 8:30～ 講演開始 9:00～
9:00	特別講演（Jaime C. Grunlan） 9:00–9:30
9:30	一般講演 3件 （ナノチューブの物性・ 原子層） 9:30–10:15
10:15	休憩 10:15–10:30
10:30	特別講演 （中村 潤児） 10:30–11:00
11:00	一般講演 2件 （原子層・ グラフェンの応用）11:00–11:30
11:30	ポスタープレビュー （ 2P–1 ～ 2P–30 ） 11:30–12:15
12:15	昼食 12:15–13:30
13:30	ポスターセッション 【 多目的スペース 】 13:30–15:15 13:30–14:00 若手奨励賞候補審査優先時間
15:15	授賞式 15:15–16:00
16:00	記念セッション （阿知波 洋次） （斎藤 晋） （飯島 澄男） 16:00–17:15
17:15	休憩 17:15–17:30
17:30	記念セッション （大澤 映二） （大塚 雅昭） （磯部 寛之） 17:30–18:45
18:45	

3月17日 （火）

	受付開始 8:30～ 講演開始 9:00～
9:00	特別講演（YuHuang Wang） 9:00–9:30
9:30	一般講演 3件 （ナノチューブの応用・ナノチュ ーブの生成と精製）9:30–10:15
10:15	休憩 10:15–10:30
10:30	特別講演（Christophe Bichara） 10:30–11:00
11:00	一般講演 2件 （その他・ ナノチューブの物性）11:00–11:30
11:30	ポスタープレビュー （ 3P–1 ～ 3P–31 ） 11:30–12:15
12:15	昼食 12:15–13:30
13:30	ポスターセッション 【 多目的スペース 】 13:30–15:15 13:30–14:00 若手奨励賞候補審査優先時間
15:15	特別講演（Yan Li） 15:15–15:45
15:45	一般講演 2件（ナノチューブの 物性・ナノホーン）15:45–16:15
16:15	特別講演 （千賀 亮典） 16:15–16:45
16:45	一般講演 3件 （原子層） 16:45–17:30
17:30	

3月18日 （水）

第14回ﾅﾉｶｰﾎﾞﾝ実用化推進研究会
【 伊藤謝恩ホール 】
10:00–18:00

講演会場 伊藤謝恩ホール
特別講演 発表25分・質疑5分
招待講演 発表10分・質疑5分
一般講演 発表10分・質疑5分
ﾎﾟｽﾀｰﾌﾟﾚﾋﾞｭｰ 発表1分・質疑なし

Time table

March 15 (Sun.)	
	Registration begins at 8:30 Lectures begin at 9:30
9:30	Invited Lecture (Esko I. Kauppinen) 9:30–9:45
9:45	General Lectures [3] (Formation and purification of nanotubes・Applications of nanotubes) 9:45–10:30
10:30	Coffee Break 10:30–10:45
10:45	General Lectures [3] (Applications of nanotubes) 10:45–11:30
11:30	Poster Preview (1P–1 through 1P–31) 11:30–12:15
12:15	Lunch (Administrative meeting) 12:15–13:30
13:30	Poster Session 【 Event Space 】 13:30–15:15 During 13:30–14:00, please give priority to selection of candidates for Young Scientist Poster Award
15:15	Special Lecture (Masaki Nakano) 15:15–15:45
15:45	General Lectures [3] (Graphene synthesis・Atomic Layers ・ Properties of graphene) 15:45–16:30
16:30	Special Lecture (Yoshiyuki Kubota) 16:30–17:00
17:00	General Lectures [4] (Endohedral nanotubes ・ Endohedral metallofullerenes ・ Other topics) 17:00–18:00
18:00	Coffee Break 18:00–18:15
18:15	Tutorial Lecturer : (Kazunari Matsuda) Kyoto University 【 Ito Hall 】 18:15–19:45
19:45	

March 16 (Mon.)	
	Registration begins at 8:30 Lectures begin at 9:00
9:00	Special Lecture (Jaime C. Grunlan) 9:00–9:30
9:30	General Lectures [3] (Properties of nanotubes ・ Atomic Layers) 9:30–10:15
10:15	Coffee Break 10:15–10:30
10:30	Special Lecture (Junji Nakamura) 10:30–11:00
11:00	General Lectures [2] (Atomic Layers ・Applications of graphene) 11:00–11:30
11:30	Poster Preview (2P–1 through 2P–30) 11:30–12:15
12:15	Lunch 12:15–13:30
13:30	Poster Session 【 Event Space 】 13:30–15:15 During 13:30–14:00, please give priority to selection of candidates for Young Scientist Poster Award
15:15	Award Ceremony 15:15–16:00
16:00	Commemorative Session (Yohji Achiba) (Susumu Saito) (Sumio Iijima) 16:00–17:15
17:15	Coffee Break 17:15–17:30
17:30	Commemorative Session (Eiji Osawa) (Masaaki Otsuka) (Hiroyuki Isobe) 17:30–18:45
18:45	

March 17 (Tue.)	
	Registration begins at 8:30 Lectures begin at 9:00
9:00	Special Lecture (YuHuang Wang) 9:00–9:30
9:30	General Lectures [3] (Applications of nanotubes ・ Formation and purification of nanotubes) 9:30–10:15
10:15	Coffee Break 10:15–10:30
10:30	Special Lecture (Christophe Bichara) 10:30–11:00
11:00	General Lectures [2] (Other topics ・ Properties of nanotubes) 11:00–11:30
11:30	Poster Preview (3P–1 through 3P–31) 11:30–12:15
12:15	Lunch 12:15–13:30
13:30	Poster Session 【 Event Space 】 13:30–15:15 During 13:30–14:00, please give priority to selection of candidates for Young Scientist Poster Award
15:15	Special Lecture (Yan Li) 15:15–15:45
15:45	General Lectures [2] (Properties of nanotubes・Nanohorns) 15:45–16:15
16:15	Special Lecture (Ryosuke Senga) 16:15–16:45
16:45	General Lectures [3] (Atomic Layers) 16:45–17:30
17:30	

March 18 (Wed.)
The 14th NanoCarbon Application Forum 【 Ito Hall 】 10:00–18:00

Place : Ito Hall
Special Lecture : 25 min (Presentation) + 5 min (Discussion)
Invited Lecture : 10 min (Presentation) + 5 min (Discussion)
General Lecture : 10 min (Presentation) + 5 min (Discussion)
Poster Preview : 1 min (Presentation)

座長一覧 (Chairpersons)

3月15日 (日) **(敬称略)**

セッション	時　　間	座　　長
招待講演(Esko I. Kauppinen)	9:30 ～ 9:45	丸山 茂夫
一般講演	9:45 ～ 10:30	
一般講演	10:45 ～ 11:30	田中 丈士
ポスタープレビュー	11:30 ～ 12:15	杉目 恒志 / 井ノ上 泰輝
特別講演(中野 匡規)	15:15 ～ 15:45	北浦 良
一般講演	15:45 ～ 16:30	
特別講演(窪田 芳之)	16:30 ～ 17:00	湯田坂 雅子
一般講演	17:00 ～ 18:00	松尾 豊
チュートリアル(松田 一成)	18:15 ～ 19:45	丸山 茂夫

3月16日 (月)

セッション	時　　間	座　　長
特別講演(Jaime C. Grunlan)	9:00 ～ 9:30	柳 和宏
一般講演	9:30 ～ 10:15	宮内 雄平
特別講演(中村 潤児)	10:30 ～ 11:00	高井 和之
一般講演	11:00 ～ 11:30	
ポスタープレビュー	11:30 ～ 12:15	中西 勇介 / 丸山 実那
記念セッション (阿知波 洋次) (斎藤 晋) (飯島 澄男) 祝辞紹介	16:00 ～ 17:15	岡田 晋 若林 知成
記念セッション (大澤 映二) (大塚 雅昭) (磯部 寛之)	17:30 ～ 18:45	若林 知成 / 小澤 理樹 菅井 俊樹 竹延 大志

3月17日 (火)

セッション	時　　間	座　　長
特別講演(YuHuang Wang)	9:00 ～ 9:30	宮内 雄平
一般講演	9:30 ～ 10:15	柳 和宏
特別講演(Christophe Bichara)	10:30 ～ 11:00	千足 昇平
一般講演	11:00 ～ 11:30	
ポスタープレビュー	11:30 ～ 12:15	小澤 大知 / 岡田 光博
特別講演(Yan Li)	15:15 ～ 15:45	Don N. Futaba
一般講演	15:45 ～ 16:15	
特別講演(千賀 亮典)	16:15 ～ 16:45	項 榮
一般講演	16:45 ～ 17:30	

3月 15日（日）

特別講演　　発表 25分 ・ 質疑応答 5分
招待講演　　発表 10分 ・ 質疑応答 5分
一般講演　　発表 10分 ・ 質疑応答 5分
ポスタープレビュー　　発表 1分 ・ 質疑応答 なし

招待講演（ 9:30-9:45 ）

1I-1　FC-CVD synthesis of CNTs from methane for transparent conductor applications　9
＊*Esko I. Kauppinen, Qiang Zhang, Datta Sukanta, Hua Jiang*

一般講演（ 9:45-10:30 ）
ナノチューブの生成と精製 ・ ナノチューブの応用

1-1　超分子化学による半導体性SWNTのone-pot分離　17
＊*中嶋 直敏*

1-2　1cmを超える長尺CNTフォレストの高速成長　18
＊*桜井 俊介, 辻 享志, 山田 真保, 畠 賢治, Futaba Don*

1-3　ホタル由来ルシフェリン/ルシフェラーゼ反応を利用したCNTの発光　19
＊*田中 丈士, 樋口 麗保子, 平塚 淳典, 片浦 弘道*

＞＞＞＞＞＞＞ 休憩（ 10:30-10:45 ）＜＜＜＜＜＜＜

一般講演（ 10:45-11:30 ）
ナノチューブの応用

1-4　Selective Activation of Singlet/Triplet Reaction Paths Enabled by Carbon-nanotube-mediated Energy Attenuation　20
＊*Dongxin Liu, Dominik Lungerich, Satori Kowashi, Takayuki Nakamuro, Kaoru Yamanouchi, Koji Harano, Eiichi Nakamura*

1-5　Polyaromatic Anthracene Nano-tweezer on Semiconducting Carbon Nanotubes for Growth and Bridging of Perovskite Crystal Grains in Perovskite Solar Cells　21
＊*林 昊升, 大川 脩平, 田 日, 松尾 豊, 丸山 茂夫*

1-6　Optimization of the Alignment Relay Technique for the Controlled Orientation and Selection of Single-Walled Carbon Nanotubes　22
＊*Monika Snowdon, Derek Schipper, Dai-ming Tang*

ポスタープレビュー（ 11:30-12:15 ）　（☆） 若手奨励賞候補
若手奨励賞候補

1P-1　針状のフラーレンC_{70}単結晶を用いた有機電界効果トランジスタ　45
☆　＊*山本 亮平, 平井 匡彦, 青木 伸之, 橘 勝*

1P-2　Alteration of Fermi-Level of Single-Wall Carbon Nanotubes via Protein Adsorption Observed by Ultrafast Spectroscopy　46
☆　＊*Tomohito Nakayama, Takeshi Tanaka, Atsushi Hirano, Muneaki Hase*

3月 15日（日）

1P-3 ☆ カーボンナノチューブ複合樹脂材料の力学特性と相構造 47
＊村岡 慶美, 福森 健三

1P-4 ☆ Understanding the Effect of Sulfur on the Synthesis of Carbon Nanotubes 48
＊仲川 黎, 江戸 倫子, 杉目 恒志, 野田 優

1P-5 ☆ Evaluation of various nitrogen-doping in graphene on the performance as a supercapacitor electrode 49
＊Rohit Yadav, Prerna Joshi, Masanori Hara, Masamichi Yoshimura

1P-6 ☆ Gene expression analysis of macrophages on carbon nanohorn coated titanium 50
＊Sadahito Kimura, Eri Hirata, Sari Takada, Masatoshi Sakairi, Masako Yudasaka, Atsuro Yokoyama

1P-7 ☆ Unidirectional bright exciton transport in a $WS_{2x}Se_{(2-2x)}$ alloy monolayer 51
＊Masafumi Shimasaki, Taishi Nishihara, Naoki Wada, Zheng Liu, Kana Kojima, Keisuke Shinokita, Kazunari Matsuda, Yasumitsu Miyata, Yuhei Miyauchi

ナノチューブの物性 【CREST】

1P-8 MoS_2 ナノチューブバンドルの電子状態 52
＊久間 馨, 丸山 実那, 岡田 晋, 千足 昇平, 丸山 茂夫

1P-9 Rayleigh scattering measurement of suspended SWCNTs coaxially wrapped with BNNTs 53
＊Satoshi Yotsumoto, Hayato Arai, Yongjia Zheng, Taiki Inoue, Rong Xiang, Shigeo Maruyama, Shohei Chiashi

1P-10 Optical properties of inorganic nanotubes with different diameters 54
＊Yohei Yomogida, Yasumitsu Miyata, Kazuhiro Yanagi

1P-11 Chemical vapor deposition of one-dimensional heterostructures 55
＊Yongjia Zheng, Yang Qian, Ming Liu, Akinito Kumamoto, Yuichi Ikuhara, Esko I. Kauppinen, Shohei Chiashi, Taiki Inoue, Rong Xiang, Shigeo Maruyama

1P-12 h-BN上へのガス流配向CNTの合成とラマン分光測定 56
＊佐藤 周, 四元 聡, 番場 雅典, 井ノ上 泰輝, 丸山 茂夫, 千足 昇平

1P-13 In-Plane Thermal Conductance of Thin Films Composed of Coaxially Combined Single-Walled Carbon Nanotubes and Boron Nitride Nanotubes 57
＊Pengyingkai Wang, Yongjia Zheng, Taiki Inoue, Rong Xiang, Ahmed Shawky, Makoto Watanabe, Anton Anisimov, Esko I. Kauppinen, Shohei Chiashi, Shigeo Maruyama

ナノチューブの応用 【CREST】

1P-14 Fabrication of ribbon-like films with highly oriented carbon nanotubes using a robotic dispenser 58
＊Manish Pandey, Ryo Abe, Naofumi Okamoto, Yuki Sekimoto, Masakazu Nakamura

3月 15日（日）

フラーレンの化学

1P-15 ポリインのリン光：新規ポリイン誘導体検出の鍵となる探針 59
＊若林 知成, 北村 望, 大澤 綾人, 岡田 大貴, 鈴木 晴, 森澤 勇介, 畑中 美穂

1P-16 CuCl-Mediated Reaction of C_{60} with Propargylic Phosphate 60
＊石塚 明日美, 前田 優, 山田 道夫

フラーレンの応用

1P-17 Catalytic activity for the reduction of 4-nitrophenol using on gadolinium oxide nanoparticle-[C_{60}]fullerene nanowhisker composites 61
＊Jeong Won Ko, Sugyeong Jeon, Weon Bae Ko

金属内包フラーレン

1P-18 Reactions of S-Heterocyclic Carbenes with Fullerenes: Preparation and Characterization of Dithiomethano-derivatives 62
＊前田 勇太, 官澤 伸治, 加固 昌寛, 山田 道夫, 前田 優, 古川 真, 赤阪 健

ナノチューブの応用

1P-19 CNT/HDPE複合材料の破断挙動の解明 63
＊宇津木 孝一, 大槻 南央, 関戸 大

ナノチューブの生成と精製

1P-20 TDDFT計算により示唆される直径1nm以下のカーボンナノチューブの直線偏光レーザー照射下の優先的安定性 64
＊宮本 良之

1P-21 ナノジルコニア分散カーボンペーパー上へのカーボンナノチューブ合成 65
＊神戸 大, 山口 宣朝, 山際 清史

グラフェン生成

1P-22 錯体ナノ空間を利用したグラフェンナノリボンの精密合成 66
＊北尾 岳史, マクレーン マイケル, 中田 和希, 植村 卓史

1P-23 Direct precipitation growth of multi-layer graphene using W capping layer -Dependence of growth atmosphere- 67
＊山田 純平, 上田 悠貴, 丸山 隆浩, 成塚 重弥

グラフェンの応用

1P-24 ナノグラフェン集合体におけるNO_x吸着ダイナミクス 68
＊日景 結理奈, 西嶌 里美, 高井 和之

1P-25 酸化グラフェンの化学構造と触媒活性との相関 69
＊鈴木 隆太郎, 井坂 琢也, 田嶋 健太郎, 中原 花菜, 松尾 吉晃, 赤井 伸行, 高井 和之

グラフェンの物性

1P-26 Investigation of surface potential variations of thermally reduced graphene oxide 70
＊K. Kanishka H. De Silva, Shuhei Ogawa, Pamarti Vishwanath, Masamichi Yoshimura

3月 15日（日）

1P-27 グラフェンの電子輸送特性に対する水素分子の吸着効果 71
＊重久 雄大, 小幡 吉徳, 石黒 康志, 高井 和之

原子層

1P-28 Multi-ferroic response of two-dimensional hexagonal materials 72
＊Fenda Rizky Pratama, M. Shoufie Ukhtary, Riichiro Saito

1P-29 Carrier-dependent photoluminescence properties of CVD-grown monolayer MoS_2 73
＊Kana Kojima, Hong En Lim, Yusuke Nakanishi, Takahiko Endo, Yutaka Maniwa, Yasumitsu Miyata

ナノ炭素粒子

1P-30 ナノダイヤモンドの溶液からソフトゲルを経由した自己組織化 74
＊田中 利彦, 三浦 康弘, 青山 哲也, 根本 雅哉, 安藤 柊介, 板橋 佑歩, 宮本 和範, 村中 厚哉, 内山 真伸, 大澤 映二

その他

1P-31 化学的手法により発生させた二原子炭素(C_2)による炭素同素体の合成 75
＊宮本 和範, 成田 将大, 増本 優衣, 橋新 崇広, 大澤 泰生, 木村 睦, 落合 正仁, 内山 真伸

>>>>>>> 昼食（ 12:15-13:30 ）<<<<<<<

ポスターセッション（ 13:30-15:15 ）
13:30-14:00 若手奨励賞候補審査優先時間

特別講演（ 15:15-15:45 ）

1S-1 ファンデルワールス界面の創発物性 1
＊中野 匡規

一般講演（ 15:45-16:30 ）
グラフェン生成 ・ 原子層 ・ グラフェンの物性

1-7 伝導ギャップ制御に向けたホモ接合グラフェンナノリボンの合成 23
＊小倉 士忠, 金子 俊郎, 加藤 俊顕

1-8 遷移金属酸化物ナノシート単層膜を用いたメタン酸化反応の電気的モニタリング 24
＊野内 亮, 石原 良晃, 杉本 渉

1-9 Mechanical properties of 2D materials, scaling from monolayer to macroscale 25
＊Dai-Ming Tang, Xin Zhou, Fengchun Hsia, Yoshio Bando, Dmitri Golberg

特別講演（ 16:30-17:00 ）

1S-2 導電性カーボンナノチューブコートPETテープに乗せた神経組織の高解像度電子顕微鏡撮影とその解析法 2
＊窪田 芳之

3月 15日（日）

一般講演（ 17:00–18:00 ）
内包ナノチューブ ・ 金属内包フラーレン ・ その他

1–10 Long Linear Carbon Chains inside CNT Formed by Electric Discharge of a SWCNT film 26
＊齋藤 弥八, 安坂 幸師, 石田 稔幸

1–11 Plasma Implantation of Lithium-Ion into Inner Space of C_{70}: Synthesis and Characterization of Lithium-Ion-Encapsulated C_{70} ($Li^{+}@C_{70}$) 27
＊Hiroshi Ueno, Kazuhiko Kawachi, Daiki Kitabatake, Keijiro Ohshimo, Hiroshi Okada, Eunsang Kwon, Shinobu Aoyagi, Yasuhiko Kasama, Fuminori Misaizu

1–12 The Cage Dependence of Single Molecule Magnet Properties of Dy-dimetallofullerene Anions 28
＊髙井 良也, 東中 隆二, 青木 勇二, 菊地 耕一, 阿知波 洋次, 兒玉 健

1–13 ナノ物質のための移動度・電荷・光測定システムの開発 29
＊菅井 俊樹, 内山 史章, 大石 祐也, 宮本 莉央奈, 佐々木 諒, 仲安 貴紀, 小栗 奏太, 小野 智也

>>>>>>> 休憩（ 18:00–18:15 ）<<<<<<<

チュートリアル（ 18:15–19:45 ）

ナノカーボン・原子層物質における光物性の基礎と応用
＊松田 一成

3月 16日（月）

特別講演　　発表 25分 ・ 質疑応答 5分
一般講演　　発表 10分 ・ 質疑応答 5分
ポスタープレビュー　　発表 1分 ・ 質疑応答 なし

特別講演（ 9:00-9:30 ）【CREST】

2S-1 High power factor, completely organic thermoelectric nanocomposites enabled by carbon nanoparticles 3
＊Jaime C. Grunlan

一般講演（ 9:30-10:15 ）【CREST】
ナノチューブの物性 ・ 原子層 【CREST】

2-1 半導体型単層カーボンナノチューブの熱電特性における一次元性 30
一ノ瀬 遥太, 上治 寛, 蓬田 陽平, ＊柳 和宏

2-2 Synthesis of Boron Nitride Nanotubes and MoS_2@BNNTs Heteronanotubes 31
＊Ming Liu, Yongjia Zheng, Yang Qian, Rong Xiang, Taiki Inoue, Shohei Chiashi, Esko I. Kauppinen, Shigeo Maruyama

2-3 Influence of interlayer stacking on gate-induced carrier accumulation in a van der Waals heterostructure comprising MoS_2 and WS_2 32
＊Mina Maruyama, Susumu Okada

>>>>>>> 休憩（ 10:15-10:30 ）<<<<<<<

特別講演（ 10:30-11:00 ）

2S-2 燃料電池用窒素ドープカーボン触媒の活性点 4
＊中村 潤児

一般講演（ 11:00-11:30 ）
原子層 ・ グラフェンの応用

2-4 First-principles electronic-structure study of stabilities and electronic properties of trilayer h-BN 33
＊芳賀 太史, 松浦 雄斗, 藤本 義隆, 斎藤 晋

2-5 グラフェン/Au電極への分子修飾の評価とプロトン透過能への影響 34
＊福島 知宏, 駒井 貴羽, 長谷部 秀尭, 村越 敬

ポスタープレビュー（ 11:30-12:15 ）　（☆） 若手奨励賞候補
若手奨励賞候補

2P-1 超音波照射による簡便で効果的な単層カーボンナノチューブの発光特性制御 76
☆ *＊紺野 優以, 西野 朱音, 山田 道夫, 前田 優, 奥平 早紀, 宮内 雄平, 松田 一成, 松井 淳, 三ツ石 方也, 鈴木 光明*

2P-2 Stable MoO_3 Doping of Carbon Nanotube Top Electrodes for Highly Efficient Metal-Electrode-Free Perovskite Solar Cells 77
☆ *＊Seungju Seo, Il Jeon, Esko I. Kauppinen, Yutaka Matsuo, Shigeo Maruyama*

3月 16日（月）

2P-3 ☆ Macrocyclic bis(dipyrrinato) metal complex for single-walled carbon nanotube separation 78
＊Guoqing Cheng, Naoki Komatsu

2P-4 ☆ Influence of the carbon-rich domain in hexagonal boron nitride on transport properties of adjacent graphene 79
＊小野寺 桃子, 渡邊 賢司, 諫山 都子, 増渕 覚, 守谷 頼, 谷口 尚, 町田 友樹

2P-5 ☆ Dielectric screening effects on photoluminescence of carbon nanotubes on hexagonal boron nitride 80
＊Nan Fang, Keigo Otsuka, Takashi Taniguchi, Kenji Watanabe, Kosuke Nagashio, Yuichiro Kato

2P-6 ☆ Synthesis of 3D hybrid Structures composed of Single-walled CNTs and Mesopores Carbon by Chemical Vapor Deposition 81
＊Aliza Khaniya Sharma, Kamal P Sharma, Takahiro Saida, Shigeya Naritsuka, Takahiro Maruyama

2P-7 ☆ 電気・熱回路網解析によるCNT薄膜の熱電性能の理論設計 82
＊小林 遵栄, 藤崎 小太郎, 山本 貴博

ナノチューブの物性 【CREST】

2P-8 Evaluation of Thermal Transport in a Single-walled Carbon Nanotube Film by Ionic-liquid Gating 83
＊Kan Ueji, Yuya Matsuoka, Takashi Yagi, Kengo Fukuhara, Yota Ichinose, Akari Yoshida, Yohei Yomogida, Kazuhiro Yanagi

2P-9 Thermal stability of single-chirality-enriched carbon nanotube thin films 84
＊Akira Takakura, Taishi Nishihara, Kazunari Matsuda, Takeshi Tanaka, Hiromichi Kataura, Yuhei Miyauchi

2P-10 Relationships between Seebeck coefficient and Conduction Directions in Aligned Semiconducting Single-wall Carbon Nanotube Films 85
＊Kengo Fukuhara, Yota Ichinose, Kanako Horiuchi, Akari Yoshida, Yohei Yomogida, Weilu Gao, Natsumi Komatsu, Junichiro Kono, Kazuhiro Yanagi

ナノチューブの応用 【CREST】

2P-11 カーボンナノチューブ繊維のマクロスケール四端子熱伝導測定 86
佐藤 彰斗, 足立 建人, ＊児玉 高志

グラフェンの応用 【CREST】

2P-12 Bubble induced damage on graphene liquid cells during TEM observation 87
＊廣川 颯汰, 手嶋 秀彰, Pablo S. Fernandez, 吾郷 浩樹, 塘 陽子, Qin-Yi Li, 高橋 厚史

グラフェンの物性 【CREST】

2P-13 歪印加によるグラフェンのPFの向上 88
＊鈴木 康平, 笹岡 健二, 山本 貴博

2P-14 端の欠陥によるグラフェンナノリボンのスピンフィルター効果 89
＊安部 直梛, 笹岡 健二, 山本 貴博

原子層 【CREST】

2P-15 Anomalous electroluminescence from WS_2/WSe_2 in-plane heterostructures 90
＊Naoki Wada, Jiang Pu, Tomoyuki Yamada, Wenjin Zhang, Zheng Liu, Yusuke Nakanishi, Yutaka Maniwa, Kazunari Matsuda, Yuhei Miyauchi, Taishi Takenobu, Yasumitsu Miyata

フラーレンの化学

2P-16 C_{60}赤外吸収の絶対強度と相対強度 91
＊若林 知成, 百瀬 孝昌, ファハールト マリオ E.

2P-17 A one-step direct oxidation of alkoxy to ketone: oxidation of alkoxy indano[60]fullerenes to [60]fullerene-fused ketones *via* weak copper oxidant 92
＊Yue Ma, Hao-Sheng Lin, Yun Yu, Shigeo Maruyama, Il Jeon, Yutaka Matsuo

金属内包フラーレン

2P-18 ESR study of La and Y hetero-dimetallofullerene anions 93
＊前島 萌乃, 菊地 耕一, 阿知波 洋次, 兒玉 健

2P-19 ESR Study of two isomers of $[Sc_2C_{80}]^-$: $[Sc_2C_{80}(1)]^-$ and $[Sc_2C_{80}(2)]^-$ 94
＊吉田 俊, 古川 貢, 菊地 耕一, 阿知波 洋次, 兒玉 健

ナノチューブの物性

2P-20 局所化学修飾単層カーボンナノチューブのドープ構造の違いに依存した発光ソルバトクロミズム挙動 95
＊白木 智丈, 新留 嘉彬, 藤ヶ谷 剛彦

ナノチューブの応用

2P-21 PEN基板上のCNT薄膜電極を用いたX線の電気的検出 96
＊松田 裕之, 鈴木 慧, 石川 剛弘, 小西 輝昭, 濱野 毅, 大野 雄高, 平尾 敏雄, 石井 聡

ナノチューブの生成と精製

2P-22 Understanding and controlling the pyrolysis of C_3H_8 for uniform synthesis of vertically-aligned single-wall carbon nanotubes 97
＊MengJu Yang, Pengfei Chen, Rei Nakagawa, Hisashi Sugime, Hitoshi Mazaki, Suguru Noda

2P-23 新しいホウ素原料を用いた化学気相成長法による窒化ホウ素ナノチューブの合成 98
＊沢田 哲郎, 高橋 宏夢, 清 智弘, 安積 茉由, 大沢 利男, 杉目 恒志, 野田 優

2P-24 CNT分散剤フラビンの昇華性 99
＊加藤 雄一, 小橋 和文, 山田 健郎, 畠 賢治

2P-25 CVD synthesis of sub-nanometer diameter single-walled CNTs 100
＊Kamal Prasad Sharma, Daiki Yamamoto, Aliza Khaniya Sharma, Takahiro Maruyama

3月 16日（月）

グラフェン生成

2P-26 a面サファイア上のグラフェンのCVD成長メカニズムの検討 101
＊上田 悠貴, 山田 純平, 丸山 隆浩, 成塚 重弥

グラフェンの応用

2P-27 Heteroatom-doped Nanocarbons as Active Support for IrO_2 as an OER Electrocatalyst 102
＊Prerna Joshi, Rohit Yadav, Masanori Hara, Masamichi Yoshimura

ナノ炭素粒子

2P-28 溶液中のナノダイヤモンドとの相互作用その1：イオン 103
＊根本 雅哉, 安藤 柊介, 板橋 佑歩, 田中 利彦, 三浦 康弘, 青山 哲也, 村中 厚哉, 内山 真伸, 大澤 映二

2P-29 溶液中のナノダイヤモンドとの相互作用その2：色素イオン 104
＊板橋 佑歩, 安藤 柊介, 根本 雅哉, 田中 利彦, 三浦 康弘, 青山 哲也, 村中 厚哉, 内山 真伸, 大澤 映二

バイオ

2P-30 Detection of odor molecules by transistor-type graphene biosensor 105
＊本間 千柊, 野口 紘長, 磯林 厚伸, 杉崎 吉昭, 早水 裕平

＞＞＞＞＞＞＞ 昼食（ 12:15-13:30 ）＜＜＜＜＜＜＜

ポスターセッション（ 13:30-15:15 ）
13:30-14:00 若手奨励賞候補審査優先時間

大澤賞・飯島賞・若手奨励賞の授賞式（ 15:15-16:00 ）

3月 16日（月）

C_{60}芳香族安定性予言50周年
記念セッション（ 16:00-17:15 ）

2C-1 The beginning of nano-carbon era －Prediction and discovery of C_{60}－ 11
＊阿知波 洋次

2C-2 炭素クラスターC_{60} 12
＊斎藤 晋

2C-3 炭素のTEM観察：アモルファス炭素、フラーレンそしてカーボンナノチューブ 13
＊飯島 澄男

祝辞紹介
＊若林 知成

>>>>>>> 休憩（ 17:15-17:30 ）<<<<<<<

C_{60}芳香族安定性予言50周年
記念セッション（ 17:30-18:45 ）

2C-4 サッカーボール分子C_{60}の50年 14
＊大澤 映二

2C-5 宇宙におけるフラーレンの起源を解明する －フラーレンを有する惑星状星雲の物理的性質についてー 15
＊大塚 雅昭, F.Kemper, J.Cami, E.Peeters, Fullerene PN consortium

2C-6 簡便・汎用合成が生み出す湾曲ナノカーボン分子 16
＊磯部 寛之

3月 17日（火）

特別講演　　発表 25分 ・ 質疑応答 5分
一般講演　　発表 10分 ・ 質疑応答 5分
ポスタープレビュー　　発表 1分 ・ 質疑応答 なし

特別講演（ 9:00-9:30 ）【CREST】

3S-1 Gating IR in Textiles 5
＊YuHuang Wang

一般講演（ 9:30-10:15 ）【CREST】
ナノチューブの応用 ・ ナノチューブの生成と精製 【CREST】

3-1 Carbon nanotube-based excitonic wavelength-selective absorber and emitter for solar thermal energy harvesting 35
＊Yuhei Miyauchi, Taishi Nishihara, Akira Takakura, Kazunari Matsuda, Takeshi Tanaka, Hiromichi Kataura

3-2 Machine-learned 100 %-yield carbon nanotube dissolution in arbitrary organic solvents 36
＊野々口 斐之, 宮尾 知幸, 後藤 千草, 村山 智子, 船津 公人, 河合 壯

3-3 ゲル、SWCNTおよび界面活性剤間のマルチスケール疎水性相互作用：詳細議論 37
王 国偉, 田中 丈士, ＊片浦 弘道

＞＞＞＞＞＞＞ 休憩（ 10:15-10:30 ）＜＜＜＜＜＜＜

特別講演（ 10:30-11:00 ）

3S-2 Selective growth of single walled carbon nanotubes : thermodynamics versus kinetics 6
＊Christophe Bichara

一般講演（ 11:00-11:30 ）
その他 ・ ナノチューブの物性

3-4 WS_2ナノチューブにおけるバルク光起電力効果 38
＊張 奕勁, 井手上 敏也, 恩河 大, 秦 峰, 鈴木 龍二, Alla Zak, Reshef Tenne, Jurgen Smet, 岩佐 義宏

3-5 Radiative quantum efficiency of bright excitons in carbon nanotubes 39
＊Hidenori Machiya, Akihiro Ishii, Yuichiro K. Kato

ポスタープレビュー（ 11:30-12:15 ）　（☆） 若手奨励賞候補
若手奨励賞候補

3P-1 Highly Selective and Scalable Fullerene-Cation-Mediated Synthesis acessing Cyclo[60]fullerenes with 5-Membered-Carbon-Ring and their Application to Perovskite Solar Cells 106
☆ *＊林 昊升, 田 日, 丸山 茂夫, 松尾 豊*

3P-2 Flattening of 2D materials encapsulated by hBN flakes 107
☆ *＊Takato Hotta, Akihiro Ueda, Shohei Higuchi, Keiji Ueno, Kenji Watanabe, Takashi Taniguchi, Ryo Kitaura*

3月 17日（火）

3P-3 ☆ SMART-EM法によるペプチド及びその凝集体解析のための修飾CNHの開発 108
＊中室 貴幸, 孫 克己, Bode Jeffery W., 原野 幸治, 中村 栄一

3P-4 ☆ 周期構造修飾されたグラフェンの電子物性 109
＊田口 裕太, 斎藤 晋

3P-5 ☆ In-plane heterostructure of MoS_2 polytypes 110
＊Ruben Canton Vitoria, Ryo Kitaura

3P-6 ☆ その場観測により観測された単層WS_2の高速成長 111
＊亀山 智矢, 金子 俊郎, 加藤 俊顕

3P-7 ☆ 単層CNT成長における添加ガスの効果の同位体ラベル分析 112
＊小矢野 文章, 山元 隼, 小林 明香里, 石丸 亮哉, 大塚 慶吾, 井ノ上 泰輝, 項 栄, 千足 昇平, 丸山 茂夫

ナノチューブの物性 【CREST】

3P-8 Electronic property of CNT thin film under external electric field 113
＊高 燕林, 岡田 晋

3P-9 金属型単層カーボンナノチューブ配列薄膜におけるホール効果と弱局在伝導 114
＊堀内 加奈子, Ryotaro Okada, Hideki Kawai, Yohei Yomogida, Natsumi Komatsu, Weilu Gao, Junichiro Kono, Kazuhiro Yanagi

グラフェンの物性 【CREST】

3P-10 Influence of interlayer stacking arrangements on carrier accumulation in bilayer graphene field effect transistors 115
＊Susumu Okada, Yanlin Gao, Mina Maruyama

3P-11 Study on effects of twist on phonon transport in graphene nanoribbons 116
＊Yukihiko Terada, Takuma Shiga

バイオ 【CREST】

3P-12 鉄イオンが媒介するカーボンナノチューブによる補酵素NADHの酸化反応 117
＊平野 篤, 和田 百代, 田中 丈士, 片浦 弘道

その他 【CREST】

3P-13 超高速膜ろ過用の六方晶窒化ホウ素ナノシート 118
＊Rasel Das, Pablo Solís-Fernández, Hiroki Ago

3P-14 Mechanical and electronic properties of copolymers of centrohexaquinane and cyclooctatetraene 119
＊藤井 康丸, 丸山 実那, 岡田 晋

金属内包フラーレン

3P-15 Single molecule magnet properties of Tb-dimetallofullerene anions: $[Tb_2@C_{80}(I_h)]^-$ and $[Tb_2@C_{78}(D_{3h})]^-$ 120
＊山岸 主暉, 東中 隆二, 青木 勇二, 菊地 耕一, 阿知波 洋次, 兒玉 健

3P-16 Attempt to produce Sm-dimetallofullerenes 121
＊藤田 直也, 菊地 耕一, 阿知波 洋次, 兒玉 健

ナノ環境と安全評価

3P-17 In vivo evaluation of biodistribution, toxicity and clearance of single wall carbon nanotubes depending on the dispersants 122
＊Ying Xu, Minfang Zhang, Mei Yang, Masako Yudasaka, Toshiya Okazaki

ナノチューブの応用

3P-18 Importance of structural parameters of CNTs for the Pt electrochemical durability in CNT based Pt electrocatalysts in PEMFCs 123
＊Don Terrence Dhammika Weerathunga, Tsuyohiko Fujigaya

3P-19 A semitransparent terahertz imager made from chemically doped semiconducting carbon nanotube thin films 124
＊大井 かなえ, 李 恒, 鈴木 大地, 河合 壯, 河野 行雄, 野々口 斐之

3P-20 Compact Wearable Foot Pressure Sensors from MWCNT Coated Cotton Fibers for Human Activity and Sporting Performance Monitoring 125
＊Md. Abdul Momin, Mohammad Jellur Rahman, Tetsu Mieno

ナノチューブの生成と精製

3P-21 Activation of Alkane for CVD Growfh of Single-Wall Carbon Nanotubes 126
＊Pengfei Chen, Mengju Yang, Rei Nakagawa, Hisashi Sugime, Hitoshi Mazaki, Suguru Noda

3P-22 石英ウールへの配向カーボンナノチューブの合成および形態評価 127
＊山口 宣朝, 神戸 大, 山際 清史

3P-23 化学気相成長法による窒化ホウ素ナノチューブ合成における触媒と原料の独立制御 128
＊高橋 宏夢, 沢田 哲郎, 清 智弘, 安積 茉由, 大沢 利男, 杉目 恒志, 野田 優

3P-24 Selective dispersion of semiconducting single-walled carbon nanotubes by using alkyl cellulose 129
＊八木 智子, 河合 壯, 野々口 斐之

ナノワイヤー

3P-25 Scaling laws on enhancement of the electric field inside a hollow cylinder 130
＊Yuan Tian, Muhammad Shoufie Ukhtary, Riichiro Saito

グラフェンの応用

3P-26 酸化グラフェンPLの増強：ジオキサン分散状態でのUV照射 131
＊金澤 克樹, 佐野 正人

3P-27 グラフェンと量子ドットとの界面における相互作用の影響 132
＊井上 禅, 石黒 康志, Alexader Baranov, Igor Nabiev, 高井 和之

3月 17日（火）

原子層

3P-28 First-principles calculation of exciton of transition metal dichalcogenide 133
＊Pang Xiaoqi, Nguyen T. Hung, Riichiro Saito

3P-29 Theoretic Study on Raman Active Modes of SnS Thin Films 134
＊米盛 樹生, Sudipta Dutta, 長汐 晃輔, 若林 克法

3P-30 表面修飾された基板上のMoS_2の電気伝導における分子吸着効果 135
＊皆川 勇気, 梅原 太一, 高井 和之

その他

3P-31 Thermal conductivity of low-cost thermoelectric Mg_3Bi_2 136
＊Nguyen T. Hung, Riichiro Saito

＞＞＞＞＞＞＞ 昼食（ 12:15-13:30 ）＜＜＜＜＜＜＜

ポスターセッション（ 13:30-15:15 ）
13:30-14:00 若手奨励賞候補審査優先時間

特別講演（ 15:15-15:45 ）

3S-3 *In situ* Study of Catalysts for Single-Walled Carbon Nanotube Growth 7
＊Yan Li, Feng Yang

一般講演（ 15:45-16:15 ）
ナノチューブの物性 ・ ナノホーン

3-6 Vapor-Phase Functionalization of Air-Suspended Single-Walled Carbon Nanotubes Using an Aryl-Halide 40
＊Daichi Kozawa, Xiaojian Wu, Akihiro Ishii, Jacob Fortner, Keigo Otsuka, Rong Xiang, Taiki Inoue, Shigeo Maruyama, YuHuang Wang, Yuichiro K. Kato

3-7 化学修飾カーボンナノホーンを用いた反応中間体の捕捉と原子分解能電顕構造解析 41
＊原野 幸治, Xing Junfei, Schweighauser Luca, 岡田 賢, 中村 栄一

特別講演（ 16:15-16:45 ）

3S-4 電子顕微鏡を使った低次元材料のナノスケール光学及び振動吸収スペクトル計測 8
＊千賀 亮典, 末永 和知, Thomas Pichler

一般講演（ 16:45-17:30 ）
原子層

3-8 Independent degrees of freedom in two-dimensional materials 42
＊Sake Wang, F. R. Pratama, M. Shoufie Ukhtary, Riichiro Saito

3-9 極性に依存したGaN表面上での遷移金属ダイカルコゲナイドの光学特性 43
＊毛利 真一郎, 小路 悠馬, 篠北 啓介, 松田 一成, 荒木 努

3-10 TaP における異常な偏光ラマンスペクトル 44
＊齋藤 理一郎, Pang Xiaoqi, Wang Tong, Nguyen T. Hung

March 15th, Sun.

Special Lecture: 25min (Presentation) + 5min (Discussion)
Invited Lecture: 10min (Presentation) + 5min (Discussion)
General Lecture: 10min (Presentation) + 5min (Discussion)
Poster Preview: 1min (Presentation)

Invited Lecture (9:30–9:45)

1I–1 FC-CVD synthesis of CNTs from methane for transparent conductor applications 9
** Esko I. Kauppinen, Qiang Zhang, Datta Sukanta, Hua Jiang*

General Lecture (9:45–10:30)
Formation and purification of nanotubes ・ Applications of nanotubes

1–1 One-pot Separation of Semiconducting Single-walled Carbon Nanotubes Based on Supramolecular Chemistry 17
** Naotoshi Nakashima*

1–2 Fast synthesis of vertically aligned CNTs array exceeding one-centimeter height 18
** Shunsuke Sakurai, Takashi Tsuji, Maho Yamada, Kenji Hata, Don N. Futaba*

1–3 Luminescence of CNTs by luciferin/luciferase reaction from firefly 19
** Takeshi Tanaka, Mahoko Higuchi, Atsunori Hiratsuka, Hiromichi Kataura*

>>>>>>> Coffee Break (10:30–10:45) <<<<<<<

General Lecture (10:45–11:30)
Applications of nanotubes

1–4 Selective Activation of Singlet/Triplet Reaction Paths Enabled by Carbon-nanotube-mediated Energy Attenuation 20
** Dongxin Liu, Dominik Lungerich, Satori Kowashi, Takayuki Nakamuro, Kaoru Yamanouchi, Koji Harano, Eiichi Nakamura*

1–5 Polyaromatic Anthracene Nano-tweezer on Semiconducting Carbon Nanotubes for Growth and Bridging of Perovskite Crystal Grains in Perovskite Solar Cells 21
** Hao-Sheng Lin, Shuhei Okawa, IL Jeon, Yutaka Matsuo, Shigeo Maruyama*

1–6 Optimization of the Alignment Relay Technique for the Controlled Orientation and Selection of Single-Walled Carbon Nanotubes 22
** Monika Snowdon, Derek Schipper, Dai-ming Tang*

Poster Preview (11:30–12:15) (☆)Candidates for the Young Scientist Poster Award
Candidates for the Young Scientist Poster Award

1P–1 Organic field effect transistor of C_{70} single crystals with rod shape 45
☆ ** Ryohei Yamamoto, Tadahiko Hirai, Nobuyuki Aoki, Masaru Tachibana*

1P-2 ☆ Alteration of Fermi-Level of Single-Wall Carbon Nanotubes via Protein Adsorption Observed by Ultrafast Spectroscopy 46
** Tomohito Nakayama, Takeshi Tanaka, Atsushi Hirano, Muneaki Hase*

1P-3 ☆ Mechanical properties and morphology of polypropylene/ethylene-1-butene copolymer rubber/CNT composites 47
** Yoshimi Muraoka, Kenzo Fukumori*

1P-4 ☆ Understanding the Effect of Sulfur on the Synthesis of Carbon Nanotubes 48
** Rei Nakagawa, Michiko Edo, Hisashi Sugime, Suguru Noda*

1P-5 ☆ Evaluation of various nitrogen-doping in graphene on the performance as a supercapacitor electrode 49
** Rohit Yadav, Prerna Joshi, Masanori Hara, Masamichi Yoshimura*

1P-6 ☆ Gene expression analysis of macrophages on carbon nanohorn coated titanium 50
** Sadahito Kimura, Eri Hirata, Sari Takada, Masatoshi Sakairi, Masako Yudasaka, Atsuro Yokoyama*

1P-7 ☆ Unidirectional bright exciton transport in a $WS_{2x}Se_{(2-2x)}$ alloy monolayer 51
** Masafumi Shimasaki, Taishi Nishihara, Naoki Wada, Zheng Liu, Kana Kojima, Keisuke Shinokita, Kazunari Matsuda, Yasumitsu Miyata, Yuhei Miyauchi*

Properties of nanotubes 【CREST】

1P-8 Electronic structures of bundles of molybdenum disulfide nanotubes 52
** Kaoru Hisama, Mina Maruyama, Susumu Okada, Shohei Chiashi, Shigeo Maruyama*

1P-9 Rayleigh scattering measurement of suspended SWCNTs coaxially wrapped with BNNTs 53
** Satoshi Yotsumoto, Hayato Arai, Yongjia Zheng, Taiki Inoue, Rong Xiang, Shigeo Maruyama, Shohei Chiashi*

1P-10 Optical properties of inorganic nanotubes with different diameters 54
** Yohei Yomogida, Yasumitsu Miyata, Kazuhiro Yanagi*

1P-11 Chemical vapor deposition of one-dimensional heterostructures 55
** Yongjia Zheng, Yang Qian, Ming Liu, Akinito Kumamoto, Yuichi Ikuhara, Esko I. Kauppinen, Shohei Chiashi, Taiki Inoue, Rong Xiang, Shigeo Maruyama*

1P-12 Synthesis and Raman scattering spectroscopy of gas-flow oriented single-walled carbon nanotubes on hexagonal boron-nitride 56
** Shu Sato, Satoshi Yotsumoto, Masanori Bamba, Taiki Inoue, Shigeo Maruyama, Shohei Chiashi*

1P-13 In-Plane Thermal Conductance of Thin Films Composed of Coaxially Combined Single-Walled Carbon Nanotubes and Boron Nitride Nanotubes 57
** Pengyingkai Wang, Yongjia Zheng, Taiki Inoue, Rong Xiang, Ahmed Shawky, Makoto Watanabe, Anton Anisimov, Esko I. Kauppinen, Shohei Chiashi, Shigeo Maruyama*

Applications of nanotubes 【CREST】

1P-14 Fabrication of ribbon-like films with highly oriented carbon nanotubes using a robotic dispenser 58
** Manish Pandey, Ryo Abe, Naofumi Okamoto, Yuki Sekimoto, Masakazu Nakamura*

Chemistry of fullerenes

1P-15 Phosphorescence of polyynes: A key probe for the detection of a new series of laser ablated polyyne derivatives 59
** Tomonari Wakabayashi, Nozomu Kitamura, Ayato Osawa, Daiki Okada, Hal Suzuki, Yusuke Morisawa, Miho Hatanaka*

1P-16 CuCl-Mediated Reaction of C_{60} with Propargylic Phosphate 60
** Asumi Ishitsuka, Yutaka Maeda, Michio Yamada*

Applications of fullerenes

1P-17 Catalytic activity for the reduction of 4-nitrophenol using on gadolinium oxide nanoparticle-[C_{60}]fullerene nanowhisker composites 61
** Jeong Won Ko, Sugyeong Jeon, Weon Bae Ko*

Endohedral metallofullerenes

1P-18 Reactions of S-Heterocyclic Carbenes with Fullerenes: Preparation and Characterization of Dithiomethano-derivatives 62
** Yuta Maeda, Shinji Kanzawa, Masahiro Kako, Michio Yamada, Yutaka Maeda, Makoto Furukawa, Takeshi Akasaka*

Applications of nanotubes

1P-19 Research of Fracture Behavior of CNT/HDPE Composites *via* Melt Blending 63
** Koichi Utsugi, Nao Otsuki, Masaru Sekido*

Formation and purification of nanotubes

1P-20 Preferential stability of carbon nanotubes with sub-nm diameter under linearly polarized laser irradiation: An *ab initio* TDDFT study 64
** Yoshiyuki Miyamoto*

1P-21 Synthesis of carbon nanotubes on nanozirconia-dispersed carbon paper 65
** Dai Goudo, Nobutomo Yamaguchi, Kiyofumi Yamagiwa*

Graphene synthesis

1P-22 Scalable Synthesis of Atomically Precise Graphene Nanoribbons in Metal-Organic Framework 66
** Takashi Kitao, Michael MacLean, Kazuki Nakata, Takashi Uemura*

1P-23 Direct precipitation growth of multi-layer graphene using W capping layer -Dependence of growth atmosphere- 67
** Jumpei Yamada, Yuki Ueda, Takahiro Maruyama, Shigeya Naritsuka*

Applications of graphene

1P-24 NO_x adsorption dynamics on Nanographene assembly system 68
** Yurina Hikage, Satomi Nishijima, Kazuyuki Takai*

1P-25 Correlation between chemical structure and catalytic activity of graphene oxide 69
** Ryutaro Suzuki, Takuya Isaka, Kentaro Tajima, Kana Nakahara, Yoshiaki Matsuo, Nobuyuki Akai, Kazuyuki Takai*

Properties of graphene

1P-26 Investigation of surface potential variations of thermally reduced graphene oxide 70
** K. Kanishka H. De Silva, Shuhei Ogawa, Pamarti Vishwanath, Masamichi Yoshimura*

1P-27 Adsorption effects of molecular Hydrogen on the electronic transport properties of Graphene 71
** Yudai Shigehisa, Yoshinori Obata, Yasushi Ishiguro, Kazuyuki Takai*

Atomic Layers

1P-28 Multi-ferroic response of two-dimensional hexagonal materials 72
** Fenda Rizky Pratama, M. Shoufie Ukhtary, Riichiro Saito*

1P-29 Carrier-dependent photoluminescence properties of CVD-grown monolayer MoS_2 73
** Kana Kojima, Hong En Lim, Yusuke Nakanishi, Takahiko Endo, Yutaka Maniwa, Yasumitsu Miyata*

Carbon nanoparticles

1P-30 Self-Assembly of Nanodiamonds through Soft Gel from their Solutions 74
** Toshihiko Tanaka, Yasuhiro F. Miura, Tetsuya Aoyama, Masaya Nemoto, Shusuke Ando, Yuho Itabashi, Kazunori Miyamoto, Atsuya Muranaka, Masanobu Uchiyama, Eiji Osawa*

Other topics

1P-31 Chemically synthesized ground state diatomic carbon (C_2) serves as an origin of carbon allotropes 75
** Kazunori Miyamoto, Shodai Narita, Yui Masumoto, Takahiro Hashishin, Taisei Osawa, Mutsumi Kimura, Masahito Ochiai, Masanobu Uchiyama*

March 15th, Sun.

>>>>>>> Lunch Time (12:15-13:30) <<<<<<<

Poster Session (13:30-15:15)
During 13:30-14:00, please give priority to selection of candidates for Young Scientist Poster Award

Special Lecture (15:15-15:45)

1S-1 Emergent phenomena at van der Waals interfaces 1
** Masaki Nakano*

General Lecture (15:45-16:30)
Graphene synthesis ・ Atomic Layers ・ Properties of graphene

1-7 Fabrication of graphene nanoribbon homojunction for transport gap control 23
** Noritada Ogura, Toshiro Kaneko, Toshiaki Kato*

1-8 Electrical monitoring of methane oxidation reaction using monolayered films of transition-metal oxide nanosheets 24
** Ryo Nouchi, Yoshiaki Ishihara, Wataru Sugimoto*

1-9 Mechanical properties of 2D materials, scaling from monolayer to macroscale 25
** Dai-Ming Tang, Xin Zhou, Fengchun Hsia, Yoshio Bando, Dmitri Golberg*

Special Lecture (16:30-17:00)

1S-2 High resolution electron micrographs of serial brain tissue sections on conductive carbon nanotube coated PET tape and neural microcircuit analysis 2
** Yoshiyuki Kubota*

General Lecture (17:00-18:00)
Endohedral nanotubes ・ Endohedral metallofullerenes ・ Other topics

1-10 Long Linear Carbon Chains inside CNT Formed by Electric Discharge of a SWCNT film 26
** Yahachi Saito, Koji Asaka, Toshiyuki Ishida*

1-11 Plasma Implantation of Lithium-Ion into Inner Space of C_{70}: Synthesis and Characterization of Lithium-Ion-Encapsulated C_{70} ($Li^{+}@C_{70}$) 27
** Hiroshi Ueno, Kazuhiko Kawachi, Daiki Kitabatake, Keijiro Ohshimo, Hiroshi Okada, Eunsang Kwon, Shinobu Aoyagi, Yasuhiko Kasama, Fuminori Misaizu*

1-12 The Cage Dependence of Single Molecule Magnet Properties of Dy-dimetallofullerene Anions 28
** Ryoya Takai, Ryuji Higashinaka, Yuji Aoki, Koichi Kikuchi, Yohji Achiba, Takeshi Kodama*

1-13 Development of Mobility, Charge and Optical Measurement System for Nanomaterials 29
* *Toshiki Sugai, Fumiaki Uchiyama, Yuya Ooishi, Reona Miyamoto, Ryo Sasaki, Takanori Nakayasu, Kanata Oguri, Tomoya Ono*

>>>>>>> Coffee Break（18:00-18:15）<<<<<<<

Tutorial（18:15-19:45）

Fundamental and application of optical physics in nano-carbon and atomically thin materials
* *Kazunari Matsuda*

March 16th, Mon.

Special Lecture: 25min (Presentation) + 5min (Discussion)
General Lecture: 10min (Presentation) + 5min (Discussion)
Poster Preview: 1min (Presentation)

Special Lecture （ 9:00–9:30 ）【CREST】

2S–1 High power factor, completely organic thermoelectric nanocomposites enabled by carbon nanoparticles 3
** Jaime C. Grunlan*

General Lecture （ 9:30–10:15 ）【CREST】
Properties of nanotubes ・ Atomic Layers 【CREST】

2–1 One dimensional characteristics in thermoelectric properties of semiconducting single walled carbon nanotubes 30
*Yota Ichinose, Kan Ueji, Yohei Yomogida, * Kazuhiro Yanagi*

2–2 Synthesis of Boron Nitride Nanotubes and MoS_2@BNNTs Heteronanotubes 31
** Ming Liu, Yongjia Zheng, Yang Qian, Rong Xiang, Taiki Inoue, Shohei Chiashi, Esko I. Kauppinen, Shigeo Maruyama*

2–3 Influence of interlayer stacking on gate-induced carrier accumulation in a van der Waals heterostructure comprising MoS_2 and WS_2 32
** Mina Maruyama, Susumu Okada*

>>>>>>> Coffee Break （ 10:15–10:30 ）<<<<<<<

Special Lecture （ 10:30–11:00 ）

2S–2 Active site of nitrogen-doped carbon catalysts for fuel cell 4
** Junji Nakamura*

General Lecture （ 11:00–11:30 ）
Atomic Layers ・ Applications of graphene

2–4 First-principles electronic-structure study of stabilities and electronic properties of trilayer h-BN 33
** Taishi Haga, Yuuto Matsuura, Yoshitaka Fujimoto, Susumu Saito*

2–5 Molecular modification of graphene/Au electrode for controlled proton permeability 34
** Tomohiro Fukushima, Takaha Komai, Hidetaka Hasebe, Kei Murakoshi*

Poster Preview （ 11:30–12:15 ）（☆）Candidates for the Young Scientist Poster Award Candidates for the Young Scientist Poster Award

2P–1 Simple and Effective Method to Control Photoluminescence Properties of Single-walled Carbon Nanotubes by Ultrasonic Irradiation 76
☆ ** Yui Konno, Akane Nishino, Michio Yamada, Yutaka Maeda, Saki Okudaira, Yuhei Miyauchi, Kazunari Matsuda, Jun Matsui, Masaya Mitsuishi, Mitsuaki Suzuki*

2P-2 ☆ Stable MoO_3 Doping of Carbon Nanotube Top Electrodes for Highly Efficient Metal-Electrode-Free Perovskite Solar Cells 77
** Seungju Seo, Il Jeon, Esko I. Kauppinen, Yutaka Matsuo, Shigeo Maruyama*

2P-3 ☆ Macrocyclic bis(dipyrrinato) metal complex for single-walled carbon nanotube separation 78
** Guoqing Cheng, Naoki Komatsu*

2P-4 ☆ Influence of the carbon-rich domain in hexagonal boron nitride on transport properties of adjacent graphene 79
** Momoko Onodera, Kenji Watanabe, Miyako Isayama, Satoru Masubuchi, Rai Moriya, Takashi Taniguchi, Tomoki Machida*

2P-5 ☆ Dielectric screening effects on photoluminescence of carbon nanotubes on hexagonal boron nitride 80
** Nan Fang, Keigo Otsuka, Takashi Taniguchi, Kenji Watanabe, Kosuke Nagashio, Yuichiro Kato*

2P-6 ☆ Synthesis of 3D hybrid Structures composed of Single-walled CNTs and Mesopores Carbon by Chemical Vapor Deposition 81
** Aliza Khaniya Sharma, Kamal P Sharma, Takahiro Saida, Shigeya Naritsuka, Takahiro Maruyama*

2P-7 ☆ Theoretical Design of Thermoelectric Performance of Carbon Nanotube Thin Films based on Electrical and Thermal Circuit Network Analysis 82
** Junei Kobayashi, Kotaro Fujisaki, Takahiro Yamamoto*

Properties of nanotubes 【CREST】

2P-8 Evaluation of Thermal Transport in a Single-walled Carbon Nanotube Film by Ionic-liquid Gating 83
** Kan Ueji, Yuya Matsuoka, Takashi Yagi, Kengo Fukuhara, Yota Ichinose, Akari Yoshida, Yohei Yomogida, Kazuhiro Yanagi*

2P-9 Thermal stability of single-chirality-enriched carbon nanotube thin films 84
** Akira Takakura, Taishi Nishihara, Kazunari Matsuda, Takeshi Tanaka, Hiromichi Kataura, Yuhei Miyauchi*

2P-10 Relationships between Seebeck coefficient and Conduction Directions in Aligned Semiconducting Single-wall Carbon Nanotube Films 85
** Kengo Fukuhara, Yota Ichinose, Kanako Horiuchi, Akari Yoshida, Yohei Yomogida, Weilu Gao, Natsumi Komatsu, Junichiro Kono, Kazuhiro Yanagi*

Applications of nanotubes 【CREST】

2P-11 Macroscopic four probe thermal and thermoelectric measurement of carbon nanotube fibers 86
*Akito Sato, Kento Adachi, * Takashi Kodama*

Applications of graphene 【CREST】

2P-12 Bubble induced damage on graphene liquid cells during TEM observation 87
** Sota Hirokawa, Hideaki Teshima, Pablo S. Fernandez, Hiroki Ago, Yoko Tomo, Qin-Yi Li, Koji Takahashi*

Properties of graphene 【CREST】

2P-13 Strain-Induced Enhancement of Thermoelectric Power Factor of Graphene 88
** Kohei Suzuki, Kenji Sasaoka, Takahiro Yamamoto*

2P-14 Spin-Filter Effect of Zigzag Graphene Nanoribbons with Egde Defects 89
** Naoya Abe, Kenji Sasaoka, Takahiro Yamamoto*

Atomic Layers 【CREST】

2P-15 Anomalous electroluminescence from WS_2/WSe_2 in-plane heterostructures 90
** Naoki Wada, Jiang Pu, Tomoyuki Yamada, Wenjin Zhang, Zheng Liu, Yusuke Nakanishi, Yutaka Maniwa, Kazunari Matsuda, Yuhei Miyauchi, Taishi Takenobu, Yasumitsu Miyata*

Chemistry of fullerenes

2P-16 Absolute and relative intensity of the C_{60} IR absorption 91
** Tomonari Wakabayashi, Takamasa Momose, Mario E. Fajardo*

2P-17 A one-step direct oxidation of alkoxy to ketone: oxidation of alkoxy indano[60]fullerenes to [60]fullerene-fused ketones *via* weak copper oxidant 92
** Yue Ma, Hao-Sheng Lin, Yun Yu, Shigeo Maruyama, Il Jeon, Yutaka Matsuo*

Endohedral metallofullerenes

2P-18 ESR study of La and Y hetero-dimetallofullerene anions 93
** Moeno Maejima, Koichi Kikuchi, Yohji Achiba, Takeshi Kodama*

2P-19 ESR Study of two isomers of $[Sc_2C_{80}]^-$: $[Sc_2C_{80}(1)]^-$ and $[Sc_2C_{80}(2)]^-$ 94
** Shun Yoshida, Ko Furukawa, Koichi Kikuchi, Yohji Achiba, Takeshi Kodama*

Properties of nanotubes

2P-20 Doped-site structure dependent energy shifts of photoluminescence from locally functionalized single-walled carbon nanotubes in organic solvent environments 95
** Tomohiro Shiraki, Yoshiaki Niidome, Tsuyohiko Fujigaya*

Applications of nanotubes

2P-21 Electrical detection of X-ray by using coplanar CNT thin-film electrodes on PEN substrate 96
** Hiroyuki Matsuda, Satoru Suzuki, Takahiro Ishikawa, Teruaki Konishi, Tsuyoshi Hamano, Yutaka Ohno, Toshio Hirao, Satoshi Ishii*

Formation and purification of nanotubes

2P-22 Understanding and controlling the pyrolysis of C_3H_8 for uniform synthesis of vertically-aligned single-wall carbon nanotubes 97
** MengJu Yang, Pengfei Chen, Rei Nakagawa, Hisashi Sugime, Hitoshi Mazaki, Suguru Noda*

2P-23 Synthesis of boron nitride nanotube by chemical vapor deposition using new boron source 98
** Tetsuro Sawada, Hiromu Takahashi, Tomohiro Sei, Mayu Asaka, Toshio Osawa, Hisashi Sugime, Suguru Noda*

2P-24 Sublimation property of a flavin compound which is a surfactant for carbon nanotube dispersion 99
** Yuichi Kato, Kazufumi Kobashi, Takeo Yamada, Kenji Hata*

2P-25 CVD synthesis of sub-nanometer diameter single-walled CNTs 100
** Kamal Prasad Sharma, Daiki Yamamoto, Aliza Khaniya Sharma, Takahiro Maruyama*

Graphene synthesis

2P-26 Study of CVD growth mechanism of graphene on a-plane sapphire 101
** Yuki Ueda, Jumpei Yamada, Takahiro Maruyama, Shigeya Naritsuka*

Applications of graphene

2P-27 Heteroatom-doped Nanocarbons as Active Support for IrO_2 as an OER Electrocatalyst 102
** Prerna Joshi, Rohit Yadav, Masanori Hara, Masamichi Yoshimura*

Carbon nanoparticles

2P-28 Interactions of Nanodiamonds #1: with Ions in their Solutions 103
** Masaya Nemoto, Shusuke Ando, Yuho Itabashi, Toshihiko Tanaka, Yasuhiro F. Miura, Tetsuya Aoyama, Atsuya Muranaka, Masanobu Uchiyama, Eiji Osawa*

2P-29 Interactions of Nanodiamonds #2: with Dye Ions in their Solutions 104
** Yuho Itabashi, Shusuke Ando, Masaya Nemoto, Toshihiko Tanaka, Yasuhiro F. Miura, Tetsuya Aoyama, Atsuya Muranaka, Masanobu Uchiyama, Eiji Osawa*

March 16th, Mon.

Bio

2P-30 Detection of odor molecules by transistor-type graphene biosensor 105
** Chishu Homma, Hironaga Noguchi, Atsunobu Isobayashi, Yoshiaki Sugizaki, Yuhei Hayamizu*

>>>>>>> Lunch Time (12:15-13:30) <<<<<<<

Poster Session (13:30-15:15)
During 13:30-14:00, please give priority to selection of candidates for Young Scientist Poster Award

Awards Ceremony (15:15-16:00)

The 50th Anniversary of the Prediction of Aromatic Stability of C_{60}
Commemorative Session (16:00-17:15)

2C-1 The beginning of nano-carbon era －Prediction and discovery of C_{60}－ 11
** Yohji Achiba*

2C-2 C_{60} as a carbon cluster 12
** Susumu Saito*

2C-3 TEM Observations of Carbon: Amorphous, Fullerenes and Carbon nanotubes 13
** Sumio Iijima*

Celebration Messages
** Tomonari Wakabayashi*

>>>>>>> Coffee Break (17:15-17:30) <<<<<<<

The 50th Anniversary of the Prediction of Aromatic Stability of C_{60}
Commemorative Session (17:30-18:45)

2C-4 The 50 years of a soccer-ball molecule C_{60} 14
** Eiji Osawa*

2C-5 Unveiling the origin of cosmic fullerenes through investigations into physical properties of fullerene-containing planetary nebulae 15
** Masaaki Otsuka, F. Kemper, J. Cami, E. Peeters, Fullerene PN consortium*

2C-6 Curved nanocarbon molecules from concise and versatile synthesis 16
** Hiroyuki Isobe*

March 17th, Tue.

Special Lecture: 25min (Presentation) + 5min (Discussion)
General Lecture: 10min (Presentation) + 5min (Discussion)
Poster Preview: 1min (Presentation)

Special Lecture （ 9:00–9:30 ）【CREST】

3S–1 Gating IR in Textiles 5
** YuHuang Wang*

General Lecture （ 9:30–10:15 ）【CREST】
Applications of nanotubes ・ Formation and purification of nanotubes 【CREST】

3–1 Carbon nanotube-based excitonic wavelength-selective absorber and emitter for solar thermal energy harvesting 35
** Yuhei Miyauchi, Taishi Nishihara, Akira Takakura, Kazunari Matsuda, Takeshi Tanaka, Hiromichi Kataura*

3–2 Machine-learned 100 %-yield carbon nanotube dissolution in arbitrary organic solvents 36
** Yoshiyuki Nonoguchi, Tomoyuki Miyao, Chigusa Goto, Tomoko Murayama, Kimito Funatsu, Tsuyoshi Kawai*

3–3 Multiscale hydrophobic interactions between gel, SWCNTs, and surfactants: detailed discussions 37
*Guowei Wang, Takeshi Tanaka, * Hiromichi Kataura*

>>>>>>> Coffee Break （ 10:15–10:30 ）<<<<<<<

Special Lecture （ 10:30–11:00 ）

3S–2 Selective growth of single walled carbon nanotubes : thermodynamics versus kinetics 6
** Christophe Bichara*

General Lecture （ 11:00–11:30 ）
Other topics ・ Properties of nanotubes

3–4 Enhanced intrinsic photovoltaic effect in tungsten disulfide nanotubes 38
** Yijin Zhang, Toshiya Ideue, Masaru Onga, Feng Qin, Ryuji Suzuki, Alla Zak, Reshef Tenne, Jurgen Smet, Yoshihiro Iwasa*

3–5 Radiative quantum efficiency of bright excitons in carbon nanotubes 39
** Hidenori Machiya, Akihiro Ishii, Yuichiro K. Kato*

Poster Preview （ 11:30–12:15 ）（☆）Candidates for the Young Scientist Poster Award
Candidates for the Young Scientist Poster Award

3P–1 ☆ Highly Selective and Scalable Fullerene-Cation-Mediated Synthesis acessing Cyclo[60]fullerenes with 5-Membered-Carbon-Ring and their Application to Perovskite Solar Cells 106
** Hao-Sheng Lin, IL Jeon, Shigeo Maruyama, Yutaka Matsuo*

3P-2 ☆ Flattening of 2D materials encapsulated by hBN flakes 107
** Takato Hotta, Akihiro Ueda, Shohei Higuchi, Keiji Ueno, Kenji Watanabe, Takashi Taniguchi, Ryo Kitaura*

3P-3 ☆ Development of Chemical CNH Fishhok for Analyzing Peptide and Its Assemblies by SMART-EM 108
** Takayuki Nakamuro, Keyi Sun, Jeffery W. Bode, Koji Harano, Eiichi Nakamura*

3P-4 ☆ Electrical properties of periodically modified graphene 109
** Yuta Taguchi, Susumu Saito*

3P-5 ☆ In-plane heterostructure of MoS_2 polytypes 110
** Ruben Canton Vitoria, Ryo Kitaura*

3P-6 ☆ Ultra fast growth of monolayer WS_2 measured by in-situ monitoring 111
** Tomoya Kameyama, Toshiro Kaneko, Toshiaki Kato*

3P-7 ☆ Isotope Labelling Analysis of Additive Gas Effects on Single-Walled Carbon Nanotube Growth 112
** Bunsho Koyano, Shun Yamamoto, Akari Kobayashi, Ryoya Ishimaru, Keigo Otsuka, Taiki Inoue, Rong Xiang, Shohei Chiashi, Shigeo Maruyama*

Properties of nanotubes 【CREST】

3P-8 Electronic property of CNT thin film under external electric field 113
** Yanlin Gao, Susumu Okada*

3P-9 Hall Effect and weak-localization conduction in aligned metallic single-walled carbon nanotube thin films 114
** Kanako Horiuchi, Ryotaro Okada, Hideki Kawai, Yohei Yomogida, Natsumi Komatsu, Weilu Gao, Junichiro Kono, Kazuhiro Yanagi*

Properties of graphene 【CREST】

3P-10 Influence of interlayer stacking arrangements on carrier accumulation in bilayer graphene field effect transistors 115
** Susumu Okada, Yanlin Gao, Mina Maruyama*

3P-11 Study on effects of twist on phonon transport in graphene nanoribbons 116
** Yukihiko Terada, Takuma Shiga*

Bio 【CREST】

3P-12 Iron ion-mediated oxidation of coenzyme NADH by carbon nanotubes 117
** Atsushi Hirano, Momoyo Wada, Takeshi Tanaka, Hiromichi Kataura*

Other topics 【CREST】

3P-13 Hexagonal boron nitride nanosheets for ultrafast membrane filtration 118
** Rasel Das, Pablo Solís-Fernández, Hiroki Ago*

3P-14 Mechanical and electronic properties of copolymers of centrohexaquinane and cyclooctatetraene 119
** Yasumaru Fujii, Mina Maruyama, Susumu Okada*

Endohedral metallofullerenes

3P-15 Single molecule magnet properties of Tb-dimetallofullerene anions: $[Tb_2@C_{80}(I_h)]^-$ and $[Tb_2@C_{78}(D_{3h})]^-$ 120
** Kazuki Yamagishi, Ryuji Higashinaka, Yuji Aoki, Koichi Kikuchi, Yohji Achiba, Takeshi Kodama*

3P-16 Attempt to produce Sm-dimetallofullerenes 121
** Naoya Fujita, Koichi Kikuchi, Yohji Achiba, Takeshi Kodama*

Environmental/Safety characterization of nanomaterials

3P-17 In vivo evaluation of biodistribution, toxicity and clearance of single wall carbon nanotubes depending on the dispersants 122
** Ying Xu, Minfang Zhang, Mei Yang, Masako Yudasaka, Toshiya Okazaki*

Applications of nanotubes

3P-18 Importance of structural parameters of CNTs for the Pt electrochemical durability in CNT based Pt electrocatalysts in PEMFCs 123
** Don Terrence Dhammika Weerathunga, Tsuyohiko Fujigaya*

3P-19 A semitransparent terahertz imager made from chemically doped semiconducting carbon nanotube thin films 124
** Kanae Oi, Kou Li, Daichi Suzuki, Tsuyoshi Kawai, Yukio Kawano, Yoshiyuki Nonoguchi*

3P-20 Compact Wearable Foot Pressure Sensors from MWCNT Coated Cotton Fibers for Human Activity and Sporting Performance Monitoring 125
** Md. Abdul Momin, Mohammad Jellur Rahman, Tetsu Mieno*

Formation and purification of nanotubes

3P-21 Activation of Alkane for CVD Growth of Single-Wall Carbon Nanotubes 126
** Pengfei Chen, Mengju Yang, Rei Nakagawa, Hisashi Sugime, Hitoshi Mazaki, Suguru Noda*

3P-22 Synthesis of aligned carbon nanotube arrays on quartz wool and its morphological characterization 127
** Nobutomo Yamaguchi, Dai Goudo, Kiyofumi Yamagiwa*

3P-23 Separate control of catalyst and source gases in synthesis of boron nitride nanotubes by chemical vapor deposition 128
* *Hiromu Takahashi, Tetsuro Sawada, Tomohiro Sei, Mayu Asaka, Toshio Osawa, Hisashi Sugime, Suguru Noda*

3P-24 Selective dispersion of semiconducting single-walled carbon nanotubes by using alkyl cellulose 129
* *Tomoko Yagi, Tsuyoshi Kawai, Yoshiyuki Nonoguchi*

Nanowires

3P-25 Scaling laws on enhancement of the electric field inside a hollow cylinder 130
* *Yuan Tian, Muhammad Shoufie Ukhtary, Riichiro Saito*

Applications of graphene

3P-26 Photoluminescence of Graphene Oxide Enhanced by UV-radiation in Dioxane 131
* *Katsuki Kanazawa, Masahito Sano*

3P-27 Effects of interactions at the interface between graphene and quantum dots on their electronic properties 132
* *Zen Inoue, Yasushi Ishiguro, Alexader Baranov, Igor Nabiev, Kazuyuki Takai*

Atomic Layers

3P-28 First-principles calculation of exciton of transition metal dichalcogenide 133
* *Pang Xiaoqi, Nguyen T. Hung, Riichiro Saito*

3P-29 Theoretic Study on Raman Active Modes of SnS Thin Films 134
* *Itsuki Yonemori, Sudipta Dutta, Kosuke Nagashio, Katsunori Wakabayashi*

3P-30 Molecular adsorption effects on the electrical conduction of MoS_2 on surface-modified substrates 135
* *Yuki Minakawa, Taichi Umehara, Kazuyuki Takai*

Other topics

3P-31 Thermal conductivity of low-cost thermoelectric Mg_3Bi_2 136
* *Nguyen T. Hung, Riichiro Saito*

>>>>>>> Lunch Time （12:15-13:30）<<<<<<<

Poster Session （13:30-15:15）

During 13:30-14:00, please give priority to selection of candidates for Young Scientist Poster Award

Special Lecture （15:15-15:45）

3S-3 *In situ* Study of Catalysts for Single-Walled Carbon Nanotube Growth 7
* *Yan Li, Feng Yang*

General Lecture （ 15:45–16:15 ）
Properties of nanotubes ・ Nanohorns

3–6 Vapor-Phase Functionalization of Air-Suspended Single-Walled Carbon Nanotubes Using an Aryl-Halide 40
** Daichi Kozawa, Xiaojian Wu, Akihiro Ishii, Jacob Fortner, Keigo Otsuka, Rong Xiang, Taiki Inoue, Shigeo Maruyama, YuHuang Wang, Yuichiro K. Kato*

3–7 Atomistic Structural Analysis of Reaction Intermediates Captured on Functionalized Carbon Nanohorns 41
** Koji Harano, Junfei Xing, Luca Schweighauser, Satoshi Okada, Eiichi Nakamura*

Special Lecture （ 16:15–16:45 ）

3S–4 Nanoscale optical and vibrational spectroscopy of low-dimensional materials in electron microscope 8
** Ryosuke Senga, Kazu Suenaga, Thomas Pichler*

General Lecture （ 16:45–17:30 ）
Atomic Layers

3–8 Independent degrees of freedom in two-dimensional materials 42
** Sake Wang, F. R. Pratama, M. Shoufie Ukhtary, Riichiro Saito*

3–9 Optical Properties of Monolayer Transition Metal Dichalcogenides on GaN Surface Depending on their Polarity 43
** Shinichiro Mouri, Yuma Komichi, Keisuke Shinokita, Kazunari Matsuda, Tsutomu Araki*

3–10 Anomalous polarized Raman spectra of TaP 44
** Riichiro Saito, Pang Xiaoqi, Wang Tong, Nguyen Hung*

特別講演
Special Lecture

1 S – 1 ～ 1 S – 2
2 S – 1 ～ 2 S – 2
3 S – 1 ～ 3 S – 4

Emergent phenomena at van der Waals interfaces

○Masaki Nakano[1,2]

[1] *QPEC and Department of Applied Physics, The University of Tokyo, Tokyo 113-8656, Japan*
[2] *RIKEN Center for Emergent Matter Science (CEMS), Wako 351-0198, Japan*

Since the discovery of graphene, a family of layered materials with nanometer-scale thickness called '2D materials' and their integrated superstructures named 'van der Waals (vdW) heterostructures' have become an invaluable material platform for condensed-matter research, providing intriguing properties and functionalities that are missing in their 3D bulk counterparts. There, the most-frequently-used sample fabrication method has been 'top-down' mechanical exfoliation combined with the pick-up and transfer methods, while 'bottom-up' molecular-beam epitaxy (MBE) should provide a complementary and unique approach in 2D materials research. Successful examples are the application of MBE-grown monolayer films to spectroscopic studies like ARPES and STM/STS measurements that require large-area monolayer films, unveiling fundamental aspects of a variety of 2D materials emerging at the monolayer limit. From materials science viewpoint, however, one of the biggest advantages of the MBE-based approach apart from large-area synthesis should be that we can design and create novel material systems that could not be achieved by simple exfoliation based on bulk crystals, although such attempts are almost missing in this rising research field.

We have recently established a versatile route to layer-by-layer epitaxial growth of a wide variety of 2D materials on insulating substrates by MBE [1], opening a door for exploration of emergent transport phenomena arising with reducing thickness [2-6] even based on hardly-cleavable [2, 3] and/or thermodynamically-metastable [5, 6] compounds as well as at the interface between dissimilar materials [7, 8]. In this presentation, we will introduce our recent achievements in particular on the emergent transport phenomena at the vdW interfaces. The first topic is for the vdW heterostructures composed of insulating 2D materials [7], where we found emergent electrical conduction despite that the individual materials are highly insulating, which could be simply understood by taking into account the band alignment at the interface and the relevant interface charge transfer. The second topic is for the vdW heterostructures made of metallic 2D material and itinerant 2D ferromagnet [8], where we found significant modulation of the magnetic properties including the magnetic anisotropy as well as the transition temperature, which could be naturally understood by considering a new-type of magnetic proximity effect mediated by Zeeman-type spin-orbit interaction.

[1] M. Nakano *et al*., Nano Lett. **17**, 5595 (2017).
[2] Y. Wang *et al*., Appl. Phys. Lett. **113**, 073101 (2018).
[3] M. Nakano *et al*., Nano Lett. **19**, 8806 (2019).
[4] H. Matsuoka *et al*., *submitted*.
[5] Y. Tanaka *et al*., *submitted*.
[6] S. Yoshida *et al*., *submitted*.
[7] Y. Kashiwabara *et al*., Adv. Funct. Mater. **29**, 1900354 (2019).
[8] H. Matsuoka *et al*., *submitted*.

Corresponding Author: M. Nakano
Tel: +81-3-5841-6871, Fax: +81-3-5841-6822, E-mail: nakano@ap.t.u-tokyo.ac.jp

High resolution electron micrographs of serial brain tissue sections on conductive carbon nanotube coated PET tape and neural microcircuit analysis

○Yoshiyuki Kubota[1,2]

[1] Division of Cerebral Circuitry, National Institute for Physiological Sciences, *Okazaki 444-8787, Japan*

[2] Department of Physiological Sciences, SOKENDAI, *Okazaki 444-8787, Japan*

The electron microscopy (EM)-based reconstruction of neuronal circuits from serial ultrathin sections has attracted considerable recent attention, despite the emergence of super resolution microscopy, because EM is a reliable method for the diverse-scale analysis of dense nanoscale details in biological structures. Here, we focus on the automated tape-collecting ultramicrotome (ATUM) method which allows the collection of many serial ultrathin sections of consistent quality quickly and automatically by producing ultrathin sections on a tape that can be repeatedly imaged using SEM. Currently, the most commonly used tape for ATUM is carbon coated (cc)-Kapton tape (polyimide film, DuPont, Wilmington, USA), but it has deficiencies due to a relatively high sheet resistance (19-6530 Mohm/sq), non-uniform carbon coating that causes mottled surface resistance, and scratching. Moreover, there is no assurance of a regular supply of high-quality cc-Kapton tape due to inconsistent industrial production procedures. Therefore, an improved alternative tape would have a valuable role the field of ATUM-based EM. In this study, we address these issues by introducing an improved tape and tissue staining protocol. We screened candidates and found that plasma-hydrophilized-carbon nanotube (CNT) tape is optimal due to its extremely high surface conductivity (240-500 ohm/sq) and low endogenous signal, and it can provide high quality images of tissue sections with SEM. The ATUM-SEM method impressively alters current research strategy using an electron microscope on functional architecture of the brain microcircuit.

[1] Kubota Y et al., Front. Neural Circuits, fncir.2018.00098 (2018)
[2]窪田芳之，電子顕微鏡を使った革新的脳組織解析法―コネクトーム研究；実験医学増刊「脳神経回路と高次脳機能 スクラップ＆ビルドによる心の発達と脳疾患の謎を解く」（榎本和生，岡部繁男編集）羊土社、東京、p158-16 ISBN 978-4-7581-0372-5 (2018)
[3] Kubota Y et al., Nature Communications, **9**, 437 (2018)

Corresponding Author: Y. Kubota
Tel: +81-564-59-5282, Fax: +81-564-59-5284,
E-mail: yoshiy@nips.ac.jp

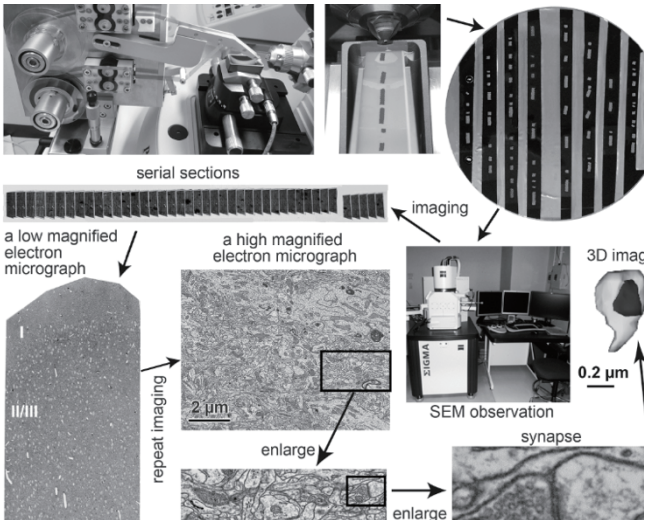

Figure 1　Pipeline of the ATUM-SEM method

High power factor, completely organic thermoelectric nanocomposites enabled by carbon nanoparticles

○Jaime C. Grunlan [1,2,3]

[1] *Department of Mechanical Engineering, Texas A&M University, USA*
[2] *Department of Materials Science and Engineering, Texas A&M University, USA*
[3] *Department of Chemistry, Texas A&M University, USA*

In an effort to create a paintable/printable thermoelectric material, comprised exclusively of organic components, polyaniline (PANi), graphene, and double-walled carbon nanotubes (DWNT) were alternately deposited from aqueous solutions using the layer-by-layer assembly technique. Graphene and DWNT are stabilized with an intrinsically conductive polymer, poly(3,4-ethylenedioxythiophene): poly(styrene sulfonate) (PEDOT:PSS). A 1 μm thick film, composed of 80 PANi/graphene-PEDOT:PSS/PANi/DWNT-PEDOT:PSS quadlayers (QL) exhibits electrical conductivity (σ) of 1.88 x 10^5 S/m and a Seebeck coefficient (S) of 120 μV/K, producing a thermoelectric power factor ($S^2 \cdot \sigma$) of 2710 μW/(m·K^2) [1]. This is the highest value ever reported for a completely organic material measured at room temperature. Furthermore, this performance matches or exceeds that of commercial bismuth telluride. These outstanding properties are attributed to the highly ordered structure in the multilayer assembly. The thermoelectric power output increased with the number of cycles deposited, yielding 8.5 nW at 80 QL for ΔT = 5.6 K. A simple thermoelectric generator was prepared with selectively-patterned, fabric-based system. The electric voltage generated by each TE device increased in a linear relationship with both ΔT and the number of TE legs, producing ~ 5 mV with just five legs and a ΔT of 9.7 K, as shown in Figure 1. By stabilizing, nanotubes and graphene with nitrogen-rich molecules, n-type multilayer thin films with relatively high power factor have also been produced [2]. This unique TE coating system is water-based and uses only organic components. For the first time, there is a real opportunity to harness waste heat from unconventional sources, such as body heat to power devices in an environmentally-benign way.

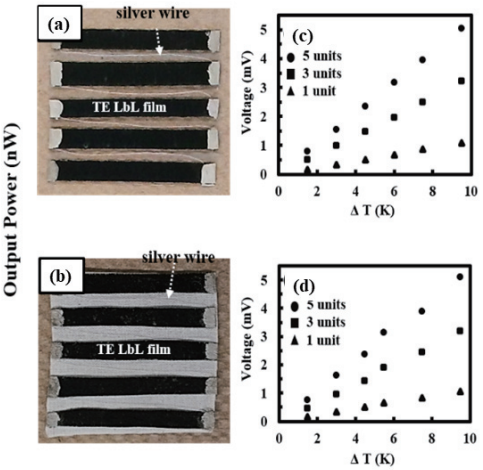

Fig.1 (a) and (b) are images of the patterned and fabric-based 80 QL thermoelectric generator modules connected with silver ink and wires. (c) and (d) are TE voltage generated by the patterned PET film and fabric-based devices as a function of ΔT [1].

[1] J. Grunlan *et al*. Adv. Energy Mater. **6**, 1502168 (2016).
[2] J. Grunlan *et al*. Nano Energy **28**, 426 (2016).

Corresponding Author: J. Grunlan
Tel: +1-979-845-3027, Fax: +1-979-845-3081,
E-mail: jgrunlan@tamu.edu

Active site of nitrogen-doped carbon catalysts for fuel cell

○Junji Nakamura[1]

[1] *Faculty of Pure and Applied Sciences, Tsukuba Research Center for Energy Materials Science (TREMS), University of Tsukuba. 1-1-1 Tennodai, Tsukbua 305-8573, Ibaraki, Japan*

Nitrogen-doped graphitic carbons as non-Pt catalysts for oxygen reduction reaction (ORR) have been paid much attention in recent years because commercialization of fuel cells requires less expensive and abundant catalytic materials. Identification of the active site of nitrogen-doped carbon materials for ORR is thus urgently required, but still under debate. Currently, the debate focuses on whether the active site is created by pyridinic N (N bonded to two carbon atoms) or graphitic N (N bonded to three carbon atoms, also called substituted N or quaternary N). To determine the active site conclusively, we prepared model catalysts of highly oriented pyrolytic graphite (HOPG) with pyridinic N (pyri-HOPG) or graphitic N (grap-HOPG). The active sites and adsorption properties were examined by ORR and post-ORR X-ray photoelectron spectroscopy (XPS). We have thus determined the active nitrogen species in carbon [1,2]. The graphitic-N doping was performed by mild bombardment with a nitrogen ion beam. To prepare the pyri-HOPG samples, edge patterning was first performed by bombarding the sample with an Ar^+ ion beam through a slit-patterned Ni mask as shown in Fig.1 A-D. The edged HOPG samples were then exposed to NH_3 at 973 K. The catalytic performances of the model catalysts were measured by cyclic voltammetry (CV) in acidic electrolyte (0.1 M H_2SO_4). It was found that the pyri- HOPG model catalyst shows high activity at high voltages, compared to the very low ORR activities of the N-free model catalysts (Fig.1 E, F). Since the pyri-HOPG sample is nearly free of graphitic N, the ORR results indicate that it is pyridinic N rather than the graphitic N that reduces the ORR overpotential and creates the active site. It is thus concluded that the ORR active sites in nitrogen-doped carbon materials are created by pyridinic N.

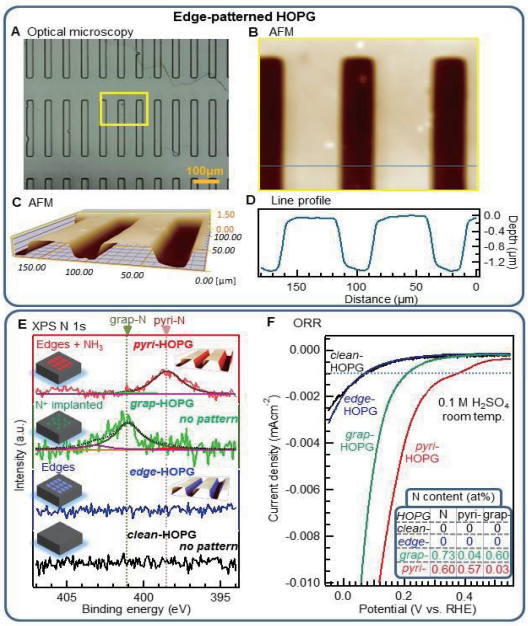

Figure.1 Structural and elemental characterization of four types of N-HOPG model catalysts and their ORR performance. (A) Optical image of patterned edge-N^+-HOPG. (B) The AFM image obtained from the region indicated by the yellow rectangle in (A). (C) 3D representation of (B). (D) Line profile of the AFM image obtained along the blue line in (B). (E) N 1s XPS spectra of model catalysts. (F) ORR results for model catalysts corresponding to (E). Nitrogen contents of the model catalysts are shown as inset in (F).

[1] D. Guo, R. Shibuya, C. Akiba, S. Saji, T. Kondo, J. Nakamura, Science, **351**, 361 (2016).
[2] S. K. Singh, K. Takeyasu, J. Nakamura, Advanced Materials, 1804297 (2018).

Gating IR in Textiles

YuHuang Wang [1]

[1] *Department of Chemistry and Biochemistry, University of Maryland, 8051 Regents Drive, College Park, MD 20742, United States*

Our human body absorbs and loses heat largely through infrared radiation that peaks at around 10 μm. However, despite thousands of years' development, none of our clothing systems are capable of controlling this major heat exchange channel. The infrared properties of both clothing and our own skin are fixed at a nearly constant level, regardless of whether one feels hot or cold. In contrast, many species in nature have evolved elegant strategies to manipulate light for the purpose of cooling and surviving harsh environments. For instance, Saharan silver ants feature triangular shaped hairs that can reflect near-infrared rays according to the position of the sun to keep themselves cool, while the geckos of Madagascar have photonic skins with changeable colors that can blend in the environment to hide from predators. In this talk, I will discuss a clothing textile that is capable of dynamically gating infrared radiation through the fabric in response to personal thermal discomfort. We show that by simply coating triacetate-cellulose fibers with a thin layer of carbon nanotubes we can modulate the infrared radiation through the fabric by as much as 35% as a function of the relative humidity of skin. Both opportunities and challenges ahead will also be discussed if time permits.

[1] Zhang, X.; Yu, S.J.; Xu, B.B.; Li, M.; Peng, Z. W.; Wang, Y.; Deng, S.L.; Wu, X.J.; Wu, Z.P.; Ouyang, M.; Wang, Y. H. *Science 363*, 619-623 (2019).

[2] Xu, B.B.; Peng, Z.W.; Wu, Z.P.; Zhang, X.A.; Wang, Y. H. *Reviews of Scientific Instruments* 90, 113102 (2019).

Corresponding Author: Y. H. Wang
Tel: +1-301-405-3368
E-mail: yhw@umd.edu

Selective growth of single walled carbon nanotubes: thermodynamics versus kinetics

Christophe Bichara

Centre Interdisciplinaire de Nanoscience de Marseille - CINaM

CNRS and Aix-Marseille University, Marseille, France

In classical crystal growth, the interaction of the growing object with its support and the energies of the different facets determine the growth mode and the resulting crystalline structure. The synthesis of carbon nanotubes by chemical vapor deposition poses somewhat similar yet more complex issues. The catalytic particle is both a support and a reactive interface with the growing tube, and many properties are altered because of the nanometric size of the objects. With this in mind, we have identified different growth modes driven by the thermodynamic properties of the interface [1, 2] and developed a modeling of the interface [3], emphasizing the importance of the configurational entropy of the nanotube edge to stabilize chiral tubes and to account for the temperature dependence of tubes' helicity distributions.

We present here further developments of this very simple thermodynamic model, including more general interface structures and the corresponding evaluation of the entropy. We also use Monte Carlo simulations to analyze the growth mechanisms and related growth rates, to address the process kinetics in relation with the chiral selectivity of the synthesis.

References

[1] Fiawoo, M.-F. C. *et al.* Phys. Rev. Lett. **108,** 195503 (2012).

[2] He, M. *et al.* Nanoscale **10**, 6744, (2018)

[3] Magnin, Y. *et al.*, Science **362,** 212–215 (2018)

3S-3

In situ Study of Catalysts for Single-Walled Carbon Nanotube Growth

Feng Yang and Yan Li
College of Chemistry and Molecular Engineering, Peking University, Beijing 100871, China

Metallic Co and intermetallic compound Co_7W_6 are both catalysts for the growth of single-walled carbon nanotubes (SWCNTs) but have shown great difference in the chirality selectivity. We studied the composition and structure of Co and Co_7W_6 nanocrystals in methane, carbon monoxide, and hydrogen at the temperature of 700–1100 ^oC by using environmental aberration-corrected transmission electron microscopy in combination with *in situ* synchrotron X-ray absorption spectroscopy. we directly present the structural and composition evolution of cobalt catalysts during the nucleation and growth of SWCNTs under carbon feeding. In the case of Co nanoparticles, the co-existence of cobalt and cobalt carbide was generally observed among the catalysts which are active in nucleating tubes. It was found that the tubes grown from solid state Co nanoparticles always present smaller diameter than the catalysts and no structure-correlation between catalyst and nanotube was found. However, the structure and chemical composition of the Co_7W_6 nanocrystals were stable under the atmosphere of methane, carbon monoxide, and hydrogen at high temperature. The SWCNTs grown from Co_7W_6 nanocrystals also show smaller diameter than the catalysts. But the distribution of the tube diameters is discrete. The above observations reveal the difference in growth mechanism of the two types of catalysts.

Corresponding Author: Yan. Li
Tel & Fax: +86-10-6275-6773
E-mail: yanli@pku.edu.cn

Nanoscale optical and vibrational spectroscopy of low-dimensional materials in electron microscope

○Ryosuke Senga[1], Kazu Suenaga[1], Thomas Pichler[2]

[1] *Nanomaterial research institute, AIST, Tsukuba 305-8565, Japan*
[2] *Faculty of Physics, University of Vienna, Vienna, Austria*

Excitations of quasiparticles govern physical properties of low-dimensional materials. Especially their behaviors at non-perfect structures like boundaries, edges, defects or irregular stacking sequence are undoubtedly important to understand the performance of nanodevices consisting of nanomaterials. However, such local information has been usually averaged in conventional inelastic scattering techniques using x-ray, neutron and light sources because of their diffraction limit. Here we demonstrate the nanoscale optical and vibrational spectroscopy of 1D/2D materials by using a monochromatic electron source mounted in a scanning transmission electron microscope. Its energy resolution, better than 30 meV, allows to access the quasiparticle excitations (i.e. phonon, exciton and plasmon) of low-dimensional materials by electron energy-loss spectroscopy (EELS). The spatial and momentum resolutions balance each other and can be finely tuned with magnetic/electrostatic lenses. For instance, an atomically thin probe can be formed with an integration of large momentum space. This allows us to extract local information from single defects. Indeed, we have successfully measured the optical gap transitions from a defect of an individual semiconducting carbon nanotube [1,2]. In contrast, an electron probe with a higher momentum resolution can provide a full phonon dispersion of 2D materials (Fig. 1) such as hexagonal boron nitride or graphene at a few tens nanometer scale [3]. Thus, the propagation of each phonon mode at defects such as edges in graphene has been unambiguously visualized. This local spectroscopy with a large flexibility will open up a wide possibility to unravel the defect physics of quantum matters.

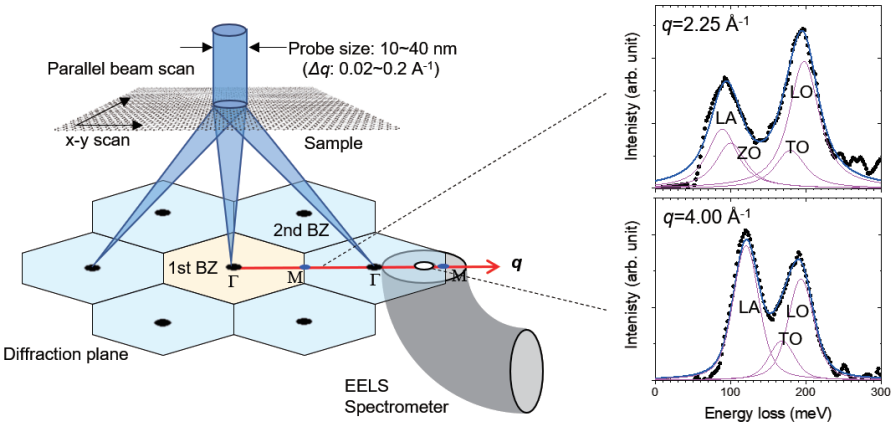

Fig. 1 Experimental setup for the momentum-resolved EELS and examples of momentum-resolved EEL spectra taken at q=2.25 and 4.00 Å^{-1} along the GMGM direction. The spectrometer entrance aperture is placed at a given position in the diffraction plane including the first, second, or third Brillouin zones.

[1] R. Senga, T. Pichler and K. Suenaga Nano Letters **16**, 3661 (2016).
[2] R. Senga *et al*., Nano Letters **18**, 3920 (2018).
[3] R. Senga *et al*., Nature **573**, 247 (2019)

Corresponding Author: R. Senga
Tel: +81-29-862-6518
E-mail: ryosuke-senga@aist.go.jp

招待講演
Invited Lecture

1 I – 1

FC-CVD synthesis of CNTs from methane for transparent conductor applications.

Qiang Zhang, Datta Sukanta, Hua Jiang, Esko I. Kauppinen

Department of Applied Physics, Aalto University School of Science, PO Box 15100, FI-00076 Aalto, Espoo, FINLAND

Due to scalability, low-cost and good control of carbon nanotube (CNT) synthesis, floating catalyst chemical vapor deposition (FC-CVD) keep attracting intense attention in both academic and industrial fields [1,2]. Especially, the CNT aerosol from FC-CVD can be directly deposited into transparent conducting films (TCFs) which are critical components of many optoelectronic devices that pervade modern technology [1]. Currently, one of the ideal models of high-performance CNT TCFs is the net-work containing long, straight, individual, high-quality single-wall CNTs (SWCNTs) [3]. Many efforts in FC-CVD have been devoted to increasing the conductivity of CNT TCFs based on this model. However, intrinsic nanotube collisions in the aerosol process of FC-CVD lead to a tread-off between yield and performance [3], because bundling increases when increasing the yield i.e. production rate, with the bundling increasing sheet resistance at the given film transmittance. Here, we report TCFs of large-diameter CNTs from methane-based FC-CVD overcoming the performance–yield tradeoff. Based on the Fe-C-S system, the double-wall CNTs (DWCNTs) with a mean diameter of 4.15 nm and a mean bundle length of 20 um have been produced into TCFs via FC-CVD. After gold chloride solution doping, the TCFs have an excellent performance of 42 ohm/sq sheet resistance at 90% transmittance. Unexpectedly, these high-performance DWCNTs films have an ultra-high yield i.e. production rate, being two orders of magnitude higher than that of SWCNT based TCFs with similar performance. Especially, these high-yield DWCNTs films contain ‘small’ bundles with around 50% of CNTs being individual, which is completely different from other FC-CVD results for SWCNTs produced at much lower yield. Moreover, the large-diameter DWCNTs will flatten at the junctions, which can provide a larger contact area between the tubes and reduce the contact resistance. These unique features of large-diameter CNTs in ‘small’ bundles are the key to obtain high-performance CNT TCFs with high yield. These results imply a new model with optimization windows for high-performance CNT TCFs with high yields and accordingly at reduced cost, and may accelerate the practical application of CNTs TCFs.

[1] Zhang, Qiang, et al. Topics in Current Chemistry, 99-128 (2019).

[2] Liao, Yongping, et al. Journal of the American Chemical Society 140.31 (2018).

[3] Mustonen, Kimmo, et al. Applied Physics Letters 107.14 (2015).

Corresponding Author: Esko I. Kauppinen
Tel: +358 40 509 8064 Fax: +358 9 2451 3517
E-mail: esko.kauppinen@aalto.fi

記念セッション
Commemorative Session

2 C – 1 ～ 2 C – 6

The beginning of nano-carbon era
— Prediction and discovery of C_{60}—

○Yohji Achiba

Department of Chemistry, Tokyo Metropolitan University, Tokyo 192-0397, Japan

Nano carbon materials so called “fullerenes” are closed-cage molecules containing only pentagonal and hexagonal rings, of which the celebrated icosahedral C_{60} molecule is the archetype. Although hollow-shell graphite molecules were mentioned in the scientific diversions column in 1966, the first article of the theoretical speculation on the possibility of a sixty-carbon framework based on the truncated icosahedron was published fifty years ago in 1970 by Osawa[1)] in the study of “superaromaticity”.

Like so many important scientific discoveries, experimental evidence of the predicted C_{60} structure suddenly appeared while alert individuals were looking for something else. In 1985, Kroto, Heath, O’Brien, Curl and Smalley were studying the formation of long-chain carbon molecules in circumstances analogous to interstellar space and stellar atmospheres. They observed that under certain conditions, clusters consisting of sixty carbon atoms were produced in unusual abundance. The truncated icosahedron C_{60} cage structure was proposed and then named “buckminsterfullerene”, because geodesic dome concepts had played an important part in the arriving at their solution.

An explosive of fullerene research occurred with the invention of techniques for the production and isolation of bulk quantities of fullerenes by Kraetschmer, Lamb, Fostiropoulos and Huffman in 1990. Since then, due to the relative simplicity of the sample preparation, many research groups have been able to bring tools and insights of their specialty to the study of fullerenes. The present talk is an attempt to bring a brief history of the discovery of C_{60} molecule by which so called nano-carbon era has certainly begun.

[1] E. Osawa, Kagaku (Kyoto) 25, 245 (1970)
[2] H. W. Kroto, J. R. Heath, S. C. O’Brien, R.F. Curl, and R. E. Smalley, Nature, 318, 162 (1985).
[3] W. Kraetschmer, LO. D. Lamb, K. Fostiropoulos, and D. R. Huffman, Nature, 347, 354 (1990).
Corresponding Author: Y. Achiba
Tel: +81-42-677-2534,
E-mail: achiba-yohji@tmu.ac.jp

C_{60} as a carbon cluster

○Susumu Saito[1-3]

[1] Department of Physics, Tokyo Institute of Technology,
2-12-1 Oh-okayama, Meguro-ku, Tokyo 152-8551, Japan
[2] Advanced Research Center for Nanoscience and Quantum Physics,
Tokyo Institute of Technology, 2-12-1 Oh-okayama, Meguro-ku, Tokyo 152-8551, Japan
[3]Materials Research Center for Element Strategy, Tokyo Institute of Technology,
4259 Nagatsuta-cho, Midori-ku, Yokohama, Kanagawa 226-8503, Japan

In 1980s, the field of “clusters”, the systems of finite number of atoms, emerged as one of new exciting research fields due to the development of experimental techniques to deal with clusters and to the advancement of first-principles electronic-structure theory, and Japanese researchers have played many important roles to further develop the field which is now called nanoscience and nanotechnology. I will review the history of cluster research field from the viewpoint of physics, and discuss the importance of the prediction of C_{60} by Professor Eiji Osawa in 1970 in this field.

Corresponding Author: S. Saito
E-mail: saito@stat.phys.titech.ac.jp

TEM Observations of Carbon: Amorphous, Fullerenes and Carbon nanotubes

Sumio Iijima

Meijo University, Graduate School of Science and Technology
University Professor of Nagoya University & NEC Senior Research Fellow

In early years of development of amorphous silicon for solar battery (1970s), there was a big dispute concerning what is the atomic structure of amorphous silicon.
Knowing this issue, I started to examine amorphous carbon films that have been familiar among electron microscopists.
During those studies I came across onion-like spheres of graphite (1980).
The TEM pictures of the onions were appreciated by Kroto & Smalley, discoverers of fullerene, because the picture supports their postulated C60 model (1987).
It was 8 years before they received Nobel prize.
In this way I was acquainted with them, and they persuaded me to work on fullerene, and soon later, fortunately I discovered carbon nanotubes (1991).
By the way, google citation of the Nature paper reached more than 50,000.

Corresponding Author: S. Iijima
Phone/Fax: +81-(0)52-834-4001,
E-mail: iijimas@meijo-u.ac.jp

The 50 years of a soccer-ball molecule C_{60}[†]

Eiji Osawa

Nanocarbon Research Institute Co., Ltd., Ueda, Nagano 386-8567, Japan

Interviewed by

Masaki Ozawa[1] and Tomonari Wakabayashi[2]

[1]*Department of Applied Chemistry, Meijo University, Nagoya 468-8502, Japan*
[2]*Department of Chemistry, Kindai University, Higashi-Osaka 577-8502, Japan*

In 1970, Eiji Osawa issued a prophetic idea for aromatic stability of a soccer-ball molecule, namely C_{60}, from a saucer-shaped hydrocarbon molecule, corannulene, as a building block [1]. Upon 50-years anniversary of his earliest record of the truncated icosahedral molecule (Fig. 1), we trace back the story from the original idea to the series of epoch-making events succeeding afterward: the discovery of the ultra-stable gas-phase carbon cluster, Buckminsterfullerene, in 1985 [2] and explosion of experimental as well as theoretical researches triggered by the preparation of macroscopic amounts of C_{60} as a new form of solid carbon in 1990 [3], eventually leading to the detection of C_{60} in space [4,5]. The story is more than most dramatic dramas, in which a vast number of researchers have been involved successfully or unsuccessfully.

Since 1991, The C_{60} Research Society, currently The Fullerenes, Nanotubes and Graphene (FNTG) Research Society, has been the most active interdisciplinary forum for exchange and collaboration of researchers from a wide variety of fields, *i.e.*, physics, chemistry, mathematics, astrophysics, biology, electrical and mechanical engineering, and materials science in particular. Professor Eiji Osawa had long been servicing as The First President of The Society during the period of 1991-2003. He is now Head of Nanocarbon Research Institute and pursuing a long-standing issue on the formation mechanism of C_{60} in natural environments including detonation diamonds and nanodiamonds.

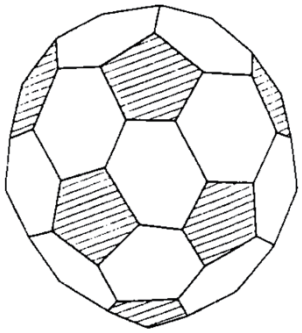

Fig. 1 A soccer-ball molecule in 1970 [1].

[1] E. Osawa, *Kagaku* **25**, 854 (1970); Z. Yoshida & E. Osawa, *Aromaticity*, Kagaku Dojin, p.p. 174-178 (1971).
[2] H. W. Kroto, J. R. Heath, S. C. O'Brien, R. F. Curl, and R. E. Smalley, *Nature* **318**, 162 (1985).
[3] W. Krätschmer, L. D. Lamb, K. Fostiropoulos, and D. R. Huffman, *Nature* **347**, 354 (1990).
[4] J. Cami, J. Bernard-Salas, E. Peeters, and S. E. Maleck, *Science* **329**, 1180 (2010).
[5] E. K. Campbell, M. Holz, D. Gerlich, and J. P. Maier, *Nature* **523**, 322 (2015).

[†]Topic in The Special Session, FNTG58, dedicated to Professor Eiji Osawa for his prediction of icosahedral C_{60}. Executive Committee Members: Tomonari Wakabayashi, Toshiki Sugai, Taishi Takenobu, and Susumu Okada. Advisory Panel: Susumu Saito. Reprint Production: Yutaka Matsuo is acknowledged for his efforts to realize kind offer by Kagaku Dojin of 300 copies with English translation of the original article in Japanese in 1970 [1].

Unveiling the origin of cosmic fullerenes through investigations into physical properties of fullerene-containing planetary nebulae

○M. Otsuka[1], F. Kemper[2], J. Cami[3,4], E. Peeters[3,4], and Fullerene PN consortium
[1]*Okayama Observatory, Kyoto University, 719-0232 Okayama, Japan*
[2]*European Southern Observatory, Karl-Schwarzschild-Str. 2, 85748 Garching b., München, Germany*
[3]*The University of Western Ontario, London, ON N6A 3K7, Canada*
[4]*SETI Institute, 189 Bernardo Ave, Suite 100, Mountain View, CA 94043, USA*

Since the prediction of the existence in 1970 [1] and their laboratory discoveries in 1985 [2], fullerenes have drawn considerable interest from astrochemists looking for them in circumstellar and interstellar conditions; because fullerenes are extremely stable and easily formed in laboratories on Earth, and therefore it had been thought that they should abundantly exist even in interstellar space. However, the first confirmed detection of cosmic fullerene C_{60} and C_{70} emission at mid-infrared wavelengths was only recently reported in the carbon-rich (i.e., the number density ratio of C/O $>$ 1) planetary nebula (PN) Tc1 [3] with mid-infrared space telescope *Spitzer* [4]. PNe are in the last evolutionary phase of Sun-like stars of the initial $1-8$ solar mass, and more than 3000 PNe have been found in the Milky Way galaxy, so far. After the detection report by [3], spectroscopic observations by *Spitzer* detected fullerenes in a variety of space environments. At the moment, PNe represent the largest fraction of fullerene detection; 24 fullerene-containing PNe have been identified in the Milky Way galaxy and the Magellanic Clouds [5-10, references therein]. Emission from planner graphene sheet C_{24} is potentially detected in some PNe [7]. Thus, the case of the detection has been increased, however, it remains unclear why these objects exhibit fullerene features and how fullerenes were formed in such evolved star environments. To answer these questions is directly related to understand the formation and evolution of large organic molecules in the solar system. Therefore, we have investigated physical properties of fullerene-containing objects, in particular, PNe based on multiwavelength data [8-10]. In this talk, we introduce our recent results and also discuss potential collaboration between astrophysicists and chemists towards understanding the origin of cosmic fullerenes.

[1] E. Osawa, Kagaku, 25, 854 (1970).
[2] H. W. Kroto et al. Nature, 318, 162 (1985).
[3] J. Cami et al. Science, 329, 1180 (2010).
[4] `http://www.spitzer.caltech.edu`
[5] J. Bernard-Salas et al. ApJ, 757, 41 (2012).
[6] D. A. García-Hernández et al. ApJ, 760, 107 (2012).
[7] D. A. García-Hernández et al. ApJ, 737, 30 (2011).
[8] M. Otsuka, MNRAS, 482, 4354 (2019).
[9] M. Otsuka et al. MNRAS, 462, 12 (2016).
[10] M. Otsuka et al. MNRAS, 437, 2577 (2014).

Corresponding Author: M. Otsuka
Tel: +81-865-47-0138, Fax: +81-865-47-0139,
E-mail: otsuka@kusastro.kyoto-u.ac.jp

Curved nanocarbon molecules from concise and versatile synthesis
簡便・汎用合成が生み出す湾曲ナノカーボン分子

Hiroyuki Isobe
Department of Chemistry, The University of Tokyo, Hongo, Tokyo 113-0033, Japan
JST ERATO Isobe Degenerate π-Integration Project, Hongo, Tokyo 113-0033, Japan

"A sphere made of sp^2-carbon atoms." This anomalous structure of [60]fullerene was a spark to ignited a new science of curved π-systems. A series of unique curved structures emerged from the planar trigonal structure of sp^2-carbon atoms, which revealed anomalous properties of the curved systems. Synthetically, the synthesis of curved π-molecules has been, and still is, a challenge for chemists. Introduction of a conceptually new "planar trigonal" structure with 1,3,5-trisubstituted benzene (named "phenine") opens up a new stream of curved π-design, and our explorations of the first series of "geodesic phenine molecules" will be presented at the symposium.

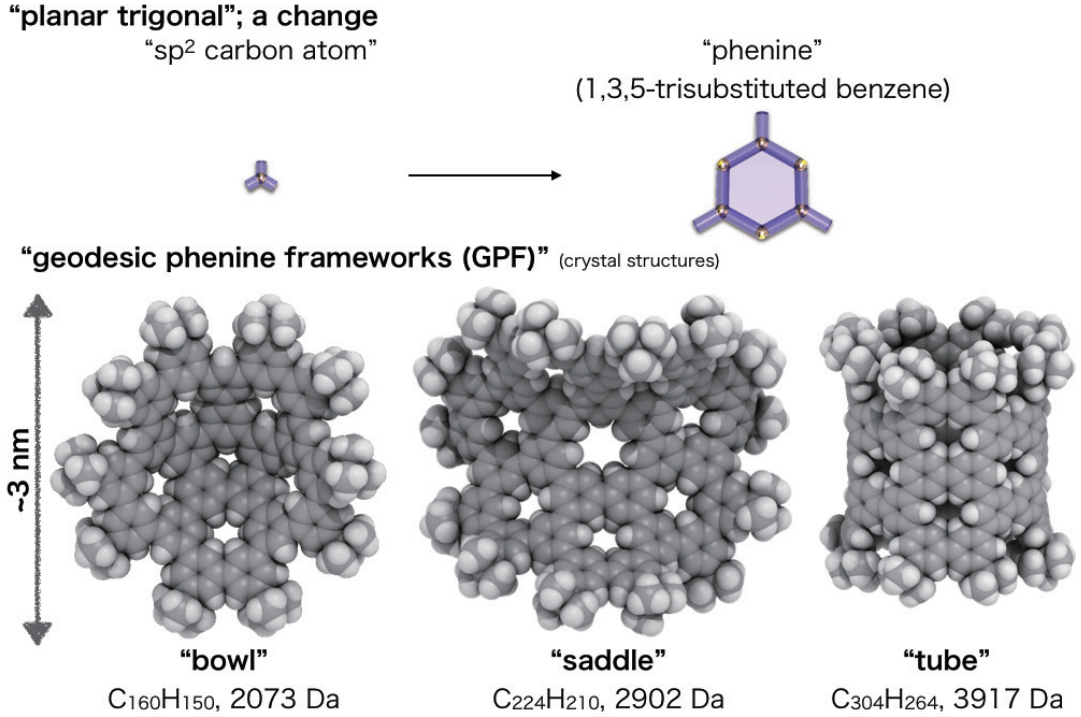

Fig. Geodesic phenine frameworks; the first series.

[1] Ikemoto, K.; Kobayashi, R.; Sato, S.; Isobe, H. *Angew. Chem. Int. Ed.* **2017**, *56* (23), 6511-6514. Ikemoto, K.; Kobayashi, R.; Sato, S.; Isobe, H. *Org. Lett.* **2017**, *19* (9), 2362-2365.
[2] Ikemoto, K.; Lin, J.; Kobayashi, R.; Sato, S.; Isobe, H. *Angew. Chem. Int. Ed.* **2018**, *57* (28), 8555-8559.
[3] Finite phenine nanotubes with periodic vacancy defects. Sun, Z.; Ikemoto, K.; Fukunaga, T.M.; Koretsune, T.; Arita, R.; Sato, S.; Isobe, H. *Science* **2019**, *363* (6423), 151-155. Sun, Z.; Mio, T.; Ikemoto, K.; Sato, S.; Isobe, H. *J. Org. Chem.* **2019**, *84* (6), 3500-3507.

Tel: +81-(0)3-5481-4777, Fax: +81-(0)3-5841-4162; Web: https://www.chem.s.u-tokyo.ac.jp/users/physorg/
E-mail: isobe@chem.s.u-tokyo.ac.jp

一般講演
General Lecture

1 – 1 ～ 1 – 13
2 – 1 ～ 2 – 5
3 – 1 ～ 3 – 10

One-pot Separation of Semiconducting Single-walled Carbon Nanotubes Based on Supramolecular Chemistry

Naotoshi Nakashima

International Institute for Carbon-Neutral Energy Research, Kyushu University, Fukuoka, Japan

The separation/purification of semiconducting single-walled carbon nanotubes (sem-SWNTs) with high quality is one of the most important issues in the science and technology of carbon nanotubes. In the meeting, I summarize our developed supramolecular chemistry-based one-pot separation of sem-SWMTs. The methods contain:

i) use of fluorene copolymers with a (n,m)chirality recognition moiety[1-7] and enantiomer recognition moiety [8]
ii) use of a supramolecular coordination polymer [9] : adsorbent removable system
iii) use of a hydrogen bonding supramolecular system [10] : adsorbent removable system
iv) use of assembled flavin molecules with thioalkyl substituents at 7- and 8 positions [11-14]: adsorbent removable system

References

[1] N. Nakashima et al., *Chem. Lett.*, 40, 239-241 (2011).
[2] N. Nakashima et al., *Chem. Lett*. **40**, 470-472 (2011).
[3] N. Nakashima et al., *Chem. Eur. J*. **17**, 13438-13444 (2011).
[4] N. Nakashima et al., *J. Am. Chem. Soc*., **133**, 14771–14777(2011).
[5] N. Nakashima et al., *Nanoscale*, **2014**, *6*, 5879–588.
[6] N. Nakashima et al., *Chem. Eur. J*., **2015**, *21*, 3359-3366.
[7] N. Nakashima et al., *Polymer Chem*. **2015**, 6, 5103-5109.
[8] N. Nakashima et al., *J. Am. Chem. Soc*. **2012**, *134*, 12700-12707.
[9] N. Nakashima et al., *Nature Communications*, **2014**, *5*, art no. 5041.
[10] N. Nakashima et al., *Scientific Reports*, **2015**, 5, art. no.18066.
[11] N. Nakashima et al., *Chem. Lett.* **2015**, 44, 566-567.
[12] N. Nakashima et al., *Bull. Chem. Soc. Jpn*. **2018**, *91*, 1646-1651.
[13] N. Nakashima et al., *Bull. Chem. Soc. Jpn*. **2019**, *92*, 1679-1683.
[14] N. Nakashima et al., submitted

Corresponding Author: N. Nakashima
Tel: +81-92-802-6745
E-mail: nakashima.naotoshi.614@m.kyushu-u.ac.jp

Fast synthesis of vertically aligned CNTs array exceeding one-centimeter height

○Shunsuke Sakurai, Takashi Tsuji, Maho Yamada, Kenji Hata, Don N. Futaba

CNT-Application Research Center, National Institute of Advanced Industrial Science and Technology (AIST), Tsukuba, Ibaraki 305-8565, Japan

Vertically aligned arrays of long carbon nanotube (CNT) have attracted much attention due to its potential for the application such as electrodes and actuators. Although many groups demonstrated the synthesis of millimeter-long CNT arrays [1], centimeter-long CNT array has been rarely reported. Cho *et al*. has reported record-long (21.7 mm) MWNT array by using Fe-Gd catalyst, instead of commonly used Fe catalyst, with maintaining catalyst lifetime up to 790 minutes [2]. In contrast, an advance of catalyst support material from a commonly used Al_2O_3 layer was rarely studied yet.

In this paper, a wide variety of double-layered catalyst support system, composed of a very thin (c.a. 1 nm) top layer (Al_2O_3 or MgO) deposited on a thick bottom layer (various metal oxides such as Al_2O_3, MgO, SiO_2, HfO_2, or ZrO_2) has been demonstrated to enhance catalyst lifetime and the resulting CNT array height. Especially, a specific combination of top/bottom layer, c.a. 2-3 nm as-sputtered Al_2O_3 top layer with >100 nm SiO_2 (thermally-grown from Si wafer) bottom layer, has been found to have an unexpected effect to enhance the initial growth rate of CNT array. As a result, a uniform CNT array exceeding 10 mm height was obtained after only 60 minutes growth (Fig.1). Our detailed study shows the importance of annealing procedure in prior to the supply of carbon feedstock to catalyst substrate.

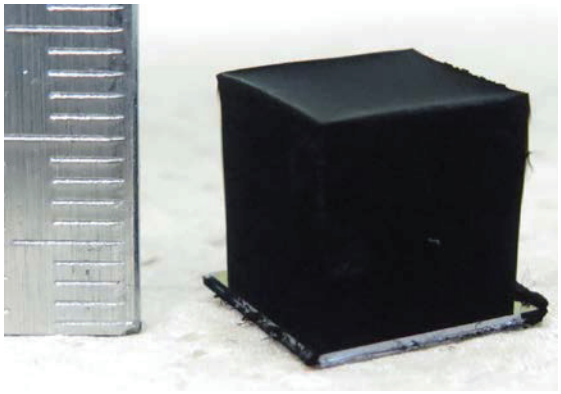

Fig.1 Photograph of CNT array exceeding 1 cm height.

[1] K. Hata, D. N. Futaba, K. Mizuno, T. Namai, M. Yumura, and S. Iijima, Science **306**, 1362 (2004).
[2] W. Cho, M. Schulz, and V. Shanov, Carbon **72**, 264 (2014).

Corresponding Author: S. Sakurai
Tel: +29-861-6205, Fax: +81-29-861-4851,
E-mail: shunsuke-sakurai@aist.go.jp

Luminescence of CNTs by luciferin/luciferase reaction from firefly

○Takeshi Tanaka, Mahoko Higuchi, Atsunori Hiratsuka, Hiromichi Kataura

Nanomaterials Research Institute, National Institute of Advanced Industrial Science and Technology (AIST), Tsukuba 305-8565, Japan

Near infrared (NIR) light emission from carbon nanotubes (CNTs) draws great attention to medical applications, such as bio-imaging, because NIR light shows high-transparency and low-scattering in biological tissues [1]. Although photoluminescence is widely used for the applications, there is a problem that visible excitation light cannot reach deep part of the tissues. In this study, we tried to utilize the luminescence reaction of firefly luciferase to excite CNTs and successfully obtained NIR luminescence derived from CNTs. Because the NIR luminescence of CNTs by luciferase does not need external excitation light, it could be powerful tool for bio-imaging at deep tissues.

The luminescence reaction catalyzed by firefly luciferase uses luciferin, ATP, and O_2 as substrates and produces luminescence at ~562 nm (Fig. 1, broken line). CoMoCAT-CNT (SG65) containing (6,5) CNTs as a major component was chosen to prepare aqueous dispersion, because the excitation (S_{22}) wavelength of (6,5) CNTs (~570 nm) matches the luminescence wavelength by luciferase reaction. Although the difference of the signal with or without CNTs was very small, we could detect the luminescence of CNT/luciferase system using IR camera. After optimization of the reaction condition, such as concentrations of substrates and luciferase, pH, CNTs, etc., luminescence spectrum of the reaction could be taken by a spectrophotometer (Fig. 2). The peak wavelength of the luminescence was consistent with that of photoluminescence of (6,5) CNTs (984 nm), indicating the luminescence of CNT/luciferase system is derived from (6,5) CNTs. Detailed results are given at the symposium.

This work was partly supported by KAKENHI No. 19H02539 and Suzuken Memorial Foundation.

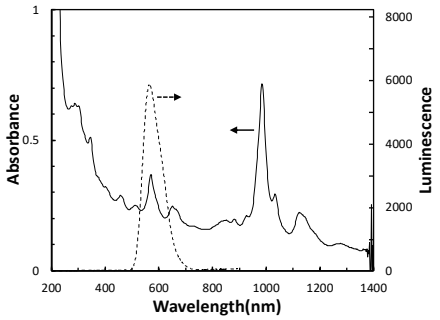

Fig. 1 Luminescence spectrum by luciferin/luciferase reaction from firefly (broken line) and absorption spectrum of CoMoCAT-CNT aqueous dispersion (solid line).

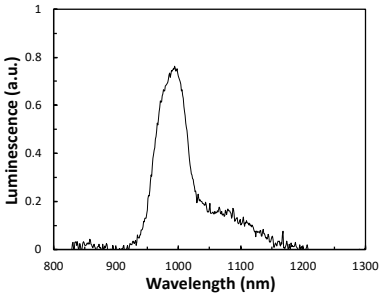

Fig. 2 Luminescence spectrum of (6,5) CNTs excited by luciferase reaction.

[1] Y. Yomogida *et al. Nat. Commun.* **7**, 12056 (2016).

Corresponding Author: T. Tanaka
Tel: +81-29-861-2903, Fax: +81-29-861-2786,
E-mail: tanaka-t@aist.go.jp

Selective Activation of Singlet/Triplet Reaction Paths Enabled by Carbon-nanotube-mediated Energy Attenuation

○Dongxin Liu[1], Dominik Lungerich[1], Satori Kowashi[1], Takayuki Nakamuro[1], Kaoru Yamanouchi[1], Koji Harano[1], Eiichi Nakamura[1]

[1] *Department of Chemistry, The University of Tokyo, Tokyo 113-0033, Japan*

In spite of its long history of application of an electron beam (e-beam) for a variety of chemical applications, e-beam has scarcely considered as an energy source for a precise control of molecular transformations. In this context, our group recently demonstrated [1] that [2 + 2] cyclization of C_{60} molecules (denoted as C_{60} dimerization) in carbon nanotubes (CNTs) can be controlled by e-beam. In the report, we performed single-molecule kinetics through video-imaging by transmission electron microscopy: we counted events of C_{60} dimerization one by one and provided rate constants based on observation of several tens of the events. In this work, we investigated the effects of e-beam with variable energy and found that CNTs attenuate the energy of e-beam and enable selective activation of singlet/triplet reaction paths of C_{60} dimerization.

Following the previous report [1], single-molecule kinetic study of C_{60} dimerization was conducted at 393-493 K with e-beam of 60-120 keV. With an e-beam of 60 keV, C_{60} dimerization did not take place. However, the dimerization took place with an e-beam of 80, 100 and 120 keV. We observed two activation energies (E_a), 13 kJ/mol at 80 keV and 34 kJ/mol at 100 and 120 keV, that are ascribed to two different excited states. Since the [2 + 2] dimerization is ground-state-forbidden, we assigned the path with the lower E_a at 80 keV to triplet (T_1), and the one with the higher E_a at 100 and 120 keV to singlet (S_1), following the order of e-beam energy. Because the energy of such electrons is over ten thousand times higher than that of the excited states of C_{60} molecule (1.6–2.0 eV), we suggest that the CNT container attenuates the energy of e-beam by the factor of 10^{-5}, and thus the energy given to the molecules becomes small enough to enable spin-state-selective electronic excitations.

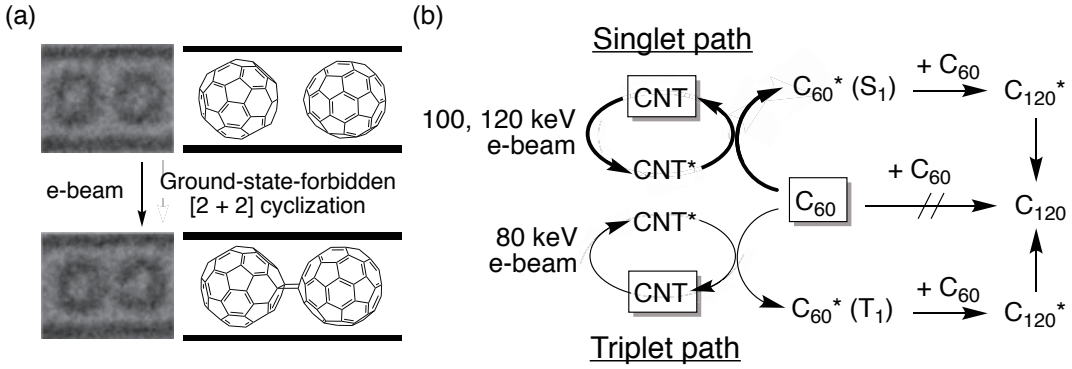

Fig.1 Selective activation of singlet/triplet reaction paths. (a) TEM images and schematic drawings of [2 + 2] cyclization of C_{60} molecules. (b) Processes of energy attenuation mediated by carbon nanotubes (CNTs).

[1] S. Okada *et al*. *J. Am. Chem. Soc.* **139**, 18281 (2017).

Corresponding Author: K. Harano and E. Nakamura
Tel: +81-3-5841-4369, Fax: +81-3-5841-4367,
E-mail: dongxin@chem.s.u-tokyo.ac.jp

Polyaromatic Anthracene Nano-tweezer on Semiconducting Carbon Nanotubes for Growth and Bridging of Perovskite Crystal Grains in Perovskite Solar Cells

○Hao-Sheng Lin [1], Shuhei Okawa,[1] Il Jeon [1], Yutaka Matsuo [1], Shigeo Maruyama [1]

[1] *Department of Mechanical Engineering, The University of Tokyo, Tokyo 113-8656, Japan*

Polyaromatic anthracene, which contains a bent polyaromatic group on one end and a functional group on the other end, has been reported to clench SWNTs. While the polyaromatic end induces strong π-π interaction with the SWNTs, the functional end can easily be modified chemically. In our group, the modified polyaromatic anthracenes were used as charge-transporting layers in optoelectronics, harnessing their bandgaps and high mobility arising from the conjugated sp^2 bonds. Hence, we designed and synthesized 4,6-di(anthracen-9-yl)-1,3-phenylene bis(dimethylcarbamate) (DPB), which is essentially polyaromatic anthracene with two urea-analogues functional groups. Subsequently, we used them as new surfactants for s-SWNTs in the PSC application. DPB successfully attached to s-SWNTs and replaced DOC surfactants as confirmed by photoluminescence (PL) and UV-visible absorption spectroscopy (UV-Vis). DPB-attached s-SWNTs showed much higher solubility in both DMF and dimethyl sulfoxide (DMSO) than the DOC-attached s-SWNTs. Accordingly, higher concentration of s-SWNTs could be added to the perovskite precursor solution. The DPB on SWNTs expectedly manifested a stronger interaction on Pb^{2+} than DOC owing to the strongly electron donating nature of the lone pair electrons on the carbamate group enhanced by its configurational orientation facing outwards. DPB-attached s-SWNT-added perovskite films exhibited excellent charge-selectivity and reduced charge trap density. The suitable molecular energy levels and higher mobility of DPB compared with DOC led to higher device performance. DPB-attached s-SWNTs-added PSCs exhibited a PCE of 20.7%, which is higher than those of DOC-attached s-SWNT-added PSCs (19.7%) and pristine PSCs (18.4%). All of the three photovoltaic parameters, namely, high short-circuit current density (J_{SC}), open-circuit voltage (V_{OC}), and filling factor (FF) contributed to the high power conversion efficiency (PCE) of the DPB-attached s-SWNTs-added PSCs. The high J_{SC} came from the large perovskite crystal size of over 500 nm. The high V_{OC} came from strong passivation effect of the DPB-attached s-SWNTs. The high FF came from the improved carrier mobility and charge selectivity of DPBs on s-SWNTs.

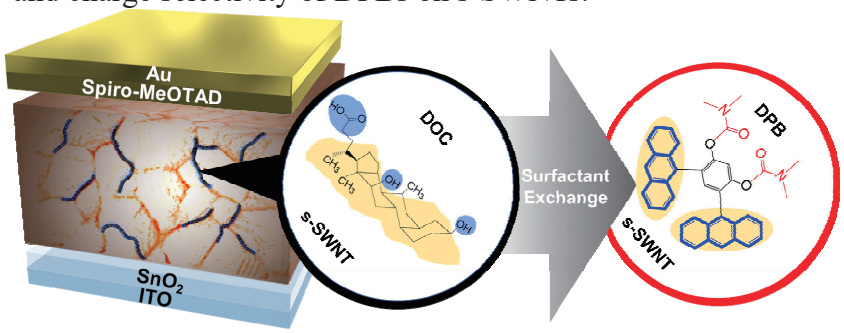

Corresponding Author: S. Maruyama
Tel: +81-3-5841-6408
E-mail: maruyama@photon.t.u-tokyo.ac.jp

Optimization of the Alignment Relay Technique for the Controlled Orientation and Selection of Single-Walled Carbon Nanotubes

○Monika Snowdon[1], Derek Schipper [1], Dai-Ming Tang [2]

[1] *Department of Chemistry, University of Waterloo, ON, N1G 2L9, Canada*
[2] *National Institute for Materials Science, Tsukuba 305-0044, Japan*

The semiconducting industry has grown immensely over the last 40 years, moving towards smaller and faster devices that correspond with the predictions of Moore's law. However, current technology cannot be tailored to progressively smaller dimensions without compromising functionality. Instead, advances in the manipulation of nanomaterials can resolve this challenge and provide information on the chemical-physical properties needed for higher-performance electronics at significantly smaller dimensions. Within these lines, one possibility is to replace silicon transistors with single-walled carbon nanotubes (SWNTs). [1] Nonetheless, there are a few problems that must be solved before SWNTs can be integrated into devices. The main difficulty is separation of the diverse kinds of SWNTs, as only certain tube conformations have the desirable semiconducting properties. [2] Additionally, SWNTs favor a random conformation when deposited onto a surface, which renders them ineffective; therefore, assembling them into tight alignment with one another is quite a complex challenge.[3] In this work, we portray the alignment relay technique (ART) for the simultaneous alignment and sorting of SWNTs toward transistor applications. The technique and methods for improving alignment will be discussed. and an example of the aligned molecules interacting with the SWNTs is schematically represented in Figure 1.

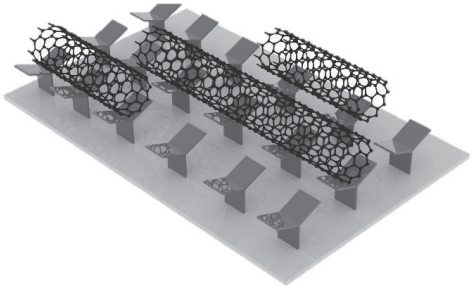

Fig.1 Schematic example of the alignment relay technique (ART) on controlling the orientation of single-walled carbon nanotubes (SWNTs).

[1] Baughman, R. H.; Zakhidov, A. A.; de Heer, W. A. Science. ***297***, 787-792 (2002).

[2] Cao, Q. *et al.* Science. ***350*****,** 68-72 (2015).

[3] Ieong, M.; Doris, B.; Kedzierski, J.; Rim, K.; Yang, M. Science. ***306***, 2057-2060 (2014).

Corresponding Author: D. Tang
Tel: +81-0-29-859-2000, Fax: +81-0-29-859-2029
E-mail: tang.daiming@nims.co.jp

Fabrication of graphene nanoribbon homojunction for transport gap control

○Noritada Ogura[1], Toshiro Kaneko[1], and Toshiaki Kato[1,2]

[1] *Graduate School of Engineering, Tohoku University, Sendai 980-8579, Japan*
[2] *JST-PRESTO*

Graphene nanoribbon (GNR), strips of two-dimensional (2D) graphene into one-dimensional (1D) structure, attracts intense attentions because of their novel electrical features. Although GNR can be synthesized by various methods, the reliable site and alignment control of GNR with high on/off current ratio remains a challenge. Our research group succeeded in fabricating suspended GNRs by an advanced plasma CVD process combining with unique nanobar structures as a catalyst [1-3]. Wafer scale integration of millions of suspended GNR can be also fabricated with our method [2]. Unfortunately, however, the on/off current ratio is still distributed in low level (~10) and further improvement of device performances are required for the practical use of our GNR devices.

In general, the formation of armchair edge structures with narrow width is required to open the bandgap in GNRs. This edge control in atomic level requires very high technical skills, which is difficult to realize in the wafer scale. It is theoretically predicted that the potential barrier can be naturally formed between GNRs junctions (homojunction GNR) independent of edge structures. However, the accuracy of this prediction and effects of junction angle have not been experimentally confirmed yet.

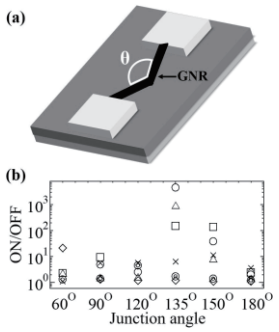

Fig.1 (a) Schematic illustration of GNR homojunction growth with plasma CVD from nanobar catalyst. (b) The distribution of on/off current ration of GNR homojunction transistor in various junction angles.

In this study, we attempted to fabricate GNR homojunction (Fig.1 (a)) with various junction angles and elucidate the correlation between junction structures and electrical properties of GNR devices. The GNR homojunctions with various junction angles were grown by designing the initial nanobar structures. Various nanobars including the contact angle from 60 to 180 º were drawn by a conventional electron-beam lithography technique. Based on this approaches, GNRs were found to be grown even from the junction structure of nanobar, indicating the GNR homojunction devices with various junction angle can be fabricated with our method. Then, on/off current ratio of GNR homojunction device was investigated as a function of junction angle. It is found that the relatively high on/off can be obtained at the specific junction angle around 135º (Fig.1 (b)). Although the critical mechanism for arising of this high on/off at specific junction angle is under investigations, this unique structures may contribute to opening a new direction for controlling the electrical properties of GNRs.

[1] T. Kato and R. Hatakeyama: Nature Nanotechnology, **7** (2012) 651.
[2] H. Suzuki, T. Kaneko, Y. Shibuta, M. Ohno, Y. Maekawa, and T. Kato: Nature Communications, **7** (2016) 11797.
[3] H. Suzuki, N. Ogura, T. Kaneko, and T. Kato: Scientific Reports **8** (2018) 11819.
Corresponding Author: N. Ogura, Tel: +81-22-795-7046, E-mail: noritada.ogura.p6@dc.tohoku.ac.jp

Electrical monitoring of methane oxidation reaction using monolayered films of transition-metal oxide nanosheets

○Ryo Nouchi[1,2], Yoshiaki Ishihara[1], Wataru Sugimoto[3]

[1] *Department of Physics and Electronics, Osaka Prefecture University, Sakai 599-8570, Japan*
[2] *PRESTO, Japan Science and Technology Agency, Kawaguchi 332-0012, Japan*
[3] *Research Initiative for Supra-Materials (RISM) and Faculty of Textile Science and Technology, Shinshu University, Ueda 386-8567, Japan*

A change in electrical resistance is a facile platform for monitoring chemical reactions. However, a reaction-induced change in resistance is usually masked by a high bulk conductivity of the sensing layer. Thus, an ultrathin sensing layer is desired to enhance the surface sensitivity. In addition, the sensitivity originates from reactivity and/or catalytic activity of the sensing layer towards a chemical reaction to be sensed. Therefore, an atomically thin material that possesses reactivity towards a target chemical reaction should be employed as the sensing layer to achieve electrical monitoring of the reaction.

Methane (CH_4) is the main component of natural gas such as shale gas and now regarded as an alternative carbon source to petroleum for producing useful chemicals. Oxidation (dehydrogenation) is the first step to produce the chemicals, but CH_4 possesses the most stable C–H bond among all hydrocarbons. Thus, a lot of efforts have been devoted to finding a material that enables facile dehydrogenation of CH_4. Recently, Weaver *et al*. reported that CH_4 undergoes dehydrogenation at low temperatures on a surface of iridium oxide single crystals [1].

In this study, the electrical monitoring of CH_4 oxidation is achieved by employing monolayered iridium oxide nanosheet films as an atomically thin sensing layer. The nanosheet films were fabricated on a SiO_2/Si substrate by the layer-by-layer method using a nanosheet suspension [2]. Two types of changes in electrical resistance were observed upon CH_4 exposure, depending on the thickness of the sensing layer: (1) a resistance decrease in a monolayered film due to (partial) reduction of the iridium oxide nanosheets (bulk resistivity: IrO_2 > Ir [3]) [Fig. 1(a)], and (2) a resistance increase in a thicker film due to increased surface scattering [4] upon adsorption of CH_4 and/or reaction products [Fig. 1(b)]. The observation of the resistance decrease with a monolayered film is a verification of the occurrence of the CH_4 oxidation reaction.

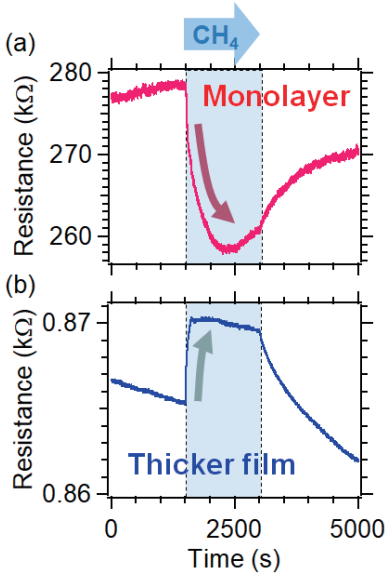

Fig. 1 Change in electrical resistance of (a) monolayered and (b) thicker films of IrO_2 nanosheets upon CH_4 exposure.

[1] Z. Liang, J. F. Weaver *et al*., Science **356**, 299 (2017).
[2] D. Takimoto, W. Sugimoto *et al*., Electrocatalysis **8**, 144 (2017).
[3] S.-W. Kim *et al*., J. Appl. Phys. **103**, 023517 (2008).
[4] R. Nouchi and I. Kanno, J. Appl. Phys. **97**, 103716 (2005).

Corresponding Author: R. Nouchi
Tel: +81-72-254-8394, Fax: +81-72-254-8394,
E-mail: r-nouchi@pe.osakafu-u.ac.jp

Mechanical properties of 2D materials, scaling from monolayer to macroscale

○ Dai-Ming Tang [1], Xin Zhou [1], Fengchun Hsia [1], Yoshio Bando [1], Dmitri Golberg [1]

[1] *World Premier International Center for Materials Nanoarchitectonics, National Institute for Materials Science, Namiki 1-1, Tsukuba, Ibaraki 305-0044, Japan*

It is essential to understand the mechanical properties of individual and assembled low-dimensional materials for their applications in nanoelectromechanical systems (NEMS), structural composite materials and some functional materials such as energy storage devices. In our research, in situ transmission electron microscopy (TEM) method is developed and applied to measure the mechanical properties of nanostructures and to directly correlate with the microstructures at multiple length scales. We developed a high-order resonance method to precisely evaluate the elastic properties of individual nanostructures with the error ~ 1%.[1-2] Plastic deformation was realized for individual carbon nanotubes by elongation under Joule heating, and metal-to-semiconductor transition was realized by modifying the chirality.[3]

In this talk, I will firstly discuss the bending behaviors of two dimensional (2D) atomic layers during nanomechanical cleavage,[4-5] which was the key process for discovering 2D materials. In situ observations combined with molecular dynamics simulations reveal layer-dependent mechanisms, from spontaneous rippling (~5 atomic layers) to homogeneous curving (~10 layers) and finally to kinking (20 or more layers). The second part will focus on the size effects on the mechanical properties of nanoporous graphene networks.[6] A strong size effect was revealed by in situ compression of micro- and nano-pillars inside electron microscopes. Both the modulus and strength are drastically increased as the specimen size reduces to ~100 nm, because of the reduced weak links in a small volume. Molecular dynamics simulations reveal the deformation mechanism involving slip-stick sliding, bending, buckling of graphene sheets, collapsing and densification of graphene cells.

[1] X. Zhou, D.-M. Tang, *et al.*, *Nano Lett* **19**, 4974 (2019).
[2] F.-C. Hsia, D.-M. Tang, *et al.*, *Nanoscale Advances*, 10.1039/C8NA00373D (2019).
[3] D.-M. Tang *et al.*, *Ultramicroscopy* **194**, 108 (2018).
[4] I. Nikiforov, D.-M. Tang, et al., *Phys Rev Lett* 109, 025504 (2012).
[5] D.-M. Tang *et al.*, *Nat Commun* **5**, 3631 (2014).
[6] D.-M. Tang *et al.*, *Adv Funct Mater* **0**, 1900311 (2019).

Corresponding Author: D.-M. Tang
Tel: +81-29-860-4949,
E-mail: Tang.Daiming@nims.go.jp

Long Linear Carbon Chains inside CNT Formed by Electric Discharge of a SWCNT film

○Yahachi Saito[1], Koji Asaka[2], Toshiyuki Ishida[3]

[1] *Toyota Physical and Chemical Research Institute, Nagakute-city 480-1192, Japan*
[2] *Department of Applied Physics, Nagoya University, Nagoya 464-8603, Japan*
[3] *ARS. Inc., Toyohashi 441-8031, Japan*

Carbyne, an infinite carbon chain, has attracted much interest and induced significant controversy for many decades. The presence of long linear carbon chains (LCCs) inside carbon nanotubes (CNTs) was substantiated in CNT produced by arc-discharge [1], by high-temperature annealing [2] and X-ray irradiation followed by thermal annealing [3] of a lump of CNTs. Last year, we found that long LCCs were encapsulated in CNTs on a film scale after field emission (FE) experiments of CNT films [4]. In the present report, an electric discharge that introduces damage to CNTs is shown to play a key role in the formation of LCC@CNT, and additional findings by Raman spectroscopy are presented.

Thick films of eDIPS CNT (Meijo Nano Carbon) were used for FE in vacuum and for a target of high-voltage electric discharge in atmosphere. Raman spectroscopy of the CNT films damaged after discharge was carried out with a range of excitation photon energies from 1.58 to 3.49 eV (Fig. 1). Raman bands at ~1850 cm^{-1} characteristic of LCCs were observed at excitation wavelengths from 488, 532, 633, and 671 nm. The strong resonant Raman scatterings at excitation photons (1.85 - 2.54 eV) indicate that the energy gaps of LCCs inside CNTs are distributed in this energy range. Transmission electron microscopy (TEM) revealed the presence of long LCCs within a channel of CNT (Fig. 2). Not only a single LCC but also two LCCs in parallel inside a CNT are found.

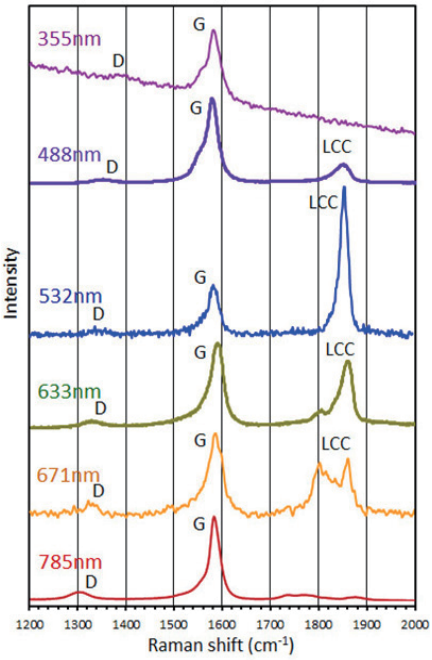

Fig. 1 Raman spectra.

Acknowledgement: Raman measurement with 671 nm excitation was conducted by Nanophoton Corp. Prof. T. Wakabayashi for valuable discussion and Prof. H. Ogata for measuring Raman spectra with 488 and 633 nm excitation are acknowledged. Thanks also to Meijo Nano Carbon Co. Ltd. for supplying SWCNT mats.

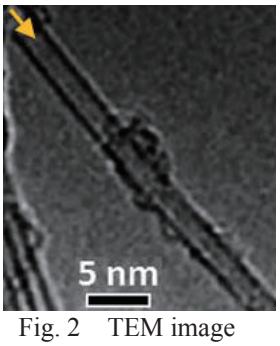

Fig. 2 TEM image

[1] X. Zhao et al, Phys. Rev. Lett. **90** (2003) 187401.
[2] L. Shi et al, Nature Mater. **15** (2016) 634.
[3] T. Murakami, et al., AIP Advances **6** (2016) 085303.
[4] S. Toma, K. Asaka, M. Irita, Y. Saito, Surf. Interface Anal. **51** (2019) 131.

Corresponding Author: Y. Saito
Tel: +81-561-57-9516, Fax: +81-561-63-6302, E-mail: ysaito@toyotariken.jp

Plasma Implantation of Lithium-Ion into Inner Space of C_{70}: Synthesis and Characterization of Lithium-Ion-Encapsulated C_{70} ($Li^+@C_{70}$)

○Hiroshi Ueno,[1,2] Kazuhiko Kawachi,[3] Daiki Kitabatake,[2] Keijiro Ohshimo,[2] Hiroshi Okada,[3] Eunsang Kwon,[4] Shinobu Aoyagi,[5] Yasuhiko Kasama,[3] Fuminori Misaizu[2,6]

[1] *The Frontier Research Institute for Interdisciplinary Sciences (FRIS), Tohoku University, Sendai 980-8578, Japan*
[2] *Department of Chemistry, Graduate School of Science, Tohoku University,*
[3] *Idea International Co. Ltd.*
[4] *Research and Analytical Center for Giant Molecules, Tohoku University*
[5] *Department of Information and Basic Science, Nagoya City University*
[6] *New Industry Creation Hatchery Center, Tohoku University*

Ion-implantation is one of the powerful tools to access endohedral metallofullerenes. Previously, we have reported an efficient implantation of lithium ion into C_{60} by using improved ion-implantation technique, so-called "plasma shower method".[1,2] This approach allowed us to achieve scalable synthesis of lithium-ion-encapsulated fullerene $Li^+@C_{60}$ X^-, a stable ionic form of lithium encapsulated fullerene consisting of Li^+ inside, neutral C_{60} cage and external counter anion X^-.[3] Despite the unique properties arising from their ionic natures, no other ionic metallofullerenes have been well studied so far.

In this work, mixed fullerene containing C_{60}, C_{70}, and several kinds of higher fullerenes was used as target of lithium plasma implantation.[4] Laser desorption ionization (LDI) mass spectrum of the crude product indicated the formation of $Li@C_{60}$, $Li@C_{70}$, $Li@C_{76}$, $Li@C_{78}$, and $Li@C_{84}$ (**Figure 1**). The products were purified according to previously developed oxidative purification process followed by electrolyte-added HPLC.[2] Till now, scalable amount of $Li^+@C_{70}$ has been successfully isolated as $TFSI^-$ (TFSI= bis(trifluoromethanesulfonyl)imide) salt. Details of the synthetic process along with basic properties of $Li^+@C_{70}$ salt will be discussed in the presentation.

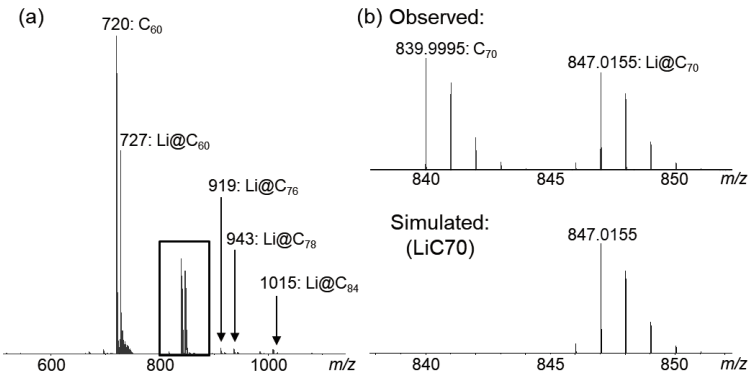

Figure 1. (a) Positive mode LDI-TOF mass spectrum of crude product. (b) Expanded view around m/z = 845. Simulated spectrum of $Li@C_{70}$ are also shown.

[1] Aoyagi, S. *et al.*, *Nature Chem.* **2010**, *2*, 678.
[2] Okada, H. *et al., RSC Adv*. **2012**, *2*, 10624.
[3] For the difference between $Li@C_{60}$ and $Li^+@C_{60}$, see Ueno, H. *et al.*, *Chem. Sci.* **2016**, *7*, 5770.
[4] Major component of the sample used was estimated by HPLC: C_{60} (ca. 60%) and C_{70} (ca. 20%).

Corresponding Author: H. Ueno
Tel: +81-22-795-7645, Fax: +81-22-795-6580, E-mail: hiroshi.ueno.d5@tohoku.ac.jp

The Cage Dependence of Single Molecule Magnet Properties of Dy-dimetallofullerene Anions

○Ryoya Takai[1], Ryuji Higashinaka[2], Yuji Aoki[2], Koichi Kikuchi[1], Yohji Achiba[1], Takeshi Kodama[1]

[1]*Department of Chemistry, Tokyo Metropolitan University, Tokyo 192-0397, Japan*
[2]*Department of Physics, Tokyo Metropolitan University, Tokyo 192-0397, Japan*

Since the discovery of single molecule magnet (SMM), SMM has been attracted large attention due to the expectation to application for high-density storage and quantum computer. In 2017, Liu et al. reported $Dy_2@C_{80}(I_h)CH_2Ph$ has over 3000 s of the relaxation time of magnetization at low temperature[1]. On the other hand, in 2019, Velkos et al. theoretically calculated the intra-cage electrostatic potentials for $C_{80}(I_h)$, $C_{80}(I_h)CH_2Ph$, and $C_{79}N$, and pointed out the different potentials would lead to the different SMM properties[2].

In the previous symposium[3], we reported the isolation of $[Dy_2@C_{78}(D_{3h})]^-$ and $[Dy_2@C_{80}(I_h)]^-$. In this work, to elucidate SMM properties of them, we measured M-T curve, M-H curve, and relaxation time (τ_m) of magnetization.

The τ_m vs $1/T$ plots for $[Dy_2@C_{78}(D_{3h})]^-$ and $[Dy_2@C_{80}(I_h)]^-$ are shown in Fig. 1. The fit function of τ_m is eq. (1). The first, the second, and the last terms represent quantum tunneling, Raman, and Orbach processes, respectively.

$$\tau_m^{-1} = \tau_{QTM}^{-1} + CT^n + \tau_0^{-1}\exp(-U_{eff}/T) \quad (1)$$

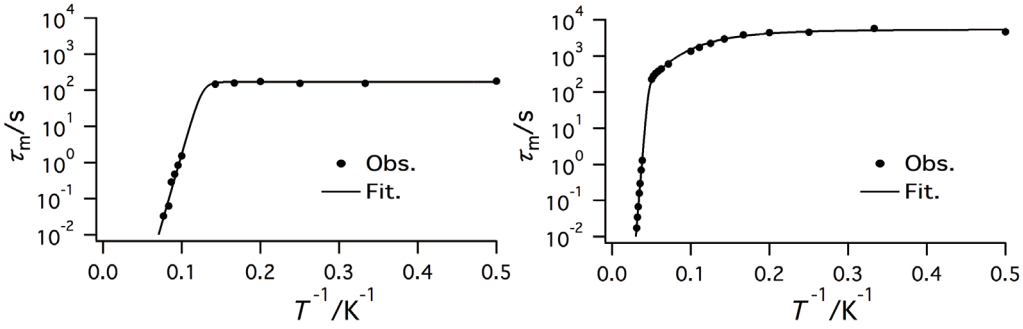

Fig. 1 τ_m vs $1/T$ plots for (left) $[Dy_2@C_{78}(D_{3h})]^-$ and (right) $[Dy_2@C_{80}(I_h)]^-$

The obtained parameters, τ_{QTM} and U_{eff}, are listed in Table 1. Comparing the results obtained in the present work between $C_{78}(D_{3h})$ and $C_{80}(I_h)$, we can easily notice that both τ_{QTM} and U_{eff} are largely different. On the other hand, U_{eff} of $C_{80}(I_h)$ and $C_{80}(I_h)CH_2Ph$ is almost identical but τ_{QTM} is different.

Table 1 τ_{QTM} and U_{eff}

	$[Dy_2@C_{78}(D_{3h})]^-$	$[Dy_2@C_{80}(I_h)]^-$	$Dy_2@C_{80}(I_h)CH_2Ph$ [ref. 1]
τ_{QTM}/s	170	5438	3257
U_{eff}/K	176	606	613

[1] F. Liu et al., *Nat. Commun*. **8**, 16098(2017).
[2] G. Velkos et al., *Angew. Chem. Int. Ed*. **58**, 5891(2019).
[3] R. Takai et al., *The 55th Fullerenes-Nanotubes-Graphene General Symposium* 127(2018).

Corresponding Author: Takeshi Kodama
Tell: +81-42-677-2530, Fax: +81-42-677-2525
E-mail: kodama-takeshi@tmu.ac.jp

Development of Mobility, Charge and Optical Measurement System for Nanomaterials

○Toshiki Sugai, Fumiaki Uchiyama, Yuya Ooishi, Reona Miyamoto, Ryo Sasaki, Takanori Nakayasu, Kanata Oguri, and Tomoya Ono

Department of Chemistry, Toho University, Miyama 2-2-1 Funabashi, 274-8510, Japan

Ion mobility spectrometry (IMS) combined with mass spectrometry has revealed novel information on nanomaterials such as fullerenes[1]. However, the sizes of nanomaterials have been growing wider and wider from carbon nanotubes to graphene for example. These materials cannot be detected mass spectrometry so other measurement systems should be combined with IMS to study them. We also have been working on nanocarbon materials such as graphene quantum dots with our newly developed IMS combined with ion trap and optical measurement system. Even with the new system it is still difficult to clarify their structures because mobility observed by IMS depends on both of structures and charges of samples. To overcome this difficulty, here we present simultaneous mobility, charge, and optical measurement system.

The system consists of an electrospray ion source (ESI) for production of positively charged nanodroplets, a trap type IMS, and a charge detector. Charged droplets were produced and trapped in the IMS system under ambient condition. Then the droplets were drifted around several cm, and then were detected by the charge detector. Figure 1 shows the detected charge and drift time profile of the droplets. The horizontal axis shows the drift time and the vertical axis shows the amount of the charge. From those peaks of the profile, the size around 100 nm and charge around thousands of e were identified, which is consistent with ESI condition. This system can be applied general nanomaterials with optical measurements.

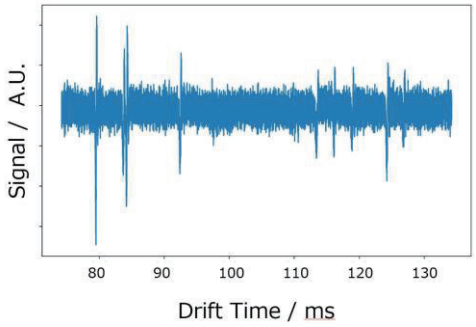

Fig. 1 Charge and Drift Time Profile of Nanodroplets

[1] G. von Helden *et al.*, *J. Chem. Phys.*, **95**, 3835 (1991).

TEL: +81-47-472-4406, E-mail: sugai@chem.sci.toho-u.ac.jp

One dimensional characteristics in thermoelectric properties of semiconducting single walled carbon nanotubes

Yota Ichinose[1], Kan Ueji[1], Yohei Yomogida[1], Kazuhiro Yanagi[1]

[1] *Department of Physics, Tokyo Metropolitan University, Hachioji Tokyo 192-0397, Japan*

Thermoelecrics are a very important technology for efficient conversion of waste heat to electrical power. Theoretical studies have suggested that lowering dimensionality can enhance thermoelectric performance due to the following two factors, (1) quantum confinement effect and (2) reduction of thermal conductivity.[1] Enhancement of thermoelectric performance by reduction of thermal conductivity is well confirmed, but experimental clarification on how the low-dimensional electronic structure can enhance thermoelectric performance has been elusive. Single walled carbon nanotubes (SWCNTs) are a very good model for studying relationships between one-dimensional electric structure and thermoelectric properties. Our recent study revealed unique one-dimensional characteristics in their thermoelectric properties.[2] For example, in conventional metallic materials, the increase of their conductivity induces the decrease of their Seebeck coefficient, which is called as thermoelectric trade-off. However, in the case of metallic SWCNTs, the trade-off is violated. In metallic SWCNTs, we can observe enhancement of both Seebeck coefficient and conductivity because of the presence of van-Hove singularity (vHs) in density of states, reflecting 1D electronic structure. In the case of semiconducting SWCNTs, however, it has been very difficult to discuss 1D characteristics in their thermoelectric properties. We cannot distinguish three, two or one-dimensional characteristics in the line-shapes of Seebeck coefficients as a function of Fermi-level in semiconductor materials.

However, a recent theoretical study pointed out the importance of thermoelectrical conductivity.[3] Only in the case of 1D materials, a sharp peak structure can be observed around 1st vHs in thermoelectrical conductivity. Thus, in this study, we investigated the thermoelectrical conductivity of semiconducting SWCNTs with various chiralities. Figure 1 shows thermoelectrical conductivities as a function of gate voltages in semiconducting SWCNTs with various chiralities. When we prepare (6,5) SWCNTs with purity more than 99%, we could observe a sharp peak structure in thermoelectrical conductivity. This sharp peak structure in thermoelectrical conductivity clearly reflects vHs structure. In this talk, we will discuss the background.

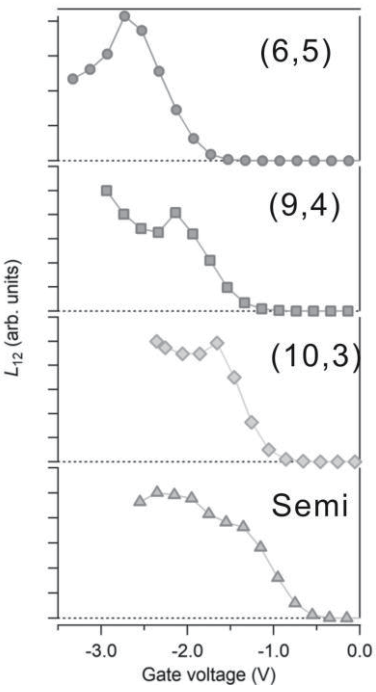

Fig1. Thermoelectric conductivity, the L_{12} term, of (6,5), (9,4), (10,3) and Semi (semiconducting SWCNT with diameter of 1.4 nm) as a function of gate voltage.

References: [1] Hicks&Dresselhaus,*PRB* 47, 16631 (1993) [2] Ichinose et al., Nano Lett. 19, 7370 (2019) [3] Yamamoto & Fukuyama, JPSJ 87, 114710 (2018)

Corresponding Author: K. Yanagi, E-mail: yanagi-kazuhiro@tmu.ac.jp

Synthesis of Boron Nitride Nanotubes and MoS_2@BNNTs Heteronanotubes

○ Ming Liu[1], Yongjia Zheng[1], Yang Qian[1], Rong Xiang[1], Taiki Inoue[1], Shohei Chiashi[1], Esko I. Kauppinen[2], Shigeo Maruyama[1,3*]

[1] *Department of Mechanical Engineering, The University of Tokyo, Tokyo 113-8656, Japan*
[2] *Department of Applied Physics, Aalto University School of Science, PO Box 15100, FI-00076 Aalto, Finland*
[3] *Energy NanoEngineering Lab., National Institute of Advanced Industrial Science and Technology (AIST), Tsukuba 305-8564, Japan*

Inorganic nanotubes have initiated a surge of intensive research in the last few years since the discovery of tungsten disulphide nanotubes in 1992 [1]. Lately, MoS_2 nanotubes [2] have been started to be produced in decent amounts and with promising potentials for large scale application, mostly as superior solid lubricants and in nanocomposites. The synthesis of single-walled MoS_2 nanotubes is still a challenge in the field, however, due to a combined theoretical and experimental work indicated that multiwall MoS_2 nanotubes with inner core larger than 6 nm are more stable than single-walled nanotubes [3]. Moreover, a boron nitride nanotube (BNNT), a structural analogue of a carbon nanotube in nature, is an electrical insulator with a bandgap of ca. 5.5 eV, basically independent of tube chirality and morphology.

In this work, firstly, we present a template-assisted synthesis method for producing high quality and single crystalline BNNTs via a CVD coating BN on pristine single-walled carbon nanotubes and subsequent removal of the template. The coating method of synthesizing coaxial nanotubes of single walled carbon nanotubes and BNNTs is recently developed in our group [4]. The quality and crystalline structure of BNNTs are examined by TEM and Raman spectroscopy characterizations (Figure 1 (a)). The optical bandgap of as-synthesized BNNTs is proven as 5.76 eV by absorption spectra. Moreover, we also demonstrate a facile CVD process of producing a hetero nanotube structure of combining MoS_2 nanotubes and BNNTs (MoS_2@BNNTs), as shown in Figure 1(b). BNNTs provides a wide cavity for a layered MoS_2 to fit into the core and enfold within it to form a tubes, as well as serves as an optically and electrically passive template for investigating the optical properties of single-walled MoS_2 nanotubes. The comparison of Raman spectra and PL spectra between multi-walled and single-walled MoS_2 nanotubes is discussed in this work.

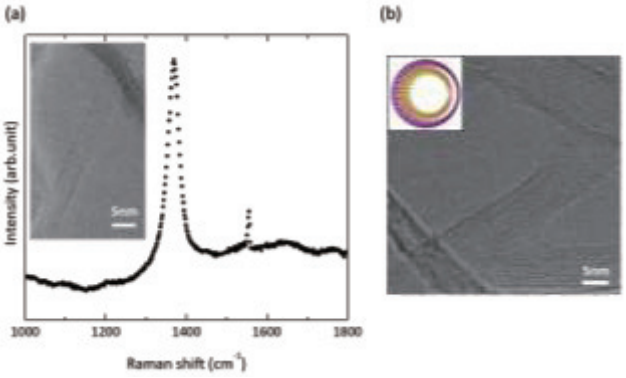

Figure 1 (a) Representative Raman spectrum and TEM image of BNNTs. (b) Representative TEM image and atomic model of MoS_2@BNNTs.

[1] R. Tenne *et al.* Nature **360**, 444 (1992).
[2] Y. Feldman *et al*. Science **267**, 222 (1995).
[3] G. Seifert *et al.* J. Phys. Chem. B **106**, 2497 (2002).
[4] R. Xiang *et al.* arXiv: 1807.06154 (2019).

Corresponding Author: Shigeo Maruyama
Tel: +81-3-5841-6421
E-mail: maruyama@photon.t.u-tokyo.ac.jp

Influence of interlayer stacking on gate-induced carrier accumulation in a van der Waals heterostructure comprising MoS_2 and WS_2

○Mina Maruyama, Susumu Okada

Department of Physics, Graduate School of Pure and Applied Sciences, University of Tsukuba, Tsukuba 305-8571, Japan

Transition metal dichalcogenides (TMDCs) are regarded as channel materials of field effect transistors (FET) because of their semiconducting electronic properties and chemically inert sheet structure. In addition, TMDCs can form van der Waals (vdW) heterostructures which exhibit interesting variations in their electronic structures depending on the electronic band structures of constituent layers and interlayer interaction. Accordingly, asymmetric carrier accumulation occurs in the vdW heterostructure comprising MoS_2 and WS_2, owing to its type-II band-offset [1]. We further demonstrated similar asymmetric carrier doping in bilayer MoS_2 in dual gate FET by controlling perpendicular electric field and carrier concentration. Thus, in the present work, we aim to investigate the influence of band offset and the electric field on carrier accumulation in bilayer MoS_2/WS_2 FET, using density functional theory with effective screening medium method. To simulate the bilayer MoS_2/WS_2-FET, we consider the structural model shown in Fig. 1 where the MoS_2/WS_2 is sandwiched by top and bottom gate electrodes which are simulated by effective screening medium with infinite dielectric constant.

Our calculations showed that carrier distribution in MoS_2/WS_2 is sensitive to field direction, field strength, carrier concentration, and interlayer stacking arrangement (Table I). Under the electric field whose direction enhances the band offset, the electron localization in MoS_2 layer increases with increasing the field strength. On the contrary, electron is spilled over WS_2 layer with the increase of the field whose direction suppresses the band offset. The electron localization is substantially suppressed by increasing the electron concentration. We further found that the interlayer stacking misorientation causes the enhancement of electron accumulation in MoS_2 layer owing to the decease of the interlayer interaction.

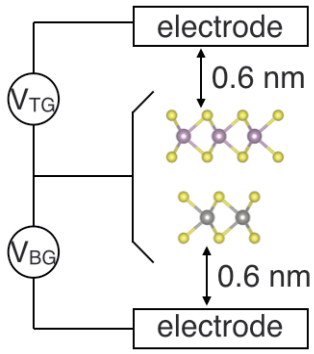

Fig.1 Structural model of bilayer MoS_2/WS_2–FET with top and bottom gate electrodes.

Table 1. Carrier distribution in bilayer WS_2/MoS_2 (AB stacking) under an electric field.

	-1.0 V/nm	-0.1 V/nm	0.1 V/nm	1.0 V/nm
	W/Mo	W/Mo	W/Mo	W/Mo
10^{13} e/cm^2	45%/55%	36%/64%	34%/66%	27%/73%
10^{14} e/cm^2	47%/53%	43%/57%	42%/58%	38%/62%

[1] M. Maruyama and S. Okada, *Appl. Phys. Express* **12**, 075008 (2019).

Corresponding Author: M. Maruyama
Tel: +81-29-853-5921, Fax: +81-29-853-5924, E-mail: mmaruyama@comas.frsc.tsukuba.ac.jp

First-principles electronic-structure study of stabilities and electronic properties of trilayer h-BN

○Taishi Haga[1], Yuuto Matsuura[1], Yoshitaka Fujimoto[1], and Susumu Saito[1,2,3]

[1] Department of Physics, Tokyo Institute of Technology, Tokyo 152-8551, Japan
[2] Advanced Research Center for Quantum Physics and Nanoscience, Tokyo Institute of Technology, Tokyo 152-8551, Japan
[3] Materials Research Center for Element Strategy, Tokyo Institute of Technology, Kanagawa 226-8503, Japan

Hexagonal boron nitride (h-BN) thin layers as well as its bulk phase attract much attention as not only substrate but also future wide-gap semiconductor materials. Unlike graphene with a sixfold symmetry, the *h*-BN layer has only a threefold symmetry, and they accordingly have different stacking directions. Therefore, in *h*-BN multilayer systems, there are many more possible stacking sequences than in the graphene multilayer. Hence, various electronic properties of *h*-BN layers depending on its stacking sequence should appear. Actually, it has been reported that *h*-BN bilayers show various electronic properties depending on their stacking sequences [1]. Defects in semiconductors often play a key role to modify and determine the electronic properties of the system. Therefore, it is important to theoretically study how an impurity in h-BN affects the electronic properties. In the present work, we study stabilities and electronic structure of h-BN trilayers using first-principles electronic-structure calculations within the framework of the density functional theory. It is found that the relative donor and acceptor ionization energies depend on the stacking sequence [2]. It is also found that spatial distributions of the valence band top and conduction band bottom states can be localized in specific h-BN layer. By using this result, we design the C-doped h-BN trilayer that allows modulation doping [Fig. 1].

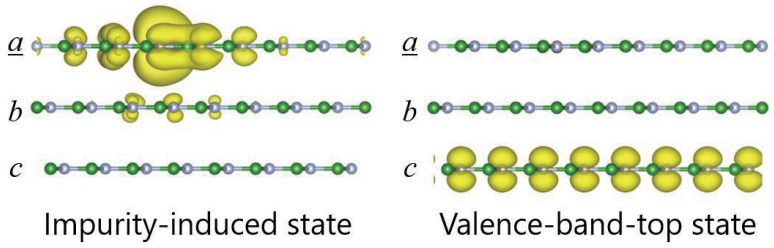

Figure 1 Spatial distributions of the impurity-induced states and the valence-band-top states of the *abc*-stacked h-BN trilayer. The top h-BN layer is doped with C atom at the N site. The doped layer and the carrier conductive layer are separated from each other.

[1] Y. Fujimoto, and S. Saito, Phys. Rev. B **94**, 245427 (2016).
[2] T. Haga, Y. Matsuura, Y. Fujimoto, and S. Saito, to be published.
Corresponding Author: T. Haga
E-mail: haga.t@stat.phys.titech.ac.jp

Molecular modification of graphene/Au electrode for controlled proton permeability

○Tomohiro Fukushima, Takaha Komai, Hidetaka Hasebe, Kei Murakoshi

Department of Chemistry, Faculty of Science, Hokkaido University, Sapporo, 060-0810, Japan

The electronic and chemical properties of graphene can be modulated through the interfacial interaction.[1] Recently, Geim *et al.*, reported that graphene can be uniquely used as proton permeable membrane.[2] The control of the proton permeability can be useful for the applications such as the separator for electrochemical systems. However, it is still difficult to control the structure of graphene. Here, we show that molecular modification of graphene surface can modulate the proton permeability from in-situ Raman spectroscopy under electrochemical potential control.

We prepared Au (111) surface through the Cavalier method, and graphene was prepared through the chemical vapor deposition. Molecular modification of graphene was accomplished by the electrochemical oxidation of phenylhydrazine derivatives. Electrochemical measurements were conducted in 0.1 M $NaClO_4$ in the presence of 2 mM phenylhydrizene as shown in Figure 1. In the absence of phenylhydrazine, anodic current was not observed. On the other hand, in the presence of phenylhydrazine, anodic current was observed from -0.2 V vs. Ag/AgCl. The anodic feature was different from second cycle suggesting that deposition of phenyl groups on G/Au electrode (Ph-G/Au). Figure 2 shows the Raman spectra of G/Au and Ph-G/Au. G band (1580 cm^{-1}) and 2D band (2700 cm^{-1}) were observed for the as-prepared G/Au electrode. On the other hand, D band (1350 cm^{-1}) was additionally observed for Ph-G/Au. Raman spectroscopy revealed that successful modification of graphene surface by phenylhydrazine. Figure 3 shows the electrochemical potential-dependent G band and 2D band position of G/Au electrode. G band and 2D band remains similar position. 2D band suddenly droped at -1.9 V and reversibly. The observed 2D band shift is due to the intercalation of H_2 molecules between graphene and Au through the proton tunneling. Effect of molecular modification will be discussed.

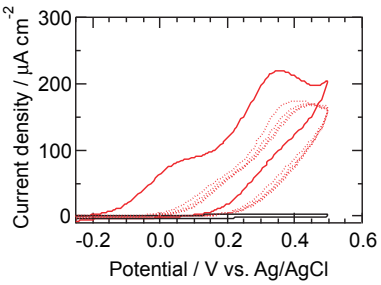

Figure 1. Cyclic voltammogram of G/Au in the absence (black) and presence of phenylhydrazine (red) in 0.1 M $NaClO_4$. Sweep rate: 50 mV/s.

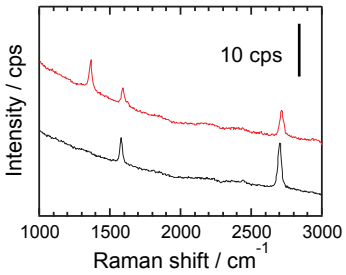

Figure 2. Raman spectra of G/Au (black) and Ph-G/Au (red) (514 nm, 0.5 mW).

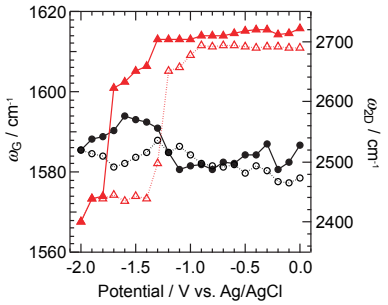

Figure 3. G band (black) and 2D band (red) peak position of G/Au electrode.

[1] T. Fukushima, K. Murakoshi, Current Opinion in Electrochemistry, **17**, 158 (2019).

[2] M. Lozada-Hidalgo, H. A. Wu, A. K. Geim *et al.*, Nature **516**, 227 (2014).

Corresponding Author: K. Murakoshi

Tel: +81-11-706-2704, Fax: +81-11-706-4810,

E-mail: kei@sci.hokudai.ac.jp

Carbon nanotube-based excitonic wavelength-selective absorber and emitter for solar thermal energy harvesting

○Yuhei Miyauchi[1], Taishi Nishihara[1], Akira Takakura[1], Kazunari Matsuda[1], Takeshi Tanaka[2], and Hiromichi Kataura[2]

[1] *Institute of Advanced Energy, Kyoto University, Uji, Kyoto 611-0011, Japan.*
[2] *Nanomaterials Research Institute, AIST, Tsukuba, Ibaraki 305-8565, Japan.*

Technologies for solar energy harvesting have been of central importance in society over recent years because their developments are considered as the key to conquer the urgent social requirement for reducing CO_2 emission on a global scale. In addition to solar photovoltaics (PV), utilization/management technologies of solar thermal energy have been of strong interest because of their high thermodynamic energy conversion efficiency and low cost. One of the key components in solar thermal technologies is a device with wavelength-controlled absorptivity/emissivity, called selective absorber/emitter. A pair of selective absorber and emitter is used for spectrally shaping the broadband solar spectrum into a narrow-band near-infrared thermal radiation, which can be used as an input to a semiconductor PV cell to efficiently generate electricity; this scheme is called solar thermophotovoltaics (STPV). Owing to the reduced thermalization loss in the PV cell, if an ideal selective absorber/emitter pair is available, STPV has a very high principle energy conversion efficiency of more than 60 %, which far exceeds the Shockley–Queisser limit of a standard Si solar cell (~ 30 % [1]). Thus, STPV has attracted growing attention as an emerging concept of the solar energy harvesting. However, the reported conversion efficiency of the state-of-the-art STPV (< 10 % [2]) is still much lower than the principle efficiency, partially due to non-ideality of the realistic selective absorber/emitter pairs.

Here, we demonstrate application of single-chirality enriched semiconducting single-walled carbon nanotubes (SWNTs) for the selective absorbers and emitters with an excellent wavelength tunability via selection of the SWNT chirality. Optical spectra of semiconducting SWNTs are dominated by thermally stable excitons whose resonant wavelengths depend on the chirality of SWNTs, and excitonic spectra are stable even at elevated temperatures more than 2000 K [3] owing to the large binding energy of one-dimensional excitons. This unique exciton property provides an excellent tunability of the wavelength cut off of the absorber composed of chirality-selected SWNTs. Moreover, thermal radiation with very narrow spectral bandwidth arising from thermal generation and radiative recombination of excitons is available [3], which offers an ideal thermal optical property as a selective emitter. We will discuss the thermal and optical characteristics of the macroscopic selective absorber/emitter thin films fabricated using single-chirality enriched SWNTs [4].

[1] W. Shockley and H. J. Queisser, *J. Appl. Phys*. **32**, 510 (1961).
[2] D. M. Bierman, A. Lenert, W. R. Chan, B. Bhatia, I. Celanović, M. Soljačić, and E. N. Wang, *Nat. Energy* **1**, 16068 (2016).
[3] T. Nishihara, A. Takakura, Y. Miyauchi, and K. Itami, *Nat. Commun.* **9**, 3144 (2018).
[4] Y. Yomogida, T. Tanaka, M. Zhang, M. Yudasaka, X. Wei, and H. Kataura, *Nat. Commun*. **7**, 12056 (2016).
Corresponding Author: Y. Miyauchi
Tel: +81-774-38-3463
E-mail: miyauchi@iae.kyoto-u.ac.jp

Machine-learned 100 %-yield carbon nanotube dissolution in arbitrary organic solvents

○Yoshiyuki Nonoguchi[1,2], Tomoyuki Miyao[1,3], Chigusa Goto[1], Tomoko Murayama[1], Kimito Funatsu[1,3,4], Tsuyoshi Kawai[1]

[1] *Division of Materials Science, Nara Institute of Science and Technology, Ikoma 630-0192, Japan*
[2] *JST, PRESTO, Kawaguchi 332-0012, Japan*
[3] *Data Science Center, Nara Institute of Science and Technology, Ikoma 630-0192, Japan*
[4] *Department of Chemical System Engineering, School of Engineering, The University of Tokyo, Tokyo 113-8656, Japan*

The insolubility of single-walled carbon nanotubes (SWCNTs) into organic solvents has been a common sense except for the uses of aqueous amphiphilic surfactant systems and a few magic solvents such as N-cyclohexylpyrrolidone [1,2]. Despite tremendous practical requirements, the preparation of organic SWCNT inks with complete homogeneity and long shelf time is rarely allowed. Few successful organic inks include dispersions with conducting polymers and polyvinyl ketone in nonpolar solvents. In order to make the inks with more arbitrary, more practical, and more preferred organic solvents, the understanding of SWCNT-surfactant-solvent interactions is indispensable.

This work demonstrates the surfactant-assisted, high yield dissolution of SWCNTs in ordinary organic solvents including alcohol, ketone, ester and ether. The surfactants used here are commercially available acid-base pairing compounds, where the polarity of dispersing solvents is apparently associated with surfactant ionicity. Representatively, cellulose derivatives such as ethyl cellulose enabled the efficient dissolution of SWCNTs in organic solvents (Fig. 1A). A feature extraction based on the multivariate analysis and genetic algorithm reveals seemingly important physicochemical requirements for the efficient dissolution (Fig. 1B). These elucidated factors are associated with not only solvents-surfactant, but also solvent-SWCNT interactions. The free and universalized SWCNT dispersion design described here will lay the groundwork for many applications ranging from fundamental nanofluidics to solution-based fabrication.

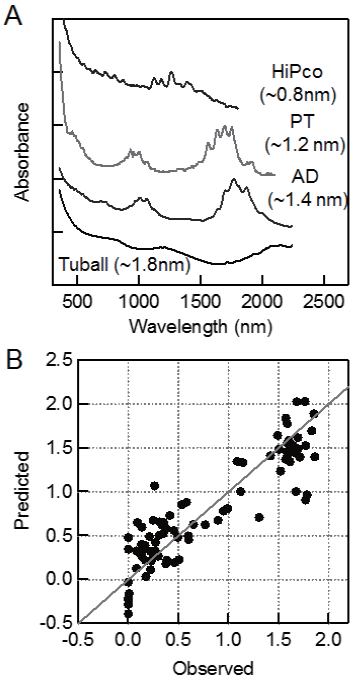

Fig. 1 (A) Dispersion of SWCNTs in THF with the aid of ethyl cellulose. (B) Cross-validation analysis of SWCNT solubility in 81 solvents examined using S_{22} absorption.

[1] M. J. O'Connell, *et al.* Science **297**, 593 (2002).
[2] S. D. Bergin, *et al.* ACS Nano **3**, 2340 (2009).

Corresponding Author: Y. Nonoguchi
Tel: +81-743-72-6028, Fax: +81-743-72-6179
E-mail: nonoguchi@ms.naist.jp

Multiscale hydrophobic interactions between gel, SWCNTs, and surfactants: detailed discussions

Guowei Wang, Takeshi Tanaka, ○Hiromichi Kataura

Nanomaterials Research Institute, AIST, Tsukuba, Ibaraki 305-8565, Japan

We have enjoyed adsorption chromatography for structure sorting of single-wall carbon nanotubes (SWCNTs), for long time. In this method, semiconducting (S-) SWCNTs are selectively adsorbed in polysaccharide gels when we used sodium dodecyl sulfate (SDS) for individually dispersing SWCNTs in water. Furthermore, diameter selective elution process can be realized diameter sorting of S-SWCNTs. In this method, we expected that the hydrophobic surfaces in polymer network in the gel work as effective adsorption sites for S-SWCNTs, because such gels have no apparent interactions to analyte except hydrophobic interactions. However, detailed adsorption mechanism was not well understood. In the previous presentation, we claimed multiscale hydrophobic interactions can explain the adsorption of S-SWCNTs to the gel. Where, the "wet-dry transition" is mesoscopic hydrophobic interaction and surfactant adsorption to SWCNTs is nanoscale hydrophobic interaction. If the mesoscopic interaction is more stable, SWCNTs can be adsorbed in the gel by removing surfactant molecules from the surface. This is the mechanism of the selective adsorption of S-SWCNT to the gels. In this presentation, we will try to discuss this interesting phenomenon by introducing "excluded water volume" as a scale of free energy gain in the hydrogen bonding system without theoretical calculations. Excluded water volume by surfactant is estimated from the number of surfactants on the surface of SWCNTs, which depends on the electronic structure of the SWCNT [1]. The other excluded water volume can be estimated from the gel volume of the adsorption site. This model clearly explains why the dry state, in which SWCNTs are directly adsorbed in gels, is stable when the adsorption site is large enough (mesoscopic). Furthermore, our model suggests that similar mechanisms will be seen everywhere when we handle nano materials with hydrophobic surfaces.

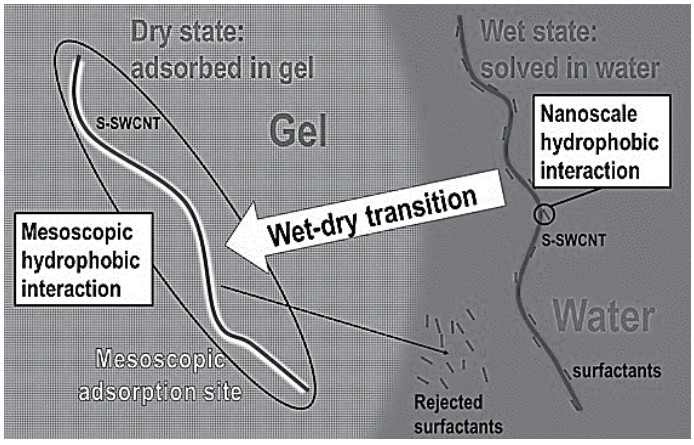

This work was supported by JST CREST, Grant Nos. JPMJCR16Q2 and JPMJCR18I5, Japan.

[1] M. Ohfuchi, J. Phys. Chem. C 2018, **122**, 4691-4697.

Corresponding Author: Hiromichi Kataura
Tel: +81-29-861-2551
E-mail: h-kataura@aist.go.jp

Enhanced intrinsic photovoltaic effect in tungsten disulfide nanotubes

○Yijin Zhang[1,2,*], Toshiya Ideue[3], Masaru Onga, Feng Qin, Ryuji Suzuki, Alla Zak, Reshef Tenne, Jurgen H. Smet, Yoshihiro Iwasa [1]

[1] *The Institute of Science and Industrial Research, Osaka University, Osaka 567-0047, Japan*
[2] *Max Planck Institute for Solid State Research, Stuttgart 70569, Germany*
[3] *Department of Applied Physics, The University of Tokyo, Tokyo 113-8656, Japan*
[4] *Faculty of Sciences, HIT-Holon Institute of Technology, Holon 5810201, Israel*
[5] *Department of Materials and Interfaces, Weizmann Institute of Science, Rehovot, Israel*
[6] *RIKEN Center for Emergent Matter Science (CEMS), Wako 351-0198, Japan*

Transition metal dichalcogenides (TMDs) such as tungsten disulphide (WS_2) are representative 2D materials. One of their unique features is the controllability of the crystal symmetry. The unit cell of the centrosymmetric bulk TMD is represented by two layers (Fig. 1). Since the inversion centre is located at the wan der Waals gap, isolation of a monolayer from bulk crystal naturally breaks the inversion symmetry. When the 2D sheets are rolled up to form a tubular structure, the mirror and rotational symmetries are broken as well. Such TMD nanotubes can be synthesized chemically. Most of them are multiwall nanotube with a polar structure [1].

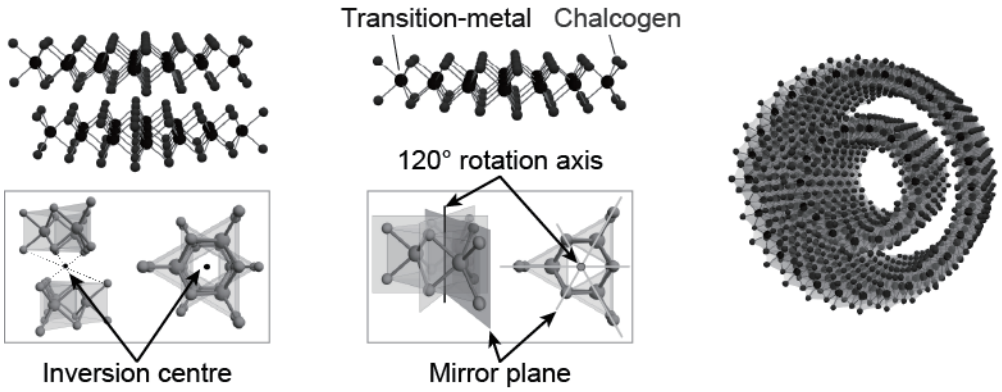

Fig.1 Crystal structures of TMD bilayer (left), monolayer (middle), and nanotube (right).

In this study, we fabricated two metal contacts at ends of an individual multiwall WS_2 nanotube and studied the electrical response upon light irradiation. We observed a sizable photovoltaic effect from intrinsic WS_2 nanotubes without formation of a *p-n* junction, while such effect was negligibly small in devices out of monolayer and bilayer 2D WS_2 flakes [2]. This difference indicates the importance of symmetry breaking for enhancing the photovoltaic effect occurring in intrinsic materials.

[1] F. Qin *et al*. Nature Commun. **8**, 14465 (2017).
[2] Y. J. Zhang, *et al.* Nature **570**, 349-353 (2019).

Corresponding Author: Y. J. Zhang
Tel: +81-3-5452-6158, Fax: +81-3-5452-6157,
E-mail: yzhang@iis.u-tokyo.ac.jp
*Present address: Institute of Industrial Science, The University of Tokyo, Tokyo 153-8505, Japan

Radiative quantum efficiency of bright excitons in carbon nanotubes

○H. Machiya[1,2], A. Ishii[1,3], Y. K. Kato[1,3]

[1] *Nanoscale Quantum Photonics Laboratory, RIKEN Cluster for Pioneering Research, Saitama 351-0198, Japan*
[2] *Department of Electrical Engineering, The University of Tokyo, Tokyo 113-8656, Japan*
[3] *Quantum Optoelectronics Research Team, RIKEN Center for Advanced Photonics, Saitama 351-0198, Japan*

Carbon nanotubes have potential applications as telecom-band single-photon emitters at room temperature, and coupling to microcavities can further improve the performance through the Purcell effect that accelerates the radiative decay into the cavity mode [1,2,3]. One of the key physical quantity in this process is the radiative quantum efficiency, or the fraction of photons emitted from excitons. The accelerated decay can be directly observed in the time domain if the radiative quantum efficiency is high enough, and this behavior allows for determination of the radiative quantum efficiency without the need to deconvolve the exciton generation efficiency from the photoluminescence (PL) quantum yield.

Here we experimentally determine the radiative quantum efficiency of bright excitons in carbon nanotubes [4]. Utilizing ultralow-mode-volume air-mode cavities, the radiative decay rates are enhanced through the Purcell effect. Time-resolved PL measurements are used to probe the overall decay process including the non-radiative paths, and we observe PL decay rates accelerated by as much as 3 times compared to typical uncoupled air-suspended nanotubes [5]. We further analyze the PL spectra by Monte-Carlo simulation of the cavity-enhanced dynamics of the exciton, extracting the Purcell factors in these devices. Combining the results from time-domain and spectral-domain measurements, we find that the radiative quantum efficiency of the bright exciton is unexpectedly high.

Work supported in part by RIKEN (Incentive Research Projects), MIC (SCOPE 191503001), JSPS (KAKENHI JP16H05962) and MEXT (Nanotechnology Platform). H.M. is supported by JSPS Research Fellowship. We thank the Advanced Manufacturing Support Team at RIKEN for technical assistance.

[1] R. Miura, S. Imamura, R. Ohta, A. Ishii, X. Liu, T. Shimada, S. Iwamoto, Y. Arakawa, Y. K. Kato, *Nat. Commun.* **5**, 5580 (2014).
[2] A. Jeantet, Y. Chassagneux, C. Raynaud, P. Roussignol, J. S. Lauret, B. Besga, J. Estève, J. Reichel, C. Voisin, *Phys. Rev. Lett.* **116**, 247402 (2016).
[3] A. Ishii, X. He, N. F. Hartmann, H. Machiya, H. Htoon, S. K. Doorn, Y. K. Kato, *Nano Lett.* **18**, 3873 (2018).
[4] H. Machiya, A. Ishii, Y. K. Kato, in preparation.
[5] A. Ishii, H. Machiya, Y. K. Kato, *Phys. Rev. X.* **9**, 041048 (2019).

Corresponding Author: Y. K. Kato
Tel: +81-48-462-1449
Web: http://katogroup.riken.jp/ E-mail: yuichiro.kato@riken.jp

Vapor-Phase Functionalization of Air-Suspended Single-Walled Carbon Nanotubes Using an Aryl-Halide

○Daichi Kozawa[1], Xiaojian Wu[2], Akihiro Ishii[1,3], Jacob Fortner[2], Keigo Otsuka[3], Rong Xiang[4], Taiki Inoue[4], Shigeo Maruyama[4,5], YuHuang Wang[2,6], Yuichiro K. Kato[1,3]

[1] *Quantum Optoelectronics Research Team, RIKEN Center for Advanced Photonics, Saitama 351-0198, Japan*
[2] *Department of Chemistry and Biochemistry, University of Maryland, College Park, Maryland 20742, United States*
[3] *Nanoscale Quantum Photonics Laboratory, RIKEN Cluster for Pioneering Research, Saitama 351-0198, Japan*
[4] *Department of Mechanical Engineering, The University of Tokyo, Tokyo 113-8656, Japan*
[5] *Energy NanoEngineering Laboratory, National Institute of Advanced Industrial Science and Technology (AIST), Ibaraki 305-8564, Japan*
[6] *Maryland NanoCenter, University of Maryland, College Park, Maryland 20742 United States*

Color centers in single-walled carbon nanotubes attract interest because of their single-photon emission at room temperature in the telecom range [1, 2]. However, the lack of vapor-phase reaction route for forming color centers hinders the use of the excellent optical properties of air-suspended carbon nanotubes. We herein demonstrate the functionalization of air-suspended carbon nanotubes using iodobenzene as a precursor. The chemical reaction procedure is rationally designed to maintain the suspended structure and fluorescent properties of carbon nanotubes. The formed phenyl group serves as a color center and exhibits localized exciton emission peaks E_{11}^{*} and E_{11}^{*-} in addition to the free exciton emission peak E_{11}. We characterize over 12 different chiralities, covering nanotubes with diameters d ranging from 0.981 to 1.29 nm, to elucidate the reactivity and optical property of the color centers. We find that the reactivity of iodobenzene scales as $1/d$, where the inherent strain on the curvature of nanotubes promotes the reaction. The trapping potential of E_{11}^{*} and E_{11}^{*-} are both close to the singlet-triplet splitting. The minimum value of $g^{(2)}(0)$ in the photon correlation verifies the photon antibunching at the color centers. These findings should lead to further development of quantum photon sources that utilize color centers in carbon nanotubes.

This work was supported in part by RIKEN (Special Postdoctoral Researcher Program, Incentive Research Projects), MIC (SCOPE 191503001), JSPS (KAKENHI JP15H05760, JP16H05962, JP18H05329), and MEXT (Nanotechnology Platform). We thank the Advanced Manufacturing Support Team at RIKEN for technical assistance.

[1] A. Ishii, X. He, N. F. Hartmann, H. Machiya, H. Htoon, S. K. Doorn, and Y. K. Kato, *Nano Lett.* **18**, 3873 (2018).

[2] X. He, N. F. Hartmann, X. Ma, Y. Kim, R. Ihly, J. L. Blackburn, W. Gao, J. Kono, Y. Yomogida, A. Hirano, T. Tanaka, H. Kataura, H. Htoon, and S. K. Doorn, *Nat. Photonics* **11**, 577 (2017).

Tel: +81-48-462-1449
E-mail: yuichiro.kato@riken.jp

Atomistic Structural Analysis of Reaction Intermediates Captured on Functionalized Carbon Nanohorns

○Koji Harano[1], Junfei Xing[1], Luca Schweighauser[1], Satoshi Okada[1], Eiichi Nakamura[1]

[1] *Department of Chemistry, The University of Tokyo, Tokyo 113-0033, Japan*

Chemical reactions in solution almost always take place via a series of minute intermediates that are often in rapid equilibrium with each other, and hence hardly characterizable at the level of atomistic molecular structures. We found that single-molecule atomic-resolution real-time electron microscopic (SMART-EM) video imaging [1] provides a unique methodology for capturing and analyzing the minute reaction intermediates, as illustrated here for the isolation, characterization, and semi-statistical analysis of single prenucleation clusters (PNCs) in the reaction mixture of crystallization of metal–organic frameworks (MOFs) by using functionalized carbon nanohorns [2]. Specifically, we found two different types of PNCs are involved in the formation of MOF-2 and MOF-5 from a mixture of zinc nitrate and benzene dicarboxylates in DMF at 95 °C and 120 °C, respectively [3]. SMART-EM identified many 1-nm-sized PNCs, among which a small amount of cube and cube-like clusters are involved in the MOF-5 synthesis, but not in the MOF-2 synthesis. In the latter, we instead found only linear and square PNCs, which suggest that the MOF-2/-5 bifurcation takes place at the PNC stage. Such a dataset is uniquely available by the use of the 'fishing' strategy, combined with the TEM video imaging, and highlight the potential of the SMART-EM technology in the study of the mechanisms of chemical reactions in solution.

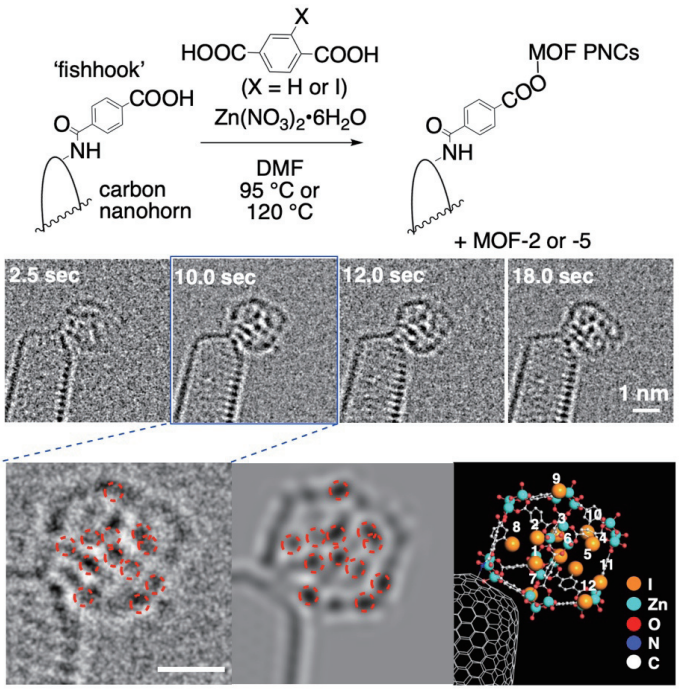

Fig.1 SMART-EM video imaging of PNCs in MOF-2 and MOF-5 syntheses from Zn^{2+} and benzene dicarboxylates. TEM images of a cubic PNC of I-MOF-5 (X = I) captured on carbon nanohorn with a carboxylate moiety are shown.

[1] E. Nakamura, *Acc. Chem. Res.* **50**, 1281 (2017).
[2] J. Xing, L. Schweighauser, S. Okada, K. Harano, E. Nakamura, *Nat. Commun.* **10**, 3608 (2019).
[3] L. Schweighauser, K. Harano, E. Nakamura, *Inorg. Chem. Commun.* **84**, 1 (2017).

Corresponding Authors: K. Harano and E. Nakamura
Tel: +81-3-5841-4369, Fax: +81-3-5841-4367
E-mail: harano@chem.s.u-tokyo.ac.jp

Independent degrees of freedom in two-dimensional materials

Sake Wang, F. R. Pratama, M. Shoufie Ukhtary, Riichiro Saito

Department of Physics, Tohoku University, Sendai 980-8578, Japan

Future semiconductor industry that utilizes the intrinsic degrees of freedom (DOFs) of electrons has been proved superior to their conventional counterpart, which depends thoroughly on energy-consuming charge. The three DOFs in two-dimensional (2D) materials have been discussed so far, that are sublattice pseudospin [1], electronic real spin [2], and valley-spin [3]. The fields concerning these DOFs are known as pseudospintronics, spintronics and valleytronics, respectively. 2D materials possess both high carrier mobilities and DOFs, which enables them to be a premium choice for the semiconductor industry [4].

Optical properties of the 2D materials have been studied extensively because the energy bandgap covers a wide range of frequencies of electromagnetic wave, from far infrared to ultraviolet [5–9]. The combination of electrical and optical properties offers possibilities for controlling electronic current or optical transitions characterized by different DOFs, which results in huge potential in fundamental physics and the applications in electronic–photonic devices.

In the monolayer transition metal dichalcogenides, thanks to the broken inversion symmetry and strong spin-orbit coupling (SOC) [6], the polarization of the three DOFs [7, 10] is observed experimentally. However, the three DOFs cannot be independent of one another for any existing materials or theoretical models, which disable independent usage of the spins. Therefore, in order to obtain the complete independence of the DOFs, a special material that offers independent control of each DOF is needed for exploring physics and material science.

Here we propose a general Hamiltonian based on the Haldane model with SOC which realizes the independence of all the DOFs that can tune optical absorption spectra as a function of the SOC [11]. The present result suggests a new 2D material or a new 2D electronic device which offers any combinations of pseudospintronics, spintronics and valleytronics applications by means of circularly polarized light.

[1] K.-i. Sasaki, R. Saito, Prog. Theor. Phys. Suppl. **176**, 253 (2008).
[2] M.N. Baibich, J.M. Broto, A. Fert, F. Nguyen Van Dau, F. Petroff, P. Etienne, G. Creuzet, A. Friederich, J. Chazelas, Phys. Rev. Lett. **61**, 2472 (1988).
[3] A. Rycerz, J. Tworzydlo, C.W.J. Beenakker, Nat. Phys. **3**, 172 (2007).
[4] K.S. Novoselov, D. Jiang, F. Schedin, T.J. Booth, V.V. Khotkevich, S.V. Morozov, A.K. Geim, Proc. Natl. Acad. Sci. U.S.A. **102**, 10451 (2005).
[5] M. Ezawa, Phys. Rev. B **86**, 161407(R) (2012).
[6] D. Xiao, G.-B. Liu, W. Feng, X. Xu, W. Yao, Phys. Rev. Lett. **108**, 196802 (2012).
[7] K.F. Mak, K. He, J. Shan, T.F. Heinz, Nat. Nanotechnol. **7**, 494 (2012).
[8] F. Bechstedt, L. Matthes, P. Gori, O. Pulci, Appl. Phys. Lett. **100**, 261906 (2012).
[9] A. Zunger, A. Katzir, A. Halperin, Phys. Rev. B **13**, 5560 (1976).
[10] H. Yuan, X. Wang, B. Lian, H. Zhang, X. Fang, B. Shen, G. Xu, Y. Xu, S.-C. Zhang, H.Y. Hwang, Y. Cui, Nat. Nanotechnol. **9**, 851 (2014).
[11] S. Wang, F. R. Pratama, M. S. Ukhtary, R. Saito, under review.

Corresponding Author: S. Wang
Tel: +81-22-795-7754, Fax: +81-22-795-6447,
E-mail: sake@flex.phys.tohoku.ac.jp

Optical Properties of Monolayer Transition Metal Dichalcogenides on GaN Surface Depending on their Polarity

S. Mouri[1], Y. Komichi[1], K. Shinokita[2], K. Matsuda[2] and T. Araki[1]

[1]*Ritsumeikan University, Nojihigashi 1-1-1, Kusatsu, Shiga, Japan,525-8577*
[2]*Institute of Advanced Energy, Kyoto University, Gokanosho, Uji, Japan 611-0011*

Optical properties of monolayer (1L) transition metal dichalcogenides (TMDs) show attractive properties such as strong light-matter interactions [1], stable excitonic features [2-4] and valley-spin polarization [5]. Therefore, they have enough potential as future novel optoelectronic devices. Understanding of charge injection or extraction effect is indispensable towards the control of these optical properties. One of the pathways to control the optical properties is to use the interaction 1L-TMDs and supported substrate. GaN is known as the polar semiconductor whose surface state is strongly modulated depending on its polarity. Here, we demonstrate the photoluminescence (PL) properties of 1L-TMDs due to the charge doping and/or charge transfer induced by GaN substrate.

The 1L-TMDs (MoS_2, WSe_2, and $MoSe_2$) were transferred on the free standing GaN (Chino Nitrides Co.) with Ga polar (+c) or N polar (-c) surface, and onto the standard SiO_2/Si substrates as a reference. Fig.1 shows the PL spectra of 1L-MoS_2 supported on each substrate measured at room temperature. The PL intensity of 1L-MoS_2 on GaN substrates becomes weak around quarter as compared with that on SiO_2/Si, as shown in Figs. 1. These results suggest that the photocarrier transfer between MoS_2 and GaN surface at room temperature.

On the other hand, the spectral shape was changed depending on the polarity of supported GaN substrate (+c, or –c). The exciton PL (X) of MoS_2 was almost disappeared on N polar (-c) GaN, while the trion (T) PL was slightly increased. The increase of trion spectral weight on N polar (-c) GaN suggests the increase of doped-carrier density interacting with the excitons, which can be explained by the electron accumulation at the interface of MoS_2 and N polar (-c) GaN. From the band alignment in MoS_2/GaN interface, the downward band bending of N polar GaN [6] could causes the surface accumulation of photo-induced electrons, which is responsible to increase the trion population. The PL quenching and increase of trion spectral weight in MoS_2 were also observed in other TMDs (WSe_2 and $MoSe_2$) on the GaN. These results strongly suggest that the engineering of polarity of supported substrate is one of important pathways towards the optical device applications of 1L-TMDs.

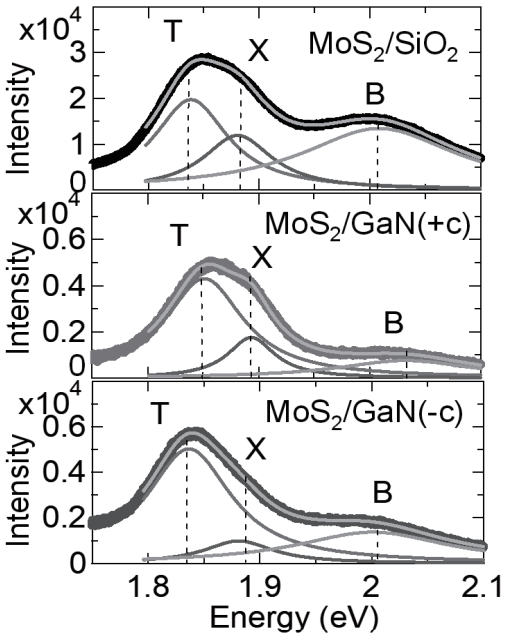

Fig. 1. PL spectra of 1L-MoS_2 on different substrates, SiO_2/Si, GaN (+c face), GaN (-c face) measured at room temperature.

References

[1] L. Britnell et al., Science **340**, 1311 (2013).
[2] K. Fai. Mak et.al., Phys. Rev. Lett **105**, 136805 (2010).
[3] A. Chernikov et.al., Phys. Rev. Lett **113**, 076802 (2014).
[4] S. Mouri et.al., Phys. Rev. **B 90**, 155463 (2014).
[5] K. Fai. Mak et.al., Nat. Nanotech. **7**, 494 (2012).
[6] M. Tangi *et.al.*, Appl. Phys. Lett. **109**, 032104 (2016).

Corresponding Author: S. Mouri
Tel:+81-77-561-2884
E-mail; iguchan@fc.ritsumei.ac.jp

Anomalous polarized Raman spectra of TaP

○Riichiro Saito, Pang Xiaoqi, Wang Tong, Nguyen T. Hung

[1] *Department of physics, Tohoku University, Sendai 980-8578, Japan*

Polarized Raman spectra of TaP Weyl semimetal is discussed by analyzing resonant Raman calculation. TaP is one of topological Weyl semimetals which attract much attention of researchers as an emerging material for discussing new physics such as the chiral Weyl fermion. Recently Kunyan Zhang et al. observed the polarized Raman spectra of a single crystal of TaP and they found that the polarized Raman spectra show anomalous patterns as a function of the polarization direction of light that depends on laser excitation energy [1] . In the normal polarized Raman spectroscopy, the polarized Raman has a fixed shape for a given symmetry of the Raman active mode, which does not change by changing the laser energy [2]. Thus the present results are exceptional in the theory of Raman spectroscopy.

In order to understand the anomalous behavior, we calculated the polarized Raman intensity by the home-made program of resonant Raman intensity with using the calculated data of the Quantum Espresso [3]. The calculate results reproduce the laser energy dependent polarized Raman spectra. In order to understand the anomalous behavior of the polarized Raman spectra, we restrict the Raman sub-processes intentionally in the resonant Raman calculation which gives the conventional polarized Raman spectra. From this analysis we found that the origin of the anomalous polarized Raman spectra comes from the quantum interference effect on Raman processes for nearly degenerate conduction bands. In particular, for a specific laser energy, some Raman intensity vanished by the interference effect. In the presentation, we will show the analysis based on the calculated results, which are compared with the experimental results.

This work is supported JSPS KAKENHI No. JPB18H01810.

References:

[1] Kunyan Zhang et al., Phys. Rev. B, in press (2020). Related papers therein.

[2] R. Saito, Y. Tatsumi, S. Huang, X. Ling, M. S. Dresselhaus, J. of Phys: Cond. Matt., 28, 353002, (2016)

[3] Y. Tatsumi, R. Saito, Phys. Rev. B 97, 115407 (2018).

Corresponding Author: Riichiro Saito
Tel: +81-22-795-7754, Fax: +81-22-795-6447,
Web: http://flex.phys.tohoku.ac.jp/
E-mail: rsaito@flex.phys.tohoku.ac.jp

ポスター発表
Poster Preview

1 P – 1 ～ 1 P – 31
2 P – 1 ～ 2 P – 30
3 P – 1 ～ 3 P – 31

Organic field effect transistor of fullerene C_{70} single crystals with rod shape

○Ryohei Yamamoto[1], Tadahiko Hirai [2], Nobuyuki Aoki [3] and Masaru Tachibana [1]

[1] Department of Materials System Science, Yokohama City University, Kanagawa 236-0004, Japan
[2] Commonwealth Scientific and Industrial Research Organisation
[3] Graduate School of Advanced Integration Science, Chiba University, Chiba 263-8522

Organic semiconductors have received attention from both technological and academic standpoints [1]. So the electrical properties of organic semiconductor are actively studied by using field effect transistor. In p-type organic field effect transistors (OFETs) with single crystals such as rubrene and tetacene, many studies showing high mobility have been reported [2] [3]. On the other hand n-type OFETs have been limited such as fullerenes [4] [5] and F_{16}CuPc [6].

It is hoped that the mobility of the fullerene C_{70} is higher than that of C_{60} due to the structure and electronic state [7]. However, researches on C_{70} FETs were limited in thin films [8] because of difficulty of the growing single crystals. To understand the mechanism of electrical properties, it is important to use a single crystal.

Recently, we succeeded in the growth of C_{70} single crystals by the liquid-liquid interface precipitation (LLIP) method. In this study, we report the results of structure and electrical measurements of C_{70} single crystals FETs.

The C_{70} crystals were grown by the LLIP method with using *m*-xylene and 2-propanol as good and poor solvents. The C_{70} crystals ware evaluated by an optical microscope, scanning electron microscope (Fig.1), Fourier-transform infrared spectroscopy and powder X-ray structural analysis.

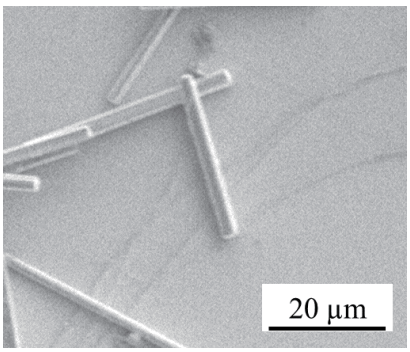

Fig.1 Scanning electron microscope image of C_{70} crystals

Output characteristics of C_{70} single crystals FETs exhibits typical feature of n-type of OFETs. It is known that water and oxygen are easily adsorbed into C_{70} crystals in air and degrade mobility of C_{70} crystals. To remove water and oxygen, the FET devices were annealed at 374 K under vacuum condition. The carrier mobility was significantly increased by the annealing treatment, and value was 1.22×10^{-2} cm^2/Vs.

[1] R. W. I. de Boer, M. E. Gershenson, A. F. Morpurgo, and V. Podzorov, *phys. Stat. sol.,* **201**, 1302 (2004).
[2] A. L. Briseno, *et al., Nature*, **444**, 913 (2006).
[3] S. Terao, *et al., J. Appl. Phys*., **108**, 124511 (2010).
[4] K. Ogawa, *et al*., *Appl. Phys. Lett.* **88,** 112109 (2006).
[5] H. Li, *et al*., *J. Am Chem. Soc*. **134**, 2760-5 (2012).
[6] H. Jiang, *et al*., *J. Mater. Chem*., **21**, 4771 (2011).
[7] S. Saito and A. Oshiyama, *phys. Rev* B **44**, 11532 (1991).
[8] S. Zheng and X. Lu, *RSC Adv.,* **5**, 38202 (2015).

Alteration of Fermi-Level of Single-Wall Carbon Nanotubes via Protein Adsorption Observed by Ultrafast Spectroscopy

○Tomohito Nakayama[1,2], Takeshi Tanaka[2],
Atsushi Hirano[2], Muneaki Hase[1]

[1] Division of Applied Physics, Faculty of Pure and Applied Sciences, University of Tsukuba, Tsukuba, Ibaraki 305-8573, Japan
[2] Nanomaterials Research Institute, National Institute of Advanced Industrial Science and Technology (AIST), Tsukuba, Ibaraki 305-8565, Japan

For over two decades, the single-wall carbon nanotubes (SWCNTs) have attracted great interest because of their remarkable features, such as high conductivity and high strength. The SWCNTs show the different types of electronic conductivity, i.e. metallic and semiconducting types [1]. One of the most important physical parameters of semiconducting SWCNTs is the Fermi-level (E_F) that is the highest energy level occupied by electrons. By controlling the Fermi-level, it is possible to make the semiconducting SWCNT p-type or n-type.

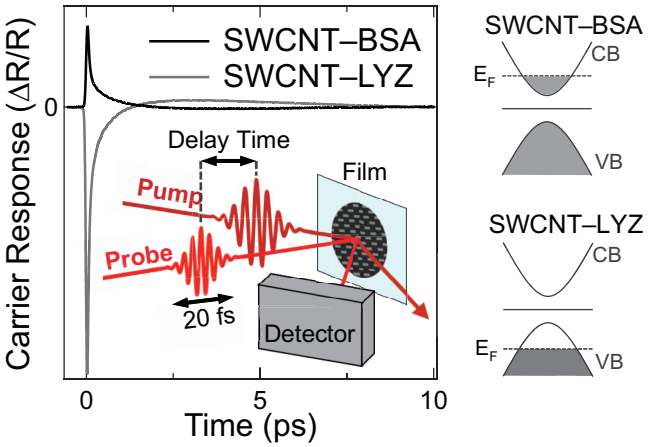

Fig.1| Carrier Response of SWCNT–BSA (Black) and SWCNT–LYZ (Gray) and schematic band structure (Left side). It can be seen that the signal of SWCNT–BSA and SWCNT–LYZ appeared in the opposite. The inset scheme indicates the experimental setup. VB and CB denote the valance and conduction bands, respectively.

In this study, we fabricated an SWCNT film whose Fermi-level is changed via adsorption of proteins, such as bovine serum albumin (BSA) [2] and hen egg-white lysozyme (LYZ) [3], which was observed from ultrafast carrier response and coherent phonon dynamics of the SWCNTs in the film using pump-probe spectroscopy with a femtosecond pulse laser. As a control sample, we used an SWCNT–SDS film. While the ultrafast carrier response of the SWCNT–LYZ film in sub-picosecond time scale exhibited the same sign as that of the SWCNT–SDS film, that of the SWCNT–BSA film exhibited a reversed sign (Fig.1). This result suggests that proteins alter the Fermi-level of the SWCNTs and have a potential to induce the reversal of surface charge of the SWCNTs. The surface charge of the SWCNTs changes by proteins should be applied to electronic materials.

[1] R. Saito, Appl. Phys. Lett. 60. (1992) [2] T. Nakayama, APEX. 11. (2018) [3] T. Nakayama, APEX. 10. (2017)
Corresponding Author: M. Hase
Tel: +81-29-853-5022, Fax: +81-29-853-5022,
E-mail: mhase@bk.tsukuba.ac.jp

Mechanical properties and morphology of polypropylene/ ethylene-1-butene copolymer rubber/CNT composites

○Yoshimi Muraoka, Kenzo Fukumori*

Toyota Central Research and Development Laboratories, Inc, Nagakute 480-1192, Japan

CNT (carbon nanotube) is one of the most promising materials as a reinforcing nanofiller for polymers since it has excellent characteristics such as high stiffness, strength, toughness and so on. Many researches have been carried out to improve mechanical properties by adding small amount of CNT to polymers[1]. Although the mechanical properties of polymer/CNT composites were improved by loading CNT, it is still unclear in detail about the effects of the incorporation of CNTs on the mechanical properties.

In this study, we have investigated the relation between flexural properties and morphologies of polypropylene (PP) based polymer blends/CNT composites, dependent on the kind of CNT, for automobile applications. The composites were prepared by melt blending of PP, ethylene-1-butene copolymer rubber (EBR) and CNTs with a twin-screw extruder. Fig. 1 shows the flexural moduli of the composites depending on the CNT amount. In the case of using CNT60 (diameter:60nm, G/D ratio:ca.8.0), the flexural modulus of CNT60 composite was superior to that of CNT15 (diameter:5nm, G/D ratio:ca.1.0) composite. The morphologies of those composites shown in Fig. 2 were observed by scanning electron microscopy (SEM). Depending on the kind of CNT, the morphology of the CNT60 composite was quite different from that of the CNT15 composite. That is, in the CNT60 composite, CNTs partially wrapped by the EBR domains were dispersed in PP matrix. On the other hand, in the CNT15 composite, CNTs were selectively localized in the EBR domains. Thus, it is confirmed that the morphology of the CNT composites, dependent on the kind of CNT related with diameter and G/D ratio, plays a key role in enhanced mechanical properties.

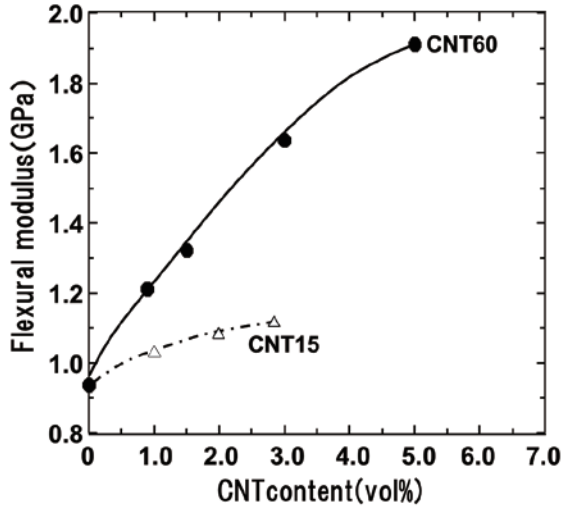

Fig.1 The relationship between CNT content and flexural modulus

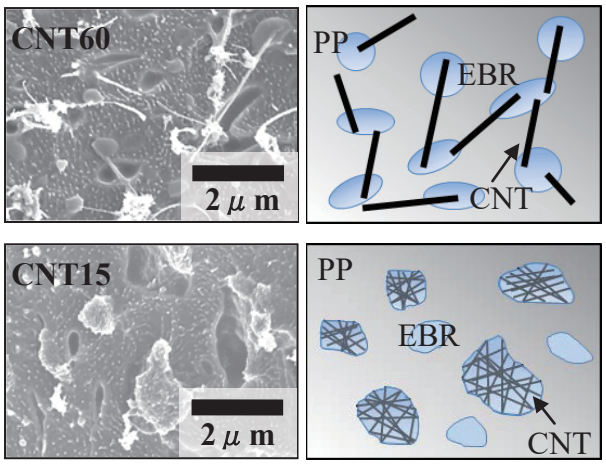

Fig.2 SEM images of composite materials and their schematic illustrations

[1] M. Khodabandelou , *et al*. Polym. Bull. **73**, 1607 (2016).

Corresponding Author: Y. Muraoka

E-mail: e4782@mosk.tytlabs.co.jp

*Present address: Aichi Institute of Technology.

Understanding the Effect of Sulfur on the Synthesis of Carbon Nanotubes

○ Rei NAKAGAWA[1], Michiko EDO[1], Hisashi SUGIME[1], Suguru NODA[1,2,*]
[1]*Department of Applied Chemistry,* [2]*Waseda Research Institute for Science and Engineering, Waseda University, Tokyo, Japan*

Carbon Nanotubes (CNTs) are attractive with high hopes in many different fields for their excellent properties. However, the practical applications of CNTs has been a challenge due to their high price and/or insufficient quality. Floating catalyst chemical vapor deposition (CVD) enables the synthesis of high quality CNTs, but it has had an issue with its low catalyst usage. To combat this situation, many groups have conducted research to improve the productivity of this process, and as a result it has been reported that the implementation of sulfur can increase the overall yield of floating catalyst CVD [1]. Many groups have proposed positive roles of sulfur; Fe-S to be the active site for catalytic reaction or reduced surface energy of Fe-S for nucleation of small Fe particles. However, these models are not supported by clear evidences and are not applicable to supported catalysts.

Here, we propose an opposite model where sulfur deactivates the Fe catalyst. Small amount of sulfur forms an inactive region on a Fe particle, and the inactive region works as an entrance for the carbon source without being covered with graphitic carbon. The analysis of this is difficult for floating catalysts, therefore for this research, supported catalysts were used by implementing graphite sheets as substrates to replicate the floating catalysts with spherical structure. Scanning electron microscope (SEM) shows that CNTs were only synthesized when S was supplied during synthesis (Fig. 1a). Additionally, to confirm the importance of having an inactive region within the catalyst particle for CNT synthesis, a thin Al_2O_3 layer was deposited on top of the Fe catalysts. The thin Al_2O_3 layer significantly enhanced the CNT growth (Fig. 1b) in a similar manner as sulfur. These results suggests a new approach for future catalyst design.

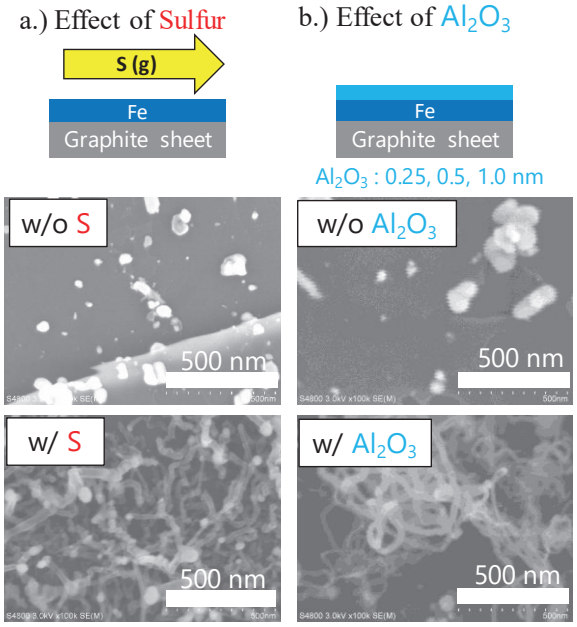

Fig. 1. SEM analysis of graphite substrates after CNT synthesis. (a) Sulfur vapor was supplied to the Fe catalyst during synthesis. (b) Al_2O_3 thin layer was deposited on the Fe catalyst.

[1] H.M. Cheng, et al., *Appl. Phys. Lett*. **72**, 3282 (1998).
Corresponding Author: S. Noda, Tel&Fax: +81-3-5286-2769, E-mail: noda@waseda.jp

Evaluation of various nitrogen-doping in graphene on the performance as a supercapacitor electrode

○Rohit Yadav, Prerna Joshi, Masanori Hara, Masamichi Yoshimura

Graduate School of Engineering, Toyota Technological Institute, Nagoya 468-8511, Japan

A supercapacitor is an energy storage device with high charge storage capacity and excellent cyclic stability due to its large surface area and easy ion accessibility. It is categorized into electric double-layer capacitors (EDLCs), pseudocapacitors and hybrid capacitors, on the basis of their charge storage mechanism. EDLC behaviour is commonly shown by carbon-based materials, where charge storage takes place via electrolyte ion intercalation inside porous electrode material forming an electrostatic double layer, resulting in the charging of EDLC. On the other hand, charge storage in pseudocapacitors takes place via oxidation and reduction (redox reaction) of the electrode with electrolyte ions. Among available carbon materials for EDLC, graphene emerged as a potential candidate due to its high mechanical strength (Young's modulus of ~490 kPa)[1], large surface area (~2630 m^2/g)[2], and high electrical conductivity (~5 $\times 10^{-3}$ S/cm)[3]. However, in the case of pristine graphene, the stacking of sheets via van der Waals interaction decreases the surface area, resulting in low intrinsic capacitance [4]. To overcome this limitation, we have incorporated nitrogen (N) into the reduced graphene oxide (N-rGO) lattice via pyrolysis in the presence of urea at various temperatures (600, 700, 800, 900 °C) in inert atmosphere. Synthesized N-rGO samples were characterized using both physical and electrochemical techniques.

X-ray photoelectron spectroscopy (XPS) and Energy-dispersive X-ray (EDX) spectroscopy showed uniform and varying nitrogen doping from 15 to 5.8 at. %, with an increase in pyrolysis temperature from 600 °C to 900 °C. N-rGO synthesized at 800 °C showed the highest specific surface area and thus the highest areal capacitance of 138.4 mF/cm^2 from the charge-discharge (CDC) profile. The capacitance shows an exceptional increment of 21.7% after 10000 cycles of charge-discharge, as shown in fig.1. The increased capacitance after stability could be due to the electrochemical activation of nitrogen functionality or oxygen functional group at the surface of the electrode upon continuous cycling, as confirmed by cyclic voltammetry (CV) after stability. The above characterizations reveal the potential use of N-rGO as an active material for supercapacitor electrode.

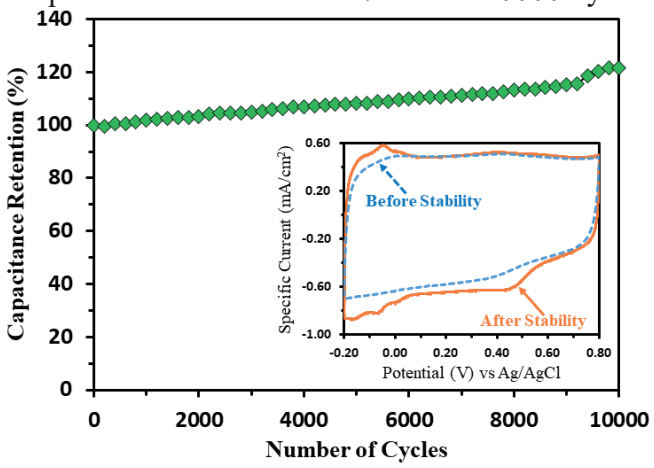

Fig. 1. Cyclic stability of N-rGO at 800 °C and inset: CV before and after stability.

[1] H. H. Huang *et al*. Sci. Rep. **8**, 6849 (2018).
[2] M. D. Stoller *et al*. Nano Lett. **8**, 3498 (2008).
[3] Y. Xu *et al*. ACS Nano **4**, 4324 (2010).
[4] L. Sun *et al*. RSC Adv. **2**, 4498 (2012).

Corresponding Author: Masamichi Yoshimura
Tel: +81-52-809-1851
E-mail: yoshi@toyota-ti.ac.jp

Gene expression analysis of macrophages on carbon nanohorn coated titanium

○Sadahito Kimura[1], Eri Hirata[1]*, Sari Takada[1], Masatoshi Sakairi[2], Masako Yudasaka[3], Atsuro Yokoyama[1]

[1] Graduate School of Dental Medicine, Hokkaido University, Kita 13, Nishi 7, Kita-ku, Sapporo 060-8586, Japan.
[2] Division of Materials Science and Engineering, Faculty of Engineering, Hokkaido University, Kita 13, Nishi 8, Kita-ku, Sapporo 060-8628, Japan.
[3]Nanomaterials Research Institute (NMRI), National Institute of Advanced Industrial Science and Technology (AIST), Tsukuba Central 5, 1-1-1 Higashi, Tsukuba 305-8565 Japan.

Carbon nanohorns (CNHs) are expected to be applied to biomaterials due to their physical and biological properties. Previously, we have concentrated on CNHs and osteogenesis and documented enhancing osteogenesis under the CNH membrane[1] and promoting osteoblast differentiation by macrophages engulfing CNHs[2]. In this study, titanium was coated with CNHs due to apply for dental implants, and inflammatory cytokines and gene expression of macrophages cultured on them were analyzed.

CNHs were electrodeposited on the Ti surface (CNH / Ti). Mouse-derived monocyte macrophage-like cells (J774A-1) were cultured on CNH / Ti. SEM and TEM observations were carried out after 24 and 72 hours. The cytokines (TNFα, IL-6, IL-10) in the culture supernatant were measured by ELISA. Microarray analysis was performed using the RNA of the cells cultured for 24 hours.

By TEM observation, some CNHs was observed in the cells. The amounts of TNFα and IL-6 on CNH / Ti were significantly lower than those on Ti, and there was no significant difference in IL-10. TNFα and IL-6 are known as inflammatory cytokines secreted by M1-type macrophages to be inhibitors of bone formation. IL-10 is known as an anti-inflammatory cytokine by M2 macrophages.

Gene Ontology analysis by microarray showed genes related to transcription, repair and replication of macrophage DNA in CNH / Ti were down-regulated compared to Ti.

Therefore, CNHs on the Ti surface might regulate transcription, repair and replication of DNA of macrophage, and effect on production of inflammatory cytokines.

[1] Kasai T, Yudasaka M,Yokoyama A,et al.: Carbon nanohorns accelerate bone regeneration in rat calvarial bone defect. Nanotechnology,2011,22,065102-065110

[2] Hirata, E,Yudasaka M,Yokoyama A,et al.: Carbon nanohorns allow acceleration of osteoblast differentiation via macrophage activation. Nanoscale, 2016, 8, 14514-145

Corresponding Author: E.Hirata
Tel: +81-011-706-4270, Fax: +81-011-706-4903,
E-mail: erieri@den.hokudai.ac.jp

Unidirectional bright exciton transport in a $WS_{2x}Se_{(2-2x)}$ alloy monolayer

○Masafumi Shimasaki[1], Taishi Nishihara[1], Naoki Wada[2], Zheng Liu[3], Kana Kojima[2], Keisuke Shinokita[1], Kazunari Matsuda[1], Yasumitsu Miyata[2], Yuhei Miyauchi[1]

[1]*Institute of Advanced Energy, Kyoto University, Uji, Kyoto 611-0011, Japan*
[2]*Department of Physics, Tokyo Metropolitan University, Hachioji, Tokyo 192-0397, Japan*
[3]*Inorganic Functional Materials Research Institute, AIST, Nagoya, Aichi 463-8560, Japan*

Recently, spatial motion of two dimensional (2D) excitons in monolayer transition metal dichalcogenides (TMDCs) has attracted growing interest because 2D exciton motion plays essential roles in intriguing phenomena such as exciton valley Hall effect [1] and Halo-shaped luminescence pattern [2]. Additionally, tunable exciton transport, which is essential for exciton transistors, has been demonstrated via exciton energy modulation by applying out-of-plane electric field on interlayer excitons in vertical heterostructure MoS_2/WSe_2 [3]. These studies clearly indicate that development of the manipulation method of the 2D exciton motion offers new opportunities for both exploring fundamental physics and developing novel optoelectronic devices relying on the 2D exciton motion and interconversion of excitons and photons. However, controlling transport of intralayer bright excitons in monolayer TMDCs, which is expected to show the strongest coupling with photons among various excitonic species in TMDCs, still remains a challenge because they are hardly driven by the electric field owing to their strongly bound nature and inherent in-plane dipole.

Here, we demonstrate unidirectional transport of bright excitons in $WS_{2x}Se_{(2-2x)}$ alloy monolayer driven by exciton energy gradient due to gradual alloy composition change in one direction. The built-in exciton energy gradient was generated using tunable exciton energy in TMDC alloys [4] depending on the composition ratio. $WS_{2x}Se_{(2-2x)}$ alloy monolayers were grown on SiO_2/Si substrate using salt-assisted chemical vapor deposition method [5]. We confirmed the emergence of the unidirectional exciton energy gradient (0-22 meV/μm) over 20 μm using spatially resolved photoluminescence (PL) mapping, and then measured PL images to examine the exciton transport on the gradient. An abrupt displacement of the exciton PL spot from the excitation spot was observed at the regions with the large energy gradient, in contrast to the coincidence of the excitation and PL spots at nearly pure WS_2 and WSe_2 regions with negligible exciton energy gradient. The displacements depending on the energy gradient could be well reproduced in numerical simulations using a drift-diffusion equation; this confirms that the observed phenomena originate from non-diffusive exciton transport driven by the gradient induced force. These findings may offer new opportunities to study exciton transport related physics and facilitate development of the 2D excitonic devices.

[1] M. Onga *et al*. *Nat. Mater*. **16**, 1193 (2017).

[2] M. Kulig *et al*. *Phys. Rev. Lett*. **120**, 207401 (2018).

[3] D. Unuchek *et al. Nature* **560**, 340 (2018).

[4] X. Duan *et al. Nano Lett*. **16**, 264 (2016).

[5] H. E. Lim *et al. Nanoscale* **11**, 19700 (2019).

Corresponding Author: Y. Miyauchi

Tel: +81-774-38-3463

E-mail: miyauchi@iae.kyoto-u.ac.jp

Electronic structures of bundles of molybdenum disulfide nanotubes

○Kaoru Hisama[1], Mina Maruyama[2], Susumu Okada[2], Shohei Chiashi[1]
and Shigeo Maruyama[1,3]

[1] *Department of Mechanical Engineering, The University of Tokyo, Tokyo 113-8656, Japan*

[2] *Department of Physics, University of Tsukuba, Tsukuba 305-8571, Japan*

[3]*Energy NanoEngineering Lab., National Institute of Advanced Industrial Science and Technology (AIST), Ibaraki 305-8564, Japan*

Transition metal dichalcogenides (TMDs) can form a tubular form, owing to their two-dimensional networks with three-atom thickness. By analogy with carbon nanotubes, TMD nanotubes are expected to exhibit unusual electronic properties that are absent in their planar form. Several theoretical works reported that the electronic structures of their tubular forms depend on their chirality [1,2]. As well as the chirality, interaction with other TMD walls in bundles must cause an electronic structure modulation, because the electronic structure of planar TMD strongly depends on the interlayer interaction. However, reports on the influence of the interwall interaction in bundled and multi-walled TMD nanotubes on their electronic structure are absent to date. Therefore, we investigate the electronic structures of bundles of molybdenum disulfide nanotubes (MoS_2 NTs) using the density functional theory.

Here, we consider a bundle of (15,0) MoS_2 NTs each of which is separated by 0.3 nm vacuum spacing with its six adjacent NTs [Fig. 1(a)]. Figure 1(b) shows the calculated band structure of the bundle of (15,0) MoS_2 NTs along the high symmetry points. Along the tube direction corresponding to the Γ-A line, the dispersion relation of the bundle retains that of an isolated NT shown in Fig. 1(c). This implies that the intertube interaction is negligible. However, it is not the case if carefully checked the dispersion relation along normal direction to the NT: The highest occupied states possessed substantial band dispersion of 0.3 eV, indicating that the intertube wave hybridization is important to determine the low energy electronic properties of the bundles. Indeed, the bundle is not the direct band gap semiconductor but indirect band gap semiconductor where the valence band and the conduction band edges are located at the K and Γ points, respectively.

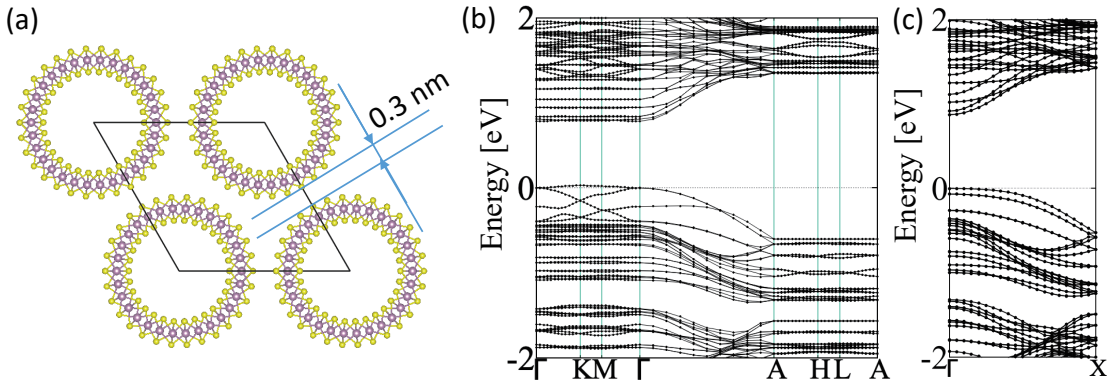

Figure 1 (a) Geometric structure of a bundle of (15,0) MoS_2 NTs with the interwall spacing of 0.3nm and electronic structures of (b) the bundle of (15,0) MoS_2 NTs and of (c) an isolated (15,0) MoS_2 NT.

[1] G. Seifert, *et al*., *Phys. Rev. Lett*. **85**, 146 (2000).[2] D. –B. Zhang, *et al., Phys. Rev. Lett*. **104**, 065502 (2010).

Corresponding Author: Shigeo Maruyama E-mail: maruyama@photon.t.u-tokyo.ac.jp

Rayleigh scattering measurement of suspended SWCNTs coaxially wrapped with BNNTs

○Satoshi Yotsumoto[1], Hayato Arai[1], Yongjia Zheng[1], Taiki Inoue[1], Rong Xiang[1], Shigeo Maruyama[1, 2], Shohei Chiashi[1]

[1]*Department of Mechanical Engineering, The University of Tokyo, Tokyo 113-8656, Japan*
[2]*Energy NanoEngineering Laboratory, National Institute of Advanced Industrial Science and Technology (AIST), Ibaraki, 305-8564, Japan*

Single-walled carbon nanotubes (SWCNTs) are one of the most promising materials for optoelectronics devices because of their unique properties, and it is known that their surrounding environment influences their physical properties. Rayleigh scattering spectroscopy [1] is a powerful method to analyze the optical properties of SWCNTs. Recently, one-dimensional van der Waals heteronanotubes which consist of SWCNTs and boron nitride nanotubes (BNNTs) are reported [2] and the BNNT is expected to work as the protect layer because of its high chemical stability. However, the influence of BNNT on the property of SWCNT is not revealed.

In this study, SWCNT-BNNT heteronanotubes were synthesized, and their Rayleigh spectra were investigated. The supercontinuum laser (the range of wavelength is 450 – 2400 nm) was used as the excitation light. Suspended SWCNTs were synthesized by fast-heating chemical vapor deposition (CVD) [3] across open slit structures (width 20 – 40 μm) fabricated on SiO_2/Si substrates. We used a thin film (~0.2 nm) of Fe as the catalyst and ethanol as the carbon source for CVD growth at 900 °C. After measuring Rayleigh scattering from pristine SWCNTs, BNNTs were synthesized by CVD using ammonia borane (NH_3BH_3) as the BNNT precursor. After BNNT growth, it was found that the optical transition energy of SWCNTs was red-shifted (Fig. 1) as a result of both increasing of the dielectric screening due to BNNT coating and decreasing of it due to desorption of water molecules.

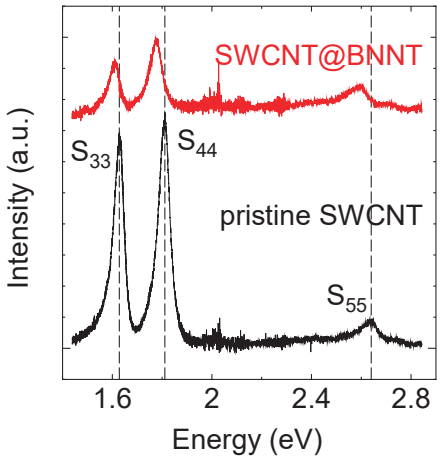

Fig. 1 Rayleigh spectra of a (28,5) SWCNT before and after BNNT growth.

[1] M. Y. Sfeir *et al.*, *Science* **306**, 1540 (2004).
[2] R. Xiang *et al.*, *Science*, in press, doi: 10.1126/science.aaz2570.
[3] S. Huang *et al.*, *Nano Lett.* **4**, 1025 (2004).

Corresponding Author: S. Chiashi
Tel: +81-3-5841-6408, Fax: +81-3-5841-6408,
E-mail: chiashi@photon.t.u-tokyo.ac.jp

Optical properties of inorganic nanotubes with different diameters

○Yohei Yomogida, Yasumitsu Miyata, and Kazuhiro Yanagi

Department of Physics, Tokyo Metropolitan University, Tokyo 192-0397, Japan

Inorganic nanotubes have a cylindrical structure of transition-metal dichalcogenide sheets and advantages for semiconductor applications because of their semiconducting properties regardless of how they are rolled. Moreover, recent studies have revealed potential applications in optoelectronics, such as high-performance photovoltaic effect [1]. Such application performance is affected by the band structure and optical properties, which is strongly dependent on their nanotube structure. Thus, it is important to understand structure-dependent optical properties. However, systematic experiment has not been investigated. Here, we prepared inorganic nanotubes with different diameters and clarified relationship between their diameters and optical properties.

Inorganic nanotubes with different diameters were prepared by two approaches: structure sorting through centrifugation [2] and synthesis via sulfurization of solution-synthesized oxide nanowires [3]. For structure sorting, inorganic nanotubes with various diameters (~100 nm in mean diameter) was used as an original sample and sorted them by density. On the other hand, the synthesis can produce relatively small-diameter WS_2 nanotubes (20 nm in mean dimeter).

Fig. 1 shows absorption spectra of the sample with different diameters. The obtained WS_2 nanotubes show optical transition peaks, including lower A-exciton peaks around 600-7

00 nm and upper B-exciton peaks around 500-600 nm. These peaks have strong correlation with diameter of the sample. The structure-sorted large-diameter sample shows longer wavelength absorption, while the synthesized small-diameter sample shows the shortest wavelength absorption. Fig. 2 shows the relationship between the diameter and absorbance peak energy. We found the absorption peak energy of A- (E_A) and B-exciton (E_B) was red-shifted with an increase in the diameter. This behavior can be understood by considering a strong coupling between the exciton and photon that is confined in cavity of inorganic nanotubes.

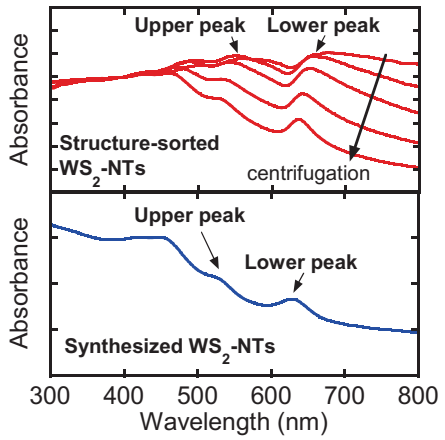

Fig. 1 Absorption spectra of WS_2 nanotubes with different diameters

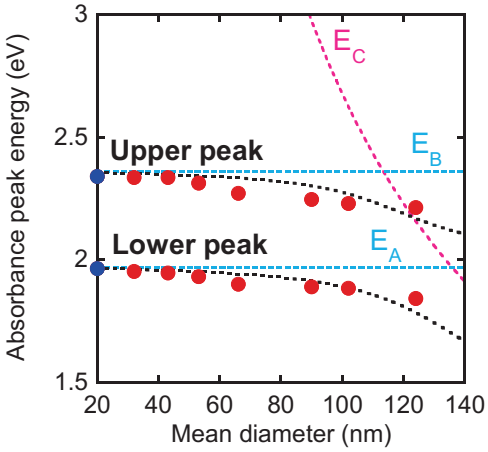

Fig. 2 Relationship between diameter and absorption peak energy.

[1] Y. J. Zhang et al, Nature 570, 350 (2019)
[2] Y. Yomogida et al, ACS Omega 9, 075001 (2018)
[3] Y. Yomogida et al, Appl. Phys. Express 12, 085001 (2019)

1P-11

Chemical vapor deposition of one-dimensional heterostructures

○Yongjia Zheng[1], Yang Qian[1], Ming Liu[1], Akihito Kumamoto[1], Yuichi Ikuhara[1], Anton Anisimov[2], Esko I. Kauppinen[3], Shohei Chiashi[1], Taiki Inoue[1], Rong Xiang[1], Shigeo Maruyama[1,4]

[1] Department of Mechanical Engineering, The University of Tokyo, Tokyo 113-8656, Japan
[2] Canatu Ltd., Konalankuja 5, FI-00390 Helsinki, Finland
[3] Department of Applied Physics, Aalto University, Otakaari 1, 02150 Espoo, FI-20742, Finland
[4] Energy NanoEngineering Lab., National Institute of Advanced Industrial Science and Technology (AIST), Tsukuba. 305-8564, Japan

In recent years researchers have focused on two-dimensional van der Waals (vdW) heterostructures, which have generated great interests recently due to the possibility of combining diverse atomic layers to create novel materials and devices [1-2]. In this work, we demonstrate a new one-dimensional structure with similar heterostructure interfaces that combines the single-walled carbon nanotubes (SWCNTs), boron nitride nanotubes (BNNTs) and Molybdenum Disulfide (MoS_2) nanotubes in the radial direction. Techniques involving direct growth of 1D vdWH by chemical vapor deposition (CVD) will be presented in detail. Ammonia borane (BH_3NH_3) as precursor was directly used to synthesize BNNTs with the aid of SWCNTs as a template by a facile CVD technique. MSNTs are synthesized on as-prepared SWCNTs/BNNTs by CVD using MoO_3 and S powders as the reactants. In Fig. 1a-d, STEM images and EELS mapping clearly show a ternary nanotube that consists of SWCNT-BNNTs-MSNTs in a coaxial structure [3]. What's more, different kinds of one-dimensional structures, such as SWCNT-BNNTs-CNTs, are also achievable using our CVD method, as shown in Fig. 1e-f. We believe these one-dimensional structures will have a broad interest and impact in many fields, which include but not limited in investigating the intrinsic optical properties of environment-isolated SWCNTs, fabricating BN-protected or gated SWCNT devices and building more sophisticated 1D material systems. It can also be used for photovoltaics and light-emitting devices when combining different kinds of transition metal dichalcogenide monolayers (TMDC) materials.

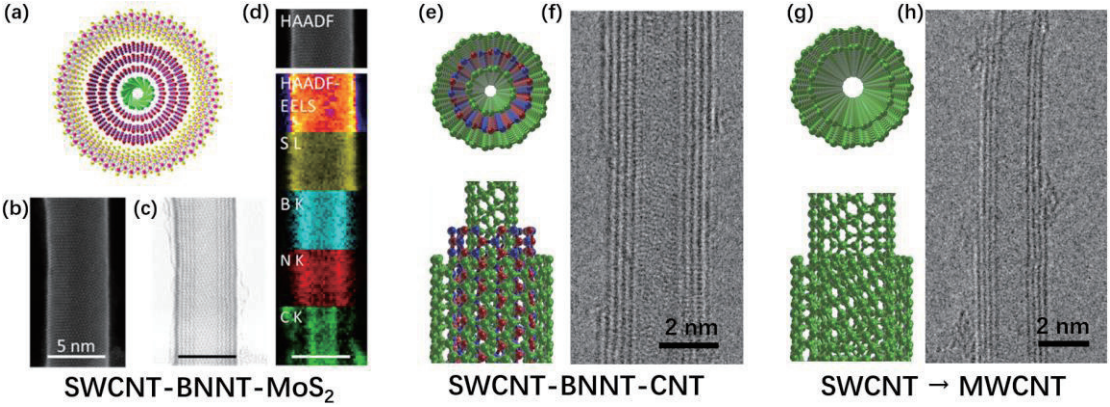

Fig. 1: (a) Atomic model, (b) HAADF-STEM image, (c) annular bright field (ABF)–STEM image and (d) EELS mapping of a 5 nm diameter ternary nanotubes consisting one layer of carbon, three layers of BN and one layer MoS_2 nanotube. Scale bar, 5 nm. (e) Atomic model and (f) TEM image of a ternary nanotubes with an inner SWCNT and outer layers of BN and carbon. (g) Atomic model and (h) TEM image of a multi-walled CNT grown from a SWCNT.

[1] D. Jariwala *et al., Nature materials,* **16,** 170 (2017).
[2] Z. Liu *et al., Nature Nanotechnology,* **8,** 119 (2013).
[3] R. Xiang *et al., Science,* accepted (2020).

Corresponding Author: S. Maruyama
Tel: +81-3-5841-6421,
Fax: +81-3-5841-6983,
E-mail: maruyama@photon.t.u-tokyo.ac.jp

Synthesis and Raman scattering spectroscopy of gas-flow oriented single-walled carbon nanotubes on hexagonal boron-nitride

○Shu Sato[1], Satoshi Yotsumoto[1], Masanori Bamba[1], Taiki Inoue[1], Shigeo Maruyama[1,2], Shohei Chiashi[1]

[1]*Department of Mechanical Engineering, The University of Tokyo, Tokyo 113-8656, Japan.*
[2]*Energy Nano Engineering Laboratory, National Institute of Advanced Industrial Science and Technology (AIST), Tsukuba 305-8564, Japan.*

It is known that the properties of single-walled carbon nanotubes (SWCNTs) are affected by the environmental conditions around them. For example, the semiconducting SWCNTs that are suspended [1] or dispersed in solution [2] emit photoluminescence (PL), while those on silicon substrate do not. On the other hand, semiconducting SWCNTs on hexagonal boron nitride (h-BN) show PL emission [3]. Recently, the synthesis of the heterostructure of SWCNTs and boron nitride nanotubes (BNNTs) [4] is reported. These complex systems of SWCNT and h-BN are interesting, however, their properties are veiled. In this study, we directly synthesized SWCNTs on h-BN based on the gas-flow oriented CVD method [5] and investigated the optical properties by using Raman scattering spectroscopy.

SWCNTs were synthesized from Fe catalyst. SEM images in Fig. 1(a, b) show the growth of gas-flow oriented SWCNTs with and without fast-heating process, which is often used for gas-oriented growth. While the fast-heating process enhanced the number of oriented SWCNTs, the enough long pre-reduction and CVD times were more important for the gas-flow oriented growth. Using the gas-flow oriented growth technique, SWCNTs were directly synthesized on exfoliated h-BN. The scanning Raman measurement (Fig. 1(c)) shows that a SWCNT was clearly lying on the surface of h-BN and that the G-band of the SWCNT on h-BN exhibited the downshift comparing to that on SiO_2 (Fig. 1(d)). The downshift was also observed from suspended SWCNT@BNNT and it might come from the interlayer interaction between SWCNTs and BNNTs.

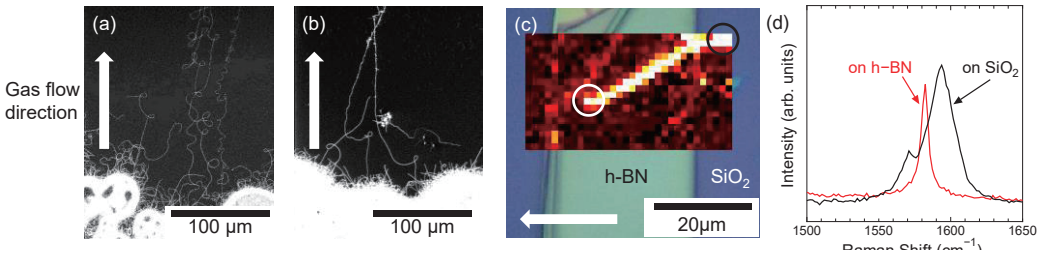

Figure 1 (a, b) SEM images of SWCNTs (a) with and (b) without using fast-heating process. (c) Scanning Raman image of the G-band intensity from SWCNT on h-BN. (d) G-band of SWCNT on h-BN (white circle of Fig.1 (c)) and on SiO_2 substrate (black circle of Fig.1 (c)).

[1] J. Lefebvre, et.al., *Phys. Rev. Let.,* **90**, 217401 (2003). [2] S. M. Bachilo, et.al., *Science*, **298**, 2361 (2002). [3] J. C. Noé, et.al., *Nano Lett.* **18**, 4136. (2018). [4] R. Xiang, et.al., *Science*, in press, doi: 10.1126/science.aaz2570. [5] S. M. Huang, et al., *Nano Letters* **4**, 1025 (2004).

Tel/Fax: +81-3-5841-6408, E-mail: chiashi@photon.t.u-tokyo.ac.jp

In-Plane Thermal Conductance of Thin Films Composed of Coaxially Combined Single-Walled Carbon Nanotubes and Boron Nitride Nanotubes

○Pengyingkai Wang[1], Yongjia Zheng[1], Taiki Inoue[1], Rong Xiang[1], Ahmed Shawky [1,2]
Makoto Watanabe[1], Anton Anisimov [3], Esko I. Kauppinen [4], Shohei Chiashi[1], Shigeo Maruyama[1, 5]

[1] *Department of Mechanical Engineering, the University of Tokyo, Tokyo 113-8656, Japan*
[2] *Nanomaterials and Nanotechnology Department, Advanced Materials Division, Central Metallurgical R&D Institute (CMRDI) P.O. Box 87 Helwan 11421, Cairo, Egypt*
[3] *Canatu, Ltd., Konalankuja 5, FI-00390 Helsinki, Finland*
[4] *Department of Applied Physics, Aalto University School of Science, 15100, FI-00076 Aalto, Finland*
[5] *Energy Nanoengineering Lab, National Institute of Advanced Industrial Science and Technology (AIST), Ibaraki 305-8564, Japan*

Carbon nanotubes (CNTs) and boron nitride nanotubes (BNNTs) are one-dimensional materials with high thermal conductivity and similar crystal structures [1, 2]. Additionally, BNNTs feature higher thermal and chemical stability in air than CNTs.

In this work, a single-walled carbon nanotube (SWCNT) film [3] was used as a template to synthesize a BNNT coating by the chemical vapor deposition (CVD) method to form a coaxial heterostructure [4]. Then, a contact-free steady-state infrared (IR) method was adopted to measure the in-plane sheet thermal conductance of the as-synthesized film [5]. The heterostructured SWCNT-BNNT film demonstrates an enhanced sheet thermal conductance compared with the bare SWCNT film. The increase in sheet thermal conductance shows a reverse relationship with SWCNT film transparency. An enhancement of over 80 % (from ~3.6 $\mu W \cdot K^{-1} \cdot sq^{-1}$ to ~6.4 $\mu W \cdot K^{-1} \cdot sq^{-1}$) is attained when the BNNT coating is applied to an SWCNT film with a transparency of 87 % as shown in Figure 1 [6]. Theoretical study on this heterostructure will be further discussed.

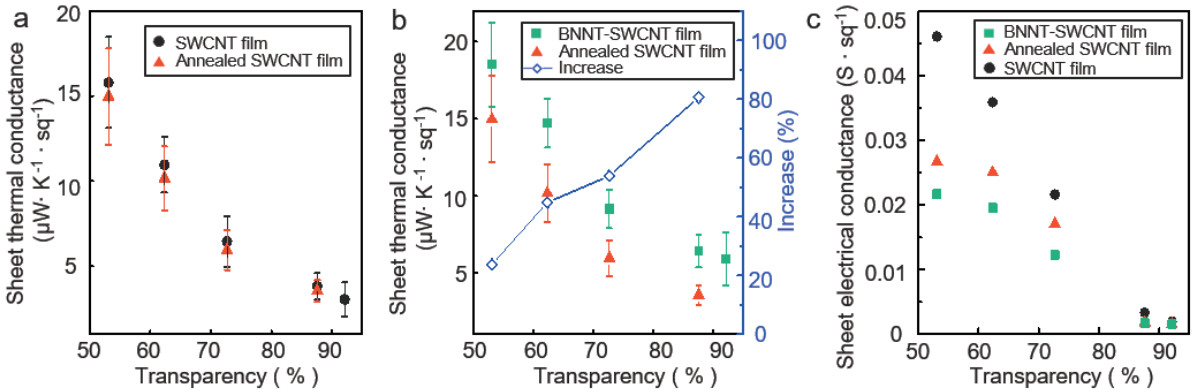

Figure 1. (a) Sheet thermal conductance of bare SWCNT films and annealed ones. (b) Comparison between annealed SWCNT films and BNNT-SWCNT films together with the increase ratio. (c) Sheet electrical conductance of bare, annealed, and BNNT-coated SWCNT films.

[1] J. Hone *et al.*, *Appl. Phys. Lett.*, **77**, 666 (2000). [2] S. Kaur *et al. Nat. Commun.*, **5**, 3082 (2014).
[3] A.G. Nasibulin *et al.*, *ACS Nano*, **4**, 5(2011).
[4] R. Xiang *et al.*, *Science*, in press, doi: 10.1126/science.aaz2570.
[5] Y. Feng *et al.*, *Jpn. J. Appl. Phys.*, **57**, 075101 (2018). [6] P. Wang *et al.*, submitted.
Corresponding Author: S. Maruyama, Tel: +81-3-5841-6421, Fax: +81-3-5800-6983,
E-mail: maruyama@photon.t.u-tokyo.ac.jp

Fabrication of ribbon-like films with highly oriented carbon nanotubes using a robotic dispenser

○Manish Pandey, Ryo Abe, Naofumi Okamoto, Yuki Sekimoto, Masakazu Nakamura

Division of Materials Science, Nara Institute of Science and Technology, 8916-5 Takayama-cho, Ikoma, Nara 630-0192, Japan

Carbon Nanotubes (CNTs) possess tremendous potential applications owing to their excellent mechanical, electrical and thermal properties [1-2]. Although experimental and theoretical studies suggest that isolated CNTs possess excellent anisotropic physical properties; however, in general, bulk CNT networks are highly random. Therefore, bulk fabrication of aligned CNT films is expected to be really important for many applications to get anisotropic and high thermal and electrical conductivity along the CNT orientation direction.

In this work, we will report a new method of fabricating the ribbon-like CNT/polymer composite films using a programmed robotic dispenser as illustrated in Fig. 1 This method can easily produce a controlled orientation of the CNTs along the length direction of the ribbon. The orientation characteristics along the length remain similar throughout the length of the film whereas width of these films and orientation intensities are interrelated and depend on the CNT composite and casting conditions which will be reported in detail. Orientation characteristics were estimated by polarized Raman mapping. These preliminary results reveal that CNTs are effectively oriented with a high degree of orientation at the center that gradually decreases towards the edges. The representative mapping of the G-band intensity ratio is shown in Fig. 2. The areas of higher intensity represent areas with highly aligned CNTs whereas areas of low intensity represent areas of randomly oriented CNTs. The thermal diffusivity of oriented films was found to be significantly higher in comparison to randomly oriented CNT films and will be reported in detail.

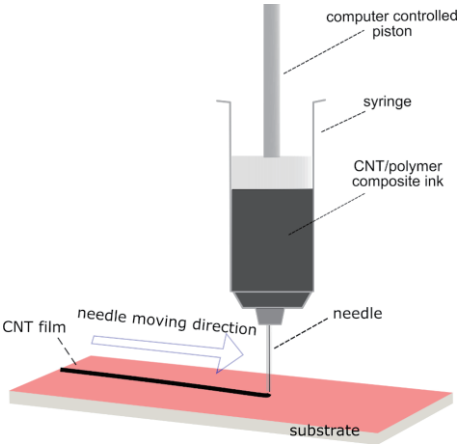

Fig. 1 Schematic of the film preparation using robot dispenser

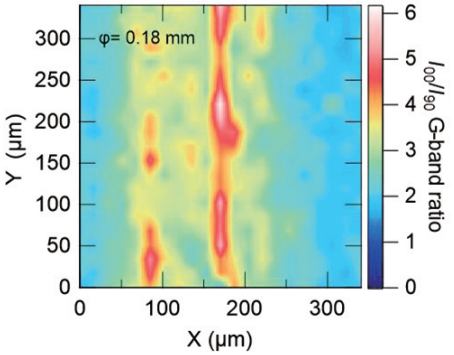

Fig. 2 Raman mapping results obtained by imaging the G-band intensity and taking their ratio with laser parallel and perpendicular to the film drawing direction.

This work was supported by JST CREST Grant Number JPMJCR18I3, Japan.

[1] Shokrieh *et al*. Mech Compos Mater **46,** 155–172 (2010).

[2] Z. Han, Alberto Fina, Progress in Polymer Science 36, 914-944 (2011).

Corresponding Author: M. Nakamura

Tel: +81- 743-72-6031, Fax: +81-743-72-6047, E-mail: mnakamura@ms.naist.jp

Phosphorescence of polyynes: A key probe for the detection of a new series of laser ablated polyyne derivatives

○Tomonari Wakabayashi[1], Nozomu Kitamura[1], Ayato Osawa[1], Daiki Okada[1], Hal Suzuki[1], Yusuke Morisawa[1], and Miho Hatanaka[2]

[1] *Department of Chemistry, Kindai University, Higashi-Osaka, Osaka 577-8502, Japan*
[2] *Institute for Research Initiatives, Graduate School of Science and Technology, and Data Science Center, Nara Institute of Science and Technology (NAIST), Ikoma 630-0192, Japan*

Laser ablation of particulate carbon in liquid organic solvents is a promising technique for production of macroscopic amounts of polyyne molecules [1]. Along with the series of hydrogen-capped polyynes, $H(C{\equiv}C)_nH$ (n = 4-9), some series of polyyne derivatives are formed as by products, e.g., methylpolyynes, $H(C{\equiv}C)_nCH_3$ (n = 5-7) [2], and cyanopolyynes, $H(C{\equiv}C)_nCN$ (n = 3-6) [3].

Phosphorescence spectroscopy is applied recently to the study of electronic transitions of polyyne derivatives embedded in cryogenic matrices [4]. We demonstrate here that phosphorescence is a key probe for the detection of a new series of polyyne derivatives with conjugate linear sp-carbon chains.

We found recently a new series of polyyne derivatives by characteristic UV absorption spectra having a peak maximum at 206, 234, 260, or 284 nm [5]. For the molecular structure, resonance-enhanced multiphoton-ionization (REMPI) mass spectroscopy, resonance Raman spectroscopy, and phosphorescence spectroscopy were examined. Fig. 1 shows a typical laser induced phosphorescence spectrum of a polyyne derivative, namely U234, isolated in a cryogenic matrix host of solid hexane at 20 K [5]. The origin band at 532 nm and the vibrational progression of ~2150 cm^{-1} are clearly seen. Lifetime of ~30 msec was derived from temporal decay of phosphorescence intensity. Fig. 2 compares the origin bands of U234 at 234 nm and 532 nm with the observed transition wavelengths for UV absorption and phosphorescence of hydrogen-capped polyynes [6].

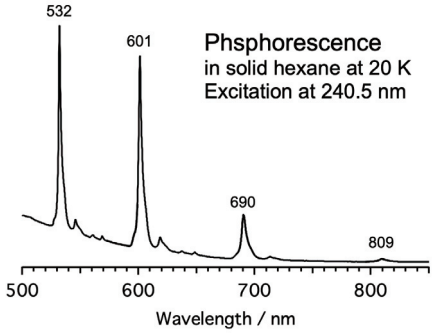

Fig. 1. Phosphorescence spectrum of a polyyne derivative U234 in a cryogenic matrix host.

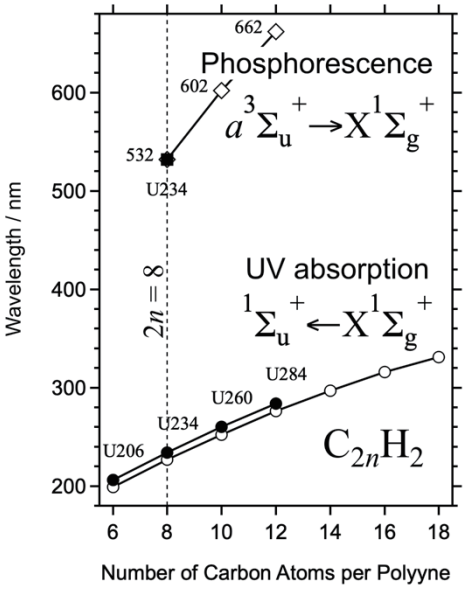

Fig. 2. Sp-carbon chain-length dependence of the electronic-transition wavelengths for hydrogen-capped polyyne molecules (open symbols) and a new series of polyyne derivatives (closed symbols).

[1] M. Tsuji et al. *Chem. Phys. Lett.* **355**, 101 (2002).
[2] Y. Wada et al. *Eur. Phys. J. D* **66**, 322 (2012).
[3] T. Wakabayashi et al. *Carbon* **50**, 47 (2012).
[4] U. Szczepaniak et al. *J. Phys. Chem. A* **122**, 89 (2019), and references therein.
[5] N. Kitamura et al. 1P-36, FNTG56, Tokyo (2019).
[6] T. Wakabayashi et al. 2P-35, FNTG55, Sendai (2018).
Corresponding Author: T. Wakabayashi, Tel: +81-6-4307-3408, E-mail: wakaba@chem.kindai.ac.jp

CuCl-Mediated Reaction of C_{60} with Propargylic Phosphate

○Asumi Ishitsuka,[1] Yutaka Maeda,[1] Michio Yamada[1]

[1] *Department of Chemistry, Tokyo Gakugei University, Koganei, Tokyo 184-8501, Japan*

Open-cage fullerenes have been attracted special interest not only as scaffolds for molecular containers in host-gest chemistry but also as precursors for endohedral fullerenes encaging small atom(s) or molecule(s) [1]. Recent studies have also showed that open-cage fullerenes are applicable for electron-accepting materials in organic photovoltaic devices [2].

Recently, we have demonstrated that transition-metal-catalyzed reactions of C_{60} and propargylic esters provided formal [2+2] and [4+2] cycloadducts via cyclization of the carbonyl group and the activated C–C triple bond of the propargylic ester in the *6-endo-dig* mode followed by cycloaddition to C_{60} [3]. During this study, we encountered an unprecedented formation of open-cage fullerenes via a one-pot CuCl-mediated reaction of C_{60} with easily accessible propargylic phosphate. In this presentation, we show that CuCl-mediated reaction of C_{60} with 1,1-dimethylprop-2-yl diphenyl phosphate (**1**) affords **2**, **3**, and **4** (Scheme 1). Notably, the yields of **2** and **4** depend strongly on the reaction conditions employed. Results also suggest that the reaction involves the formation of the phosphate to the 1,3-dienyl phosphate, which enables the reaction with C_{60} by [4+2] cycloaddition to form the cyclohexene-annulated intermediate and subsequent intramolecular *syn* elimination of the phosphodiester affords **2** as the precursor for **4**. The transformation of **2** to **4** can be explained by invoking the intramolecular [4+4] cycloaddition followed by retro-[2+2+2] cycloaddition sequence [4].

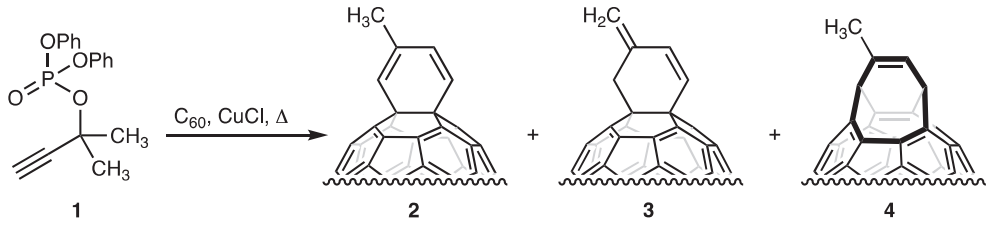

Scheme 1. CuCl-mediated reaction of C_{60} with 1.

[1] For selected reviews, see: (a) Y. Rubin Chem. Eur. J. **3**, 1009 (1997). (b) K. Komatsu et al. Chem. Lett. **34**, 886 (2005). (c) S.-i. Iwamatsu et al. Synlett **14**, 2117 (2005). (d) M. Murata et al. Chem. Commun. **46**, 6083 (2008). (e) L. Gan et al. Adv. Mater. **22**, 1498 (2010). (f) G. C. Vougioukalakis et al. Chem. Soc. Rev. **39**, 817 (2010). (g) Y. Li et al. Chem. Eur. J. **23**, 10485 (2017).

[2] (a) M. Murata et al. Chem. Commun. **47**, 7335 (2011). (b) C.-P. Cheng et al. Adv Energy Mater. **1**, 776 (2011).

[3] (a) M. Yamada et al. Org. Biomol. Chem. **15**, 8499 (2017). (b) M. Yamada et al. J. Org. Chem. **84**, 9025 (2019).

[4] M.-J. Arce et al. J. Am. Chem. Soc. **118**, 3775 (1996).

Corresponding Author: M. Yamada
Tel: +81-42-329-7493, Fax: +81-42-329-7493
E-mail: myamada@u-gakugei.ac.jp

Catalytic activity for reduction of 4-nitrophenol using on gadolinium(III) oxide nanoparticle-[C_{60}]fullerene nanowhisker composites

○Jeong Won Ko[1], Sugyeong Jeon[2], Weon Bae Ko[1,2,3]

[1] *Nanomaterials Research Institute,* [2]*Department of Convergence Science, Graduate School,*
[3]*Department of Chemistry, Sahmyook University,*
815, Hwarang-ro, Nowon-gu, Seoul 01795, Republic of Korea

Ethylamine ($C_2H_5NH_2$) was added to containing an aqueous solution of gadolinium nitrate hexahydrate ($Gd(NO_3)_3 \cdot 6H_2O$) under vigorous stirring condition. The precipitated solution was heated at 120 °C for 12 h in an oven. The resulting mixture was centrifuged several times and then washed with distilled water to obtain gadolinium hydroxide. The product was dried at 80 °C in an oven. $Gd(OH)_3$ was annealed to obtain Gd_2O_3 in an electric furnace at 700 °C for 4 h under argon atmosphere [1]. Gadolinium(III) oxide nanoparticle-[C_{60}]fullerene nanowhisker composites were synthesized using gadolinium(III) oxide nanoparticle solution, C_{60}-saturated toluene and isopropyl alcohol by the liquid liquid interfacial precipitation (LLIP) method [2]. The final product of gadolinium(III) oxide nanoparticle-[C_{60}]fullerene nanowhisker composites was characterized by X-ray diffraction, scanning electron microscopy, Raman spectroscopy, and transmission electron microscopy. The catalytic activity of their hybrid nanocomposites was investigated in the reduction of 4-nitrophenol by UV-vis spectroscopy. The kinetics study of catalytic activity for reduction of 4-nitrophenol was followed a pseudo first-order reaction.

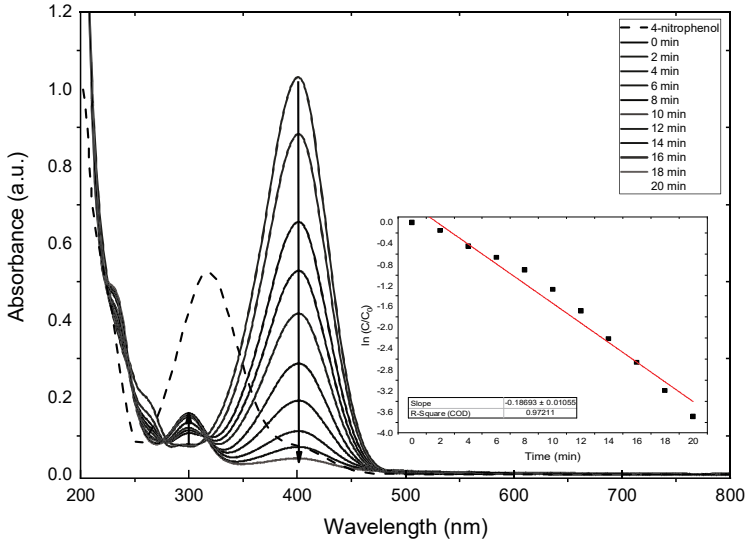

Fig.1 UV-vis spectrum and kinetics study for reduction of 4-nitrophenol with gadolinium (III) oxide nanoparticle-[C_{60}]fullerene nanowhisker composites

[1] J. Kang, B. Min, Y. Sohn, Ceram. Int. 41, 1243-1248 (2015).

[2] K. Miyazawa *et al.* Surf. Eng. doi.org/10.1080/02670844.2017.1396779 (2017).

Corresponding Author: W. B. Ko

Tel: +82-2-3399-1700, Fax:, +82-2-979-5318,

E-mail: kowb@syu.ac.kr

Reactions of *S*-Heterocyclic Carbenes with Fullerenes: Preparation and Characterization of Dithiomethano-derivatives

○Yuta Maeda[1], Shinji Kanzawa[1], Masahiro Kako*[,1], Michio Yamada[2], Yutaka Maeda[2], Makoto Furukawa[3], Takeshi Akasaka*[,2,3,4]

[1] *Department of Engineering Science, The University of Electro-Communications, Chofu 182-8585, Japan*
[2] *Department of Chemistry, Tokyo Gakugei University, Tokyo 184-8501, Japan*
[3] *Foundation for Advancement of International Science, Tsukuba, Ibaraki 305-0821, Japan*
[4] *School of Materials Science and Engineering, Huazhong University of Science and Technology, Wuhan, Hubei 430074, P. R. China*

Endohedral metallofullerenes (EMFs) have been the focus of extensive research because of their remarkable structures and properties. To date, a number of studies have been carried out to develop exohedral functionalization of EMFs, which will open up various applications such as molecular electronics and biomedicines.

The methano-bridge formation is one of the most frequently employed reactions for functionalization of EMFs. Until now, many methanofullerenes have been reported using the Bingel-Hirsch reaction, reactions of carbenes and diazoalkanes, electrochemical synthesis, the radical malonate addition, and zwitterion addition.[1] For example, $M_3N@I_h$-C_{80} (M = Sc, Y, and Lu) reacted with carbenes to afford two regioisomeric methanofullerenes.[2] As a part of our continuing study on the carbine addition of fullerenes, we previously reported the reaction of a *S*-heterocyclic carbene (SHC)[3] with C_{60} to produce the corresponding [6,6]-closed methanofullerene. Nevertheless, the synthetic efficiency of the precursor of the SHC was not sufficient to study the properties of SHCs. Although *N*-heterocyclic carbenes (NHCs) have been extensively studied for the application to catalysts or ligands for metallic complexes, examples of cyclic carbenes containing other heteroatoms such as phosphorus and sulfur are extremely sparse compared with those of NHCs.

We now report the methano-derivatives of fullerenes using novel SHCs generated by synthetically more accessible precursors. The reaction of disilene to CS_2 produced the corresponding SHC **1**, which reacted with $Sc_3N@I_h$-C_{80} to afford the corresponding [6,6]-open methano-bridged derivative **2**.[4] Similar SHC derivatives were also obtained for C_{60} and C_{70}. The details of electronic properties of these adducts will be discussed on the basis of electrochemical measurements and the density functional theory calculations.

Scheme 1.

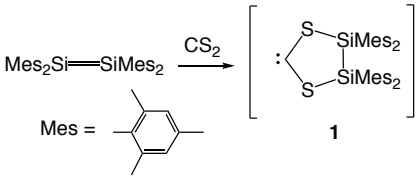

Scheme 2.

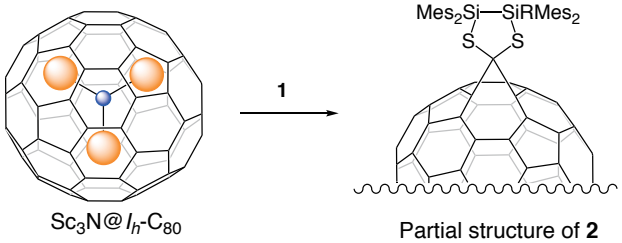

[1] M. Yamada *et al.* Chem. Rev. **113**, 7209–7264 (2013). [2] M. Yamada *et al.* Chem. Eur. J. **23**, 6552–6561 (2017). [3] H. Nikawa *et al.* Angew. Chem. Int. Ed. **117**, 7739–7742 (2005). [4] M. Kako, *et al.* Helv. Chim. Acta **102**, e21477 (2019).

Corresponding Author: Masahiro Kako Tel: +81-42-442-5570. E-mail: kako@e-one.uec.ac.jp

Research of Fracture Behavior of CNT/HDPE Composites *via* Melt Blending

○Koichi Utsugi[1], Nao Otsuki[1], Masaru Sekido[2]

[1]*Advanced Course of Production System Engineering, National Institute of Technology, Sendai College, Natori 981-1239, Japan*

[2]*Department of Materials and Environmental Engineering, National Institute of Technology, Sendai College, Natori 981-1239, Japan*

CNTs are considered as the ideal reinforcement fillers for the nanocomposite materials due to their outstanding mechanical properties, such as tensile strength, light weight, and low density. Last year we have reported tensile strength of CNT/high density polyethylene (HDPE) composites prepared by Melt Blending. As a result, the fracture strain decreased as the weight ratio of CNTs was increased [1]. Aggregation of CNTs was not observed from the composite [2]. In this work we investigated the reason why the fracture strain of CNT/HDPE composites was decreased by observing the crystal state of HDPE.

In this report the crystal state of HDPE was studied using a differential scanning calorimetry (DSC) to measure crystallinity of the composite. The difference between thermal analysis of cross section and fracture surface depending on the different weight ratio of CNT/HDPE was measured by DSC (Fig. 1). Crystallinity of HDPE increased as the weight ratio of CNTs was increased. Crystallinity of 4.8wt.% MWNT composites was 2.7% higher than 2.9wt.% MWNT composites. It is suggested that the cause of the decrease in fracture strain is not due to decreased of the crystallinity for base material.

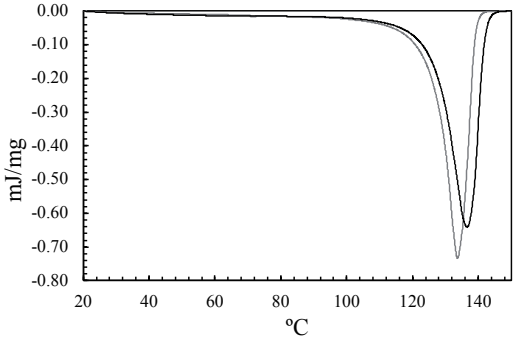

Fig. 1 DSC chart of cross section for MWNT/HDPE composites. gray is 2.9wt.%MWNT. black is 4.8wt.%MWNT.

[1] Atsushi Onodera *et al.,* The 54th fullerenes-Nanotubes-Graphene General Symposium, 1P-11(2018)

[2] Koichi Utsugi *et al.,* The 56th fullerenes-Nanotubes-Graphene General Symposium, 2P-19(2019)

Corresponding Author: Koichi Utsugi

Tel: +81-22-381-0329, Fax: +81-22-381-0329

E-mail: a1912605@sendai-nct.jp

Preferential stability of carbon nanotubes with sub-nm diameter under linearly polarized laser irradiation: An *ab initio* TDDFT study

○Yoshiyuki Miyamoto[1]

[1] *Research Center for Computational Design of Advanced Functional Materials, National Institute of Advanced Industrial Science and Technology (AIST), Central 2, 1-1-1 Umezono, Tsukuba 305-8568, Japan*

Carbon nanotubes (CNTs) with diameters less than 1 nm are thermally [1] and chemically [2] unstable compared to those with larger diameters. However, in this work, survival of such thin CNTs under irradiation with ultra-short pulse laser is demonstrated. Diameter thinning of CNTs by laser shot was reported [3], and those CNTs contained vacancies which resulted in structural defects after the thinning. On the other hand, this work targets vacancy-free CNTs.

For demonstrating the preferable stability of thin CNTs, first-principles molecular dynamics (MD) simulation based on the time-dependent density functional theory (TDDFT) was performed under a laser irradiation by using fictitious model of one-dimensional alternating array of (8,0) and (14,0) CNTs or (5,5) and (8,8) CNTs. When polarization of the laser field is set perpendicular to tube axes, the CNTs with larger diameters are destroyed while those with smaller diameter survive, as seen in snapshot of Fig. 1 for a case with (8,0) and (14,0) CNTs [4]. The assumed laser conditions were the pulse-width 10 fs, wavelength 800 nm, and the maximum field intensity 5 V/Å with corresponding fluence 3.32 J/cm^2.

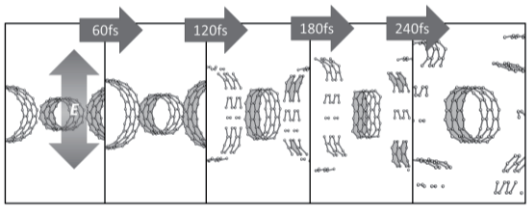

Fig.1 Snapshot of TDDFT-MD simulation of (8,0) and (14,0) CNT arrays under laser shot with a polarization as indicated by a vertical arrow in the left most panel.

The background physics of this selection is polarization direction of the laser field that makes the tangential area of CNT wall along with the laser field larger with larger diameters. More details will be discussed in the presentation of this work.

This work was performed with support from the NEDO project “Development of advanced laser processing with intelligence based on high-brightness and high-efficiency laser technologies” (TACMI project).

[1] M. Terrones, *et al*. Science, **288**, 1226 (2000).
[2] W. Zhou, *et al*. Chem. Phys. Lett **350**, 6, (2001).
[3] Y. Zhang, Z. Shi, Z. Gu, and S. Iijima, CARBON, **38**, 2055 (2000).
[4] Y. Miyamoto, *in preparation*.

Corresponding Author: Y. Miyamoto
Tel: +81-29-849-1498, Fax: +81-29-861-3171,
E-mail: yoshi-miyamoto@aist.go.jp

Synthesis of carbon nanotubes on nanozirconia-dispersed carbon paper

○Dai Goudo, Nobutomo Yamaguchi, Kiyofumi Yamagiwa

Graduate School of Science & Engineering, Teikyo University of Science, Adachi, Tokyo 120-0045, Japan

Carbon nanotubes (CNTs) are promising for use in electrode materials, such as conductive agents and catalyst supports, because of their morphological characteristics and high conductivity. Electrodes are generally produced by coating a substrate (e.g., carbon paper (CP)) with a slurry of the electrode material. A typical drawback of CNTs as electrode materials is their low dispersibility in the slurry, leading to localization of CNTs on the electrodes. This drawback can be addressed by homogeneous direct synthesis of CNTs on CP, which can also result in improvements to the electrode surface area. In this study, CNTs were synthesized on CP by chemical vapor deposition (CVD) with camphor. In particular, zirconia nanoparticles (nanozirconia) were dispersed on the surface of CP before the synthesis to examine its effects on CNT growth.

Small pieces of CP (Toray TGP-H-120) were dipped in 0.3% and 30% nanozirconia dispersion liquid, and used as substrates after drying (0.3%-Zr/CP, 30%-Zr/CP, respectively). CVD was carried out using camphor ($C_{10}H_{16}O$) and ferrocene as the carbon source and the catalyst precursor, respectively. The syntheses were performed at 750°C for 15 min under flowing Ar gas.

In the case of as-supplied CP as the substrate, a small quantity of carbonaceous material was deposited inhomogeneously on the surface. In contrast, when 0.3%-Zr/CP was used as the substrate, a large number of CNTs were observed, as shown in Fig. 1. This result indicates that the formation of Fe catalyst nanoparticles from ferrocene was promoted by the effects of dispersed nanozirconia on the surface. However, no specific product was confirmed in the case of 30%-Zr/CP, suggesting that a moderate amount of nanozirconia dispersed on the surface is critical for the promotion of CNT growth.

Detailed characterizations, including electrochemical characteristics, will be discussed in the presentation.

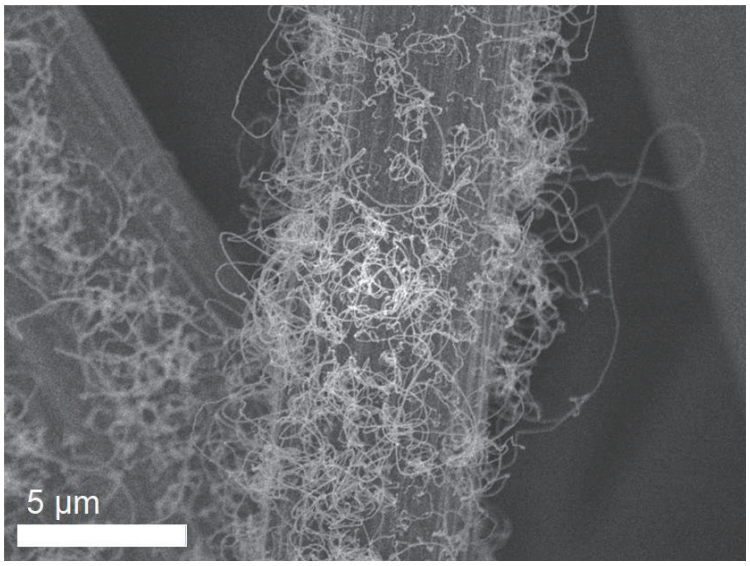

Fig. 1. Scanning electron microscopy image of CNTs grown on nanozirconia-dispersed carbon paper.

Corresponding Author: K. Yamagiwa
Tel: +81-3-6910-1010
E-mail: yamagiwa@ntu.ac.jp

Scalable Synthesis of Atomically Precise Graphene Nanoribbons in Metal–Organic Framework

○Takashi Kitao[1,2], MacLean W A Michael[2], Kazuki Nakata[2], Takashi Uemura[1,2,3]

[1]*Graduate School of Engineering, The University of Tokyo, 5-1-5 Kashiwanoha, Kashiwa, Chiba 277-8561, Japan*
[2]*Graduate School of Frontier Sciences, The University of Tokyo, 5-1-5 Kashiwanoha, Kashiwa, Chiba 277-8561, Japan*
[3]*CREST, Japan Science and Technology Agency (JST), 4-1-8 Honcho, Kawaguchi, Saitama 332-0012, Japan*

Graphene nanoribbons, defined as nanometer-wide stripes of graphene, have attracted significant attention as candidates for next-generation semiconductor materials. The structural perfection of GNRs is an essential issue because their physical properties are critically dependent on nanoribbon's width and edge geometry. In this regard, simple and effective fabrication methods for atomically precise GNRs should be developed not only for fundamental research but also for their future applications in advanced opt-electronic devices. However, the widespread implementation of GNRs into the various devices has yet to be realized, as methods for the synthesis of GNRs in precise and scalable fashion are currently lacking.

Metal–organic frameworks (MOFs), porous materials formed through the self-assembly of metal ions and organic ligands, have been applied to a variety of applications, including gas storage, separation, and catalysis. MOFs have the advantages of the tunable and regulated nature of their nanospaces and have been shown to provide an ideal compartment for controlling the arrangement of guest species through the geometrical constraint of host pores, as well as non-covalent interactions between host and guest.[1] Here, we exploited a new method that circumvents the issues surrounding the synthesis of GNRs utilizing the MOFs as a template. A series of characterizations of the GNR, including NMR, UV/vis/NIR, and Raman spectroscopy measurements, confirmed the formation of the GNR with well-controlled edge structure and width (Fig. 1).[2]

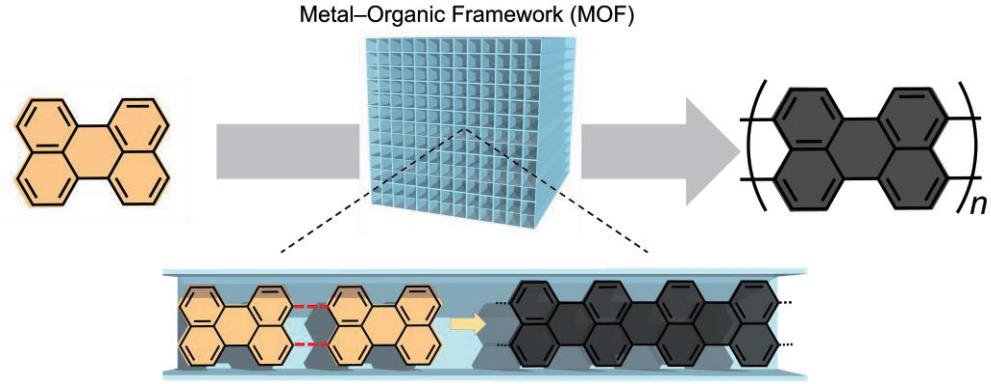

Fig. 1. Schematic image for preparation of an atomically precise GNR using a MOF as template.

[1] T. Kitao, T. Uemura *et al*. *Chem. Soc. Rev*. **2017**, *46*, 3108-3133.
[2] T. Kitao, T. Uemura *et al*. *submitted.*
Corresponding Author: T. Kitao
Tel: +81-4-7136-3791, Fax: +81-4-7136-3792,
E-mail: kitao@edu.k.u-tokyo.ac.jp

Direct precipitation growth of multi-layer graphene using W capping layer -Dependence of growth atmosphere-

○Jumpei Yamada[1], Yuki Ueda[1], Takahiro Maruyama[2], and Shigeya Naritsuka[1]

[1]Department of Materials Science and Engineering, Meijo University, Nagoya 468-8502, Japan
[2]Department of Applied Chemistry, Meijo University, Nagoya 468-8502, Japan

Recently, graphene growth on an insulating substrate has been frequently studied as an alternative method without using the transfer process. We have succeeded in the direct growth of multilayer graphene using a W capping layer in a high vacuum [1]. In this study, in order to develop its application fields, a precipitation method was also studied at atmospheric pressure.

W(20nm) / a-C(5nm)/ Ni(300nm) layers were deposited on a sapphire substrate using electron-beam deposition. These samples were annealed at 900 °C for 30min in atmospheric pressures of nitrogen (N_2:1000 [ml/min]) and nitrogen and hydrogen mixed gas (N_2:1000 [ml/min]+H_2:20 [ml/min]). After the annealing, the catalyst layers were removed to directly obtain the graphene on the substrate.

Fig.1 (a) shows the Raman spectrum of the sample annealed under N_2 atmosphere without graphene signals. The catalytic metals were observed to be oxidized by the residual oxygen in the ambient. As a result, graphene did not grow. In contrast, in the case of mixed gas, multilayer graphene was directly grown on the substrate. The G and G '(2D) peak were observed on the Raman spectra in Fig.1 (b), which indicates graphene was successfully precipitated on the substrate. This is probably because the mixing hydrogen was useful to suppress the etching effect of residual oxygen. Finally, we succeeded in the direct growth of multilayer graphene at atmospheric pressure by using a mixed gas of N_2 and H_2.

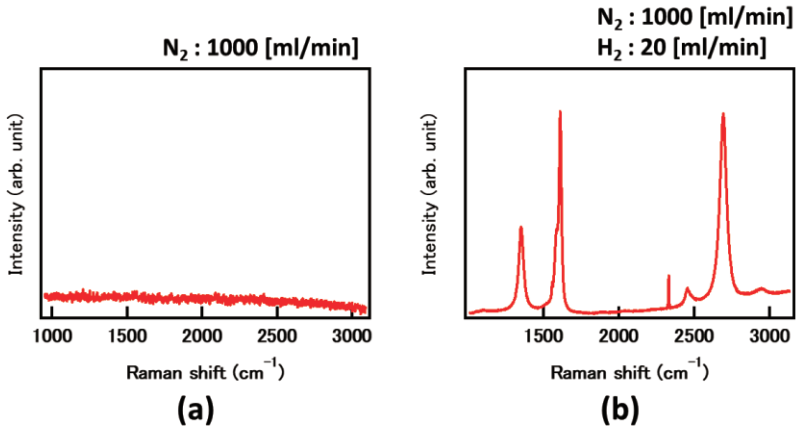

Fig.1 Raman spectrum of grown samples with (a) unmixed N2 gas, and (b) mixed gas of N2 and H2

Reference: [1] J. Yamada et al. J. Appl. Phys. 55,100302 (2016).

Acknowledgement: This work was supported in part by JSPS KAKENHI Grant Numbers 2660089, 15H03558, 26105002, 25000011.

Corresponding Author: Jumpei Yamada, **E-mail**:jjjjjjyyyyyy119@gmail.com

1P-24

NO_x adsorption dynamics on Nanographene assembly system

○Y.Hikage[1], S.Nishijima[1], K.Takai[1,2]

[1]*Graduate school of Science and Engineering, Hosei University, Tokyo 184-8584, Japan*
[2]*Department of Chemical Science and Technology, Hosei University, Tokyo 184-8584, Japan*

Activated Carbon Fibers (ACFs) consisting of 3D random network of nanographenes having localized spins induced by the edge-state on the zigzag part of its periphery are useful to remove removing NO_x pollutants due to its chemical activity and nanopore between nanographenes giving high specific surface area [1, 2]. The major species in the vicinity of the source of NO_x such as coal-fired power plants is NO molecule having spin moment (S=1/2). In this study, NO adsorption and chemical reactivity in ACFs under atomospheric condition are evaluated in terms of the presence of ambient water molecule adsorbed inside nanopore, whre the spin magnetism is used as a prove to track the adsorption daynamics of NO molecule into ACFs.

ACFs (FR-20, Kuraray) was vacuum-heated at 473 K for 30 min at 10^{-4} Pa (**ACF-HT**) and NO gas was introduced at a partial pressure of 2 kPa (**ACF-NO**), followed by evacuation down to 10^{-4} Pa (**ACF-NO-VAC**). XPS, SEM-EDS were measured by Phi5600 and SU8020, respectively. X-band ESR and SQUID magnetometer measuremernts are carried out by JEOL FA-300 at room temperature and QD-MPMS-1 at 2 - 300 K under 0 - 10000 Oe.

SEM image and EDS mapping of the fracture surface of **ACF-NO** confirmed adsorbed NO exist as nitrogen compounds uniformly distibuted inside ACFs as well as the surface (Fig. 1 (a) (b)). In the XPS N1s spectrum shown in Fig. 1 (c), the peak derived from NO_3 clealy emerges after NO adsorption. Fig. 2 shows the magnetization curves of **ACF-HT** and **ACF-NO-VAC**. By adsorption NO, the magnetization is reduced by 39%, which is similar to the difference in the ESR intensity for **ACF-HT** and **ACF-NO-VAC**. This indicates that ACFs and NO is chemically bond and cancel the edge-state spins. However, linewidth of the ESR spectrum increases sharply at the instance of the introduction of NO molecules due to dipolar interactions between edge-state spins of ACFs and adsorbed NO molecules, suggesting the physisorption of NO moleucle at the initial stage of the adsorption.

[1] T. Shimohara et al, *J. Jpn. Soc. Atmospheric Env.*, 48, 65-73 (2013).

[2] Fujita et al, *J. Phys. Soc. Jpn*, 65, 1920-1923 (1996).

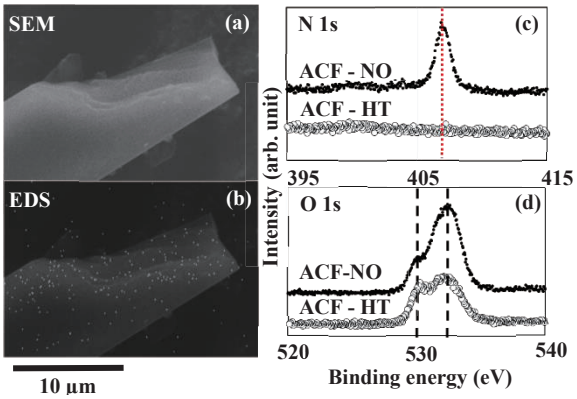

Fig. 1 SEM and EDS images after NO adsorption and XPS spectra about **ACF-HT** (○) and **ACF-NO** (●)

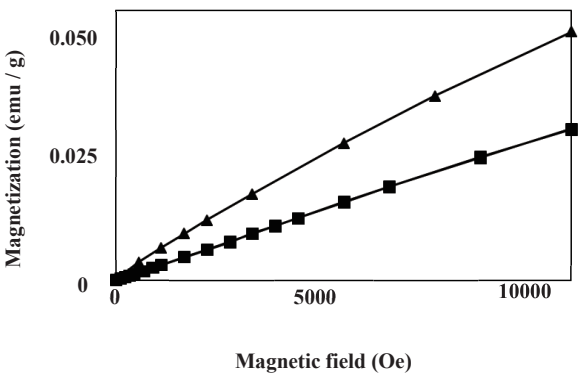

Fig. 2 Magnetic susceptibility for **ACF-HT** (▲) and **ACF-NO-VAC** (■)

Corresponding Author: Kazuyuki Takai
Tel: +81-42-387-6138, Fax: +81-42-387-7002

Correlation between chemical structure and catalytic activity of graphene oxide

○Ryutaro Suzuki[1], Takuya Isaka[1], Kentaro Tajima[1], Kana Nakahara[2], Yoshiaki Matsuo[3], Nobuyuki Akai[2], Kazuyuki Takai[1]

[1]Hosei Univ., [2]Tokyo Univ. of Agric. and Tech., [3]Univ. of Hyogo

In this study, two kinds of graphene oxide (**HGO** and **BGO**) was synthesized by the Hummers [1] and Brodie [2] methods respectively, and the correlation between their chemical structure and chemical activity was evaluated. Previous studies have shown that **HGO** has many carboxy and hydroxy groups, and **BGO** has many epoxy groups [3]. When the epoxy group is introduced, the symmetry of the AB sublattice of graphene is maintained, but the symmetry is broken in the case of attaching the hydroxy group or carboxy group, because they bond to only one of the AB sublattice sites. Therefore, the electronic state that causes the localized spin magnetism appears in the Fermi energy (E_F), suggesting that the catalytic activity of **HGO**, **BGO** was significantly different. In this study, an amine oxidation coupling reaction to obtain N-Benzylidenebenzylamine from Benzylamine was carried out with adding **HGO** and **BGO** as catalyst to evaluate the chemical activity of GOs.

Table 1 Amount of π conjugation of HGO and BGO

Sample	π conjugation (g / L)
HGO	2.61
BGO	0.62
Graphite	4.56

HGO and **BGO** was synthesized by the Hummers method in which graphite is oxidized using concentrated sulfuric acid and potassium permanganate, and Brodie method using fuming nitric acid and potassium chlorate, respectively.

The oxidative coupling reaction of amine was performed by adding **HGO** (**BGO**) sample as a catalyst to Benzylamine and stirring for 24 h while heating at 60 °C to synthesize N-Benzylidenebenzylamine.

Table 1 shows the amount of π-conjugated system in GO dispersion obtained by using empirical formula [4], which can evaluate the amount of π conjugated system of GO from the absorbance of UV-vis measurement at 660 nm. The π conjugated systems were more destroyed in **BGO** than those in **HGO**. This proved that the oxidation by the Brodie method had more epoxy groups that formed more sp^3 bonds that destroyed the π conjugated system.

Table 2 shows the conversion of Benzylamine and the molar ratio of a by-product, Benzaldoxime. **HGO** catalyst has lower Benzaldoxime yield despite higher Benzylamine conversion than **BGO** catalyst. Thus, **HGO** and **BGO** follow different reaction pathways based on the structural difference. Investigation of the correlation between active species in graphene oxide and catalytic activity in this way can enable the invention of a new green catalyst with selectivity.

Table 2 Molar ratio of byproduct and Conversion for HGO and BGO catalyst

Catalyst	GC-Yield (Molar ratio)	Conversion (%)
HGO	1	40
BGO	2.8	26
No catalyst	0	-

[1] D.C. Marcano et al, ACS Nano, 4, 4806 - 4814 (2010)

[2] B.C. Brodie, Phil. Trans. R., Soc. Lond., 149, 249 - 259 (1859)

[3] K.Tajima et al, Polyhedron, 136, (2017)

[4] Coleman et al, Nat. Nanotechnol September, 3 (2018)

Investigation of surface potential variations of thermally reduced graphene oxide

○K. Kanishka H. De Silva, Shuhei Ogawa, Pamarti Vishwanath, Masamichi Yoshimura

Graduate School of Engineering, Toyota Technological Institute, Nagoya 468-8511, Japan

Fabrication of graphene by the reduction of graphene oxide (GO) is one of the most widely studied topics due its ability of bulk production of graphene with controllable properties that can be assigned to a vast range of applications [1]. Investigation of local electronic properties of graphene and its derivatives, such as work function (WF) and surface potential (SP), is necessary for applications based on electronic devices. Kelvin probe force microscopy (KPFM) is widely used for mapping the surface potential of graphene-based materials [2]. However, depending on the properties of graphene and GO, such as amount of oxygen containing groups, number of layers, and heteroatom doping, and also on KPFM measurement conditions (humidity, mode of measurement, etc.), WF and SP values show a discrepancy [3]. Here, we focus on the SP variation of GO sheets upon thermal reduction by carrying out the KPFM measurements under same environmental conditions. For comparison, KPFM measurement of pristine graphene grown by chemical vapour deposition was also done (not shown here).

The GO flakes were deposited on SiO_2 (300 nm)/Si substrates (S) by spin coating. Thermal annealing of GO was done at 800 ºC for different times such as 5 min, 10 min, 20 min, and 30 min. Then, topography and the SP were measured at the same place and the WF was calculated.

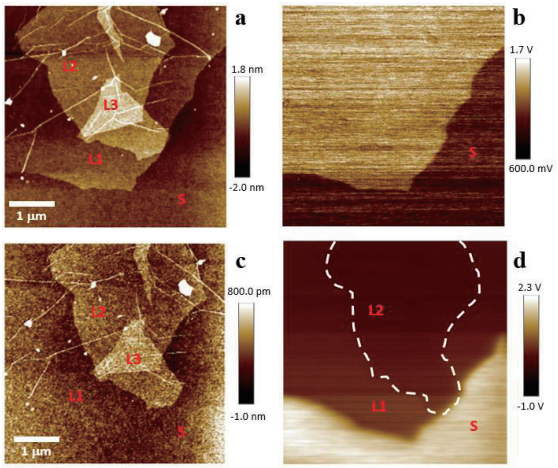

Fig.1. AFM height and potential images of GO (a and b) and GO after annealed for 5 min (c and d).

Figures 1(a) and 1(c) show the atomic force microscopic (AFM) height images of GO and GO after annealed for 5 min. The layers (L1, L2, L3) have been preserved after the thermal treatment except for the reduction in thickness from 1 nm to 0.4 nm due to the removal of oxygen functionalities. Figures 1(b) and 1(d) are the corresponding potential images. In the potential image of GO, there is no clear contrast among layers due to its insulating nature associated by oxygen functionalities. In contrast, even after 5 min of annealing, difference in potential of L1 and L2 is clearly visible (L2 is outlined) indicating the change in electronic properties. However, L3 cannot be seen clearly because of the screening effect [2]. The calculated WF of L1 was varied from 5.38 eV to 4.75 eV after annealing for 5-30 min. These results demonstrate that graphene with tunable electronic properties can be obtained by controlling the reduction conditions.

[1] K.K.H. De Silva *et al*. Appl. Surf. Sci. **447**, 338 (2018).
[2] Lee *et al*. Appl. Phys. Lett. **95**, 222107 (2009)
[3] V. Panchal *et al*. Sci. Rep. **3**, 2597 (2013)

Corresponding Author: K.K.H. De Silva
Tel: +81-52-809-1852
E-mail: sd16501@toyota-ti.ac.jp

Adsorption effects of molecular Hydrogen on the electronic transport properties of Graphene

○Y. Shigehisa[1], Y. Obata[1], Y. Ishiguro[2], K. Takai[1, 2]

[1] *Dept. Applied Chemistry, Hosei University, Tokyo 184-8584, Japan*
[2]*Department of Chemical Science and Technology, Hosei University, Tokyo 184-8584, Japan*

Molecular hydrogen adsorption is one of the most important examples in terms of applications for the transistor devices accompanied with band gap opening technology and hydrogen storage materials. Meanwhile, defect-introducing is one of the interesting strategies to give additional adsorption sites to graphene in view of enhancing the interactions between hydrogen and graphene [1]. In this study, we investigated carrier doping and scattering caused by molecular hydrogen adsorption before and after defect-introducing into graphene by Ar^+ beam irradiation by means of electric conductivity measurement.

A field effect transistor using graphene obtained by exfoliation of graphite (g-FET) was fabricated on SiO_2 / Si substrate. Time dependence of the electrical conductivity for the g-FET was measured after annealing in a vacuum chamber followed by hydrogen adsorption (1 atm) at room temperature (**NoDefect**). For defect-introduced graphene, atomic vacancies were introduced into the surface of g-FET by Ar^+ beam irradiation at 100 eV after annealing, followed by exposing to hydrogen molecules (**Defect+H_2**).

The charge neutral point (V_{CNP}) where the minimum conductivity appears in a g-FET exhibits no significant shift from 0.5 h after the molecular hydrogen adsorption up to 6 h (**NoDefect**). In contrast, V_{CNP} shift by molecular hydrogen adsorption on defect-introduced graphene was -25 V (**Defect+H_2**). Moreover, V_{CNP} shift by following evacuation was very small (Vacuum). The observed shifts indicate the strong chemical adsorption by molecular hydrogen adsorption. These results suggest that defect-introducing to graphene is important to provide additional adsorption sites for efficient molecular doping.

[1] G. Sunnardianto,et al, *Int. J. Hydrogen Energy,* **43** (2017).

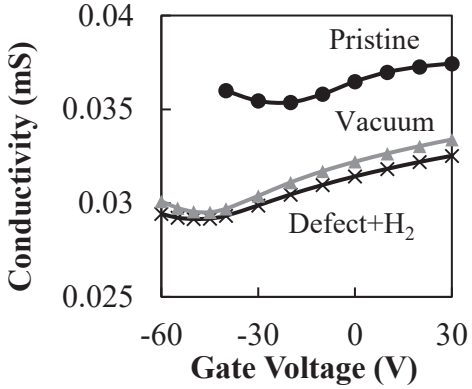

Fig. 1 Effects of H_2 adsorption on the transfer curve of g-FET that irradiated by Ar^+ beam

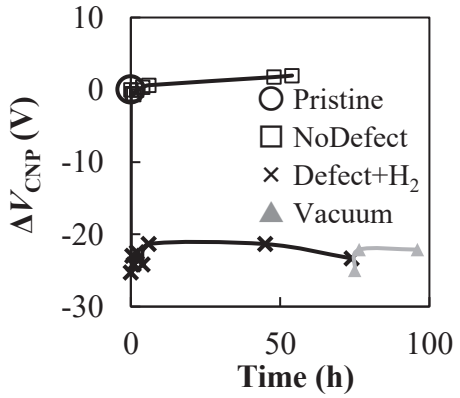

Fig. 2 Time evolution of ΔV_{CNP} upon H_2 adsorption and after evacuation

Multi-ferroic response of two-dimensional hexagonal materials

F. R. Pratama[1], M. S. Ukhtary[1], R. Saito[1]
[1]Department of Physics, Tohoku University, Sendai 980-8578, Japan

Two-dimensional (2D) hexagonal materials, such as silicene & MoS_2 have promising applications in next-generation electronics. Researches in the magnetic properties of the 2D materials are growing in the field of magneto-electronics and spintronics to realize devices with low energy consumption [1,2].

Recently, a theoretical study on the magnetic susceptibility of massive 2D Dirac systems in low temperature has been performed by Koshino and Ando [3], in which they found that the magnetic susceptibility is non-zero when the Fermi energy is smaller than the band gap. This property appears due to the spin and valley degeneracy in the Landau levels. However, in the case of silicene, the Landau levels are non-degenerate for each spin direction at the K and K' valleys due to the strong spin-orbit coupling. Moreover, the energy gap of silicene is tuneable by an external electric field perpendicular to the 2D plane [4]. Thus, we expect that the *magnetic* susceptibility can be controlled by the *electric* field.

In this study, we calculate the magnetic susceptibility of silicene for a given temperature as a function of electric field. First, we show the formation of the Landau levels around the K and K' points as a function of the external electric and magnetic fields. By obtaining the Landau levels, we calculate the thermodynamic potential, magnetization, and magnetic susceptibility of the system. We expect to find the temperature range in which the magnetic susceptibility can be effectively controlled by the electric field and address the role of spin-orbit coupling.

References:

[1] A. M. Tokmachev *et al*, Nat. Commun. **9**, 1627 (2018).
[2] M. Gilbertini *et al*, Nat. Nanotechnol. **14**, 408 (2019).
[3] M. Koshino and T. Ando, Solid State Commun. **151**, 1054 (2011).
[4] M. Ezawa, Phys. Rev. B **86,** 161407(R) (2012).

Carrier-dependent photoluminescence properties of CVD-grown monolayer MoS_2

○Kana Kojima, Hong En Lim, Yusuke Nakanishi, Takahiko Endo, Yutaka Maniwa, Yasumitsu Miyata

Department of Physics, Tokyo Metropolitan University, Hachioji, 192-0397, Japan

The optical properties of transition metal dichalcogenide (TMDC) atomic layers have attracted much attention because of their unique spin-valley coupling and excitonic optical responses. Recently, Lien *et al.* has reported that the non-radiative relaxation of TMDC depend strongly on various factors, which include supporting substrate and carrier density [1]. While we have demonstrated that the growth substrates play a major role in non-radiative relaxation of chemical vapor deposition (CVD)-grown monolayer MoS_2 [2], the effect of carrier density remains unclear. In this work, we have investigated the carrier-dependent photoluminescence (PL) response of monolayer MoS_2 grown on SiO_2 by using electrostatic doping.

A simple field effect transistor device were fabricated to regulate the carrier density of the monolayer MoS_2 by varying the backgate voltage (V_g). As shown in Fig. 1a, the increase of negative trions by such electron doping results in a red shifted PL peak with weakened intensity at V_g=30 V [3]. The PL lifetime, in contrast, is insensitive to the different V_g applied with an approximate value of 20 ps (Fig. 1b). These results suggest that the carrier density has only a minor contribution to the non-radiative relaxation of the MoS_2 grown on SiO_2. In this presentation, we will also discuss the effects of carrier density and substrate on MoS_2-based van der Waals heterostructures.

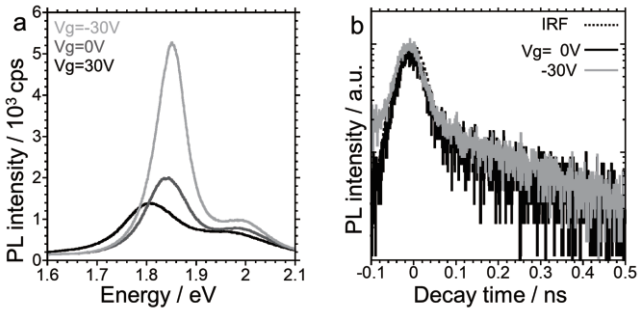

Fig. 1. (a) PL spectra and (b) time-resolved PL decay profiles of CVD-grown monolayer MoS_2 on SiO_2 under gate voltages, V_g = –30, 0, 30V.

[1] D. H. Lien *et al.*, Science **364** 468-471 (2019) [2] K. Kojima *et al.*, Nanoscale **11** 12798-12803 (2019) [3] K. F. Mak *et al.*, Nat. Mater. **12** 207-211 (2013)

Corresponding Author: Y. Miyata, Tel: 042-677-2508, E-mail: ymiyata@tmu.ac.jp

Self-Assembly of Nanodiamonds through Soft Gel from their Solutions

○Toshihiko Tanaka[1,2], Yasuhiro F. Miura[3], Tetsuya Aoyama[2], Masaya Nemoto[1,2], Shusuke Ando[1], Yuho Itabashi[1], Kazunori Miyamoto[4], Atsuya Muranaka[2], Masanobu Uchiyama[2,4], Eiji Osawa[5]

[1]Department of Chemistry and Biochemistry, National Institute of Technology, Fukushima College, 30 Aza-nagao, Tairakamiarakawa, Iwaki, Fukushima, 970-8034, Japan
[2]Elements Chemistry Laboratory, RIKEN Cluster for Pioneering Research, 2-1 Hirosawa, Wako, Saitama, 351-0198, Japan
[3]Hamamatsu University School of Medicine, 1-20-1 Handayama, Higashi-ku, Hamamatsu city, Shizuoka, 431-3192, Japan
[4] Graduate School of Pharmaceutical Sciences, the University of Tokyo, 7-3-1 Hongo, Bunkyo-ku, Tokyo 113-0033, Japan
[5]Nano Carbon Research Institute Ltd., Asama Research Extension Center, Shinshu University, 3-15-1 Tokida, Ueda, Nagano, 386-8567 Japan

We already reported two kinds of rectangular precipitates of detonation nanodiamonds (DND): one is a fine tape-like whisker[1] and the other is a nanosheet[2]. We consider that one interesting aspect of the self-assembly of DND is its application to the drug delivery systems[3] for cancer therapy and that aggregated elementary diamond nanoparticles (~50nm) play an effective role in avoiding serious side effects to hearts or to bone marrow through EPR effect[4]. We demonstrate herein further results on the precipitates.

The whiskers are formed through the gelation of DND and a kind of crystallization takes place from soft gel to hydrated colloidal crystals. Curved whiskers were precipitated on the wall of a test tube at the meniscus between air, glass and DND solutions. The meniscus was moving down slowly (<1mm/h) through the evaporation of water in vacuum and the concentrated solution became the gel because gelation takes place over 7wt.%. Their rectangular shapes depend on the concentration of the solution. If a DND solution of over 4 wt.% dries out in the tube, a ring of a long-curved whisker can be removed easily after drying. They were slightly elastic, being able to deform a little without breaking and have birefringence (**Fig.1**).

The nanosheets were crystallized from a diluted DND solution on a Langmuir monolayer of arachidic acid (AA) and we consider that they include the monolayer. The horizontal lifting technique allows us to transfer the floating DND/AA hybrid layer onto solid substrates any number of times, in such a way that a multi-layered structure of the nanosheets can be constructed. Hence the nanosheets are amphiphilic because of the AA monolayer.

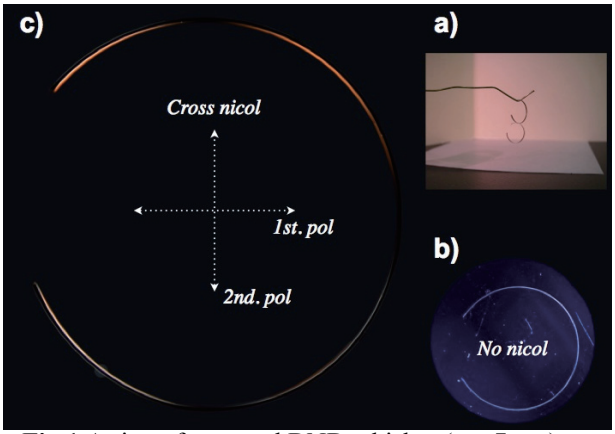

Fig.1 A ring of a curved DND whisker (ϕ ~7mm): (a) pending 2 rings; (b) an image with no nicols; (c) that with cross nicols.

[1] E. Osawa; *Diam.Rel.Maer.* 16, 2018(2007);
[2] T.Tanaka, Y.F. Miura, T. Sato, E. Osawa; *Abstract of the 53th FNTG Symposium*, 66(2017); [3] E.K.Chow, X.-Q. Zhang, M. Chen, R. Lam, E. Robinson, H. Huang, D. Schaffer, E. Osawa, A. Goga, D. Ho, *Sci. Trans. Med*., 3.73(2011); [4] Y. Matsumura. H. Maeda, *Cancer Res.*, 46, 63872 (1986).
Corresponding Author: Eiji Osawa/Tel: +81--268-75-8381 / E-mail: osawa@nano-carbon.jp

Chemically synthesized ground state diatomic carbon (C_2) serves as an origin of carbon allotropes

○Kazunori Miyamoto,[1] Shodai Narita,[1] Yui Masumoto,[1] Takahiro Hashishin,[1] Taisei Osawa,[1] Mutsumi Kimura,[2,3] Masahito Ochiai,[4] Masanobu Uchiyama[1,3,5]

[1] *Graduate School of Pharmaceutical Sciences, The University of Tokyo, 7-3-1 Hongo, Bunkyo-ku, Tokyo 113-0033, Japan*
[2] *Division of Chemistry and Materials, Faculty of Textile Science and Technology, Shinshu University, Ueda, 386-8567, Japan*
[3] *Research Initiative for Supra-Materials (RISM), Shinshu University, Ueda, 386-8567, Japan*
[4] *Graduate School of Pharmaceutical Sciences, University of Tokushima, 1-78 Shomachi, Tokushima 770-8505, Japan.*
[5] *Cluster of Pioneering Research (CPR), Advanced Elements Chemistry Laboratory, RIKEN, 2-1 Hirosawa, Wako-shi, Saitama 351-0198, Japan*

Diatomic carbon (C_2) exists in carbon vapour, comets, the stellar atmosphere, and interstellar matter, but although it was discovered in 1857,[1] it has proved frustratingly difficult to characterize, since C_2 gas occurs/exists only at extremely high temperatures (above 3500°C) (Fig. 1a).[2] Since 1930, several experimental methods to generate C_2 have been developed by using extremely high energy processes, such as electric carbon arc and multiple photon excitation,[3] and the C_2 species obtained were reported to exhibit singlet dicarbene (double bond) and/or triplet biradical (triple bond) behavior.[4] In contrast, recent theoretical simulations suggest that C_2 in the ground state should have a singlet biradical (quadruple bond) character (Fig. 1a).[5] Here, we present the first "chemical" synthesis of C_2 in a flask at room temperature or below, not only providing the first experimental evidence to support theoretical predictions that C_2 has a singlet biradical character with a quadruple bond, thus settling a long-standing controversy between experimental and theoretical chemists, but also achieving the first bottom-up chemical synthesis of carbon allotropes such as amorphous carbon, graphite, carbon nanotubes, and C_{60} (Fig 1b).[6]

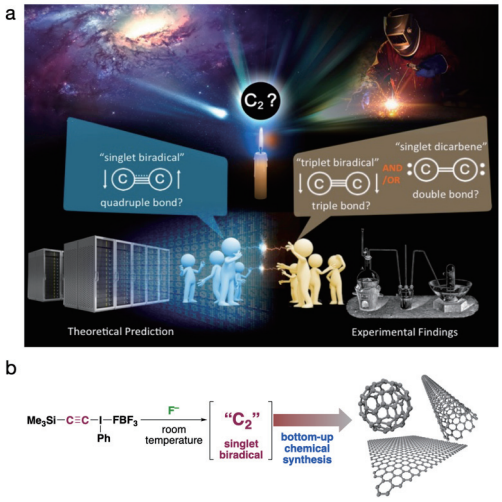

Fig.1 a) Long-standing dispute between experimental and theoretical chemists concerning the nature of diatomic carbon (C_2). b) Chemical generation of C_2 and a chemical synthesis of carbon allotropes.

[1] W. Swan, *Trans. R. Soc. Edinburgh.* **21**, 411–430 (1857). [2] G. Glockler, *J. Chem. Phys.* **22**, 159–161 (1954). [3] P. S. Skell, *et al. Acc. Chem. Res.* **6**, 97–105 (1973). [4] P. S. Skell, *et al. J. Am. Chem. Soc.* **92**, 5620–5624 (1970). [5] S. Shaik, *Nat. Chem.* **4**, 195–199 (2012). [6] K. Miyamoto, *et al. ChemRxiv* doi: 10.26434/chemrxiv.8009633.

Corresponding Author: K. Miyamoto, M. Uchiyama
Tel: +81-3-5841-0783, Fax: +81-3-5841-0733
E-mail: kmiya@mol.f.u-tokyo.ac.jp; uchiyama@mol.f.u-tokyo.ac.jp

Simple and Effective Method to Control Photoluminescence Properties of Single-walled Carbon Nanotubes by Ultrasonic Irradiation

○Yui Konno[1], Akane Nishino[1], Michio Yamada[1], Yutaka Maeda[1], Saki Okudaira[2], Yuhei Miyauchi[2], Kazunari Matsuda[2], Jun Matsui[3], Masaya Mitsuishi[4], Mitsuaki Suzuki[5]

[1] *Department of Chemistry, Tokyo Gakugei University, Tokyo 184-8501, Japan*
[2] *Institute of Advanced Energy, Kyoto University, Uji 611-0011, Japan*
[3] *Department of Material and Biological Chemistry, Yamagata University, Yamagata 990-8560, Japan*
[4] *Institute of Multidisciplinary Research for Advanced Materials, Tohoku University, Sendai 980-8577, Japan*
[5] *Department of Chemistry, Josai University, Saitama 350-0295, Japan*

It has been reported that the sidewall functionalization is effective to control the local band structures of single-walled carbon nanotubes (SWNTs), resulting in emergence of new red-shifted photoluminescence (PL) peaks in the near-infrared region [1,2,3]. This allows the excitation with the E_{11} energy to afford increase of the PL excitation efficiency, which is advantageous for bioimaging and so on. For the PL measurements, the use of low concentrated and individually dispersed solution of SWNTs is preferred for avoiding concentration quenching and unwanted interaction with other chiral SWNTs [4]. However, the sonication of SWNTs is also known to shorten and damage the SWNTs [5,6]. Meanwhile, surfactant decomposition has been studied and reported that the decomposition proceeds *via* generation of radical species from water upon ultrasonic irradiation [7]. Here we present the effects of ultrasonic irradiation on the PL properties of SWNTs under various conditions including different surfactants, concentration of SWNTs, and atmospheres.

In this study, sodium cholate (SC), sodium dodecylbenzene sulfate (SDBS), and sodium dodecyl sulfate (SDS) were selected as typical surfactants to disperse SWNTs in D_2O. To clarify the effect of ultrasonic irradiation, a small amount of SWNTs (initial concentration: 12.5 mg/L) was sonicated and centrifuged to prepare the SWNTs dispersion. The characteristic absorption and PL peaks of SWNTs were observed from the supernatant prepared using SC. On the other hand, the supernatant prepared using SDS exhibited low intrinsic absorption and PL peaks of SWNTs. When SDBS was used, the dispersibility of SWNTs was found to be as good as that obtained with SC. In this case, it is noteworthy that the new PL peaks at 1043 and 1118 nm emerged accompanied by decreasing the intrinsic PL peaks of SWNTs, as seen in the oxidation of SWNTs [1, 2]. The details of the control of the PL properties of SWNTs by ultrasonic irradiation will be discussed.

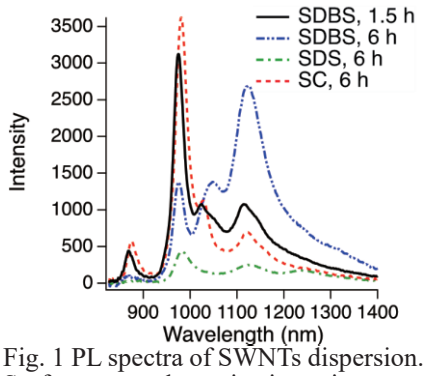

Fig. 1 PL spectra of SWNTs dispersion. Surfactant and sonication time are shown in the figure.

[1] R. B. Weisman *et al*. *Science* **330**, 1656 (2010) [2] Y. Maeda *et al. J. Am. Chem. Soc.* **135**, 6356 (2013) [3] Y. Wang *et al*. *Nat. Chem*. **5**, 840 (2013). [4] R. B. Weisman *et al*. *Science* **297**, 593 (2002). [5] M. D. Lay *et al*. *J. Phys. Chem. C* **114**, 12490 (2010). [6] F. Hennrich *et al. J. Phys. Chem. B* **111**, 1932 (2017). [7] M. Ashokkumar *et al. Aust. J. Chem*. **56**, 1045 (2003).

Corresponding Author: Y. Maeda
Tel: +81-42-329-7512
E-mail: ymaeda@u-gakugei.ac.jp

Stable MoO_3 Doping of Carbon Nanotube Top Electrodes for Highly Efficient Metal-Electrode-Free Perovskite Solar Cells

Seungju Seo[1], Il Jeon[1], Esko I. Kauppinen[2], Yutaka Matsuo[1,3], Shigeo Maruyama[1,4]

1. Department of Mechanical Engineering, School of Engineering, The University of Tokyo
2. Department of Applied Physics, Aalto University School of Science
3. Institutes of Innovation for Future Society, Nagoya University
4. Energy NanoEngineering Laboratory, National Institute of Advanced Industrial Science (AIST)

ABSTRACT

Organic-inorganic lead halide perovskite solar cells (PSCs), since the first report in 2009, have attracted great interest for the high power conversion efficiency (PCE). Now the certified power conversion efficiency (PCE) reads 25.2%. Accordingly, more research effort should be made on the device stability and the fabrication cost.

Top metal electrode in PSCs is usually thermally evaporated under vacuum. This substantially increases the fabrication cost let alone the high cost of gold and silver. Furthermore, use of the metal top electrodes deteriorates the long-term stability of PSCs as the metal ions migrate into the bulk of the perovskite layer, undermining the device performance.

As an alternative to the metal electrodes, single-walled carbon nanotube (CNT) as the top electrode has been reported to achieve high stability in PSCs owing to the hydrophobic nature of carbon and avoiding the ion migration. In addition, it drastically reduces the fabrication cost as it can be easily deposited onto devices by a simple mechanical transfer. Despite such advantages, there are three factors limiting the PCE of the CNT top electrode-based PSCs that need to be addressed: (1) the unfavorable work function of the CNT with respect to the active perovskite layer, leading to loss in voltage potential, (2) lower conductivity than the metal counterparts, limiting the fill factor (FF), and (3) less refractive nature with respect to incident light leading to loss in short-circuit current.

Here, we address those three issues by engineering the CNT top electrode. We tuned the work function of CNT electrodes, increased their conductivity by depositing MoO_3 under vacuum, without damaging underneath perovskite layers. Using photoelectron yield spectroscopy, absorbance and raman spectroscopy, we determine the necessary MoO_3 thickness and thermal annealing parameters to efficiently dope the CNT top electrode and study underlying doping mechanism between CNTs and MoO_3 to achieve highly efficient CNT top electrode-based PSCs.

Corresponding Author: Prof. Shigeo Maruyama
Tel : +81)3-5841-6421
maruyama@photon.t.u-tokyo.ac.jp

Macrocyclic bis(dipyrrinato) metal complex for single-walled carbon nanotube separation

○ Guoqing Cheng, and Naoki Komatsu

Graduate School of Human and Environmental Studies, Kyoto University, Kyoto 606-8501, Japan

We have been developing host-guest chemistry for separation of carbon nanotubes (CNTs) according to their structure and physical properties. The host molecules named "nanotweezers" and "nanocalipers" has been designed and synthesized to discriminate CNTs based on diameter, metallicity and even handedness [1].

In this work, new nanocalipers with two dipyrrin moieties at both ends were designed and synthesized. Dipyrrin moieties with the parallel alignment formed the macrocyclic homoleptic binuclear bis(dipyrrinato) metal complex in the presence of copper ion. The resulting rigid macrocycle is expected to be able to interlock single-walled carbon nanotubes (SWNTs) with a suitable structure (Fig. 1), and simultaneously disperse SWNTs into the solution phase.

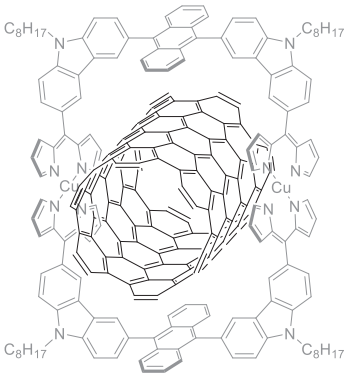

Fig.1 Schematic structure of the macrocycle-interlocked SWNT

In the extraction, nanocalipers and HiPco SWNTs are bath-sonicated in the presence of Cu(II) in THF. After centrifugation, the resultant supernatant was analyzed by absorption spectroscopy. In Fig. 2a, upward shift of the baseline and red-shift of the band around 460 nm were observed, implying the extraction of SWNTs and the complexation between the macrocycle and SWNTs, respectively. After demetallization followed by washing out the host molecules thoroughly, the resulting SWNTs were analyzed by Raman spectroscopy. At the excitation of 785 nm, the content of relatively larger diameters (1.01-1.15 nm) increase, while enrichment of semiconducting SWNTs is observed at the excitation of 633 nm.

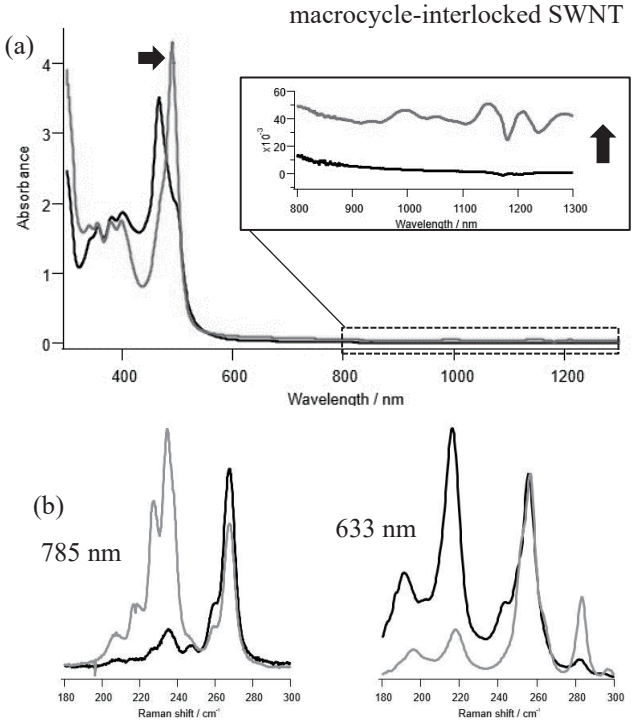

Fig.2 (a) Absorption spectra of the supernatant after 48 h sonication followed by centrifugation (gray trace) and the macrocycle in THF (black trace). Inset: expansion at the region of 800-1300 nm. (b) Normalized Raman spectra of HiPco SWNTs before and after extraction (black and gray traces, respectively) at 785 and 633 nm.

[1] G. Liu, N. Komatsu *et al*. *J. Am. Chem. Soc.*, **135**, 4805 (2013); *J. Mater. Chem. A*, **2**, 19067 (2014); *Org. Chem. Front.*, **4**, 911 (2017).

Corresponding Author: Naoki Komatsu, Tel: +81-75-753-6833, E-mail: komatsu.naoki.7w@kyoto-u.ac.jp

Influence of the carbon-rich domain in hexagonal boron nitride on transport properties of adjacent graphene

○Momoko Onodera[1], Kenji Watanabe[2], Miyako Isayama[1], Satoru Masubuchi[1], Rai Moriya[1], Takashi Taniguchi[2], and Tomoki Machida[1,3]

[1] IIS, The University of Tokyo, Tokyo 153-8505, Japan
[2] NIMS, Ibaraki 305-0044, Japan [3]CREST-JST

Hexagonal boron nitride (h-BN) crystals synthesized under high pressure and high temperature (HPHT) are known to have high quality and used in more than 200 research institutes. However, all HPHT h-BN crystals have a distinct carbon(C)-rich domain at the core region, which contains a significant amount of C impurities. We found that this domain still exists after exfoliation and cannot be identified with an optical microscope or AFM. To evaluate the influence of the C-rich domain on adjacent graphene, we detected the C-rich domain by utilizing photoluminescence in UV range and fabricated graphene/h-BN heterostructures with graphene placed across the boundary of the domain, which enabled us to measure graphene on the domain and pristine regions simultaneously. Graphene on the C-rich domain exhibited degraded carrier mobility and bending in the Landau-fan diagram [1]. The plot of the energy at the bending point suggested the formation of an acceptor level located at 0.10 eV above the Dirac point. To elucidate the role of C impurities in h-BN, we also conducted experiments using intentionally C-doped HPHT h-BN [2]. Graphene on C-doped h-BN showed bending in the Landau fan diagram and strong hysteresis upon sweeping carrier density, which further confirmed the existence of an acceptor state. Finally, we study h-BN crystals synthesized at atmospheric pressure and high temperature (APHT) as an alternative to HPHT h-BN [3]. We found that APHT h-BN does not have any distinct impurity-rich domains and can be used as a high-quality substrate of other 2D materials.

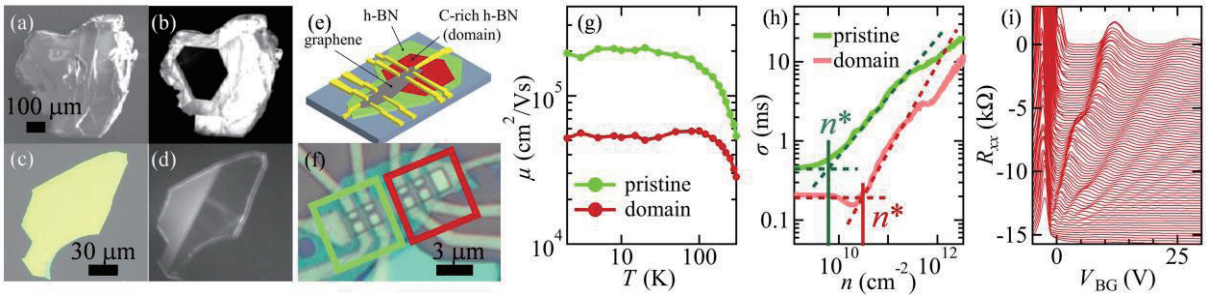

Fig. 1: (a) SEM and (b) CL (320 nm) images of an HPHT h-BN crystal. (c) Optical microscope and (d) PL (340 nm) images of an exfoliated HPHT h-BN flake. (e) Schematic and (f) photographic image of the device. (g) Temperature dependence of carrier mobility. (h) Extraction of charrier inhomogeneity n^* at T = 2 K. (i) R_{xx} vs. V_{BG} at B = 0–9 T obtained in graphene on the C-rich domain. Data are offset in proportional to B for clarity.

[1] M. Onodera, K. Watanabe, M. Isayama, M. Arai, S. Masubuchi, R. Moriya, T. Taniguchi, and T. Machida, Nano Lett. **19**, 7282 (2019).

[2] M. Onodera, M. Isayama, T. Taniguchi, K. Watanabe, S. Masubuchi, R. Moriya, Y. Hoshi, T. Haga, Y. Fujimoto, S. Saito, and T. Machida (submitted).

[3] M. Onodera, T. Taniguchi, K. Watanabe, M. Isayama, S. Masubuchi, R. Moriya, and T. Machida, Nano Lett. **20**, 735 (2020).

Corresponding Author: M. Onodera
Tel: +81-3-5452-6158, Fax: +81-3-5452-6157, E-mail: monodera@iis.u-tokyo.ac.jp

Dielectric screening effects on photoluminescence of carbon nanotubes on hexagonal boron nitride

○Nan Fang[1,2], Keigo Otsuka[1], Takashi Taniguchi[3], Kenji Watanabe[3], Kosuke Nagashio[4], Yuichiro K. Kato[1,2]

[1] *Nanoscale Quantum Photonics Laboratory, RIKEN Cluster for Pioneering Research, Saitama 351-0198, Japan*
[2] *Quantum Optoelectronics Research Team, RIKEN Center for Advanced Photonics, Saitama 351-0198, Japan*
[3] *National Institute of Materials Science, Ibaraki 305-0044, Japan*
[4] *Department of Materials Engineering, The University of Tokyo, Tokyo 113-8656, Japan*

Hexagonal boron nitride (*h*-BN), a two-dimensional (2D) material, is atomically flat with low defect density, which is widely used to support other 2D materials. We expect that the advantages of *h*-BN can also be utilized in mixed dimensional heterostructures, and single-walled carbon nanotubes (CNTs) would provide a unique opportunity in this context. The one-dimensional nature of CNTs results in enhanced Coulomb interactions, giving rise to tightly bound excitons that show photoluminescence (PL) at room temperature. CNTs directly attached on solid-state substrates such as SiO_2/Si, however, suffers from the strong substrate quenching effect.[1] By using *h*-BN as a substrate, the quenching effect is expected to be suppressed. Moreover, excitons in CNTs are sensitive to the dielectric environment, and intimate contact with the *h*-BN could result in large modifications in excitonic energies.

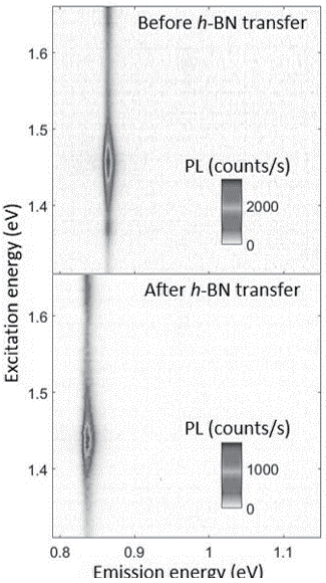

Figure 1 PLE maps of an air-suspended CNT before and after the *h*-BN transfer.

Here, we study *h*-BN effects on PL excitation (PLE) spectra of CNTs by transferring *h*-BN flakes over air-suspended CNTs grown over trenches on SiO_2/Si substrates.[2] Figure 1 shows PLE maps of a suspended CNT before and after the *h*-BN transfer with the excitation power fixed at 10 μW. Before the *h*-BN transfer, the values for the E_{11} and E_{22} are consistent with those for a (10,8) air-suspended nanotube. After the *h*-BN transfer, the PL intensity is decreased to approximately half of the initial value. This PL reduction caused by the *h*-BN flake is much weaker than that in the conventional SiO_2/Si substrates. We also observe redshifts in both E_{11} and E_{22} of 27 and 17 meV, respectively. Although the shift values show tube-to-tube variations, all the CNTs show redshifts for both E_{11} and E_{22}, which is consistent with the dielectric screening effect from *h*-BN flakes.

Work supported by JSPS (KAKENHI JP19K23593, JP16H05962), MIC (SCOPE 191503001), and MEXT (Nanotechnology Platform). K. O. is supported by JSPS Research Fellowship. We acknowledge the Advanced Manufacturing Support Team at RIKEN and T. Nishimura for technical assistance.

[1] J. Lefebvre, Y. Homma, P. Finnie, Phys. Rev. Lett. **90**, 217401 (2003).
[2] A. Ishii, M. Yoshida, Y. K. Kato, Phys. Rev. B **91**, 125427 (2015).

Corresponding Author: Yuichiro K. Kato
Tel: +81-48-462-1449, Web: http://katogroup.riken.jp/, E-mail: yuichiro.kato@riken.jp

Synthesis of 3D hybrid Structures composed of Single-walled CNTs and Mesopores Carbon by Chemical Vapor Deposition

Aliza Khaniya Sharma[1], Kamal P Sharma[1,2], Takahiro Saida[1,2],
Shigeya Naritsuka[3], Takahiro Maruyama[1,2]

[1]*Department of Applied Chemistry, Meijo University, Japan*
[2]*Nanomaterials Research Center, Meijo University, Japan*
[3]*Department of Materials Science and Engineering, Meijo University, Japan*

1. Introduction

It is highly desirable to obtain single-walled carbon nanotube (SWCNTs) and graphitic carbon hybrid structure, which could open up the wider applicability as an electrode material in lithium ion secondary battery with hybrid structure framework [1, 2]. In this study, to synthesize an SWCNTs-graphitic carbon hybrid structure, we carried out SWCNTs growth utilizing Co catalysts deposited on mesoporous carbon (MC) by alcohol catalytic chemical vapor deposition (ACCVD) method.

2. Experimental procedure

Commercially available MC (TOYO Tanso) w treated chemically in a mixture of HNO_3 and HCl (3:1 l volume), and is termed as etched MC (EMC) hereaft The EMC dispersed in acetone was spin coated onto t SiO_2/Si substrates. Co catalyst (0.2 nm in thickness) w deposited on them by using a pulsed arc plasma gun, a SWCNTs growth was carried out on those substrates 700ºC for 3 min with different partial pressure of Ethan (EtOH). The grown SWCNTs were characterized l FESEM, Raman spectroscopy, XPS, and HRTEM.

3. Results and Discussion

Figure 1(a) shows FESEM image of the SWCN grown on EMC at 100sccm EtOH and overlapp Raman spectra at 90sccm. Thread like structures we observed on both SiO_2/Si and EMC. Radial breathi mode (RBM), G-band and 2D-band peaks were seen Raman spectra after growth, indicating that SWCN were grown successfully on EMC. **Figure 1(b)** sho the HRTEM image of the SWCNTs grown at 90sc EtOH. FESEM, HRTEM and Raman analysis reveal that we successfully synthesize SWCNTs and MC 3 hybrid structure.

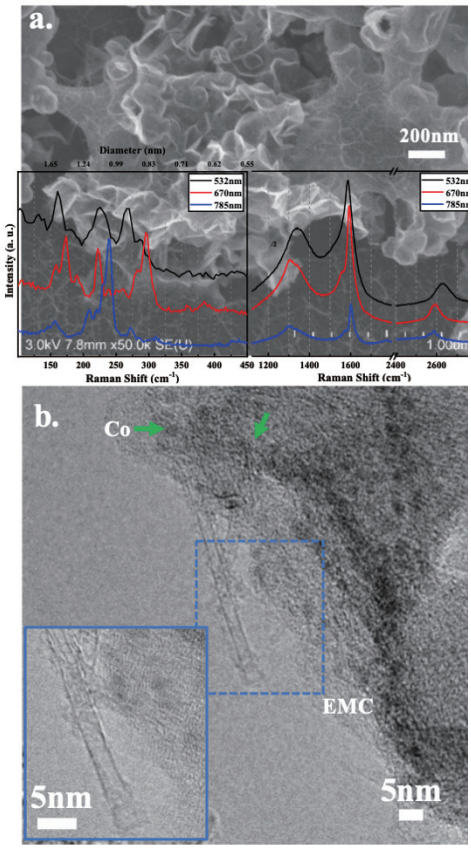

Figure 1. SWCNTs grown on EMC **(a)** FESE image of at 90sccm EtOH. **(b)** HRTEM image SWCTs grown at 100sccm EtOH. Overlappe Raman spectra in **(a)**, and high resolution TE image, inset in **(b)** are of SWCNTs grown 90sccm EtOH.

This work was supported in part by Private Univers Research Branding Project from the MEXT, Japan. We tha Prof. Takehiko Hihara at NITech for TEM observation.

[1] Y. Sang et.al. Nano 13 (2018)1850071.
[2] R. Ghosh et al. Chem. Commun. 51 (2015) 8974.

Corresponding Author: T. Maruyama
Phone: +81-52-838-2386, Fax: +81-52-832-1172
E-mail: takamaru@meijo-u.ac.jp.

Theoretical Design of Thermoelectric Performance of Carbon Nanotube Thin Films based on Electrical and Thermal Circuit Network Analysis

○Junei Kobayashi, Kotaro Fujisaki and Takahiro Yamamoto

Department of Electrical Engineering, Tokyo University of Science, Tokyo 125-8585, Japan

The thermoelectric (TE) devices based on carbon nanotubes (CNTs) thin film are expected to be flexible and sustainable power resources [1]. It is considered that the TE performance of the thin film depends not only on transport properties of individual CNTs [2] but also on the film structures such as alignment, density of CNTs and film thickness [3]. However, it has not been clarified how the macroscopic parameters derived from those structures affect the TE performance of the film. This means that there currently exist no guidelines to enhance the TE performance by controlling the macroscopic parameters. Our aim is to establish the guidelines through computational approach.

In the present study, we focus on the dependence of (i) film thickness and (ii) alignment of CNTs. We estimated electrical conductivity σ, Seebeck coefficient S and Power Factor $PF \equiv \sigma S^2$ solving both large-scale electrical and thermal circuit equations for CNT network models (Figs. 1 and 2). The obtained results are summarized as follows. (i) The averaged *PF* of CNT films with a fixed area density of CNTs increases with increasing the film thickness. (ii) The averaged *PF* of CNT films with a fixed area density of CNTs has the maximum value at the alignment where the electrical conductivity is maximized, this alignment is intermediate between perfectly random alignment and well-alignment.

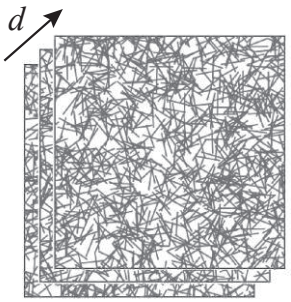

Fig. 1 Controlled film thickness d

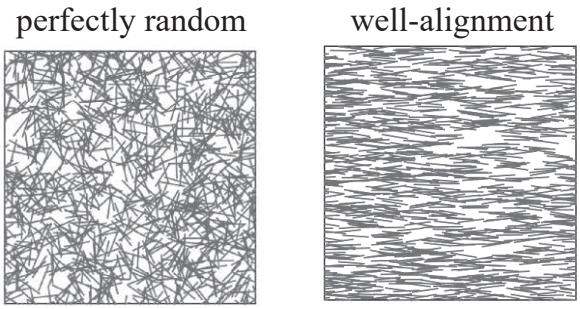

Fig. 2 Controlled alignment

[1] M. Ohnishi *et al.,* Phys. Rev. B **95**, 155405 (2017).

[2] T. Yamamoto *et al*., J. Phys. Soc. Jpn. **87**, 114710 (2018).

[3] M. Tsukuda *et al.,* Appl. Phys. Express **12**, 055006 (2019).

Corresponding Author: Takahiro Yamamoto

Tel & Fax +81-3-5876-1492 E-mail: takahiro@rs.tus.ac.jp

Evaluation of Thermal Transport in a Single-walled Carbon Nanotube Film by Ionic-liquid Gating

○Kan Ueji[1], Yuya Matsuoka[1], Takashi Yagi[2], Kengo Fukuhara[1], Yota Ichinose[1], Akari Yoshida[1], Yohei Yomogida[1], Kazuhiro Yanagi[1]

[1] *Department of Physics, Tokyo Metropolitan University, Hachioji, Tokyo 192-0397, Japan*
[2] *National Metrology Institute of Japan, National Institute of Advanced Industrial Science and Technology, Tsukuba, Ibaraki,305-8563, Japan*

A single-walled carbon nanotube (SWCNT), in which both holes and electrons can flow, is one of the most promising candidates for flexible thermoelectric generators because of the van-Hove singularity that originates from the quasi one-dimensional characteristic. The dimensionless thermoelectric figure of merit (ZT) is given as $ZT = \sigma S^2 T/\kappa$, where σ, S, T, and κ are the electric conductivity, Seebeck coefficient, absolute temperature, and thermal conductivity, respectively. A Fermi level of the SWCNT film needs to shift near the van-Hove singularity level by doping so that the power factor (σS^2) is maximized in both pure semiconducting and metallic SWCNT.[1] On the other hand, the measurement of κ after changing the doping level systematically is difficult, indicating that the Fermi level dependence of κ is indefinite. However, shifting the Fermi level of the SWCNT film results in charge carriers (hole or electron) being placed in the valence or conduction band, which may affect κ because the charge carriers can interact with acoustic phonons. In fact, Fang *et al* calculated that the mobility of acoustic phonons in a graphene nanoribbon vary depending on whether or not the Fermi level is located in the band.[2] To maximize ZT, evaluating not only the power factor but also κ as a function of the Fermi level is important. Accordingly, we have developed an equipment to simultaneously measure the σ and κ of SWCNT by means of a unique time-domain thermoreflectance method (TDTR) for Au, which is used as a stable electrode and thermal transducer. We attempt to clarify the κ of SWCNT dependent on the Fermi level.

Molybdenum (adhesion layer) and gold electrodes were deposited onto a quartz glass substrate. The semiconducting SWCNT film with a polycarbonate membrane was transferred to the substrate, and chloroform was used to rinse the membrane away, thus resulting in the adherence of the SWCNT film to the measurement substrate. The sample was annealed at 473 K in vacuo for 2 hours to remove organic impurities. The κ of SWCNT tuned by the Fermi level was measured by TDTR under vacuo. We have a successful TDTR measurement for Au during ionic liquid gating as shown in Fig.1. Both the lock-in phase signals are almost same, indicating that the gate voltage range between 0 and −2.5 V have less of an impact on Au. Therefore, it has become possible to measure the κ of SWCNT film tuning at the Fermi level. In this presentation, we will discuss the variation of thermophysical properties in the SWCNT film by ionic-liquid gating system.

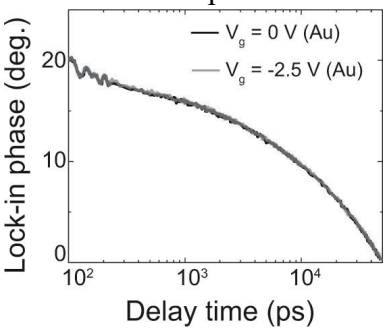

Fig. 1 TDTR signals for gold electrode when gate voltage (V_g) change.

[1] Y. Ichinose *et al*., *Nano Lett*., **19**, 7370 (2019) [2] T. Fang *et al*., *Phys. Rev. B*, **78**, 205403 (2008)

Corresponding Author: K. Ueji and K. Yanagi. Tel: +81-42-677-2494 (Ext. 3253), Fax: +81-42-677-2483,
E-mail: kueji@tmu.ac.jp, yanagi-kazuhiro@tmu.ac.jp

Thermal stability of single-chirality-enriched carbon nanotube thin films

○Akira Takakura[1], Taishi Nishihara[1], Kazunari Matsuda[1], Takeshi Tanaka[2], Hiromichi Kataura[2], and Yuhei Miyauchi[1]

[1] *Institute of Advanced Energy, Kyoto University, Uji, Kyoto 611-0011, Japan.*
[2] *Nanomaterials Research Institute, AIST, Tsukuba, Ibaraki 305-8565, Japan.*

Single-walled carbon nanotubes (SWNTs) have been considered as promising materials for various applications utilizing their superior physical properties including high thermal stability [1] and strength-to-weight ratio [2]. Moreover, recent finding of narrow-band thermal radiation in individual SWNTs relying on excitonic effect has suggested their potential application as a wavelength selective thermal emitter [1]; a core component in thermophotovoltaic energy harvesting devices [3]. This application requires macroscopic assemblies of single-chirality enriched SWNTs that can be operated at high temperature (≥ 700 °C). However, macroscopic aggregation of SWNTs often lowers their excellent intrinsic properties, and it is still unclear whether the SWNT assemblies are stable enough to be used at elevated temperatures, although individual SWNTs have been confirmed to be stable even at 1700 °C [1].

Here we report the thermal stability of single-chirality-enriched SWNT thin films on various substrates. Single chirality SWNTs were separated by gel chromatography [4], and the films composed of the SWNTs were fabricated using vacuum filtration method [5]. The SWNT films were transferred onto metal grids (for fabricating free-standing membranes) or various kinds of substrates including sapphire with different crystal planes and quartz. Typical thickness of the SWNT films was ~100 nm as confirmed via the observation using the scanning electron microscope. The SWNT films were heated up in argon gas flow conditions, and their stabilities were studied using optical techniques such as Raman scattering, absorption and photoluminescence (PL) spectroscopy.

Raman spectroscopy showed that *D*-mode feature, which is an indicative of the defect density, decreased with increasing temperature, in contrast to almost no changes in *G*-mode feature and optical absorption. The *D*-mode signals disappeared in the SWNT film after the thermal treatment at 700 °C, irrespective of substrates; this result suggests that the thermal treatment substantially heals the defects in SWNTs. Enhancement of PL intensities of the SWNT films, which is also sensitive to the defect density, were also observed. We found that the (6,5) enriched SWNT films on the C-plane sapphire were decomposed after the thermal treatment at 900 °C, in striking contrast to a little decomposition on A-, R-plane sapphire and quartz substrates. This result clearly shows that thermal stability of SWNT films depends on the kinds of substrate surface. We will discuss the possible mechanism of the substrate dependence and the thermal stability of SWNT films with various chiralities to develop a general design principle of SWNT thin film devices operating at high temperatures.

[1] T. Nishihara, A. Takakura, Y. Miyauchi, and K. Itami, *Nat. Commun.* **9**, 3144 (2018).
[2] A. Takakura *et al. Nat. Commun.* **10**, 3040 (2019).
[3] E. Rephaeli and S. Fan, *Opt. Express* **17**, 15145 (2009).
[4] Y. Yomogida *et al*. *Nat. Commun.* **7**, 12056 (2016).
[5] X. He *et al*. *Nat. Nanotechnol.* **11**, 633 (2016).

Corresponding Author: Y. Miyauchi
Tel: +81-774-38-3463, E-mail: miyauchi@iae.kyoto-u.ac.jp

Relationships between Seebeck coefficient and Conduction Directions in Aligned Semiconducting Single-wall Carbon Nanotube Films

○Kengo Fukuhara[1], Yota Ichinose[1], Kanako Horiuchi [1], Akari Yoshida [1], Yohei Yomogida [1], Weilu Gao [2], Natsumi Komatsu [2], Junichiro Kono [2], Kazuhiro Yanagi [1]

[1] *Department of Physics, Tokyo Metropolitan University, Tokyo 192-0397, Japan*
[2] *Department of Electrical and Computer Engineering, Rice University, Texas 77005, USA*

Single-wall carbon nanotubes (SWCNTs) are one-dimensional materials with sharp van Hove singularities. As proposed by Hicks and Dresselhaus, one-dimensional materials have potential to exhibit superior thermoelectric performance [1], and then their thermoelectric properties attract a lot of interest. Since SWCNTs have quite an-isotropic structure, previously, we investigated thermoelectric properties depending on conduction directions, such as parallel or perpendicular directions to the nanotube axis, using aligned SWCNT thin films [2]. We observed an-isotropic character in electrical conductivity, but completely isotropic character in Seebeck coefficient regardless of the conduction directions. Such isotropic character in Seebeck coefficient will reflect that the conduction mechanism in the parallel direction is similar hopping conduction to the perpendicular direction. However, if the mechanisms are different between the two directions, Seebeck coefficient may also exhibit an-isotropic character. To check this hypothesis, in this study, we investigated electrical conductivity and Seebeck coefficients of aligned metallic and semiconducting SWCNT films. We fabricated large-area aligned SWCNT films using the slow filtration method [3]. Then we measured electrical conductivity and Seebeck coefficient as a function of Fermi level in parallel and perpendicular directions. Figure 1 shows the relationships between Seebeck coefficient and electrical conductivity in parallel and perpendicular directions in metallic and semiconducting SWCNTs. We found that in the case of semiconducting SWCNTs, Seebeck coefficient showed something different line-shapes as shown using dash lines in small electrical conductivity region. This result may suggest an-isotropic character in Seebeck coefficient in aligned semiconducting SWCNT films.

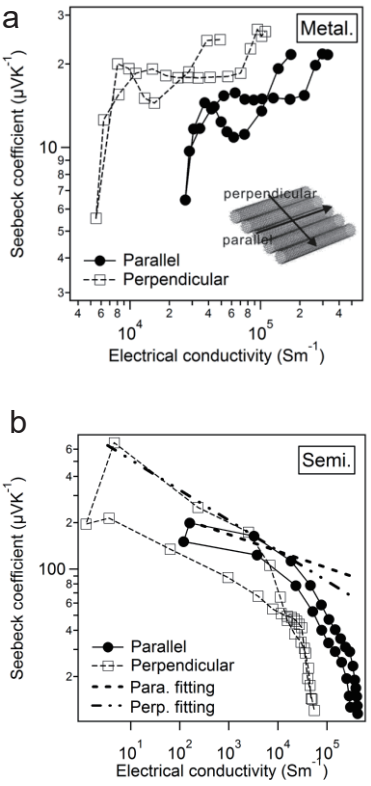

Figure 1. The correlation between Seebeck coefficient and electrical conductivity
(a) is the metallic and (b) is the semiconducting sample.

Reference: [1] Hicks & Dresselhaus, PRB **47**, 16631 (1993) [2] Fukuhara *et al*., APL **113**, 243105 (2018) [3] He *et al*., Nat. Nanotechnol. **11**, 1 (2016)

Corresponding Author: K. Yanagi, Tel: +81-42-677-2494, E-mail: yanagi-kazuhiro@tmu.ac.jp

Macroscopic four probe thermal and thermoelectric measurement of carbon nanotube fibers

Akito Sato [1], Kento Adachi [1], ○Takashi Kodama [1]

[1] *Department of Mechanical Engineering,The University of Tokyo, Tokyo 113-8656, Japan*

Carbon nanotubes (CNT) are one of most famous carbon nanomaterials and attract the interest in thermal management society for future thermal engineering application due to its excellent thermal and thermoelectric properties at nanoscale. Since most industrial applications require the bulk form, the CNTs must be made macroscopic structure such as the thin film and the CNT fibers [1] fabricated by various spinning method has been extensively investigated for the future application. However, it has been reported that the bulk properties of CNTs are varied depending on the material structure, and in particular, the structural dependent thermal and thermoelectric properties of CNTs has not been clarified so far due to lack of a simple and accurate measurement technique.

The suspended microfabricated device is generally utilized to estimate the thermal conductivity and thermoelectrical properties of nanomaterials to suppress and to define the heat loss through the measurement system [2], and a four probe thermal conduction measurement method has been recently reported to separate the thermal boundary conductance between sample and measurement structure from the measured thermal conductance, which becomes a cause of serious measurement error [3]. However, the appropriate device design is usually required depending on the material of interest and the device microfabrication cost is not neglectable for the simple evaluation of the thermal conduction properties. Furthermore, thermal conductivity measurement with the microfabricated device is not suitable for the measurement of macroscopic materials in terms of the measurement sensitivity.

Thus, we develop a simple thermal and thermoelectric measurement technique for macroscale fiber materials based on the nanoscale four probe thermal conduction measurement method. The measurement technique does not require the complicated device microfabrication process and the measurement system is composed of the suspended four bulk platinum wires with the samples at the center of the wires manipulated with a standard bonding machine. In the presentation, we demonstrate the simultaneous measurement of electrical conductivity, thermal conductivity, and the thermoelectric power of CNT fibers fabricated with a wet spinning method and report the details of the measurement technique.

[1] K. Mukai *et al*. Appl. Phys. Express **9**, 055101 (2016).
[2] T. Kodama *et al*. Nat. Mater. **16**, 892 (2017).
[3] J. Kim *et al*. Rev. Sci. Instrum. **86**, 044901 (2015).

Corresponding Author: T. Kodama
Tel: +81-3-5841-2744, Fax: +81-3-5841-8091,
E-mail: kodama@photon.t.u-tokyo.ac.jp

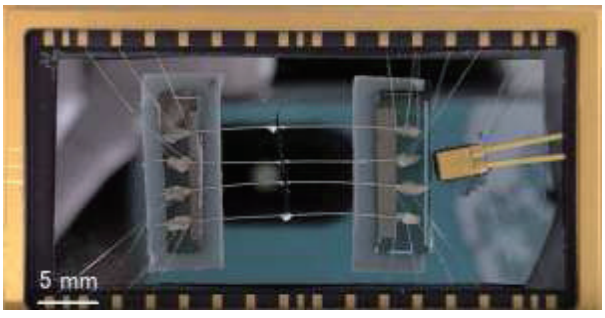

Fig.1 Photograph of the macroscopic four probe thermal measurement device

Bubble induced electron beam damage on graphene liquid cells during TEM observation

Sota Hirokawa[1], Hideaki Teshima[1,2], Pablo Solis Fernandez[3], Hiroki Ago[3], Yoko Tomo[4], Qin-Yi Li[1,2], Koji Takahashi [1,2]

[1] Department of Aeronautics and Astronautics, Kyushu University, 744 Motooka, Nishi-ku, Fukuoka 819-0395, Japan
[2] International Institute for Carbon-Neutral Energy Research (WPI-I2CNER), Kyushu University, 744 Motooka, Nishi-ku, Fukuoka 819-0395, Japan
[3] Global Innovation Center, Kyushu University, 6-1 Kasuga-koen, Kasuga-city, Fukuoka 816-8580, Japan
[4] Department of Mechanical Engineering, Kyushu University, 744 Motooka, Nishi-ku, Fukuoka 819-0395, Japan

Graphene liquid cells (GLCs) allows highest possible spatial resolution for liquid phase transmission electron microscopy (TEM)[1]. However, long time observation using GLCs is limited owing to the inevitable electron irradiation damage[2], [3]. Here, we investigate the occurrence of damage in the GLC wrapping water pockets under several electron beam conditions. Comparison of our observation proves that TEM with lower electron dose rate can reduce the damage possibility. Interestingly, during the observation of water pockets encapsulating no-bubbles, we never found the damage of GLC even with highest electron dose rate TEM. This fact indicates that electron beam induced damage in graphene depends on not only the electron dose rate but also whether there is bubbles in the GLC.

In addition, we use GLCs to study nanoscale dynamics that is induced by controllable damage in graphene. We observed air molecule leakage from bubble to water and unexpected directional nucleation of new bubbles, which is beyond the explanation of conventional diffusion theory.

[1] J. M. Yuk *et al.*, Science, **336**, 61–64, (2012).
[2] D. Shin *et al.*, Nat. Commun., **6**, 1–6, (2015).
[3] L. Wang *et al.*, Microsc. Microanal., **23**, 866–867, (2017).

Corresponding Author: K. Takahashi
Tel: +81-92-802-3015
E-mail: takahashi@aero.kyushu-u.ac.jp

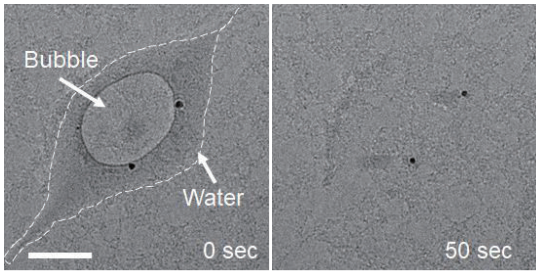

Fig.1. TEM image of a water pocket and encapsulated bubble (left). After GLC got damage, water and the bubble disappeared (right). Scale bar is 50 nm.

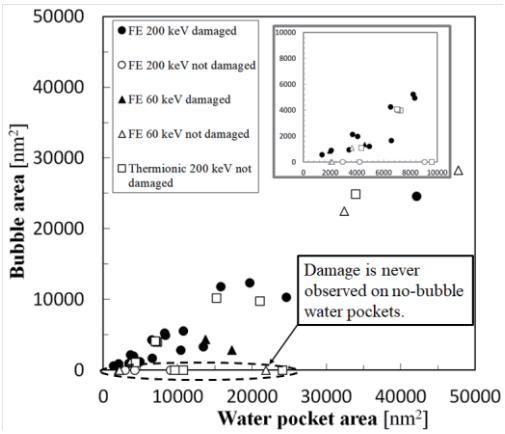

Fig.2. Relationship between GLC damage occurrences and size of water pockets and corresponding bubbles.

Strain-Induced Enhancement of Thermoelectric Power Factor of Graphene

○Kohei Suzuki[1], Kenji Sasaoka[2] and Takahiro Yamamoto[1,2]

[1] Department of Electrical Engineering, Tokyo University of Science, Tokyo 125-8585, Japan
[2] Water Frontier Science & Technology Research Center, Tokyo University of Science, Katsushika-Ku, 125-8585, Japan

Thermoelectric conversion is a key technology for sensor batteries for Internet of Things (IoT). Graphene is a potential candidate for flexible and sustainable thermoelectric materials. In fact, a previous experimental study reported the large power factor (PF=$S^2\sigma$) of graphene films[1], where σ is electrical conductivity and S is Seebeck coefficient. This large power factor originates from the high electrical conductivity, but the Seebeck coefficient is not large enough. In order to enhance the PF of graphene, we need to increase the Seebeck coefficient by introducing new technology.

As a new technology, we introduce the application of strain to the graphene, which has attracted much attention as a band-gap engineering[2]. In this study, we performed numerical simulation based on the non-equilibrium Green's function method combined with the tight-binding method. First, we calculated the chemical potential dependence of the power factor of a graphene under the local strain along the armchair direction at 300 K, which can be experimentally induced by shrinking the graphene films[3]. The obtained power factor has the peak structure at a certain chemical potential value, irrespective of the local strain. Fixing the chemical potential to this value, we estimate the strain dependence of the electrical conductance, the Seebeck coefficient and the power factor. The obtained results show that the Seebeck coefficient becomes larger with increasing the strain whereas the electrical conductance decreases. In addition, we clarified that the power factor is maximized at about 1 % strain. The maximum value becomes 1.4 times larger than the power factor of pristine graphene.

[1] K. Kanahashi, *et al*. npj 2D Materials and Applications, **44**, 3 (2019).
[2] S. Souma, *et al*., Phys. Lett. **104**, 213505 (2014)
[3] H. Shioya *et al.,* Nano Lett. **14**, 1158 (2014).
Corresponding Author: Takahiro Yamamoto
Tel & Fax: +81-03-5876-1486,
E-mail: takahiro@rs.tus.ac.jp

Spin-Filter Effect of Zigzag Graphene Nanoribbons with Edge Defects

○Naoya Abe[1], Kenji Sasaoka[2] and Takahiro Yamamoto[1,2,3]

[1] *Department of Electrical Engineering, Tokyo University of Science, Tokyo 125-8585, Japan*
[2] *Water Frontier Science & Technology Center, Tokyo University of Science, Japan*
[3] *Department of Liberal Arts, Tokyo University of Science, Tokyo 125-8585, Japan*

Spintronics is expected to one of new electronics for next generation, which utilizes not only charge degrees of freedom but also spin degrees of freedom. Many spintronic devices have been proposed, *e.g.*, a new device switching between up- and down-spin channels by the chemical potential [1]. This switching device performance can be evaluated by spin filter efficiency. One of the potential candidates for this switching device's materials is a hydrogen-terminated zigzag graphene nanoribbons (H-ZGNRs). Since the H-ZGNR is an atomic layer material, the gate voltage can be applied to the H-ZGNRs more efficiently than bulk materials. In addition, the H-ZGNRs are known to have edge magnetization [2] and their long spin relaxation time and long spin diffusion length are also advantage for the spintronics devices [3]. However, performance of spin filter effect under edge defects remains to be resolved thus far.

In this work, the spin-filter effect with edge defects of H-ZGNRs of about 10 nm in length, which is shorter than the spin diffusion length [3], is computationally examined using the density functional theory (DFT) method combined with the non-equilibrium Green's function (NEGF) technique. The exchange-correlation potential in the DFT calculation is treated as the local spin density approximation (LSDA). Moreover, we assume that the ground state of H-ZGNR is ferromagnetic. For this case, we calculate the electrical conductance of an H-ZGNR with/without edge defects. From our simulation results, we found that the spin filter efficiency exceeds 99% at characteristic chemical potential in the presence of the edge defects. This originates from Fano resonance originating from the defect level lying in the continuum electronic state of an H-ZGNR.

[1] K. Yabusaki et al., Jpn.J.Appl.Phy. **58**,045001 (2019).
[2] Y. W. Son et al., Natute **444**, 347 (2006).
[3] N.Tombros et al., Nature **448**, 571 (2007).

Corresponding Author: Takahiro Yamamoto
Tel&Fax: +81-3-5876-1492
E-mail: takahiro@rs.tus.ac.jp

Anomalous electroluminescence from WS_2/WSe_2 in-plane heterostructures

○Naoki Wada[1], Jiang Pu[2], Tomoyuki Yamada[2], Wenjin Zhang[3], Zheng Liu[4], Yusuke Nakanishi[1], Yutaka Maniwa[1], Kazunari Matsuda[3], Yuhei Miyauchi[3], Taishi Takenobu[2], Yasumitsu Miyata[1]

[1] *Department of Physics, Tokyo Metropolitan University, Hachioji 192-0397, Japan*
[2] *Department of Applied Physics, Nagoya University, Nagoya 464-8603, Japan*
[3] *Institute of Advanced Energy, Kyoto University, Uji, 611-0011, Japan*
[4] *Inorganic Functional Materials Research Institute, AIST, Nagoya, 463-8560, Japan*

Heterostructures of transition metal dichalcogenides (TMDCs) are an attractive system to realize high-performance devices such as light-emitting diodes and tunnel field-effect transistors. To investigate their electronic properties and device performance, we have developed growth processes of various in-plane heterostructures based on TMDC monolayers. In our previous studies, we have demonstrated the electric double layer light emitting diodes (EDLEDs) using these in-plane heterostructures [1-3]. In particular, we recently found that some samples show unique electroluminescence (EL) peaks, which have never been observed for photoluminescence spectra. However, the origin of these EL peaks is still unknown. In this study, we have investigated the spatially-resolved EL spectra of WS_2/WSe_2 in-plane heterostructures. The samples were grown by chemical vapor deposition (Fig.1a), and then EDLEDs were fabricated (Fig.1b). The device shows linear EL along the heterointerface by applying bias voltage (Fig. 1c). Interestingly, multiple EL peak components can be observed at a specific position along the interface as shown in Fig.1d. This suggests that the interface EL could be used to probe interface-derived electronic states and optical transitions. In this presentation, we will discuss about the detail of voltage- and site-dependent EL properties.

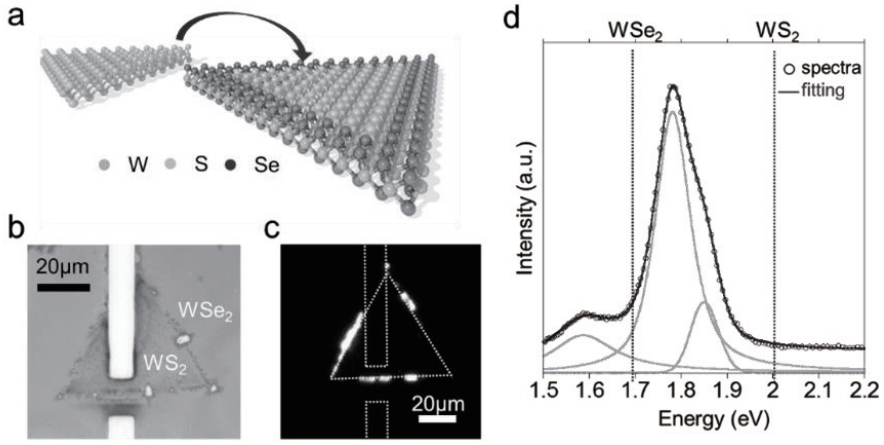

Fig.1 (a) Illustration of growth model of WS_2/WSe_2 in-plane heterostructures. (b) Optical and (c) EL images of WS_2/WSe_2-based EDLED device. (d) EL spectrum obtained at the interface.

[1] J. Pu et al., Adv. Mater. , 29, 1606918 (2017). [2] Y. Takaguchi et al., 56th FNTG symposium.
[3] N. Wada et al., 57th FNTG symposium.

Corresponding Author: Yasumitsu Miyata, Tel: 042-677-2508, E-mail: ymiyata@tmu.ac.jp

Absolute and relative intensity of the C_{60} IR absorption

○Tomonari Wakabayashi[1], Takamasa Momose[2], Mario E. Fajardo[3]

[1] Department of Chemistry, Kindai University, Higashi-Osaka, Osaka 577-8502, Japan
[2] Department of Chemistry and Department of Physics and Astronomy, The University of British Columbia, Vancouver, British Columbia 6VT 1Z1, Canada
[3] Munitions Directorate, US Air Force Research Laboratory AFRL/RWME, Eglin AFB, Florida 32542-5910, USA

The detection of C_{60} and C_{70} in space by the infrared (IR) emission spectra of planetary nebulae has rekindled interest in absolute band strengths of dipole-allowed infrared (IR) transitions of fullerenes for the estimation of their abundances [1,2]. Four IR-active vibrational modes of C_{60} are known to be key probes for the carbon molecule of high symmetry [3]. They are triply degenerate modes of T_{1u} symmetry and the behaviors are tricky when the icosahedral symmetry of I_h in $^{12}C_{60}$ is lowered by isotopic substitutions of ^{12}C nuclei by heavier ^{13}C isotopes. We studied in this work effects of isotopic substitutions on vibrational spectra by matrix isolation spectroscopy of C_{60} in cryogenic solid parahydrogen (pH_2), orthodeuterium (oD_2), and neon (Ne) matrix hosts using isotopically manipulated C_{60} samples and by molecular orbital (MO) calculations at B3LYP/6-31G(d) level of density functional theory (DFT) for the most important 328 distinct isotopomers of $^{13}C_n{}^{12}C_{60-n}$ of n = 0, 1, 2, and 3 [4].

Three-fold degeneracy of the T_{1u} mode is lifted upon ^{13}C-isotopic substitution into three distinct modes of different frequencies. The vibrational frequencies are lowered and the IR absorption intensities are decreased. IR-silent modes in I_h symmetry are activated for the IR absorption for vibrational modes of nearby frequencies to the T_{1u} modes. With increasing ^{13}C abundance, contributions from isotopically substituted species, $^{13}C_n{}^{12}C_{60-n}$ of $n \geq 1$, to the IR intensity of the other modes than T_{1u} increase. Nevertheless, the sum intensity of the split T_{1u} modes and the IR-activated modes of nearby frequencies remains constant (Fig. 1). The relative intensities observed by matrix isolation spectroscopy are well reproduced by the calculations. For a conclusion, we suggest a set of IR band strengths for the four IR-active T_{1u} modes of fullerene C_{60} based on the present DFT-MO calculation, e.g., S = 27.1 km/mol for $T_{1u}(3)$ at 1185 cm^{-1} (8.5 μm). For the others, see Fig. 1.

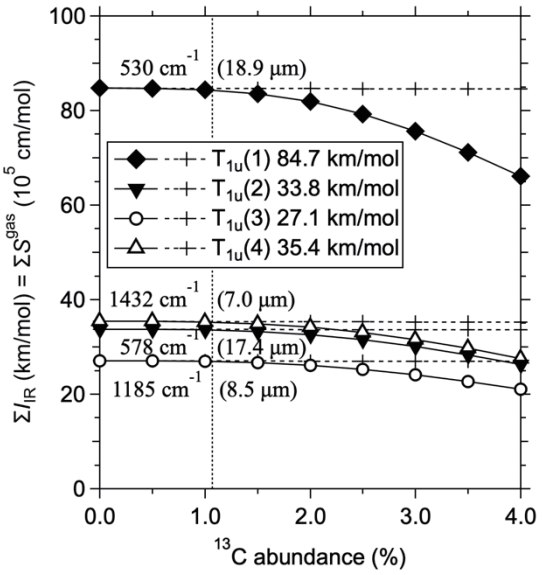

Fig. 1. Calculated band strengths of the four IR-active modes of C_{60} vs ^{13}C abundance: $T_{1u}(1)$ at 18.9 μm, $T_{1u}(2)$ at 17.4 μm, $T_{1u}(3)$ at 8.5 μm, and $T_{1u}(4)$ at 7.0 μm. Solid lines indicate IR absorption intensity of 328 isotopomers of $^{13}C_n{}^{12}C_{60-n}$ up to n = 3, while dotted lines include contributions from highly substituted isotopomers of $n \geq 4$.

[1] J. Cami, J. Bernard-Salas, E. Peeters, and S. E. Malek, *Science* **329**, 1180 (2010).
[2] M. Otsuka, F. Kemper, J Cami, E. Peeters, and J. Bernard-Salas, *Mon. Not. R. Astron. Soc.* **437**, 2577 (2014).
[3] W. Krätschmer, K. Fostiropoulos, and D. R. Huffman, *Chem. Phys. Lett.* **170**, 167 (1990).
[4] T. Wakabayashi, T. Momose, and M. E. Fajardo, *J. Chem. Phys.* **151**, 234301 (2019).
Corresponding Author: T. Wakabayashi, Tel: +81-6-4307-3408, E-mail: wakaba@chem.kindai.ac.jp

A one-step direct oxidation of alkoxy to ketone: oxidation of alkoxy indano[60]fullerenes to [60]fullerene-fused ketones *via* weak copper oxidant

○Yue Ma [1], Hao-Sheng Lin [2], Yun Yu[1] , Shigeo Maruyama[2], Il Jeon[2], Yutaka Matsuo [1,2]

[1] *Hefei National Laboratory for Physical Sciences at Microscale, University of Science and Technology of China, 96 Jin-zhai Road, Hefei, Anhui 230026, China*
[2] *Department of Mechanical Engineering, School of Engineering, The University of Tokyo, Bunkyo-ku, Tokyo 113-8656, Japan*

Considerable endeavors have been devoted to selective oxidation of alcohols to ketones in the field of organic chemistry. However, all protocols turn into ineffective once alcohols are protected/functionalized by alkyl group that forming the alkoxy group. Consequently, the one-step oxidation of alkoxy to ketone has never been unveiled and still remains great challenges, especially by using weak oxidants. Recently, carbonyl [60]fullerene and its derivatives have attracted intensive attentions due to their impressively potential applications in photovoltaics. Among these carbonyl [60]fullerene derivatives, the fullerene-fused ketone has more potential for photovoltaics owing to its unique full-carbon-five-membered ring structure, and the synthetic building block that the ketone moiety renders.

In this work we realized the one-step direct oxidation of alkoxy indano[60]fullerenes to [60]fullerene-fused ketones through weak oxidant, $CuBr_2$, in moderate yields with an excellent functional group tolerance. The products were unambiguously characterized by NMR spectroscopy, MALDI-TOF mass spectrometry. The reaction mechanism was thoroughly studied via analyzing the intermediate, isotopy effect and EPR measurement. Besides, the reaction scope was enlarged via the optimized reaction condition.

Figure 1. The concept of $CuBr_2$-promoted one-step oxidation of alkoxy indano[60]fullerenes to fullerene-fused ketones.

.

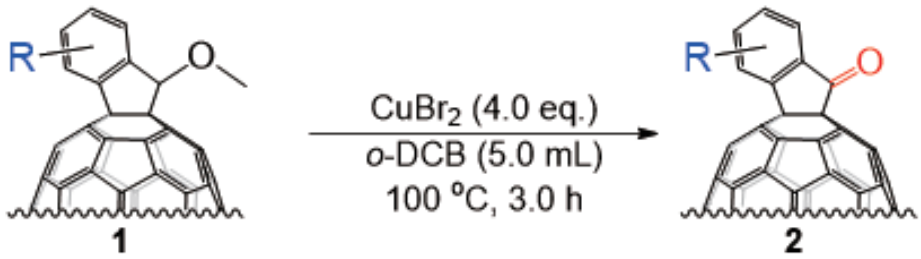

[1] Lin, H-S. *et al*. *Chem. Mater.* **2019**, 31, 8432−8439

Corresponding Author: Y. Matsuo
Tel: +81-3-5841-0978, E-mail: matsuo@photon.t.u-tokyo.ac.jp

ESR study of La and Y hetero-dimetallofullerene anions

○Moeno Maejima, Koichi Kikuchi, Yohji Achiba, Takeshi Kodama

Department of Chemistry, Tokyo Metropolitan University, Tokyo 192-0397, Japan

Dimetallofullerene anions $[M_2@C_n]^-$ (M = Y and La) (n = 78, 80) have an electron on the internal M_2 dimmer, which is mainly composed of s and d orbitals [1]. ESR is a powerful tool to reveal the nature of the dimer orbital via hyperfine coupling constants. In this study, we synthesized and isolated hetero-dimetallofullerene anions, $[LaY@C_n]^-$, to elucidate the character of the hetero-dimer orbital by ESR.

Soot containing metallofullerenes was produced by DC arc discharge under He atmosphere. The produced soot was extracted by a mixture of acetone and triethylamine. The separation was performed by HPLC. Sample isolation was confirmed by LD-TOF-MS and the cage structure was identified by UV-Vis-NIR absorption. Electronic structure of $[LaY@C_n]^-$ was investigated by X-band ESR.

Fig. 1 shows the ESR spectrum of $[LaY@C_{78}]^-$. Although the three peaks due to a small amount of not separated $[Y_2@C_{78}]^-$ was observed, the other 16 peaks were assigned to an electron spin on the internal La-Y dimmer of $[LaY@C_{78}]^-$, S=1/2, coupled with nuclear spins of ^{139}La(I=7/2) and ^{89}Y(I=1/2). From the spectrum simulation, the isotropic g factor (g_{iso}) and the hyperfine coupling constants (A_{iso}) for La and Y were obtained and listed in Table 1 with the results of $[Y_2@C_{78}]^-$ and $[La_2@C_{78}]^-$ [2, 3].

A_{iso} is proportional to the spin density on the nucleus, then it represents a degree of the s-orbital contribution. A_{iso} for Y of $[LaY@C_{78}]^-$ is larger than that of $[Y_2@C_{78}]^-$ while A_{iso} for La is smaller than that of $[La_2@C_{78}]^-$. Therefore, it was suggested that the density of an unpaired electron on Y is larger than that of La in $[LaY@C_{78}]^-$. This result is reasonable because the dimmer orbital composed of 4d, 5s-orbital of Y and 5d, 6s-orbitals of La and the energy of 5s-orbital of Y is lower than that of 6s-orbital of La.

In the symposium, the results of low temperature ESR for $[LaY@C_{78}]^-$ and $[LaY@C_{80}]^-$ will be also discussed.

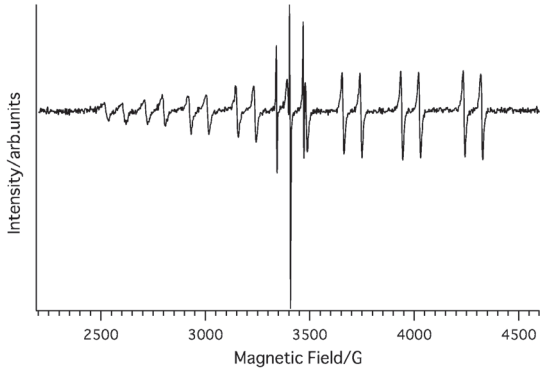

Fig.1 ESR spectrum of $[LaY@C_{78}]^-$

Table 1 ESR parameters

	$[LaY@C_{78}]^-$	$[Y_2@C_{78}]^-$	$[La_2@C_{78}]^-$
g_{iso}	1.951	1.985	1.961
A_{iso}/MHz	668 (La) 235 (Y)	170	827

[1] A. Velloth *et al*. *J. Phys. Chem.* C. **121**, 18169 (2017).

[2] N. Nakatori *et al*. *The 50th Fullerenes-Nanotubes-Graphene General Symposium* 44 (2016).

[3] S. Nishimoto *et al*. *The 52nd Fullerenes-Nanotubes-Graphene General Symposium* 129 (2017).

Corresponding Author: Takeshi Kodama

Tel: +81-42-677-2530, Fax: +81-42-677-2525, E-mail: kodama-takeshi@tmu.ac.jp

ESR Study of two isomers of $[Sc_2C_{80}]^-$: $[Sc_2C_{80}(1)]^-$ and $[Sc_2C_{80}(2)]^-$

○Shun Yoshida[1], Ko Furukawa[2], Koichi Kikuchi[1], Yohji Achiba[1], Takeshi Kodama[1]

[1]*Department of Chemistry, Tokyo Metropolitan University, Tokyo 192-0397, Japan*
[2]*Center for Coordination of Research Facilities, Niigata University, Niigata 950-2181, Japan*

In the previous symposium, we reported the isolation of two isomers of $[Sc_2C_{80}]^-$: $[Sc_2C_{80}(1)]^-$ and $[Sc_2C_{80}(2)]^-$ [1]. Moreover, X-band ESR spectra of them at room temperature were measured [2]. Both ESR spectra for $[Sc_2C_{80}(1)]^-$ and $[Sc_2C_{80}(2)]^-$ showed the isotropic patterns due to the fast motion in solution, and were essentially consisted of 64 peaks, respectively (some peaks were overlapped). The spectral simulation reproduced well the spectra, and the obtained isotropic hyperfine coupling constants (A_{iso}), which come from the interaction between an unpaired spin and nuclear spin of Sc (I=7/2), were very large: $A_{iso}(1)$=497.5 MHz, $A_{iso}(2)$=464.9 MHz. Therefore, it was concluded that an unpaired spin is located on the encaged Sc dimer because A_{iso} is proportional to spin density on the metal nucleus. In this study, to investigate the spin state of two isomers of $[Sc_2C_{80}]^-$ more in detail, we measured X-band cw-ESR spectra and Q-band ESEFS (Electron-Spin-Echo detected Field-Sweep) spectra at low temperature.

Fig. 1 is the X-band cw-ESR spectrum of $[Sc_2C_{80}(1)]^-$ and showed very complex and anisotropic pattern due to the random orientation of $[Sc_2C_{80}(1)]^-$ fixed in frozen solution. Fig. 2 is Q-band ESEFS spectrum of $[Sc_2C_{80}(1)]^-$. Because the microwave frequency for Q-band measurement is about 4 times larger than that for X-band, Zeeman interaction is dominant over hyperfine interaction, and the latter contributes as perturbation. Therefore the spectral feature for Q-band is rather simple compared with X-band. Both two spectra were simulated by the same set of parameters.

In the symposium, the assignments of the peaks of these spectra with the results of $[Sc_2C_{80}(2)]^-$ will be discussed.

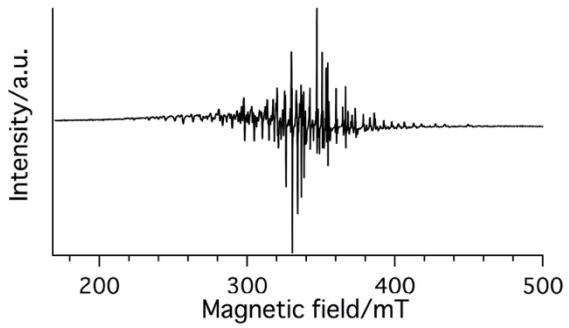

Fig. 1 X-band cw-ESR spectrum of $[Sc_2C_{80}(1)]^-$ (4 K)

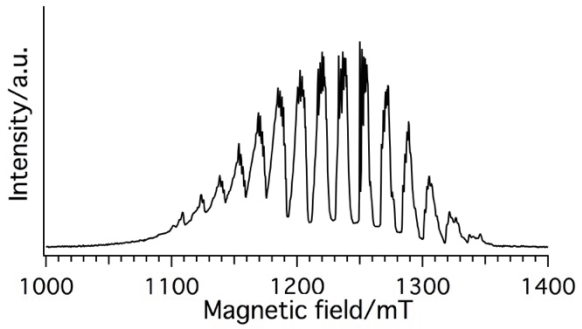

Fig. 2 Q-band ESEFS spectrum of $[Sc_2C_{80}(1)]^-$ (10 K)

[1] S.Yoshida, *et al. The 55th Fullerenes-Nanotubes-Graphene General Symposium* 126 (2018).
[2] S.Yoshida, *et al. The 56th Fullerenes-Nanotubes-Graphene General Symposium* 59 (2019).

Corresponding Author: Takeshi Kodama
Tel: +81-42-677-2530, Fax: +81-3-42-677-2525
E-mail: kodama-takeshi@tmu.ac.jp

Doped-site structure dependent energy shifts of photoluminescence from locally functionalized single-walled carbon nanotubes in organic solvent environments

○Tomohiro Shiraki[1,2], Yoshiaki Niidome[1], Tsuyohiko Fujigaya[1,2,3]

[1] *Department of Applied Chemistry, Kyushu University, Fukuoka 819-0395, Japan*
[2] *WPI-I2CNER, Kyushu University, Fukuoka 819-0395, Japan*
[3] *CMS, Kyushu University, Fukuoka 819-0395, Japan*

Single-walled carbon nanotubes (SWNTs) show near infrared photoluminescence (PL) whose energy is sensitively changed by their microenvironments composed of surfactants and solvents.[1] The PL properties have been found to be enhanced by defect doping that is achieved by local chemical functionalization of SWNTs. As one example of synthetic methods of the locally functionalized SWNTs (lf-SWNTs), diazonium chemistry using aryldiazonium salts was reported to produce sp^3 carbon defects in the sp^2 carbon network of the SWNTs via the aryl group functionalization.[2] The lf-SWNTs emit E_{11}* PL that has narrower band-gap energies with higher quantum yields compared to E_{11} PL of pristine SWNTs. In addition, E_{11}* PL energies are modulated depending on the chemical structures of the functionalized aryl groups at the doped sites. Very recently, we have reported that E_{11}* PL showed larger energy shifts than E_{11} PL when organic solvents were injected to the aqueous lf-SWNTs solubilized by surfactant micelles.[3] This result shows that the doped sites have high sensitivity to the microenviroments, and the unique properties are expected to be modulated depending on the difference in chemical structures of the doped sites of lf-SWNTs.

In this study, we examined microenvironment effects of the lf-SWNTs having different doped sites structures: bis-aryl functionalized lf-SWNTs that show E_{11}^2* PL appearing longer wavelength regions than typical E_{11}* PL [4] and oxygen(O)-doped lf-SWNTs that have defects with ether or epoxide structures.[5] Fig. 1 shows energy shifts of E_{11}^2* PL from bis-aryl functionalized lf-SWNTs (ΔE_{11}^2*) as a function of a solvent polarity parameter of $f(\varepsilon) - f(\eta^2)$. The ΔE_{11}^2* showed larger energy shifts according to the increase in the values of $f(\varepsilon) - f(\eta^2)$ with a liner correlation. By comparison of the lf-SWNTs with different structures including O-doped ones, the shifting manner was found to change with strong dependence on the chemical structures of doped sites.

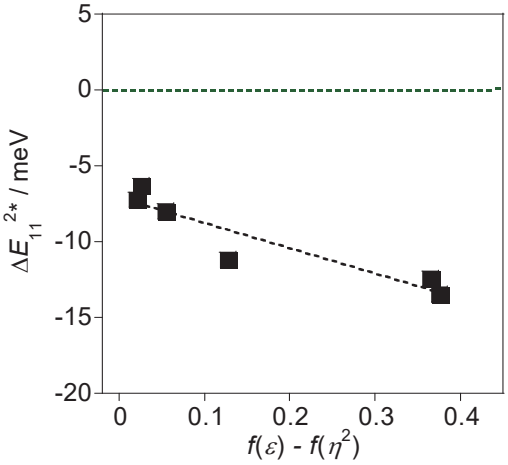

Fig.1 Plots of ΔE_{11}^2* as a function of $f(\varepsilon) - f(\eta^2)$ for bis-aryl functionalized lf-SWNTs that were treated by injection of organic solvents.

[1] Y. Ohno *et al*. Phys. Status Solidi B. **244**, 4002 (2007). [2] Y. Wang *et al*. Nat. Chem. **5**, 840 (2013). [3] T. Shiraki *et al.* Chem. Commun. **55**, 3662 (2019). [4] T. Shiraki *et al*. Sci. Rep. **6**, 28393 (2016). [5] Y. Miyauchi *et al*. Nat. Photon., **7**, 715 (2013).

Corresponding Author: T. Fujigaya
Tel: +81-92-802-2842, Fax: +81-92-802-2842
E-mail: fujigaya.tsuyohiko.948@m.kyushu-u.ac.jp

Electrical detection of X-ray by using coplanar CNT thin-film electrodes on PEN substrate

○Hiroyuki Matsuda[1], Satoru Suzuki[1], Takahiro ishikawa[2], Teruaki Konishi[2], Tsuyoshi Hamano[2], Yutaka Ohno[3,4], Toshio Hirao[2], Satoshi Ishii[1]

[1] Department of Physics, Tokyo Denki University, Saitama 350-0394, Japan
[2] National Institute for Radiological Sciences, National Institutes for Quantum and Radiological Science and Technology, Chiba 263-8555, Japan
[3] Department of Electronics, Nagoya University, Nagoya 464-8602, Japan
[4] Institute of Materials and Systems for Sustainability, Nagoya University, Nagoya 464-8601, Japan

Radiation exposure to the eye lens has been a problem for a curer in the radiation therapy. Then, the transparent real-time dosimeter is required to measure the eye dose without disturbing their eyesight. In order to develop the transparent detector, transparency is necessary not only for the substrate but also for the electrode. Carbon nanotube is known to have transparency along with radiation tolerance [1]. In this study, we have fabricated the coplanar CNT thin-film electrodes on the PEN sheet and conducted the direct electrical detection of X-ray using these.

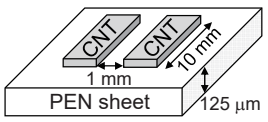

Fig.1 Device structure.

Figure 1 shows the schematic structure of the device, where the distance between the CNT thin-film electrodes was 1 mm. The electrodes were patterned on the PEN substrate by splay coating of the single-walled CNT dispersion in IPA (0.2 wt%) using the metal mask. The device was placed inside of the stainless chamber under a vacuum of 1.0×10^{-2} Pa. X-ray with an effective energy of 83 keV was irradiated to the device from outside of the chamber at a bias voltage of 10 V. The current of the device was measured in real time during turning on and off of the irradiation at each dose rate.

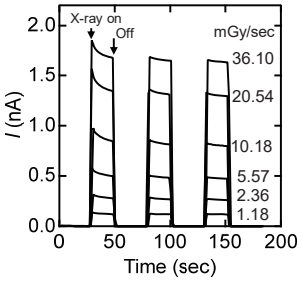

Fig.2 Time dependence of the current.

The current was confirmed to respond to the X-ray irradiation, as shown in Fig. 2. Moreover, the generated current increased linearly with the dose rate below 10.18 mGy/sec, as shown in Fig. 2, although it no longer changed linearly above 20.54 mGy/sec. It is thought that the generated current was the charges originated from the ionized residual gas inside the chamber, and that it did not reach the saturated region under the biased voltage. The CNT thin-film electrodes on the PEN sheet is applicable to the real-time transparent detector.

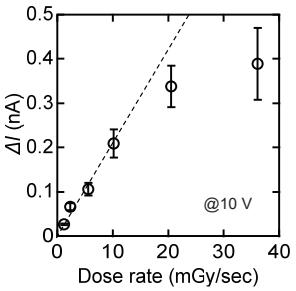

Fig.3 Dose rate dependence of the generated current.

This work was supported partially by the joint usage/research program of the Institute of Materials and Systems for Sustainability (IMaSS), Nagoya University.

[1] S. Ishii *et al*. Physica E. **86**, 297 (2017).

Corresponding Author: S. Ishii
Tel: +81-49-296-1926, Fax: +81-496-296-2915,
E-mail: s.ishii@mail.dendai.ac.jp

Understanding and controlling the pyrolysis of C_3H_8 for uniform synthesis of vertically-aligned single-wall carbon nanotubes

○Meng-Ju Yang[1], Pengfei Chen[1], Rei Nakagawa[1], Hisashi Sugime[1], Hitoshi Mazaki[2], Suguru Noda[1,3,*]

[1] *Department of Applied Chemistry, School of Advanced Science and Engineering, Waseda University, 3-4-1 Okubo, Shinjuku-ku, Tokyo 169-8555, Japan*

[2] *Central Technical Research Laboratory, JXTG Nippon Oil & Energy Corporation, 8 Chidori-cho, Naka-ku, Yokohama, Kanagawa 231-0815, Japan*

[3] *Waseda Research Institute for Science and Engineering, Waseda University, 3-4-1 Okubo, Shinjuku-ku, Tokyo 169-8555, Japan*

Single-wall carbon nanotubes (SWCNTs) have been extensively researched, but the low-cost mass production of high-quality SWCNT is still a challenge. Among others, C_2H_2 is known as a highly active carbon feedstock which can grow vertically-aligned SWCNTs (VA-SWCNTs) directly without gas-phase reactions [1]. However, larger area SWCNT growth is difficult because supplying C_2H_2 with high concentration tends to deactivate the catalysts easily [2]. Therefore, controlling the gas-phase reactions is important for the large area growth as shown with the combined feed of C_2H_2 and C_2H_4 in our previous report [3]. From this viewpoint, the low-activity carbon feedstocks are considered to play an important role. Some carbon species were previously studied [4], however the possibility of the SWCNT growth with thinner Fe conditions was overlooked since the catalyst condition was fixed. In this study, by changing Fe thickness of Fe/Al_2O_x/Si samples using our original combinatorial method [5], the growth of millimeter-tall VA-SWCNTs is studied using C_3H_8 as a carbon feedstock. It was found that, compared to C_2H_2, C_3H_8 can grow larger amount of the VA-SWCNTs with thinner Fe (Fig. 1a). With 0.40 nm Fe, the average areal SWCNT yield at 800 °C for 30 min was 3.4 mg cm^{-2} with C_3H_8 whereas it was 1.4 mg cm^{-2} with C_2H_2 (Fig. 1b). The analysis of the gas species by gas chromatography indicated that C_3H_6 which was generated by the decomposition of C_3H_8 plays a key role for the SWCNT growth.

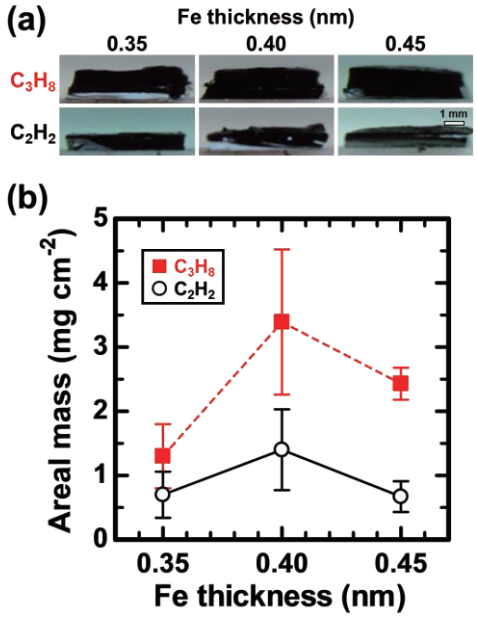

Fig. 1: (a) Side-view images of the SWCNT forests with different Fe thickness (on Al_2O_x/Si samples) at 800 °C after 30 min using C_3H_8 or C_2H_2. (b) Areal mass of the SWCNTs corresponding to the samples shown in (a).

[1] H. Sugime et al., *Carbon* **50**, 2953 (2012). [2] K. Hasegawa et al., *ACS Nano* **5**, 975 (2011). [3] T. Sato et al., *Carbon* **136**, 143 (2018). [4] H. Kimura et al., *ACS Nano* **7**, 3510 (2013). [5] S. Noda et al., *Carbon* **44**, 1414 (2006).

Corresponding Author: S. Noda, Tel: +81-3-5286-2769, E-mail: noda@waseda.jp

Synthesis of boron nitride nanotube by chemical vapor deposition using new boron source

○Tetsuro Sawada[1], Hiromu Takahashi[1], Tomohiro Sei[1], Mayu Asaka[1], Toshio Osawa[1], Hisashi Sugime[1], Suguru Noda[1,2,*]

[1] The Department of Applied Chemistry, [2]Waseda Research Institute for Science and Engineering, Waseda University, Tokyo 169-8555, Japan.

Boron Nitride Nanotube (BNNT) has high thermal stability, chemical stability, and thermal conductivity similarly to carbon nanotube (CNT) with electrical insulation and optical transparency oppositely to CNT. We may design various new devices by combining them. Physical vapor deposition (PVD) is known as a production method for high quality BNNT [1]. However impurities such as B-powder and h-BN flakes are included at high contents in the product, and high production cost stems from the very high temperature and solid source materials (B or BN powders) used in the PVD processes. Chemical vapor deposition (CVD) is another production method of BNNT that may enable its mass production at low cost due to the moderate reaction temperature and gaseous source materials. Ammonia (NH_3) is an effective nitrogen source of low cost [2], however there lack the good boron source of low cost and low risk. For example, diborane is highly explosive and poisonous while BCl_3 etch the catalyst away. Borazine and ammonia borane are widely used for h-BN atomic layers but expensive for mass production of BNNTs.

In this work, we report boric acid (H_3BO_3) as a new boron source of low cost and low risk. BNNT was synthesized on graphite substrates with sputter-deposited Fe catalyst using a conventional tubular thermal CVD reactor. BNNT was synthesized at 950 °C for 10 min by feeding H_3BO_3 vapor and NH_3 Ar carrier gas. The as-grown substrates were analyzed by scanning electron microscope (SEM) and Raman scattering spectroscopy (excitation wavelength: 633 nm). The color of the graphite substrates turned from gray to white. The SEM image showed many tube-like structures (Fig. 1), and the Raman spectroscopy showed peaks at ~ 1370 cm^{-1} (not shown) originating from h-BN structure [2]. These results showed that BNNT were synthesized using the new boron source, i.e. H_3BO_3 vapor.

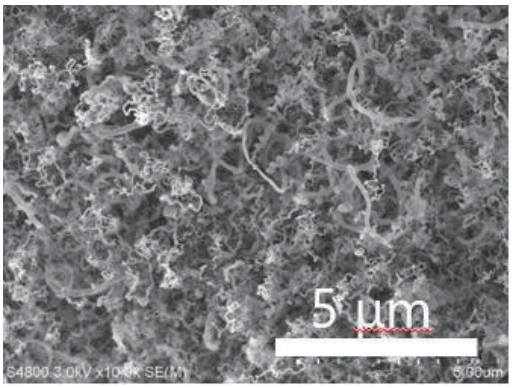

Fig. 1. SEM image of BNNT produced by CVD using H_3BO_3 and NH_3 sources and Fe/graphite substrate.

[1] K. S. Kim et al., Semicond. Sci. Technol. **32**, 013003 (2017).

[2] P. Ahmad *et al*., RSC Adv. **20**, 35116 (2015).

Corresponding Author: S. Noda, Tel: 03-5286-2769, E-mail: noda@waseda.jp

Sublimation property of a flavin compound which is a surfactant for carbon nanotube dispersion

○Yuichi Kato,[1] Kazufumi Kobashi,[1] Takeo Yamada,*[1] and Kenji Hata[1]

[1]*CNT-Application Research Center, National Institute of Advanced Industrial Science and Technology (AIST), Central 5, 1-1-1 Higashi, Tsukuba 305-8565, Japan*

Dispersing to liquid with surfactants has been an important technique to utilize unique electronic property of single-walled carbon nanotubes (SWNTs), especially in the field of electronics. Surfactants play an important role to strongly adsorb and stabilize to isolated SWNT. On the other hand, the strongly adsorbed surfactants have problems of removal. An approach to remove surfactants is a wet process; adsorption stability control has been studied. The other possible approach for removing is a dry process of gasification. In this presentation, we show the sublimability of a flavin compound, 10-dodecyl-7,8-dimethyl-10*H*-benzo[*g*]pteridine-2,4-dione (**dmC12**, Fig. 1a),[1] which is a surfactant for carbon nanotube dispersion (Fig. 1b) and chirality separation.

We heated **dmC12** in a flask to 240-260°C with a mantle heater under low pressure conditions (0.65-3×10^{3}Pa) in the absence or presence of SWNT. In both cases, we found a yellow material at the top of the flask (Fig. 2). UV-vis absorption spectroscopy and ^{1}H NMR indicate that the yellow material was **dmC12**. These results indicate **dmC12** has sublimability and show our concept; sublimation can be a useful way to remove the surfactant from SWNT surfaces. Calculated saturated vapor pressure of **dmC12** is 0.08 Pa at 250°C (Fig. 3) measured by the vapor pressure evaluation system VPE-9000 (under high vacuum 2.1×10^{-3} Pa). In this test, no residue was visually observed (98% weight decrease).

In the presentation, we would like to discuss the further improving the sublimation property of a flavin compound because thermal reactions compete with sublimation around 250°C under the practical low pressure (0.65-3×10^{3}Pa), unfortunately. We observed a red viscous material at the bottom of the flask. Considering the chemical structure, the long linear alkyl chain of **dmC12** is a steric repulsion site. It is common that saturated vapor pressure of branched hydrocarbons is higher than that of straight chained hydrocarbon. It suggests that there is room to lower the sublimation temperature by changing the chemical structure.

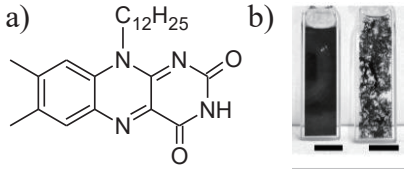

Fig.1 a) Chemical structure of **dmC12**. b) Photograph of the SWNT suspensions in toluene in the presence (left) and absence (right) of **dmC12** (scale bar=1 mm).

Fig.2 Photo of yellow material at the top of the flask.

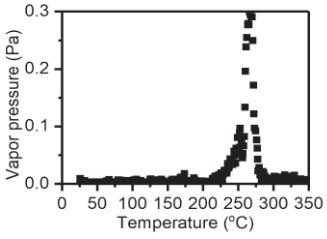

Fig.3 Saturated vapor pressure plot of **dmC12**.

[1] Y. Kato *et al*. Chem. Lett. (2020), accepted.

Corresponding Author: T. Yamada
Tel: +81-29-861-8435, Fax: +81-29-861-4851
E-mail: takeo-yamada@aist.go.jp

CVD synthesis of sub-nanometer diameter single-walled CNTs

○ Kamal P Sharma[1,2], Daiki Yamamoto[1], Aliza K. Sharma[1], Takahiro Maruyama[1,2]

[1] *Department of Applied Chemistry, Meijo University, Nagoya 468-8502, Japan*

[2] *Nanomaterials Research Center, Meijo University, Nagoya 468-8502, Japan*

Single walled carbon nanotube (SWCNT) comprised of fore frontier application due to its superior chemical, electrical and optical properties [1]. Chirality controlled SWCNT synthesis is progressing very rapidly to surpass the post growth treatment process [2]. So synthesized SWCNTs had more than 1 nm diameter and with very low yield. Narrow diameter distributed SWCNTs possesses fewer chirality and synthesis of such tubes could be an alternative technique to solve the aforementioned problem. Here we challenge to address this issue by utilizing simultaneously deposited Co and W onto SiO_2 as a catalyst.

An ultrahigh vacuum (UHV) chemical vapor deposition (CVD) system with nozzle through which ethanol vapors is supplied at vicinity substrate was used as a growth chamber as reported elsewhere [3]. 0.2 nm Co and simultaneously deposited 0.2 nm Co and 0.4 nm W onto SiO_2/Si (referred as Method-A and Method-B respectively) were utilized as growth substrates. 10^{-1} Pa ethanol vapor over the 10^{-6} Pa base pressure was utilized for 60 min at elevated temperatures. As synthesized SWCNTs under our optimized condition were analyzed by Raman spectroscopy, FESEM, XPS and TEM.

Figure 1 (a) and **Figure 1 (b)** show the Raman spectra of SWCNTs grown for 60 min at 600°C (Method A) and 800°C (Method B) respectively by keeping other conditions unchanged and were the optimal growth conditions. It is clearly observable in **Figure 1 (b)** that RBM peaks were dominantly shifted to higher energy region compared to **Figure 1(a)**, indicating sub-nanometer distributed SWCNTs. Background to **Figure 1 (a) and (b)** show the corresponding FESEM images.

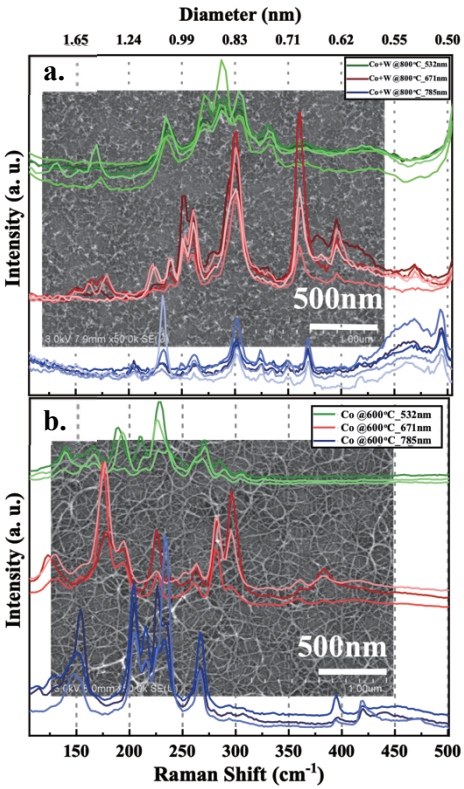

Figure 1. Raman spectrum of SWCNT grown onto SiO_2/Si by ACCVD technique at **(a)** 600°C by utilizing 0.2 nm Co and **(b)** 800°C using 0.4nm W/0.2nm Co. background show the corresponding FESEM images.

This work was supported in part by Private University Research Branding Project from the Ministry of Education, Culture, Sports, Science and Technology (MEXT), Japan.

[1] R. H. Baughman, et al. Science, 297, 787 (2002).
[2] F. Yang et al., Nature, 510, 522 (2014).
[3] T. Maruyama et al. Carbon 116, 128 (2017).

Corresponding Author: Takahiro Maruyama
E-mail: takamaru@meijo-u.ac.jp

Study of CVD growth mechanism of graphene on a-plane sapphire

○Yuki Ueda[1], Jumpei Yamada[1], Takahiro Maruyama[2], and Shigeya Naritsuka[1]

[1] *Department of Materials Science and Engineering, Meijo University, Nagoya 468-8502, Japan*
[2] *Department of Applied Chemistry, Meijo University, Nagoya 468-8502, Japan*

Direct growth of graphene on an insulating substrate has been studied to avoid the transfer process, which bring many problems upon industrial applications. Conventionally, c-plane sapphire is widely used as a growth substrate. Saito et al. demonstrated that the quality of graphene grown on a-plane sapphire was better than that grown on c-plane sapphire [1]. However, graphene growth on a-plane sapphire was rarely reported, and its growth mechanism has not been clarified yet. In this study, the influence of growth pressure on graphene CVD growth on a-plane sapphire is investigated for clarifying its growth mechanism.

Graphene was directly grown on a-plane sapphire at 1250 ºC by low-pressure CVD without metal catalyst. Mixture gas of N_2, H_2, and 3-Hexyne was flown to a reactor for the growth of graphene. Growth pressure was chosen 5 and 50 kPa.

Figure 1 shows the growth pressure dependence of Raman spectra. In both cases, the total gas flow rate, 3-Hexyne partial pressure, and H_2 partial pressure were the same. In the case of 5 kPa, the obtained D, G, and G' peaks show that graphene was already grown at 1 h. On the other hand, in the case of 50 kPa, graphene was not grown even at a longer growth time of 3 h. Figure 1 (b) and (c) show the surface AFM images of samples grown at growth pressures of 50 kPa and 5 kPa, respectively. The surface of the sample grown at 50 kPa was flat while that of the sample grown at 5 kPa was rough. These results indicate that a large amount of atoms of the sapphire surface were thermally desorbed during CVD when the growth pressure was as low as 5 kPa. As a result, it is considered that the decomposition efficiency of the carbon source was possibly improved by the catalytic effects of the thermally desorbed Al atoms, leading to a high degree of supersaturation for graphene nucleation and growth. On the other hand, when the growth pressure was as high as 50 kPa, the thermal desorption of Al atoms was suppressed. Therefore, the degree of supersaturation was insufficient for graphene nucleation because the carbon source was difficult to decompose by the weak catalytic effect of the sapphire surface.

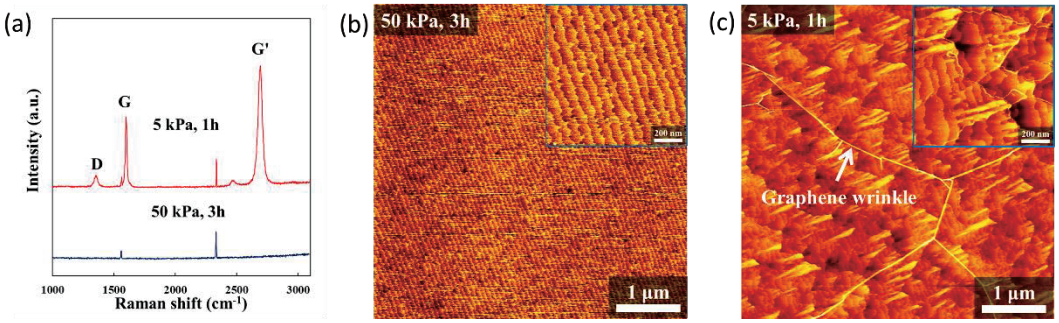

Figure 1 Growth pressure dependence of Raman spectra (a). AFM images of samples grown at 50 kPa (b) and 5 kPa (c).

Acknowledgement: This work was supported in part by JSPS KAKENHI Grant Numbers 15H03559, 26105002.

[1] K. Saito et al., J. Phys. Chem. C 118, 5523 (2014).

Corresponding Author: Y. Ueda, Tel: +81-52-838-2387, E-mail: 173441501@ccalumni.meijo-u.ac.jp

Heteroatom-doped Nanocarbons as Active Support for IrO_2 as an OER Electrocatalyst

○Prerna Joshi, Rohit Yadav, Masanori Hara, Masamichi Yoshimura

Surface Science Laboratory, Toyota Technological Institute, Nagoya, 468-8511, Japan

Increasing demand for renewable energy systems have guided us to look for environment-friendly and cheaper energy sources. In this regard, hydrogen comes as a promising candidate which can be obtained by electrochemical water splitting in water electrolyzers (WEs). However, oxygen evolution reaction (OER) occurring at anode in WEs is kinetically sluggish and requires the use of Ir based catalysts. Recent research in the field of OER electrocatalysts focusses on minimizing the overpotential and reduction in the loading amount of the catalyst. To overcome these problems, tuning the surface of the catalyst is achieved by the use of conductive nanocarbon supports doped with heteroatoms [1] such as B and/or N which increase the electrical conductivity and tolerability of the nanocarbon towards electrolyte medium [2]. Present research focusses on the mono (B or N) and bi-atom doping of graphene (B and N) as support materials and examines its effect on the OER activity of IrO_2 nanoparticles (nps).

The synthesis of nanocarbon supports was done via pyrolysis of graphene oxide (prepared by synthetic graphite via modified Hummers' method) and the dopant precursor, urea (N), boron anhydride, BA (B) and urea+ BA (B/N) at 800, 1000 and 1000 °C respectively to yield N-rGO, B-rGO and B/N-rGO in N_2 atmosphere for 60 min. Further, IrO_2 nps were decorated via hydrothermal method on the doped carbon supports. Prepared catalysts were characterized by X-ray photoelectron spectroscopy (XPS), transmission electron microscopy (TEM), energy dispersive X-ray spectroscopy (EDX) and were evaluated for their electrochemical activity towards OER by linear sweep voltammetry (LSV) with rotating disk electrode (RDE) system).

The presence of the respective elements in the catalysts was confirmed by XPS. Further, EDX analysis confirmed the homogeneity of the dopants and IrO_2 on graphene lattice. The average particle size estimated from TEM for IrO_2 nps on N-rGO, B-rGO and B-N-rGO was 1.6, 1.5 and 1.8 nm respectively. Electrochemical analysis was carried out by LSV in 0.5 M H_2SO_4 solution (Fig. 1). Catalysts with doped supports (N-rGO, B-rGO and B/N-rGO) showed low overpotential and better durability than undoped catalyst (rGO). These results demonstrate that the use of heteroatom doped nanocarbon supports can enhance the electrochemical activity towards OER.

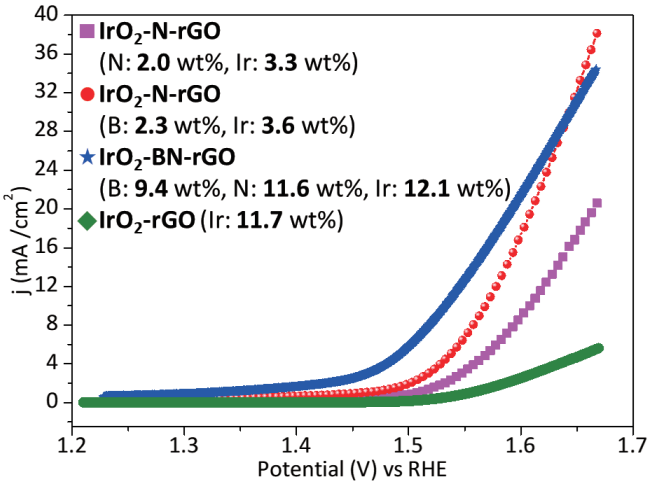

Fig. 1. LSV of IrO_2 nps decorated on the B-rGO, N-rGO and rGO sheets.

[1] M. Alattas *et al*. Scientific Reports, **8**, 17689 (2018).

[2] T. Reier *et al*. ACS Catalysis, **2**, 1765 (2012).

Corresponding Author: Dr. Prerna Joshi

Tel: +81-52-809-1852, Fax: +81-52-809-1851

Web: https://www.toyota-ti.ac.jp/surface/index.html

E-mail: joshiprerna2011@toyota-ti.ac.jp

Interactions of Nanodiamonds #1: with Ions in their Solutions

○Masaya Nemoto[1,2], Shusuke Ando[1], Yuho Itabashi[1], Toshihiko Tanaka[1,2], Yasuhiro F. Miura[3], Tetsuya Aoyama[2], Atsuya Muranaka[2], Masanobu Uchiyama[2,4], Eiji Osawa[5]

[1]Department of Chemistry and Biochemistry, National Institute of Technology, Fukushima College, 30 Aza-nagao, Tairakamiarakawa, Iwaki, Fukushima, 970-8034, Japan
[2]Elements Chemistry Laboratory, RIKEN Cluster for Pioneering Research, 2-1 Hirosawa, Wako, Saitama, 351-0198, Japan
[3]Hamamatsu University School of Medicine, 1-20-1 Handayama, Higashi-ku, Hamamatsu city, Shizuoka, 431-3192, Japan
[4] Graduate School of Pharmaceutical Sciences, the University of Tokyo, 7-3-1 Hongo, Bunkyo-ku, Tokyo 113-0033, Japan
[5]Nano Carbon Research Institute Ltd., Asama Research Extension Center, Shinshu University, 3-15-1 Tokida, Ueda, Nagano, 386-8567 Japan

Detonation nanodiamonds (DND) often sediment[1] with ions from their aqueous colloidal solutions and the interaction with ions should affect the self-assembly of DND. One aspect of the interaction is that with the ions in biological organs with respect to their applications for drug delivery systems[2]. We consider that elementary diamond nanoparticles (EDIAN) should aggregate a little with ions in the organs and that the aggregates containing drug molecules will be delivered there.

We prepared sediments with various salts from 0.25wt.% DND solutions (NanoAmando[@], *NanoCarbon Research Institute Ltd.*) and measured each minimum salt concentration c_m where a phase does not containing any DND particles is shown in a test tube through sedimentation (Table.1). Such a transparent phase was confirmed by the tyndall effect using a red laser beam. Their c_m values are $0.1\sim3\times10^{-3}$(mol/kg) , thus being smaller than those for sugars and particularly sulfate or sulfonate anions show significantly small values ($<5\times10^{-4}$). Similar results were already reported for some different sufonates.[3] Hence the interaction with anions is more important and should be larger than that with cations.

We consider that crosslinking of positively charged EDIAN (ζ -potential: ~+50 meV) can be done with negatively charged ions; the negative charge is well delocalized in the larger oxo acids, thereby can play an efficient role of the crosslinker. Salting out of proteins takes place usually at higher salt concentrations exceeding 0.01(mol/kg) and its precipitating mechanism should be different from that for DND, although the both are likely to be multi-polar charged nanoparticles[3].

Table1 c_m values of 0.25wt.% DND solutions for various salt additives.

additives	cm (mol/kg)
Li Cl	2.00E−03
Na Cl	3.00E−03
K Cl	2.00E−03
Rb Cl	3.00E−03
Cs Cl	3.00E−03
Mg Cl_2	1.50E−03
Ca Cl_2	2.00E−03
Na NO_3	2.00E−03
Na SO_4	1.00E−04
Na (p−toluenesulfonate)	5.00E−04
Na (1−naphthalenesulfonate)	5.00E−04
glucose	no detect(>0.1)
sucrose	no detect(>0.1)

[1]N.O. Mchedlov-Petrossyan, N. N. Kamneva, A. I. Marynin, A. P. Kryshtal, E. Osawa, *Phys. Chem. Chem. Phys.*, 17, 16186(2015); [2]E.K.Chow, X.-Q. Zhang, M. Chen, R. Lam, E. Robinson, H. Huang, D. Schaffer, E. Osawa, A. Goga, D. Ho, *Sci. Trans. Med*., 3.73(2011); [3]A. S. Barnard, E. Osawa; *Nanoscale* 6, 1188 (2014).
Corresponding Author:Toshihiko Tanaka / Tel: +81-246-46-0810 / E-mail: ttanaka@fukushima-nct.ac.jp

Interactions of Nanodiamonds #2: with Dye Ions in their Solutions

○Yuho Itabashi[1], Shusuke Ando[1], Masaya Nemoto[1,2], Toshihiko Tanaka[1,2], Yasuhiro F. Miura[2], Tetsuya Aoyama[3], Masanobu Uchiyama[3,4], Eiji Osawa[5]

[1]*Department of Chemistry and Biochemistry, National Institute of Technology, Fukushima College, 30 Aza-nagao, Tairakamiarakawa, Iwaki, Fukushima, 970-8034, Japan*
[2]*Elements Chemistry Laboratory, RIKEN Cluster for Pioneering Research, 2-1 Hirosawa, Wako, Saitama, 351-0198, Japan*
[3]*Hamamatsu University School of Medicine, 1-20-1 Handayama, Higashi-ku, Hamamatsu city, Shizuoka, 431-3192, Japan*
[4]*Graduate School of Pharmaceutical Sciences, the University of Tokyo, 7-3-1 Hongo, Bunkyo-ku, Tokyo 113-0033, Japan*
[5]*Nano Carbon Research Institute Ltd., Asama Research Extension Center, Shinshu University, 3-15-1 Tokida, Ueda, Nagano, 386-8567 Japan*

Doxorubicin(DX, **Fig.1**) is usually supplied in its hydrochloride salt and it was applied to drug delivery systems of detonation nanodiamonds (DND) for cancer therapy.[1] DND sediment with salts in their aqueous colloidal solutions[2] and DX cations also are likely to induce DND aggregates. One interesting aspect of DX is whether aggregated elementary diamond nanoparticles (aggregated EDIAN, ~50nm) play an effective role or not in avoiding serious side effects to hearts or to bone marrow through EPR effect[4] of a large drug spiecies exceeding 10 nm of its size.

However we cannot prepare DND sediments by adding DX to their solutions whereas we can do by adding carminic acids (CA, **Fig.1**). Why does the difference takes place? We prepared sediments with 3 anionic dyes (**Fig1**, CA, AQ, and MO) from 0.25wt.% DND solutions（NanoAmando@, *NanoCarbon Research Institute Ltd.*）and measured each minimum salt concentration $\mathbf{c}_m$ where a phase not containing any DND particles is shown in a test tube. Such a transparent phase was confirmed by the Tyndall effect using a red laser beam. We will then discuss the difference in sedimentation between DX and CA together with the other 2 dyes. Only DX is not a flocculant for the DND solution. We consider that cations are weaker flocculants than anions as shown in our other poster shown this time.

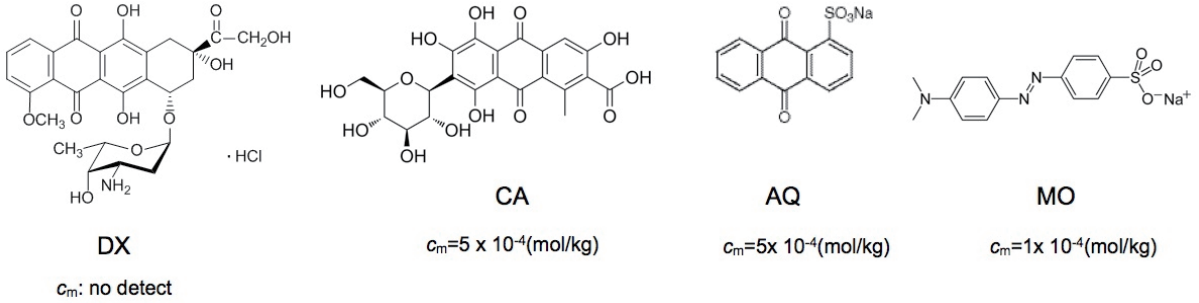

Fig.1 Dye molecules and their $\boldsymbol{c}_m$ values for a 0.25 wt.% DND aqueous solution : DX (Doxorubicin) ; CA (Carminic acid); AQ (Sodium Anthraquinone-1-sulfonate); MO(Methyl orange).

[1] E.K.Chow, X.-Q. Zhang, M. Chen, R. Lam, E. Robinson, H. Huang, D. Schaffer, E. Osawa, A. Goga, D. Ho, *Sci. Trans. Med*., 3.73(2011; [2] N.O. Mchedlov-Petrossyan, N. N. Kamneva, A. I. Marynin, A. P. Kryshtal, E. Osawa, *Phys. Chem. Chem. Phys.,* 2015, 16186(2015).

Corresponding Author:Toshihiko Tanaka / Tel: +81-246-46-0810 / E-mail: ttanaka@fukushima-nct.ac.jp

Detection of odor molecules by transistor-type graphene biosensor

Chishu Honma[1)], Hironaga Noguchi[1)], Yoshiaki Sugizaki[2)], Atsunobu Isobayashi[2)], Yuhei Hayamizu[1)]

1) Department of Materials Science and Engineering, School of Materials and Chemical Technology, Tokyo Institute of Technology, 2-12-1 Ookayama, meguroku, Tokyo, Japan
2) Corporate Research & Development Center, Toshiba Corporation,1, Komukai-Toshiba-cho, Saiwai-ku, Kawasaki 212-8583, Japan

E-mail: honma.c.aa@m.titech.ac.jp

Graphene has a high carrier mobility and specific surface area. Due to its unique properties, graphene is suitable for sensing including biosensors [1]. Immobilization of probe biomolecules on graphene surface allows us to utilize it as a biosensor. We can electrically detect the binding of target molecules as the result of its interactions with the immobilized probe biomolecules. However, immobilization of probe molecules via covalent bonds to graphene causes degradation of the intrinsic electronic properties. Furthermore, controlling the orientation of the immobilized probe biomolecules is essential to maintain the probe activity. In this study, we used self-assembled peptides, which self-assemble into ordered structures on the graphene surface. Due to its uniform structure, the peptides are suitable as a molecular scaffold enabling non-covalent immobilization of bio-probes [2]. We designed two types of peptides: (1) a scaffold peptide adsorbed on the graphene surface, and (2) a probe peptide with additional amino acid sequence attached to the scaffold peptide. By immobilizing these on graphene transistors, we succeeded to electrically monitor the binding of limonene, odor molecules of a lemon, with various concentrations (Fig. 1).

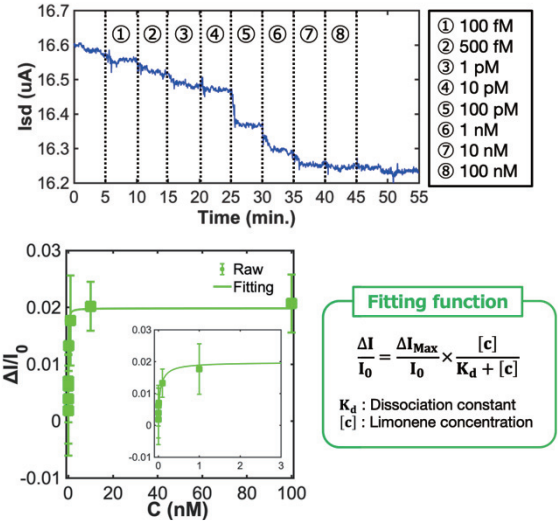

Fig.1 (top) Response of source-drain current to limonene. (bottom) a plot of current change vs concentration with a fitting curve based on Langmuir model.

This work was supported by the Cabinet Office (CAO), Cross-ministerial Strategic Innovation Promotion Program (SIP), "An intelligent knowledge processing infrastructure, integrating physical and virtual domains" (funding agency: NEDO).

[1] Ohno,Yasuhide ,et al.; J. Am. Chem. Soc., **2010**, *132* (51), 18012–18013

[2] Khatayevich, Dmitriy, et al. Langmuir 28.23 (2012): 8589-8593.

Highly Selective and Scalable Fullerene-Cation-Mediated Synthesis accessing Cyclo[60]fullerenes with 5-Membered-Carbon-Ring and their Application to Perovskite Solar Cells

○Hao-Sheng Lin [1], Il Jeon [1], Shigeo Maruyama [1], Yutaka Matsuo [1]

[1] *Department of Mechanical Engineering,The University of Tokyo, Tokyo 113-8656, Japan*

In thin-film photovoltaics, cyclo[60]fullerenes have been widely used as electron acceptors in organic solar cells and as electron-transporting layers (ETLs) in perovskite solar cells. In particular, cyclo[60]fullerenes as an over-coating layer of metal oxide ETLs have been one of the most exploited applications in perovskite solar cells, demonstrating a dramatic reduction hysteresis and enhancement of the device charge-dynamics. With respect to such applications, heterocyclo[60]fullerene, which is one of the most abundant types of cyclo[60]fullerene, have shown relatively poor performance compared with full-carbon-ring cyclo[60]fullerenes because of their electrochemical instability. Accordingly, cyclo[60]fullerenes with a full-carbon-ring, such as 3-membered-carbon-rings (e.g. $PC_{61}BM$) and 6-membered-carbon-rings (e.g. ICBA, MIF), have been the preferred choices for the over-coating layers of metal oxide ETLs. However, cyclo[60]fullerenes with a 5-membered-carbon-ring, namely indano[60]fullerenes, have never been demonstrated to date because of inefficient synthetic protocols.

In this work, a fullerene-cation-mediated synthesis,[1] accessing a new class of 5-membered-carbon-ring cyclo[60]fullerenes with high yields of up to 93% is showcased. This method utilizes aryl[60]fullerene cations, ArC_{60}^{+} as intermediates, which are generated *in situ* by heating the aryl[60]fullerenyl dimers in the presence of $CuBr_2$. In addition, 5-membered-carbon-ring cyclo[60]fullerenes display excellent device applicability when they are used in perovskite solar cells as over-coating layers of electron-transporting layers. A power conversion efficiency of 20.7% is achieved thanks to the favorable energy alignment, optimized substrate design, and electrochemical stability of the 5-membered-carbon-ring fullerenes.[2]

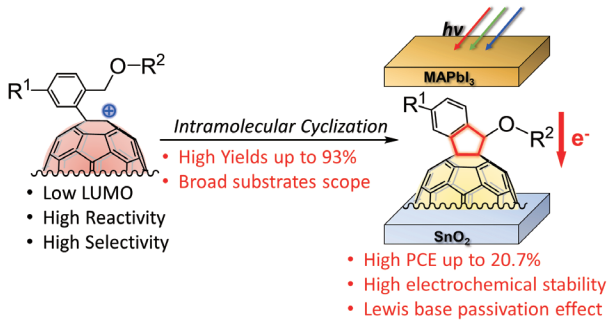

[1] H.-S. Lin, Y. Matsuo Chem. Comm. **54**, 11244 (2018).

[2] H.-S. Lin, I. Jeon, Y. Chen, X.-Y. Yang, T. Nakagawa, S. Maruyama, S. Manzhos, Y. Matsuo, Chem. Mater. **31**, 8432 (2019).

Corresponding Author: Y. Matsuo
Tel: +81-3-5841-0978
E-mail: matsuo@photon.t.u-tokyo.ac.jp

Flattening of 2D materials encapsulated by hBN flakes

○Takato Hotta [1], Akihiro Ueda [1], Shohei Higuchi [1], Keiji Ueno [2], Kenji Watanabe [3], Takashi Taniguchi [3], Ryo Kitaura [1]

[1] *Department of Chemistry, Nagoya University, Nagoya 464-8602, Japan*
[2] *Department of Chemistry, Saitama University, Saitama 338-8570, Japan*
[3] *National Institute of Materials Science, Tsukuba 305-0044, Japan*

The hBN encapsulation is one of the most important techniques to address intrinsic properties of 2D materials, such as graphene and transition metal dichalcogenides (TMDs). Through the encapsulation by hBN flakes, environmental effects arising from substrates and impurities can be suppressed. Impurities, which are inevitably encapsulated between hBN flakes and 2D materials, however, prevent us from investigating fundamental properties of 2D materials. In this paper, to obtain impurity-free hBN-encapsulated 2D materials, we have developed a fabrication technique based on the Nano-squeeze method [1].

We have fabricated hBN-encapsulated single layer $MoSe_2$ by the dry transfer method with a polymer stamp; an exfoliated $MoSe_2$ flake on SiO_2/Si substrate was picked up with a hBN flake, and then the hBN/$MoSe_2$ was transferred onto another hBN flake. Bubble-like impurities between the layers were removed by squeezing a surface of the stacking structures with an AFM probe (Brucker, RESPA-40). As you can see in Figure 1, there are almost no bubbles after the squeezing process. Although there are no the detectable bubbles in the hBN/$MoSe_2$/hBN, PL spectra at 10 K show strong signals from trions, whose intensity depends strongly on the force applied in the squeezing process. Figure 2 and 3 show the force dependence of PL spectra at 10 K and ratio of the PL intensity from excitons and trions, respectively. The ratio decreases as the force increases, meaning that applying force leads to increase of charged impurities on the surface of top-layer hBN. Based on the results obtained, we put a few-layer graphene on the top of hBN/$MoSe_2$/hBN before the squeezing process. We found that the top graphene effectively screens the charged impurities induced by the squeezing process and high-quality $MoSe_2$ can be achieved. In this presentation, we will show the details of the sample fabrication and results of characterization, including PL, Raman and transport properties.

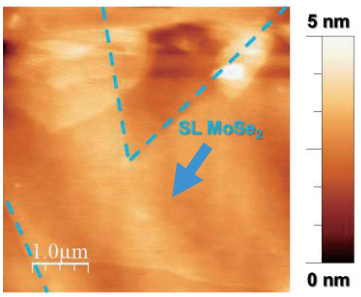

Figure 1 AFM image after removing bubbles.

[1] M. R. Rosenberger, *et. al.*, ACS Appl. Mater. Interfaces 10, 10379-10387 (2018).

Corresponding Author: R. Kitaura, Tel: +81-52-789-3660, Fax: +81-52-747-6442, E-mail: r.kitaura@nagoya-u.jp

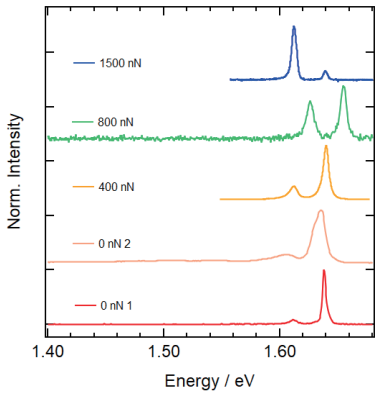

Figure 2 Strength dependence of PL spectra at 10 K.

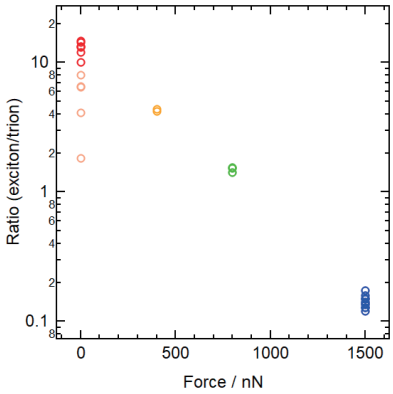

Figure 3 Force dependence of the ratio of exciton/trion.

Development of Chemical CNH Fishhook for Analyzing Peptide and Its Assemblies by SMART-EM

○Takayuki Nakamuro [1], Keyi Sun [1], Jeffrey W. Bode [2], Koji Harano [1], Eiichi Nakamura [1]

[1] *Department of Chemistry, The University of Tokyo, Tokyo 113-0033, Japan*
[2] *Department of Chemistry and Applied Biosciences, ETH Zürich, 8093 Switzerland*

Assembly of peptide is an important research area that is directly linked to various scientific events including pathology. Analysis methods such as NMR and AFM[1] have been performed to elucidate such phenomena, but it is still difficult to clarify their details because aggregates have a structure size distribution and the events occur on nanoscale. In this context, our group demonstrated a new electron microscopy, single-molecule atomic-resolution real-time transmission electron microscopy (SMART-EM)[2], for dynamic study of molecules or their assemblies in atomic resolution. Here we show that dynamics of single molecule peptide and assembly of peptides can be analyzed by SMART-EM methodology. Daptomycin[3], the active ingredient of Cubicin®, has extensively studied as a pharmaceutical for gram-positive bacteria. It is proposed that daptomycin assembles into oligomers in the presence of calcium ion which act as active species, thus daptomycin was selected as a model peptide for single molecular observation and assembly processes by SMART-EM imaging.

Single molecule daptomycin was captured at the curved surface of chemically functionalized carbon nanohorn (*Dap@CNH*), which was subjected to the SMART-EM observation. The snapshots were reconstructed to confirm their structural accuracy. We also demonstrated the new approach to evaluate calcium concentration dependent assembly processes in solution by combining DLS and SMART-EM techniques.

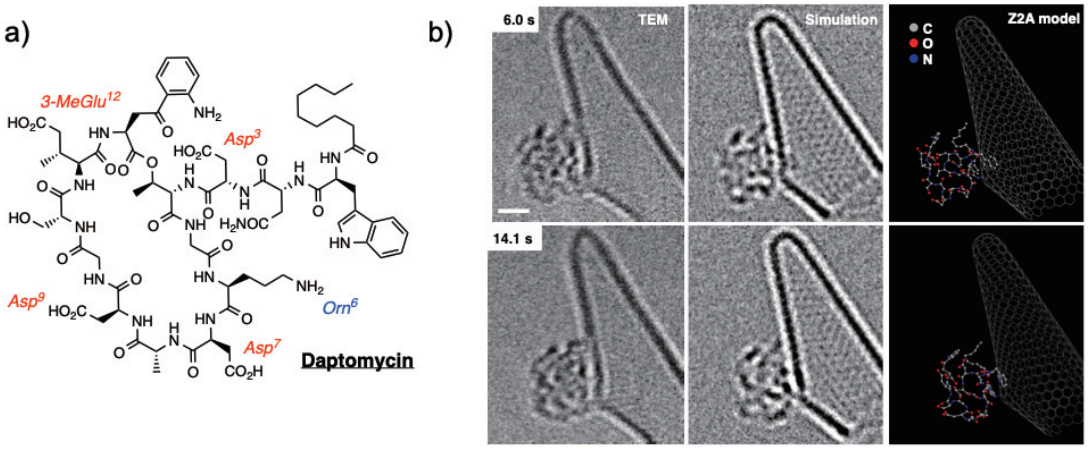

Fig. 1 a) Structure of daptomycin (Dap). b) Representative TEM images of *Dap@CNH*. (left) extracted from TEM experiments. Simulated TEM images (middle) and plausible molecular models (right) are shown. The scale bar is 1 nm.

[1] S. Banerjee *et al*. ACS Nano. **11**, 12202 (2017).
[2] E. Nakamura, Acc. Chem. Res. **50**, 1281 (2017).
[3] S. D. Taylor et al. Bioorg. Med. Chem. **24**, 6253 (2016)

Corresponding Author: E. Nakamura
Tel: +81-3-5841-4356, Fax: +81-3-5841-4368,
E-mail: muro@chem.s.u-tokyo.ac.jp

Electrical properties of periodically modified graphene

○Yuta Taguchi[1], Susumu Saito[1]

[1]*Department of Physics, Tokyo Institute of Technology, 2-12-1 Oh-okayama, Meguro-ku, Tokyo 152-8551, Japan*

Ever since the production of graphene by exfoliation, electronic properties of graphene and related atomic layer materials have been intensively studied. Its high conductivity is of scientific importance, while the semiconducting behavior of modified graphene has been studied theoretically[1,2] and experimentally[3]. Since there are infinite kinds of periodic structure modification in principle, various electronic properties are expected to be realized.

In the present work, we study the electronic properties of periodically modified graphene as shown in Fig.1 and Fig.2 . Figure1 shows a system in which structural defects in the shape of truncated triangles are arranged in the same direction, and Figure2 shows a system in which structural defects in the opposite direction are additionally arranged. In Fig.1, there is a difference between the numbers of atoms on two sublattices of the original honeycomb lattice. While in Fig.2, they are the same. Interestingly, electronic properties are considerably different from each other near the Fermi energy. We mainly discuss the electronic states near the Fermi energy in these two types of systems including the magnetic properties in some systems.

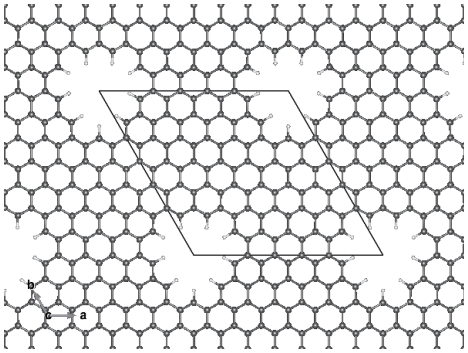

Fig.1 Hexagonal arrangements of defects on the graphene lattice

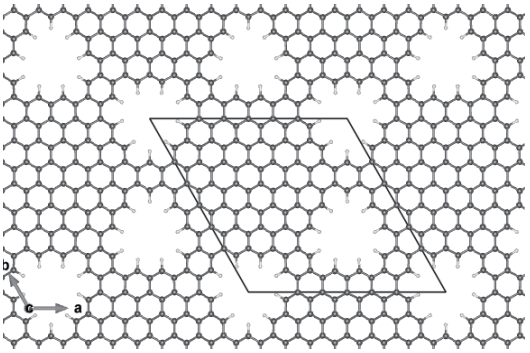

Fig.2 Super honeycomb lattice arrangement of defects

[1] T.Matsumoto and S.Saito, J. Phys. Soc. Jpn. **71**, 2765 (2002)

[2]M.Sakurai, Y.Sakai, and S.Saito, J. Phys: Conf. Ser. **302**, 012018 (2011)

[3]B.S.Jessen *et al*. , Nature Nanotech. **14**, 340 (2019)

Corresponding Author: Y. Taguchi

E-mail: taguchi.y.ae@m.titech.ac.jp

In-plane heterostructure of MoS_2 polytypes

Ruben Canton-Vitoria[1], Ryo Kitaura[1]

[1] *Department of Chemistry, Nagoya University, Nagoya 464-8602, Japan.*

During the last 7 years scientific community pay attention to 2D MoS_2 due to its high phonon-limited mobility 410 cm^2/Vs at room temperature and its high quantum yield. Recently, the combination of MoS_2 with others 2D materials e. j. WS_2 forming heterostructures results attractive for developing more advances devices.[1,2] However, heterostructures of different phases of MoS_2 (2H, 1T and 1T´) still remained unexplored.

In this poster we present a new CVD methodology which provide in-plane heterostructures involving different polytypes of MoS_2. In order to confirm changes in the phase, several techniques such as Raman mapping or solid PL mapping images were essential. Concretely, characteristic $J_{1\text{-}3}$ nodes are invisible in the semiconducting MoS_2 but were found at basal plane of monolayers, however, they were negligible at the edges (fig. 1a). Based in the spectroscopic differences between MoS_2 phases, Raman mapping clearly distinguishes 2 well defined domains (fig. 1b). Such results are in harmony with PL intensity maps, showing strong intensity emission in the semiconducting phase at the edges, but minor or nothing on the basal plane (fig. 1c). Additional spectroscopic techniques were carried out in order to support the present study. Briefly, Raman Pl not only shows 2 orders of magnitude higher at the semiconducting phase, but in addition, 15 meV blue shift. Deconvolution of Mo and S bands through XPS clearly shows the presence of 2 phases and AFM unambiguously shows homogeneous large areas of MoS_2, free of impurities, with lower height than 1 nm, which are in harmony with single layer. The controlling proportion of reagents, time of reaction and position play a relevant role in controlling the percentage of phases.

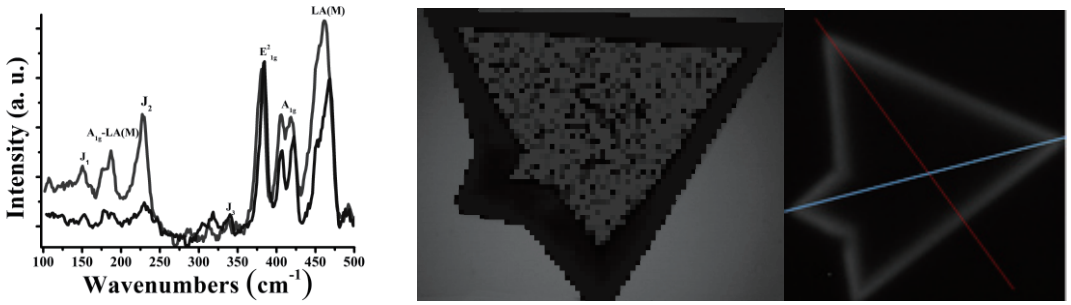

Fig.1. (a) Raman at the basal plane (gray) and at the edges (black), (b) Raman mapping showing the superposition of J_2 peak (gray) and E^1_{2g} intensities and (c) PL intensity map of in plane MoS_2 heterostructure.

Acknowledgements

This project has received funding Japan Society for the Promotion of Science (JSPS) postdoctoral fellowship grant agreement No P19368.

[1] K, Chen, *et al*. Adv. Mater. **27**, 6431 (2015)

[2] M, Okada, *et al.* ACS Nano **12**, 2498 (2018)

Corresponding Author: Ryo Kitaura

E-mail: canton.vitoria.ruben@h.mbox.nagoya-u.ac.jp

Ultra fast growth of monolayer WS_2 measured by in-situ monitoring

○Tomoya Kameyama[1], Toshiro Kaneko[1], Toshiaki Kato[1,2]

[1]*Graduate School of Engineering, Tohoku University, Sendai 980-8579, Japan*
[2] *JST-PRESTO*

Since the discovery of two dimensional (2D) materials, they have attracted intense attentions because of their ultrathin thickness, unique optical and electrical features, and high mechanical flexibility [1, 2]. Graphene is the most famous example of 2D materials which has high electrical conductivity. However, graphene is difficult to be applied for practical applications for semiconductor devices due to its zero-bandgap structure. Transition metal dichalcogenide (TMD) is known as another kind of 2D materials, which possess ultrathin thickness as similar as graphene. TMD is expected to be applied on practical semiconductor devices because it has tunable bandgap structure. Furthermore, bright photoluminescence of TMD makes them as a promising candidate for next generation optoelectrical applications [3]. To fabricate the high performance optoelectrical devices, it is greatly important to synthesize single crystal, monolayer, and large scale TMD. Unfortunately, the uncertain growth mechanism of TMD makes it difficult to realize them.

In this study, to reveal the growth mechanism of monolayer tungsten disulfide (WS_2), in-situ monitoring system has been developed, which can directly observe the time evolution of monolayer WS_2 growth [4]. The result of in-situ monitoring implies that WS_2 growth might be dominated by the transformation from liquid to solid phase rather than vapor-solid transformation. Furthermore, WS_2 growth velocity is found to be very fast (~9 μm/s) (Fig.1 (a)), which is over 100 times faster than that of typical graphene. The WS_2 growth velocity decreases with an increase in substrate temperature (Fig.1 (b)). This result suggests that WS_2 growth follows Wilson-Frenkel model, where chemical potential difference between growing site and liquid phase precursors is the dominant element to decide the growth velocity. These findings about growth mechanism of monolayer WS_2 should be useful to synthesis high quality and single crystal WS_2 in large scale.

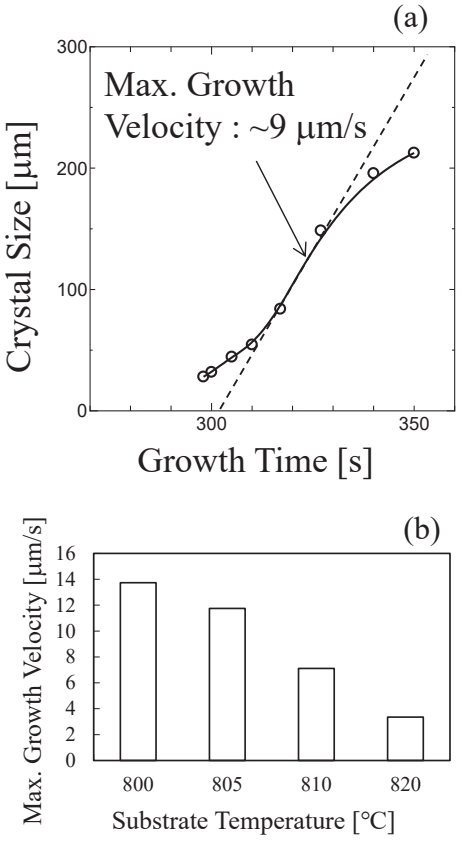

Fig.1 (a) Crystal size change as a function of growth time. (b) Histogram of maximum growth velocity as a function of substrate temperature.

[1] T. Kato and T. Kaneko: ACS Nano, **8** (2014) 12777.
[2] T. Kato and T. Kaneko: ACS Nano, **10** (2016) 9687.
[3] T. Akama, W. Okita, R. Nagai, C. Li, T. Kaneko, and T. Kato: Scientific Reports, **7** (2017) 11967.
[4] C. Li, T. Kameyama, T. Takahashi, T. Kaneko, and T. Kato: Scientific Reports, **9** (2019) 12958.

Corresponding Author: T. Kameyama
Tel: +81-22-795-7046, Fax: +81-22-263-9225,
http://www.plasma.ecei.tohoku.ac.jp/
E-mail: tomoya.kameyama.r1@dc.tohoku.ac.jp

Isotope Labelling Analysis of Additive Gas Effects on Single-Walled Carbon Nanotube Growth

○Bunsho Koyano[1], Shun Yamamoto[1], Akari Kobayashi[1], Ryoya Ishimaru[1], Keigo Otsuka[2], Taiki Inoue[1], Rong Xiang[1], Shohei Chiashi[1], Shigeo Maruyama[1, 3]

[1] *Department of Mechanical Engineering, The University of Tokyo, Tokyo 113-8656, Japan*
[2] *Nanoscale Quantum Photonics Laboratory, Riken Cluster for Pioneering Research, Wako, 351-0198, Japan*
[3] *Energy NanoEngineering Lab, National Institute of Advanced Industrial Science and Technology (AIST), Tsukuba, 305-8564, Japan*

Single-walled carbon nanotubes (SWCNTs) are carbon materials whose diameter is about 1–2 nm and expected to be applied to various devices including electronics. However, the mechanism of SWCNT growth remains unclear in many ways, which makes it difficult to synthesize dense and long SWCNTs applicable to practical electronic devices. To elucidate the growth mechanism, we proposed a method for tracing the growth profiles of individual SWCNTs by embedding digitally coded isotope labels [1]. This method unveiled various features of individual SWCNT growth including the root growth mode, monotonic growth rates, abrupt growth termination, and so on.

In this work, we investigated the effects of additive gases during a pause of a carbon precursor [2] and also during a pretreatment process [3] on growth of individual SWCNTs. In the former case, Ar, Ar/H_2 or Ar/H_2/H_2O was introduced during a pause in the supply of ethanol at growth temperature of 800 °C. In the latter case, we pretreated catalyst at 800 °C with Ar/H_2 for 10 min, Ar/H_2 for 60 min, or Ar/H_2/H_2O for 6 min before growth. We introduced ^{13}C ethanol pulses with three different ratios while introducing ^{12}C ethanol. Raman mapping was used to analyze G-band downshifts of individual SWCNTs. Growth curves constructed from Raman mapping images indicated that SWCNTs interrupted with Ar tended to show no regrowth while those interrupted with Ar/H_2 or Ar/H_2/H_2O showed regrowth (Fig. 1(a–c)). In the case of Ar/H_2/H_2O, SWCNTs were etched catalytically toward their root parts and regrown with enhanced growth rates. Also, we compared incubation time of SWCNTs grown from catalyst pretreated under three different conditions (Fig. 1(d–f)). This result shows longer time reduction and Ar/H_2/H_2O pretreatment increased incubation time. We also applied a tree-based machine learning algorithm to evaluate the additive gas effects on SWCNT growth.

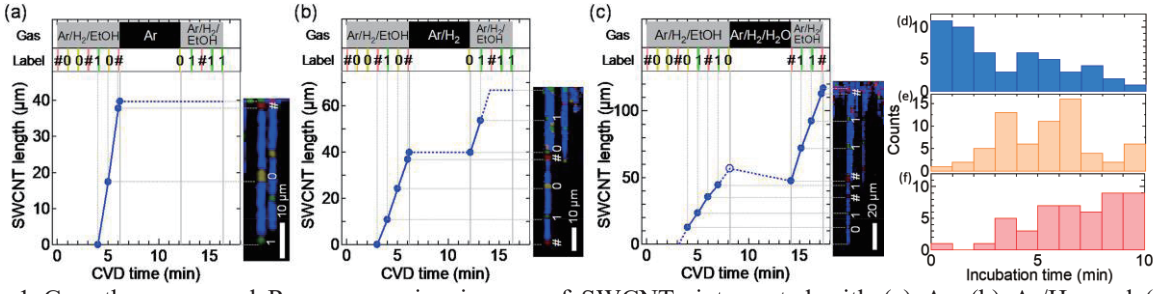

Fig. 1 Growth curves and Raman mapping images of SWCNTs interrupted with (a) Ar, (b) Ar/H_2, and (c) Ar/H_2/H_2O. Distribution of incubation time of SWCNTs grown after pretreatment with (d) Ar/H_2 for 10 min, (e) Ar/H_2 for 60 min, and (f) Ar/H_2/H_2O for 6 min[1] K. Otsuka *et al*. ACS Nano **12**, 3994 (2018). [2] B. Koyano *et al.*, Carbon **155**, 635 (2019). [3] B. Koyano *et al.*, in preparation. Corresponding Author: S. Maruyama, Tel: +81-3-5841-6421, Fax: +81-3-5800-6983, E-mail: maruyama@photon.t.u-tokyo.ac.jp

Electronic property of CNT thin film under external electric field

○Yanlin Gao, Susumu Okada

Department of Physics, Graduate School of Pure and Applied Sciences, University of Tsukuba,
Tsukuba, 305-8571, Japan

Owing to unusual structural and electronic properties, CNTs have been regarded as emerging materials in wide areas of modern technologies. It has been demonstrated that CNTs work as conducting channels in field effect transistors (FETs) and thermoelectronic devices. In usual CNT-based devices, the channels consist of mat films of CNTs, which intrinsically intersect or align with other CNTs. At the intersectional and aligned regions, the intertube interaction plays decisive roles to determine the device performance. In our previous work, we predicted that field inversion occurs at the intersectional region of two CNTs under a weak electric field. [1,2] Although the aligned CNTs can work as a conducting channel in real devices, the carrier distribution is still uncertain in densely aligned CNT thin films in the FET structure. Thus, in this work, to elucidate the carrier distribution in CNT thin films, we studied the electronic structures of CNT thin films under an external electric field using density functional theory combined with effective screening medium method (Fig.1)..

Our calculations show that the distribution of accumulated carriers by the electric field slightly depends on the field strength, constituent CNT species, and intertube spacing. For the thin films consisting only of semiconducting CNTs under large gate voltage, the carriers are primarily distributed on the CNT layer at the electrode side with a small carrier penetration into the opposite CNT layer. In contrast, the carrier penetration in the CNT layer at the opposite side of electrode is enhanced under a low gate voltage. Unlike the cases of the semiconducting CNTs, for the thin films containing metallic CNTs, accumulated carrier distribution strongly depends on the metallic CNT arrangement with respect to the electrode. In addition, a large intertube spacing in the thin films enhances the carrier concentration on the CNT at the electrode side, except in the thin films containing metallic CNTs.

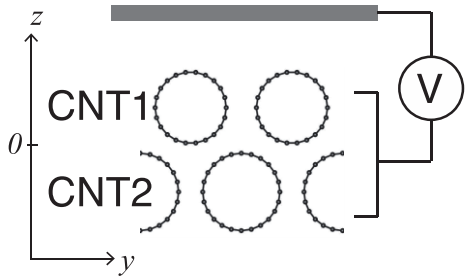

Fig.1 Structural model of CNT thin film FET.

Reference

[1] Taketo Kochi and Susumu Okada, Appl. Phys. Express 9, 085103 (2016)
[2] Taketo Kochi and Susumu Okada, Appl. Phys. Express 10, 075101 (2017)

Corresponding Author: Y. Gao
TEL: +81-29-853-5921, FAX: +81-29-853-5924
E-mail: ylgao@comas.frsc.tsukuba.ac.jp

Hall Effect and weak-localization conduction in aligned metallic single-walled carbon nanotube thin films

○Kanako Horiuchi[1], Ryotaro Okada[1], Hideki Kawai[1], Yohei Yomogida[1], Komatsu Natsumi[2], Weilu Gao[2], Junichiro Kono[2], Kazuhiro Yanagi[1]

[1] Department of Physics, Tokyo Metropolitan University, Tokyo 192-0397, Japan
[2] Department of Electrical and Computer Engineering, Rice University, Texas 77005, USA

Hall effect measurements are important for understanding the charge transport mechanisms and intrinsic carrier mobility in solid. However, in hopping conduction systems, it is not possible to correctly evaluate carrier density from the hall effect measurements, because hopping carriers only respond to the electric force, not to the Lorentz force.[1] Transport mechanisms in most of single-walled carbon nanotube (SWCNT) networks are hopping conductions, thus usually it is difficult to correctly detect hall effect in SWCNT thin films. In the case of metallic SWCNTs, we can observe weak localization conduction depending on their network morphology. Previously, we proposed to use aligned metallic SWCNTs for hall measurements because weak localization conduction can be observed in doped aligned metallic SWCNT films. In this study, we developed an approach to correctly measure hall effect in aligned SWCNTs as follows.

First we need to check conduction mechanism along the *"perpendicular"* direction to the nanotube axis, and to confirm weak localization conduction along the perpendicular direction. We usually observe weak-localization conduction along the parallel direction in aligned metallic SWCNT films, but sometimes not along the perpendicular directions. If the conduction along perpendicular direction was hopping conduction, we could not correctly observe hall effect even if we used aligned metallic SWCNT film.

When the conduction along perpendicular direction is weak-localization, we can observe hall effect in aligned metallic SWCNT films as shown in Fig. 1. We injected electrons or holes by electrolyte gating methods, and we observed the change of the sign of the hall voltage according to the types of conduction carriers. We concluded that the hall effect was correctly detected in aligned metallic SWCNT films when the conduction along the perpendicular direction is weak-localization.

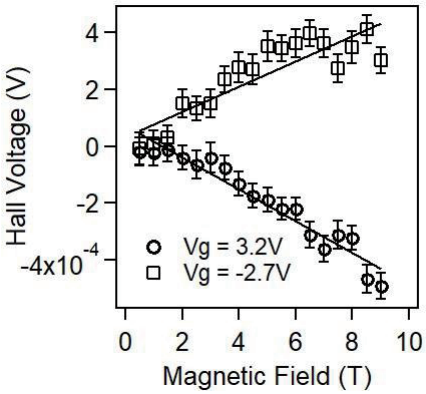

Figure 1: Hall voltage as a function of magnetic field at Vg of 3.2 V (electron conduction) and -2.7 V (hole conduction).

References: [1] Yi et al., Sci. Rep. 6 23650 (2016)

Corresponding to Kazuhiro Yanagi, yanagi-kazuhiro@tmu.ac.jp

Influence of interlayer stacking arrangements on carrier accumulation in bilayer graphene field effect transistors

Susumu Okada, Yanlin Gao, and Mina Maruyama
Department of Physics, University of Tsukuba, Tennodai, Tsukuba 305-8571, Japan

Field effects on the electronic properties of graphene thin films are an important subject for practical application of these thin films. Experimental and theoretical works demonstrate that an electric field modulate the electronic structure of graphene thin films. A perpendicular electric field induces a finite band gap in bilayer graphene with the AB interlayer arrangement, where the width of the band gap depends on the field strength. Bilayer graphene with twisted arrangement in a particular mutual angle (i.e., twisted bilayer graphene) exhibits superconductivity under carrier doping via an electric field. Although these works indicate that the electronic structure and carrier distribution of graphene thin films under an electric field depend on the mutual stacking arrangement, the detailed correlation between the electronic properties and the stacking arrangement in graphene thin films under a normal electric field remains unclear. Therefore, in this work, we aim to provide theoretical insight into the influence of the interlayer stacking arrangement on the electronic structure of bilayer graphene, using the density functional theory combined with the effective screening medium method. Our calculations show that the carriers are extended throughout the layers for graphene with the AB arrangement. Conversely, the carriers are highly localized on the layer situated at the electrode side for twisted bilayer graphene. In addition to the electronic structure, the thermal and thermoelectric properties of bilayer graphene is also found to depend on the stacking arrangement.

Corresponding Author: Susumu Okada (sokada@comas.frsc.tsukuba.ac.jp)

Study on effects of twist on phonon transport in graphene nanoribbons

○Yukihiko Terada[1] and Takuma Shiga[1,2]
[1] *Department of Mechanical Engineering, The University of Tokyo, Tokyo 113-8656, Japan*
[2] *PRESTO, Japan Science and Technology Agency, Kawaguchi, Saitama 332-0012, Japan*

CNT is a significant candidate for various applications (sensor, field emission devises, and so on) [1] because of its many advantages such as high electron mobility, high thermal conductivity, and flexibility. So far, thermal conductivity and phonon transport inside CNTs have been extensively investigated by experiments and simulations, and individual CNTs are found to have quite high thermal conductivity [2,3]. This high thermal conductivity is of course due to strong sp^2 covalent bond, low-dimensionality, and rotational symmetry of cylindrical structure [3].

From engineering viewpoint, utilization of the superior thermal conductivity of individual CNTs is demanded for CNT-based bulk materials like films. In addition to lattice imperfections, an aggregation of CNTs forming a film yields many junctions, which consequently increases overall thermal resistance. Since CNTs have empty space because of their cylindrical structure, encapsulation of substances into the space is one of effective approaches for modulating thermal properties. In general, encapsulation negatively influences heat conduction because encapsulated substances not only are scattering centers of phonons in CNTs but also break the rotational symmetry. However, influence of encapsulation on heat conduction has not been fully clarified, thus, it is still worth to exploring nanomaterials which are beneficial for enhancement of thermal conductivity of CNT-based bulk materials.

We here consider a graphene nanoribbon (GNR) as a candidate for the exploration, and investigate phonon transport in coherent ballistic regime by the combination of the atomistic Green's function[4] and mode-matching methods[5]. Since GNRs encapsulated in CNTs are experimentally observed to be twisted[6], we evaluate the effect of partial twist on overall thermal conductance of GNRs by changing a twist angle per length and a number of units of twisted GNRs. As results, we find that, while thermal conductance is strongly dependent on specific twist angle, it is surprisingly insensitive to a number of unit cells of twisted GNRs, which is intuitively opposite to a usual interpretation in terms of Fabry-Pérot interference.

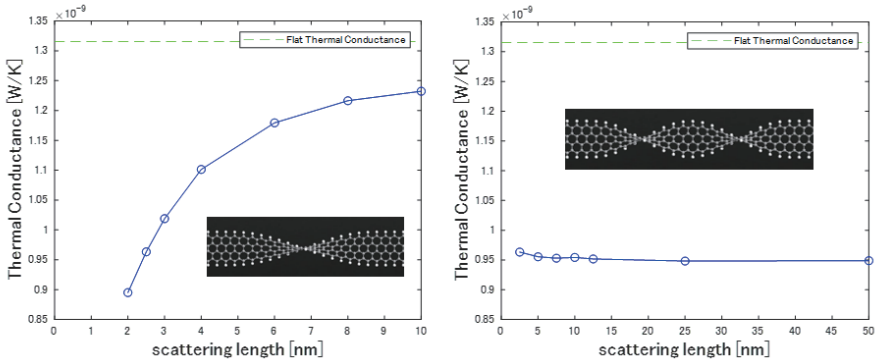

Figure Thermal boundary conductance as a function of (a) length with 180° twist angle and (b) number of unit cells of 180°-twisted GNRs at room temperature.

[1] R.Baughman, *et al*., Science, **297**, 5582 (2002)., [2] V. Lett, *et al.*, Phys. Rev. Lett. **118**, 135901 (2017).
[3] L. Lindsay, *et al*., Phys. Rev. B **82**, 161402(R) (2010). [4] W. Zhang, *et al.,* Num. Heat Trans. B **51**, 333 (2007).
[5] Z. Ong and G. Zhang, Phys. Rev. B **91**, 17 (2015) [6] A. Talyzin, *et al*., Nano Lett., **11**, 10 (2011)
Corresponding Author: Takuma Shiga, Tel&Fax: +81-3-5841-8091, E-mail: shiga@photon.t.u-tokyo.ac.jp

Iron ion-mediated oxidation of coenzyme NADH by carbon nanotubes

○Atsushi Hirano, Momoyo Wada, Takeshi Tanaka, Hiromichi Kataura

Nanomaterials Research Institute, National Institute of Advanced Industrial Science and Technology (AIST), Ibaraki 305-8565, Japan

As-grown carbon nanotube (CNT) materials have been reported to induce oxidative stress on proteins, which is facilitated by metals originating from the catalyst remains [1]. The oxidation mechanism should be generally applicable to other biomolecules, including low-molecular-weight compounds. For understanding biological impact of the CNTs, it is important to demonstrate the generality of the mechanism. In this study, we examined a redox reaction of a coenzyme—nicotinamide adenine dinucleotide (NADH) (Fig.1)—with the CNTs; NADH is a biomolecule used in metabolic systems. It was found that the CNTs with the remaining metals were reduced by NADH, which means that NADH was oxidized by the CNTs. The reaction was suppressed by the addition of a chelating agent for the metals, demonstrating that the metals mediate this reaction. The present results thus suggested that CNT materials with metals can affect biological reactions involving NADH such as metabolism.

The CNT used in this study was produced by the HiPco process; therefore, the CNT materials contain iron species as catalyst remains. NADH used as a reductant for the CNTs is a representative biological reductant and has a NAD^+/NADH redox couple with a redox potential of −0.32 V (*vs.* NHE) (Fig.1). Fig.2a shows absorption spectra of the CNTs in the presence and absence of NADH. NADH induced restoration of the spectrum, indicating reduction of the CNTs. The effect of NADH was also observed in the time courses profiles of absorbance at 1250 nm (Fig.2b). Importantly, restoration of the spectrum was kinetically suppressed in the presence of a chelating agent EDTA, which indicates that the coexisting iron ions facilitate the redox reaction between the CNTs and NADH. Similar profiles were observed for an NADH analogue—nicotinamide adenine dinucleotide phosphate (NADPH). The iron ion-mediated redox reaction should be associated with biological impacts of the CNTs in cells and animals.

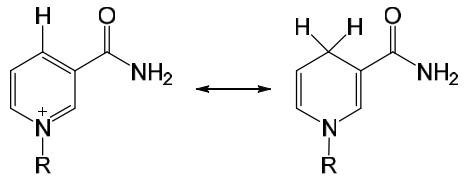

Fig. 1 Chemical structures of NAD^+ and NADH. R denotes a moiety composed of ribose–ADP complex.

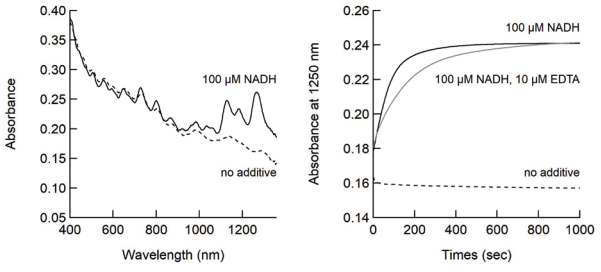

Fig. 2 Redox reaction of the CNTs with NADH. (a) Absorption spectra of the CNTs in the presence and absence of NADH. (b) Time courses of absorbance values at 1250 nm.

[1] A. Hirano *et al*. ACS Nano **13**, 1805 (2019).

Corresponding Author: A. Hirano
Tel: +81-29-849-1064, Fax: +81-29-861-2786,
E-mail: hirano-a@aist.go.jp

Hexagonal boron nitride nanosheets for ultrafast membrane filtration

○Rasel Das, Pablo Solís-Fernández, Hiroki Ago

Global Innovation Center (GIC), Kyushu University, Fukuoka 816-8580, Japan

Freshwater facilities are continuously shrinking due to the presence of toxic wastewater pollutants. It jeopardizes the human health, and diminishes the availability of hygienic foods, drinks and indirectly causes various diseases. Therefore, developing an efficient wastewater filtration technology is an urgent need. Very recently, amino functionalized hexagonal boron nitride (h-BN) membranes have shown good pollutants retention ability combined with fast permeation [1]. However, preparation of functionalized h-BN nanosheets is very difficult and requires tedious steps due to its chemical inertness.

In this study, we used N-methyl-2- pyrrolidone (NMP)-assisted simple sonication method to produce exfoliated h-BN nanosheets [2] without prior functionalization. It allowed us to fabricate a highly ordered lamellar h-BN film, having thickness about 3.0 μm onto polyvinylidene difluoride (PVDF) support membrane, as shown in Fig. 1. This membrane showed a very high pure water flux of ~360 L m^{-2} h^{-1} bar^{-1} at neutral pH. We also investigated to increase the water pollutants selectivity of this h-BN membrane by simply tuning the water pH. It allowed us to achieve a very good methyl orange (MO) rejection >90% at pH 2.0 combined with a high permeation of 433 L m^{-2} h^{-1} bar^{-1}. The mechanism of water flow through h-BN lamellar structure and MO retention was also investigated in details. This work paves the way for the development of a novel pH-responsive 2D layered material-based new filtration technology to separate molecules from many industry effluents, such as water purification, healthcare, bioprocessing, food, and environmental, because of their low energy consumption (*i.e.* high water filtration ability).

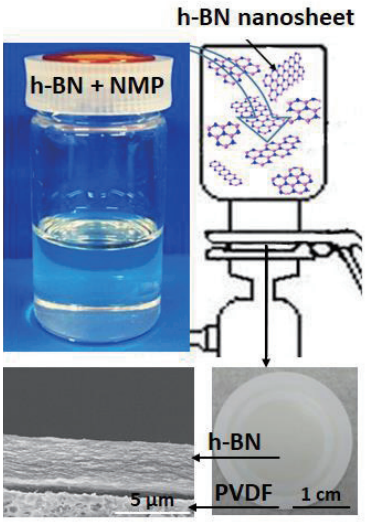

Fig. 1. Fabrication of a lamellar membrane using exfoliated h-BN nanosheets for water purification.

References

[1] C. Chen *et al. Nat. Commun.* **9**, 1902 (2018).

[2] J. N. Coleman *et al. Science* **331**, 571 (2011).

Corresponding Author: R. Das
Tel&Fax: +81-92-583-8975
E-mail: r-das@gic.kyushu-u.ac.jp

Mechanical and electronic properties of copolymers of centrohexaquinane and cyclooctatetraene

○Yasumaru Fujii, Mina Maruyama, and Susumu Okada

Graduate School of Pure and Applied Sciences, University of Tsukuba, 1-1-1 Tennodai, Tsukuba, Ibaraki 305-8571, Japan

Polyquinane has been attracting much attention as building block of various real and hypothetical carbon allotropes covering all dimensions. Because of the unsaturated π electron states of pentagonal ring, covalent networks of polyquinane occasionally possess unusual electronic structures that are absent in the networks sorely consisting of hexagonal rings. In addition to the electronic structure, the polyquinane could form three-dimensional covalent network that exhibits unusual mechanical properties: The three-dimensional network consisting only of fused pentagons (pentadiamond) possesses a moderate bulk modulus and negative Poisson's ratio, leading to the remarkable mechanical toughness against the anisotropic structural deformation. In addition to the pentadiamond, the large number of possible combinations and arrangements of polyquinane and other hydrocarbons causes the rich morphological variety of polyquinane derivatives.

In this work, using the density functional theory with generalized gradient approximation, we theoretically designed three-dimensional covalent networks consisting of centrohexaquinane [Fig1. (a)] and cyclooctatetraene, and investigated their physical properties. In these networks, centrohexaquinane and cyclooctatetraene altenately arrangement at the vertexes and faces of cubic lattice, respectively. Accordingly, the copolymers are three-dimensional carbon allotropes consisting of both sp^2 and sp^3 C atoms. Furthermore, they possess two strcural isomers with $P\bar{4}3m$ [Fig1. (b)] and $Fm\bar{3}m$ [Fig1. (c)], owing to two possible arrangements of centrohexaquinane. Our calculations demonstrated that these coploymers are metals with large Fermi level DOS. The mechanical properties strongly depend on their morphologies: The copolymer with $Fm\bar{3}m$ symmetry possesses relatively high bulk modulus with negative Poisson ratio, while that with $P\bar{4}3m$ has low bulk modulus with negative Poisson's ratio.

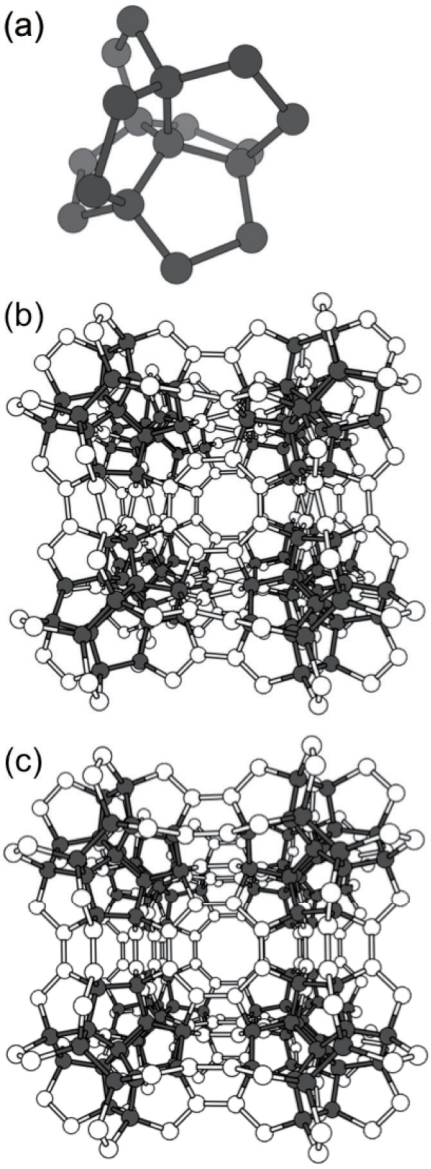

Fig.1 (a) Centrohexaquinane. Hydrogen is omitted. Optimized structures of copolymer with (b) $P\bar{4}3m$ and (c) $Fm\bar{3}m$ symmetry. Light and dark gray spheres denote sp^3 and sp^2 C atoms, respectively.

Corresponding Author: Y. Fujii
E-mail: yfujii@comas.frsc.tsukuba.ac.jp

Single molecule magnet properties of Tb-dimetallofullerene anions: $[Tb_2@C_{80}(I_h)]^-$ and $[Tb_2@C_{78}(D_{3h})]^-$

○Kazuki Yamagishi[1], Ryuji Higashinaka[2], Yuji Aoki[2], Koichi Kikuchi[1], Yohji Achiba[1], Takeshi Kodama[1]

[1]*Department of Chemistry, Tokyo Metropolitan University, Tokyo 192-0397, Japan*
[2]*Department of Physics, Tokyo Metropolitan University, Tokyo 192-0397, Japan*

Recently, single molecule magnets (SMMs) containing two lanthanide metals in a fullerene cage have been studied actively. For example, Tb-dimetallofullerenes, $Tb_2@C_{79}N$ [1] and $Tb_2@C_{80}(CH_2Ph)$ [2], exhibited the magnetic hystereses at sweep rate 2.9 mT s^{-1} up to 27 K and 28 K, respectively. This rather good SMM property originates from the ferromagnetically coupled spin system inside the cage, [Tb^{3+} - e^- - Tb^{3+}]. From the theoretical calculation [1], it was suggested that the symmetry of the electrostatic field in the fullerene cage affect the SMM properties. Therefore, in this study, we synthesized and isolated $[Tb_2@C_{80}(I_h)]^-$ and $[Tb_2@C_{78}(D_{3h})]^-$, which have carbon cages with no N-substitution and no additional group, and the magnetic properties were measured to investigate the influence of the cage.

Fig.1 and Fig. 2 show M-H curves for $[Tb_2@C_{80}(I_h)]^-$ and $[Tb_2@C_{78}(D_{3h})]^-$ at sweep rate 4.2 mT s^{-1}, and the hysteresis loops were seen up to 29 K and 15 K, respectively. For $[Tb_2@C_{80}(I_h)]^-$, the temperature of hysteresis disappearance is almost identical for $Tb_2@C_{79}N$ and $Tb_2@C_{80}(CH_2Ph)$ although the symmetry of the electrostatic field in the fullerene cage is different. On the other hand, $[Tb_2@C_{80}(I_h)]^-$ and $[Tb_2@C_{78}(D_{3h})]^-$ have rather different temperatures of hysteresis disappearance.

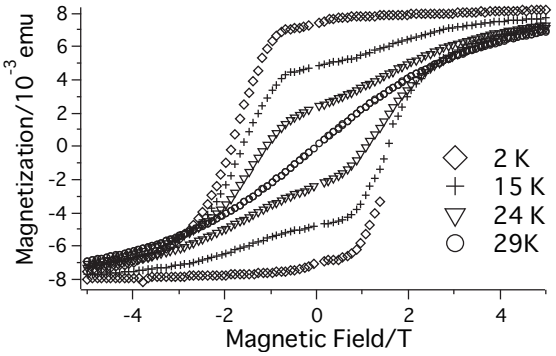

Fig. 1 M-H curve of $[Tb_2@C_{80}(I_h)]^-$

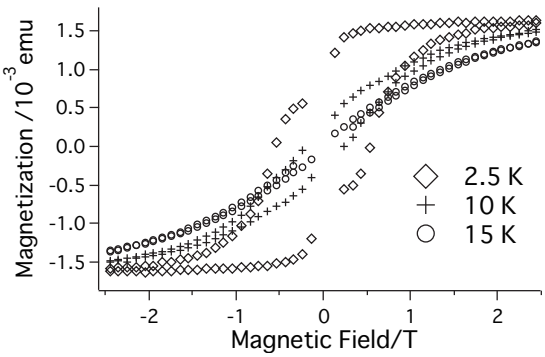

Fig. 2 M-H curve of $[Tb_2@C_{78}(D_{3h})]^-$

[1] G. Velkos *et al.* Angew. Chem. Int. Ed. **58**, 5891 (2019).
[2] F. Liu *et al.* Nature Communications **10**, 571 (2019).

Corresponding Author: Takeshi Kodama
Tel: +81-42-677-2530
Fax: +81-42-677-2525
E-mail: kodama-takeshi@tmu.ac.jp

Attempt to produce Sm-dimetallofullerenes

○Naoya Fujita, Koichi Kikuchi, Yohji Achiba, Takeshi Kodama

Department of Chemistry, Tokyo Metropolitan University, Tokyo 192-0367, Japan

The encapsulated lanthanide metals generally tend to take +3 oxidation state in monometallofullerenes (mono-EMFs) and dimetallofullerenes (di-EMFs). However, in the mono-EMFs particular case, those encapsulated metals, Sm, Eu, Tm, and Yb, take +2 oxidation state. In the previous work, while Tm-di-EMFs were obtained [1], Yb- and Eu-di-EMFs were not obtained [2, 3]. The presence of Tm-di-EMFs was understood by the following: Tm can take +3 oxidation state in di-EMFs, because the 3rd ionization energy (IE3) of Tm is lower enough forming +3 state. Since the IE3 of Sm is lower than that of Tm, it was thought that Sm-di-EMFs, which have not been reported, might be obtained. In this work, using an almost identical method previously reported [4], we tried to produce di-EMFs containing Sm.

First, we carried out the experiment for the system of only Sm and carbon, but no evidence of the presence of Sm-di-EMFs was obtained. Then, we move to the hetero metal system. The soot was obtained by direct-current arc discharge of Sm/Y/C (Sm:Y:C=2:1:97) composite rods under a 500 Torr He atmosphere. The raw soot was extracted for 8 h with a mixed solvent of triethylamine and acetone. The extract was separated by HPLC using a C_{18}-AR-II column and a Buckyprep-M column, acetone with an ion-pair reagent, tetrabutylammonium bromide, as an eluent.

Fig. 1 and 2 show 1st- and 2nd-step HPLC chromatograms and LD-TOF-MS spectra of each fraction. In the fraction A-1, the peak of Y_2C_{80} was observed but no peaks of $SmMC_{80}$ and Sm_2C_{80}. Similarly, in the fraction A-2, the peak of Y_2C_{78} was observed but no peaks of $SmYC_{78}$, Sm_2C_{78}. Therefore, it was suggested that di-EMFs containing Sm, $SmYC_n$ and Sm_2C_n, were not produced or not extracted as an anion form if existed in the raw soot. We also tried Sm/Tb system and the results will be discussed in the symposium.

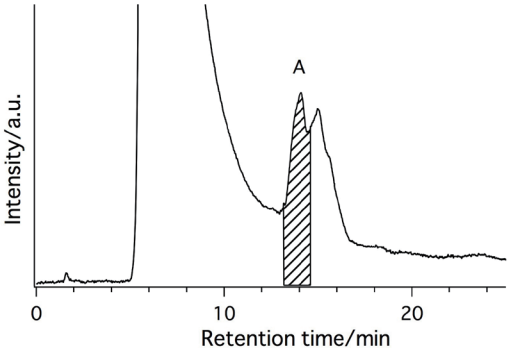

Fig.1 1st-step HPLC chromatogram

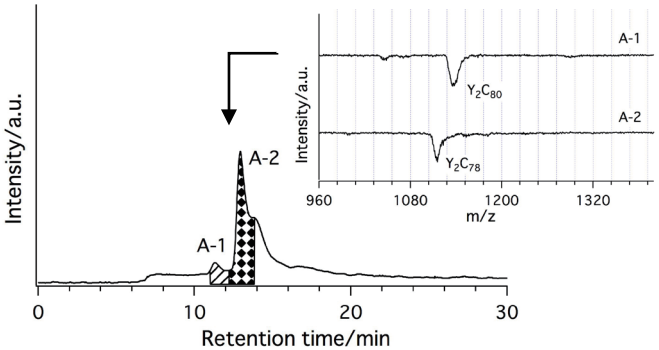

Fig.2 2nd-step HPLC chromatogram and LD-TOF-MS spectra of each fraction

[1] K. Kobayashi, et al. *The 54th Fullerenes-Nanotubes-Graphene General Symposium* 48(2018).
[2] K. Kobayashi, et al. *The 52nd Fullerenes-Nanotubes-Graphene General Symposium* 128(2017).
[3] Y. Furiya, et al. *The 56th Fullerenes-Nanotubes-Graphene General Symposium* 136(2019).
[4] N. Nakatori, et al. *The 49th Fullerenes-Nanotubes-Graphene General Symposium* 46(2015).
Corresponding Author: Takeshi Kodama
Tel: +81-42-677-2530, Fax: +81-42-677-2525, E-mail: kodama-takeshi@tmu.ac.jp

In vivo evaluation of biodistribution, toxicity and clearance of single wall carbon nanotubes depending on the dispersants

○Ying Xu[1], Minfang Zhang[1]*, Mei Yang[1], Masako Yudasaka [1, 2], Toshiya Okazaki[1]

[1]*National Institute of Advanced Science and Technology (AIST)*
[2]*Meijo University*

The toxicity and biodistribution of carbon nanotubes are believed to depend on their types, lengths or functionalization degrees. However, it has not been known that the fate of carbon nanotubes, having similar lengths and no chemical functionalization are different and depend on the types of dispersants. In this study, we have investigated the effect of two different dispersants on the biodistribution, toxicity and degradation of single-wall carbon nanotubes (CNTs) after intravenous injection into mice for 3 months.

The CNTs used in this study were produced by the super-growth method (SG-CNTs) [1]. The SG-CNTs were oxidized with H_2SO_4/HNO_3 and then dispersed in bovine serum albumin (BSA) (CNT-BSA) or a phospholipid polyethylene glycol (DSPE-PEG) solution (CNT-PEG) by sonication. The CNT-BSA or CNT-PEG dispersion solutions were intravenously injected into mice. At five time points of Day 1, 3, 7, 30, 90, the biodistribution of CNTs in the tissues of lung, liver, and spleen were estimated by an optical absorption measurement method that we developed recently.

The results showed that the tissues of lung, liver and spleen were pigmented to dark or grey on Day1 due to the accumulation of CNTs in them. For livers and spleens, tissues of CNT-BSA and CNT-PEG injection groups didn't show much difference in the color, whereas, slight difference in the quantities of CNTs. Interestingly, for lungs, the color of CNT-PEG injected group was obviously darker than that of CNT-BSA group. And the quantities of CNT-PEG in lung were much larger than that of CNT-BSA. These results indicated that the biodistribution of SWNTs was related to their dispersants. Moreover, the dark color of lungs faded away and the quantities of CNT-PEG in lung decreased with the increase of post-injection time, indicating the clearance of CNTs from lungs. This result confirmed our previous study [2]. In addition, no obvious signs of toxicity were indicated from our measurements of cytokines in blood plasma and tissue lysates of liver, lung and spleen. The results suggested that the fate of CNTs in living body was influenced by the dispersants and the clearance of CNTs from lungs is possible. The reasons for the dependence of biodistribution on the CNT dispersants are currently under study.

[1] K. Hata, *et al.* Science, **306**, 1362 (2004).

[2] X. Xu *et al*. 56th Fullerenes-Nanotubes-Graphene General Symposium.

Corresponding Author: M. Zhang

Tel: +81-29-861-6758

E-mail: m-zhang@aist.go.jp

Importance of structural parameters of CNTs for the Pt electrochemical durability in CNT based Pt electrocatalysts in PEMFCs

○Don Terrence Dhammika Weerathunga[1,2], Tsuyohiko Fujigaya[*1,2,3]

[1] *International Institute for Carbon-Neutral Energy Research (WPI-I²CNER), Kyushu University, 744 Motooka Nishi-ku, Fukuoka 891-0395, Japan*
[2] *Department of Applied Chemistry, Graduate School of Engineering, Kyushu University, 744 Motooka Nishi-ku, Fukuoka 819-0395, Japan*
[3] *Center for Molecular Systems (CMS), Kyushu University, 744 Motooka Nishi-ku, Fukuoka 819-0395, Japan*

The durability of polymer electrolyte fuel cells (PEMFC) is required to be improved largely [1]. By using carbon nanotubes (CNT) as catalyst support in place of carbon black, improvement of durability was reported [2]. To explore the structural dependency on the type of CNT for durability, accelerated durability tests from 1.0 – 1.5 V vs RHE at 0.5 Vs^{-1} in 0.1 M $HClO_4$ at 25 ºC in half-cell were performed to CNTs listed in Table 1, after loaded with Pt nanoparticles (Fig. 1).

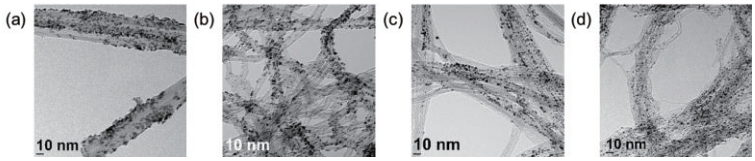

Fig. 1 CNT/Pt composites of (a) MW_{25}, (b) $MW_{9.5}$, (c) $SW_{1.5}$ and (d) $SW_{2.5}$ [3].

Table 1. List of CNTs

Label*	MW_{25}	$MW_{9.5}$	$SW_{1.5}$	$SW_{2.5}$
Manufacturer	Nikkiso	Nanocyl	Meijo NC	Nippon Zeon
Diameter / nm	20 – 30	8.5 – 10.5	1.2 – 2.8	2.0 – 3.0
Raman I_D/I_G	0.22	4.29	0.02	0.16
Pt degradation rate (k)	0.32	6.02	3.36	12.65

*(Labels are as MW for Multi-walled CNTs and SW for Single-walled CNTs with mean diameter as the suffix).

Electrochemical stability of CNTs is revealed to dominate the stability of Pt. MWs having larger diameter with lower degree of side-wall defects (witnessed by a low I_D/I_G in Raman as in Table 1) offered a lower Pt degradation rate (k) than smaller MWs and SWs (Fig. 2 and Table 1) [3]. Also the onset temperature in the thermogravimetric analysis and their profiles provide an insight for predicting durability of their Pt composites (not shown) [3].

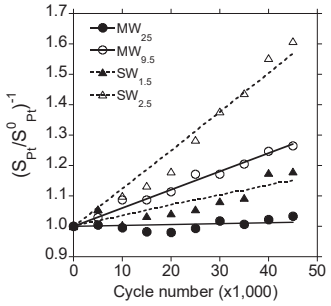

Fig. 2 $(S_{Pt}/S^0_{Pt})^{-1}$vs cycle number of Pt composites, where S_{Pt} and S^0_{Pt} is the ECSA at a particular cycle number and at 5,000 cycle number respectively, the gradient of the graphs represent the Pt degradation rate (k) and the values are shown in Table 1 [3].

[1] S. Ye *et al*. ECS Trans **16**, 2101 (2008).
[2] Y. Shao *et al.* J. Electrochem Soc. **153**, A1093 (2006).
[3] D. Weerathunga *et al.* Diam. Relat. Mater. **97**, 107459 (2019).

Corresponding Author: T. Fujigaya,
Tel. / Fax: +81-92-802-2840,
E-mail: fujigaya.tsuyohiko.948@m.kyushu-u.ac.jp

A semitransparent terahertz imager made from chemically doped semiconducting carbon nanotube thin films

○Kanae Oi,[1] Kou Li,[2] Daichi Suzuki,[3] Tsuyoshi Kawai,[1] Yukio Kawano,[2] Yoshiyuki Nonoguchi[1,4]

[1] *Division of Materials Science, Nara Institute of Science and Technology, NAIST, Takayama, Ikoma, Nara 8916-5, Japan*
[2] *Laboratory for Future Interdisciplinary Research of Science and Technology, Tokyo Institute of Technology, 2-12-1 Ookayama, Meguro-ku, Tokyo, 152-8552, Japan*
[3] *Quantum Effect Device Research Team, Center for Emergent Matter Science, RIKEN, 2-1 Hirosawa, Wako, Saitama, 351-0198, Japan*
[4] *JST PRESTO, 4-1-8 Honcho, Kawaguchi, Saitama 332-0012, Japan*

Sensing devices with terahertz (THz) wave have a great potential for the use in nondestructive inspection. Most of them rely on Si and compound semiconductor devices. Very recently, the photothermoelectric effect of single wall carbon nanotube (SWCNTs) has been employed to develop flexible THz imagers that can sense real 3D objects [1]. Herein we utilize semitransparent semiconducting (sc-) SWCNT thin films with excellent thermoelectric properties for the construction of semitransparent THz detectors.

We dispersed SWCNTs in toluene using poly(9,9-di{2-[2-(2-methoxy-ethoxy)ethoxy] ethyl}fluorenyl-2,7-diyl) ($PFEtO_3$). This SWCNTs dispersion was then used to form semitransparent thin films (~300 nm) on PET substrates. The doping level was modulated with a p-type dopant (silver bis-(trifluoromethanesulfonyl)imide) and an n-type dopant (KOH/15-crown ether).

The S_{11} absorption in the near infrared (NIR) gradually bleached and the broad peak (I_p) in the FIR evolved, depending on the concentration of dopant (**Fig.1(a)**). Assuming that the product of THz absorption and power factor is the relative sensitivity of devices, SWCNTs films has high sensitivity in the wide dopant concentration range (**Fig.1(b)**). Based on this result, we evaluated the noise equivalent power (NEP) of on-tip p–n junction devices implementing doped SWCNTs films. Along with this, we successfully demonstrated the two-dimensional inspection of X-shape metal tapes behind opaque objects (plastic plate and black tape) by scanning the detector at 29 THz (**Fig.1(c)**).

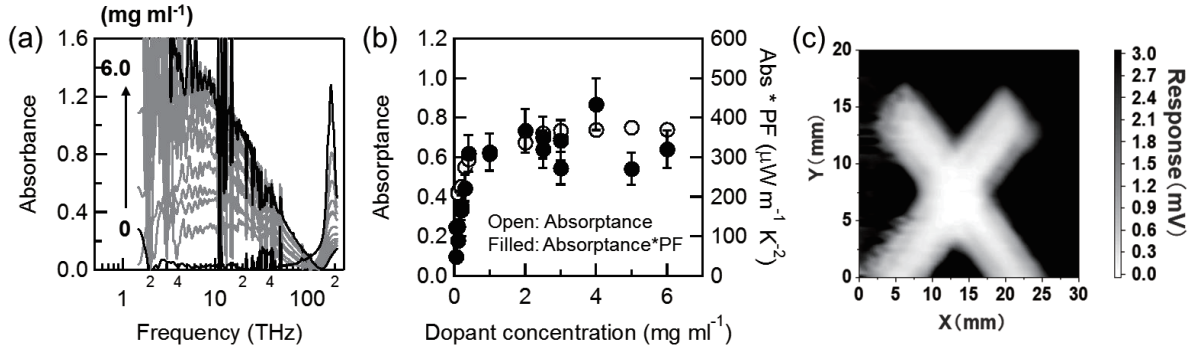

Fig.1 (a) NIR-to-FIR spectra of sc-SWCNT films dependent on p-doping concentration. (b) Relationship between sensitivity and p-dopant concentration. (c) An inspection image of a metal tape acquired at 29 THz.

[1] D. Suzuki, S. Oda, and Y.Kawano, Nat. Photonics, **10**, 809-813 (2016).

Corresponding Author: Yoshiyuki Nonoguchi
Tel: +81-743-72-6028, Fax: +81-743-72-6179
E-mail: nonoguchi@ms.naist.jp

Compact Wearable Foot Pressure Sensors from MWCNT Coated Cotton Fibers for Human Activity and Sporting Performance Monitoring

Md. Abdul Momin[1*], Mohammad Jellur Rahman[2] and Tetsu Mieno[1]

[1] *Graduate School of Science & Technology, Shizuoka University, Shizuoka 422-8529, Japan*

[2] *Department of Physics, Bangladesh University of Engineering and Technology, Dhaka, Bangladesh*

High sensitive compact pressure sensors have been developed using multiwall carbon nanotube (MWCNT) coated cotton fibers. The performance of the sensors is optimized by varying the concentration of MWCNTs and the thickness of the total fibers. Water-dispersible MWCNT derivatives is used to coat cotton textiles with high stability [1]. By the citric-acid and oxygen plasma treatments, MWCNTs are functionalized and they can easily disperse in water. This method is very safe and eco-friendly. These functionalized MWCTNs are coated on cotton fibers and used as filler material of the force/pressure sensors. These pressure sensors have sensitivities of 180–0.20 kPa^{-1} in the range of forces F= 1 mN–100 N (p= 8.84 Pa–884 kPa) [2]. These new pressure sensors have short activation and relaxation time. The reproducibility of the load cells in pressure measurements is observed, and high reproducibility under different harsh ambient conditions is demonstrated, as well as high durability in tests involving more than 11,200 repeated compression/relaxation cycles. The efficiency of the sensors remains almost the same at low and high temperatures and under low- and high-humidity conditions. The load cells can measure characteristic signals corresponding to walking, jogging, jumping and standing conditions and the center of gravity of a human foot during standing, walking and running. Schematic of sensors and recorded signals during a running are shown in Fig. 1 and Fig. 2. Therefore, the load cells have, strong potential to be used as wearable force (or pressure)-monitoring devices, for healthcare tests, rehabilitation, real-time sports activities, and robot technologies.

[1] Md. J. Rahman, T. Mieno, *J. Nanomater.*, **2014**, Article ID 508182 pp. 1–9 (2014).

[2] M. A. Momin, Md. J. Rahman, Tetsu Mieno, *J. Nanomater*, **2019**, Article ID 7658437 pp. 1-15 (2019).

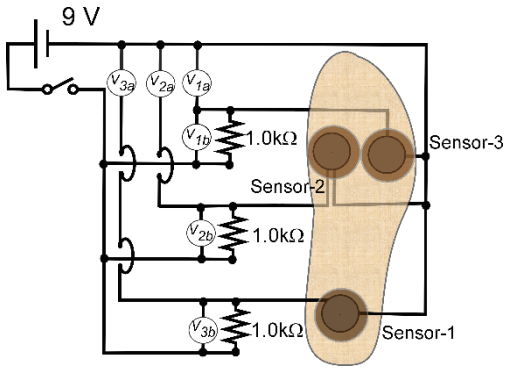

Fig.1: The 3 sensors are set in a shoe insole.

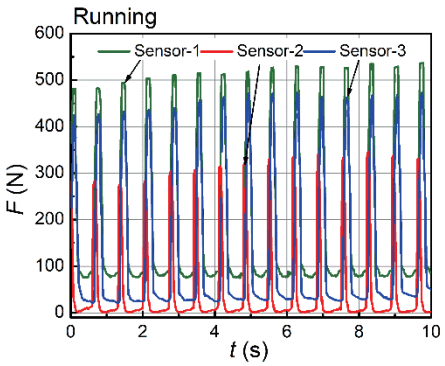

Fig. 2: Force signals of the 3 sensors during running.

*Corresponding author: Md. Abdul Momin

E-mail: mamomin89bd@gmail.com, Mobile: +8108041265887

Activation of Alkane for CVD Growth of Single-Wall Carbon Nanotubes

○Pengfei Chen[1], Mengju Yang[1], Rei Nakagawa[1], Hisashi Sugime[1], Hitoshi Mazaki[2], Suguru Noda[1,3,*]

[1] *Department of Applied Chemistry, School of Advanced Science and Engineering, Waseda University, 3-4-1 Okubo, Shinjuku-ku, Tokyo 169-8555, Japan*
[2] *Central Technical Research Laboratory, JXTG Nippon Oil & Energy Corporation, 8 Chidori-cho, Naka-ku, Yokohama, Kanagawa 231-0815, Japan*
[3] *Waseda Research Institute for Science and Engineering, Waseda University, 3-4-1 Okubo, Shinjuku-ku, Tokyo 169-8555, Japan*

Nowadays C_2H_2 is one of the commonly used carbon sources for the growth of single-wall carbon nanotubes (SWCNTs) due to its high activity [1]. However, the large-area synthesis of SWCNTs is still a problem because the C_2H_2 supply at high concentrations easily causes the catalyst deactivation [2]. We proposed the control of gas-phase reactions by combining two carbon sources of C_2H_2 and C_2H_4, which yielded SWCNTs at an improved areal yield [3]. In this study, instead of using the alkyne or alkene, we investigated less reactive alkane as the carbon source. Compared to the C_2H_2, n-hexane (n-C_6H_{14}) can be a better candidate because of the lower price and easier storage in liquid state. We studied the gas-phase reactions by gas chromatography (GC) and gas-phase kinetic simulation (CHEMKIN) to determine the factors that influence the SWCNT growth. We first checked the CNT synthesis using the combinatorial catalyst (0.2-5 nm Fe on 15 nm AlO_x) [2] and found that SWCNTs grow from thin Fe layer when n-C_6H_{14} (2 vol%) is fed with H_2 at relatively high concentrations (20-40 vol%) (Fig. 1a). Then we examined the large-area synthesis of SWCNTs using the 18 substrates (1×1 cm^2) with 0.7 nm Fe, and found that SWCNTs was produced at a higher average yield of 1.8 mg cm^{-2} from n-C_6H_{14} (Fig. 1b) than from C_2H_2 (1.4 mg cm^{-2}). The analysis of the gas-phase species showed that C_2H_2 forms from n-C_6H_{14} at a concentration similar to the optimum C_2H_2 concentration (0.3 vol%) in our previous works [2,3]. n-C_6H_{14} is an effective carbon source that yields C_2H_2 *in situ* for the large-area synthesis of SWCNTs.

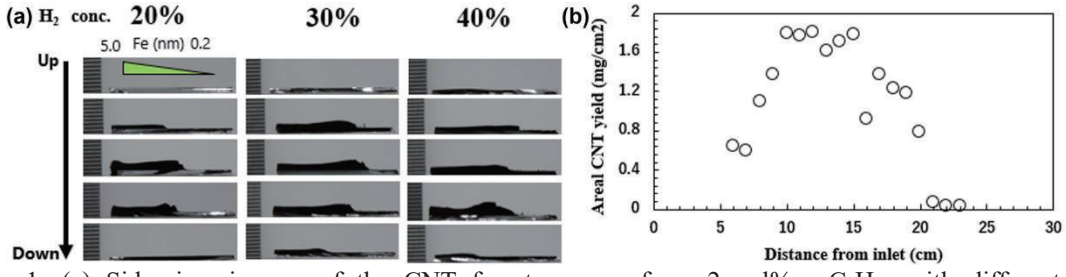

Fig. 1: (a) Side-view images of the CNT forests grown from 2 vol% n-C_6H_{14} with different H_2 concentrations on Fe (gradient)/AlO_x/Si. (b) Areal mass of the SWCNTs grown with 20 vol% H_2 and 0.7 nm Fe. CVD was carried out at 800 °C for 30 min.

[1] H. Sugime and S. Noda, *Carbon* **50**, 2953 (2012). [2] K. Hasegawa and S. Noda, *ACS Nano* **5**, 975 (2011). [3] T. Sato et al., *Carbon* **136**, 143 (2018).

Corresponding Author: S. Noda, Tel: +81-3-5286-2769, E-mail: noda@waseda.jp

Synthesis of aligned carbon nanotube arrays on quartz wool and its morphological characterization

○Nobutomo Yamaguchi, Dai Goudo, Kiyofumi Yamagiwa

Graduate School of Science & Engineering, Teikyo University of Science, Adachi, Tokyo 120-0045, Japan

Carbon nanotubes (CNTs) are generally synthesized by chemical vapor deposition (CVD) using hydrocarbons derived from fossil fuels, such as ethylene, benzene, and alcohols, as carbon sources. Meanwhile, Ando et al. has developed camphor CVD techniques using camphor ($C_{10}H_{16}O$), which is a natural tree-derived carbon source [1]. Camphor CVD systems are promising, given their environmental friendliness and high mass productivity [2]. In this study, CNTs were synthesized on various Silicon-based substrates to examine the effects of substrates on the morphology and yields of CNTs.

CVD was performed using camphor and ferrocene as the carbon source and the catalyst precursor, respectively. Silicon-based substrates (silicon wafers, quartz wools, and quartz filter papers) were placed at the center of a ceramic tube in the CVD furnace. The ceramic tube was heated to 750°C (synthetic temperature) for 15 min (synthetic time) under flowing Ar gas. After the synthesis, the products on the substrate were examined by scanning electron microscopy (SEM) and transmission electron microscopy (TEM).

Each substrate resulted in a distinctive CNT morphology. Figure 1 shows SEM images of aligned CNT arrays grown on the surface of quartz wool fibers as an example. The arrays were ~100 μm in length and have rippled plate-shaped structures. TEM images (not shown here) indicate that the arrays are composed of multi-walled CNTs with outer diameters of 10-50 nm. In typical applications, the arrays are expected to be self-supporting thin CNT films, and this is accomplished by applying a proper exfoliation process.

The CNT yield and formation mechanism of the structure will be discussed in the presentation.

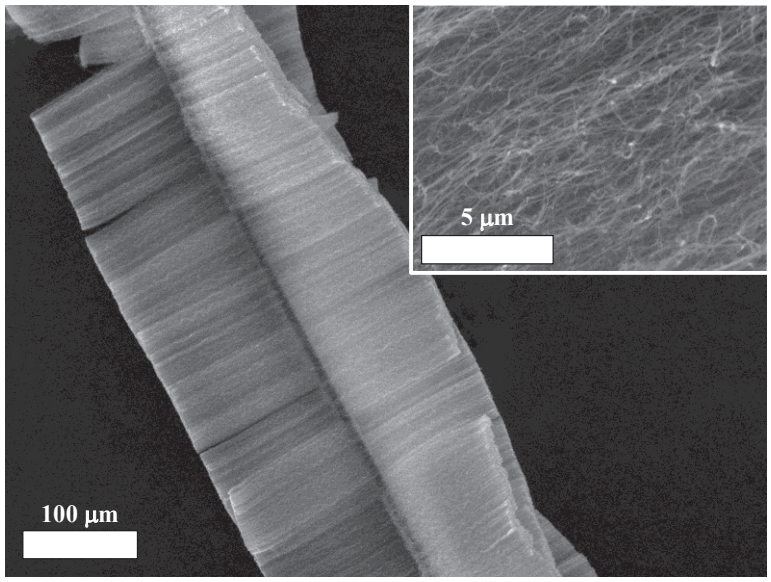

Fig. 1. SEM images of aligned CNT arrays grown on quartz wool. Inset shows high magnification SEM image of the arrays.

[1] M. Kumar and Y. Ando, *Chem. Phys. Lett.*, **374**, 521 (2003).
[2] M. Kumar and Y. Ando, *J. Nanosci.Nanotechnol.*, **10**, 3739 (2010).

Corresponding Author: K. Yamagiwa
Tel: +81-3-6910-1010
E-mail: yamagiwa@ntu.ac.jp

Separate control of catalyst and source gases in synthesis of boron nitride nanotubes by chemical vapor deposition

○Hiromu takahashi[1], Tetsuro Sawada[1], Tomohiro Sei[1], Mayu Asaka[1], Toshio Osawa[1], Hisashi Sugime[1], Suguru noda[1,2]

[1] Department of Applied Chemistry, [2]Waseda Research Institute for Science and Engineering, Waseda University, Tokyo 169-8555, Japan.

Boron nitride nanotube (BNNT) has excellent properties such as high mechanical strength, high thermal stability, high thermal conductivity and so on [1]. Applications for thermal interface material or wiring system are considered, but the high cost of BNNT is currently making this difficult [1]. In commercial production, BNNT is synthesized by physical vapor deposition (PVD) [2] using plasma or laser, therefore the producibility is limited due to the difficulty of the scaling up of the production. To realize the mass production of BNNT at low cost, chemical vapor deposition (CVD) has been focused by many researchers [1]. Boron oxide CVD has been widely researched, however the understanding of the growth mechanism of BNNT is limited. In this research, we studied the growth mechanism of BNNT focusing on understanding the effect of B sources, NH_3 supplement, and catalyst conditions.

As the B source, the mixture of B and metal oxides (e.g. Fe oxide or Mg oxide) were widely used in previous reports [1]. However, the independent control of B source and catalyst was difficult because of the mixed B and catalyst sources. In this research, we used metal-free B sources and catalysts supported on substrates. Fe catalyst with a thickness gradient was prepared on $AlO_x/SiO_2/Si$ or graphite substrates using the combinatorial masked deposition method to examine catalyst conditions carefully (Fig. 1a). B_2O_2 vapor as the boron source was generated by heating the mixed powder of B and B_2O_3 [3] in the CVD reactor. To avoid the BN formation on the B source, NH_3 was supplied through an inner tube at the downstream of the B source. The reactor was heated under Ar flow, and after reaching 1000 °C, CVD was carried out for 10 min by flowing NH_3/Ar. After CVD, the reactor was cooled down to ambient temperature under Ar flow.

Nanotubes were observed well on the graphite substrate but poorly on the $AlO_x/SiO_2/Si$ substrate possibly due to the reaction of Fe with the latter at 1000 °C. Scanning electron microscopy (SEM) (Fig. 1b) showed nanotubes with length, density and diameter changing with Fe thickness. Individual tubes showed layer structure with an interlayer distance of 0.34 nm that matches BNNT in transmission electron microscope (TEM) image (Fig. 1b). Tubes contained N as shown by the scanning electron transmission microscope-energy dispersive X-ray spectroscopy (STEM-EDS) (Fig. 1c).

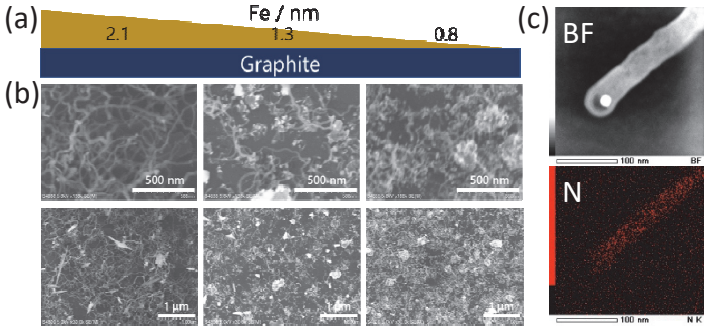

Fig. 1. (a) Catalyst structure. (b) SEM images at different positions. (c) Blight-field image and elemental map of N by STEM-EDS.

[1] P. Ahmad, et al., RSC Adv. **5**, 35116 (2015).

[2] K.S. Kim, et al., Semicond. Sci. Technol. **32**, 013003 (2017).

[3] Songfeng E., Chem. Phys. Lett. **687**, 307 (2017).

Corresponding Author: S. Noda Tel&Fax: +08-3-5286-2768 E-mail: noda@waseda.jp

Selective dispersion of semiconducting single-walled carbon nanotubes by using alkyl cellulose

○Tomoko Yagi[1], Tsuyoshi Kawai [1], Yoshiyuki Nonoguchi [1, 2]

[1] *Division of Materials Science, Nara Institute of Science and Technology, NAIST, Takayama, Ikoma, Nara 8916-5, Japan*
[2] *JST PRESTO, 4-1-8 Honcho, Kawaguchi, Saitama 332-0012, Japan*

Single-walled carbon nanotubes (SWCNTs) are classified into metallic carbon nanotubes (m-SWCNTs) and semiconductor carbon nanotubes (sc-SWCNTs). The selective extraction of sc-SWCNTs is required for the development of efficient electronic devices. Conjugated polymers have been used to selectively disperse sc-SWCNTs [1]; however, these polymers are not suitable for large scale production due to their high production cost. Here we demonstrate that alkyl cellulose can disperse sc-SWCNTs at high selectivity and yield. Alkyl cellulose is a sustainable, and environmentally friendly compound conformable to large-quantity production. We reveal that the selectivity changes depending on the side chain length of alkyl cellulose.

We dispersed SWCNTs in tetrahydrofuran (THF) using alkyl cellulose with different alkyl chain lengths (R = C_2, C_4, C_6, C_{12}) (**Figure 1**). We evaluated the selectivity of sc-SWCNTs extraction using UV-Vis-NIR spectroscopy with dispersion.

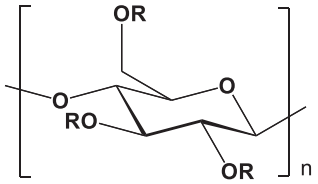

Figure 1. Chemical structure of alkyl cellulose (R = C_2, C_4, C_6, C_{12})

UV-Vis-NIR spectra indicated that the selectivity of sc-SWCNTs changes depending on the side chain length of alkyl cellulose. Particularly, hexyl cellulose selectively extracted sc-SWCNTs in THF (**Figure 2**). This successful separation expectedly relies on the difference of the polarizability between sc- and m-SWCNTs polymer complexes which can be modulated by the side chain length of alkyl cellulose. Selectivity dependences on solvents, and polymers' molecular weight along with CNT diameters are systematically investigated. We believe that this result will help elucidate the mechanism of selective dispersion of SWCNTs by polymer wrapping.

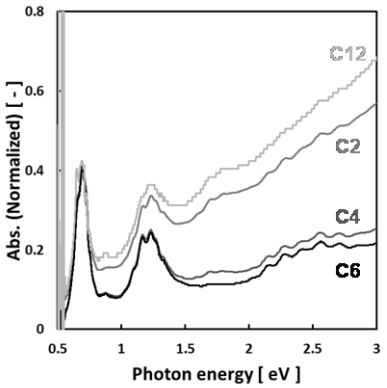

Figure 2. UV-Vis-NIR spectra of dispersions normalized by S_{11} using different alkyl cellulose (R = C_2, C_4, C_6, C_{12}) as a dispersant.

[1] A. Nish *et al*. Nat. Nanotech., **2**, 640-646 (2007).

Corresponding Author: Yoshiyuki Nonoguchi
Tel: +81-743-72-6028, Fax: +81-743-72-6179
E-mail: nonoguchi@ms.naist.jp

Scaling laws on enhancement of the electric field inside a hollow cylinder

○Yuan Tian, Muhammad Shoufie Ukhtary, Riichiro Saito
Department of Physics, Graduate School of Science, Tohoku University,
Sendai 980-8578, Japan

Nanoscale metallic tube with dielectric core (fig.1) is a good model to represent the character of tips used in tip enhanced Raman spectroscopy (TERS) [1]. Further, multi-shell nanotubes consisting of of semiconductors is predicted being able to enhance the efficiency of photoelectric devices [2]. For such application, the enhancement of electric field inside the cylinder should be optimized. E. Devaux et.al. showed that the enhancement occurs by the excitation of surface plasmon (SP) [3]. However, even though the existence of SP in a hollow core is already studied and well proved, Designing the cylinder which gives a large enhancement is not easy as a function of frequency or diameter of the core. It is because that we do not have neither analytical expression of the enhancement nor the numerical simulation. If the relationship between the enhancement of electric field, the geometry and the frequency of the light are available, we could synthesize the hollow nano cylinder which gives the best enhancement for a given frequency of light.

In this work, we calculate the enhancement of the electric field inside the cylinder with different geometries and frequencies of incident light, in which we solve the Helmholtz equation with incident light and boundary conditions.

We obtain the enhancement of electric field inside the cylinder as a function of the incident frequency ω (fig.2). We then found that the enhancement can be roughly fitted as a Lorentzian function of ω. The parameters of the Lorentzian function, such as the maximum enhancement and width can be obtained by scaling the enhancement by the thickness and radius of the hollow cylinder. Further, the ω of maximum enhancement is compared with the dispersion relation of the SPs. Further which we obtain resonant condition of SP which is relevant to the enhancement. The fitted scaling function of the enhancement is useful to find the optimized geometry of hollow cylinder for a given ω.

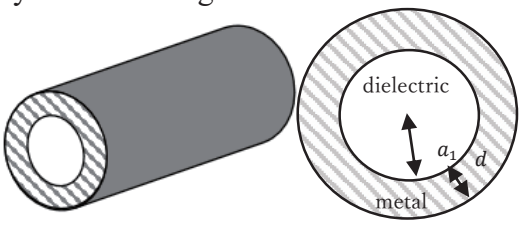

Fig.1 The layout of a hollow cylinder, with a_1 as the inner boundary radius and d as the thickness

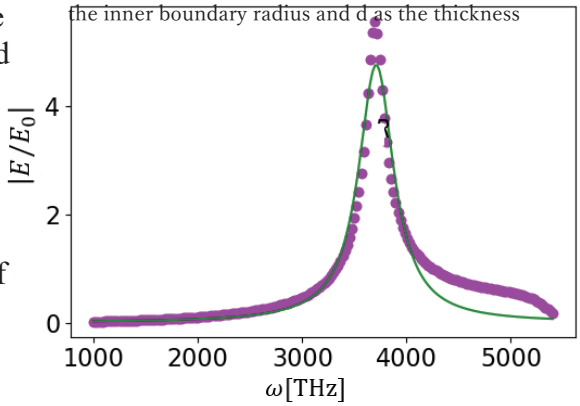

Fig.2 Plot of the electric field enhancement as a function of incident frequency ω for a certain geometry. Dot is the result from numerical calculation, line is the fitting of the result with Lorentzian function.

Reference:
[1] Alexander S. McLeod *et.al.*, Phys. Rev. B 90, 085136 (2014).
[2] Joseph D. Christesen *et.al.*, Nano Lett.12, 11, 6024-6029 (2012).
[3] U. Schröter, E. Devaux *et.al.*, Phys. Rev. B 64, 125420 (2001).

Photoluminescence of Graphene Oxide Enhanced by UV-radiation in Dioxane

○Katsuki Kanazawa[1], Masahito Sano [1]

[1] *Depart. of Organic Materials Science, Yamagata University, Yonezawa 992-0038, Japan*

Graphene oxide (GO) contains various oxygen-containing groups, such as epoxide, ether, carbonyl and hydroxyl groups attached to graphene hexagonal structures that have been damaged to some extents by oxidation. As a result, GO has lost the excellent electronic and mechanical properties of graphene, but, it has gained good dispersibility to many polar solvents and photoluminescence (PL).

GO dispersed in a solvent exhibits PL under UV radiation. Although the oxygen-containing groups are shown to be responsible for PL, the detailed mechanisms are not yet understood. When the size of GO is on the order of a few nanometers (sometimes called graphene nanodots), it has relatively strong blue emission. For GO of micrometer sizes, it emits around yellow-to-red region with much weaker intensities. For practical applications of GO's PL, it is necessary to increase the emission intensity.

Recently, we have developed Twilight fluorescence (TwiF) microscopy which is capable of imaging a single-layer graphene dispersed in solutions. Presently, it is the only technique to visualize graphene or GO floating freely in a liquid. We have also modified the microscope so that a small portion of the rays under observation is directed into a spectrometer, making the simultaneous measurement of a fluorescence spectrum possible while imaging the target GO sheet.

When GO is dispersed in N-methyl-2-pyrrolidone, PL remains stably constant under UV radiation. Surprisingly, when GO is dispersed in 1,4-dioxane, PL increases as UV radiation continues (Fig. 1). TwiF spectroscopy indicates that the longer wavelengths are enhanced more than the shorter wavelengths (Fig. 2). We will discuss possible mechanisms of the enhancement at the presentation.

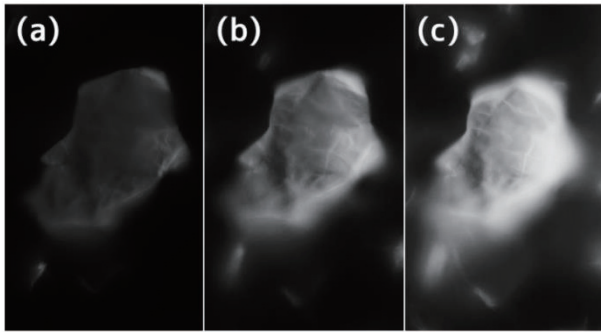

Fig.1 Enhanced photoluminescence of GO single piece in 1,4-Dioxane (a)0sec (b)900sec (c)1800sec

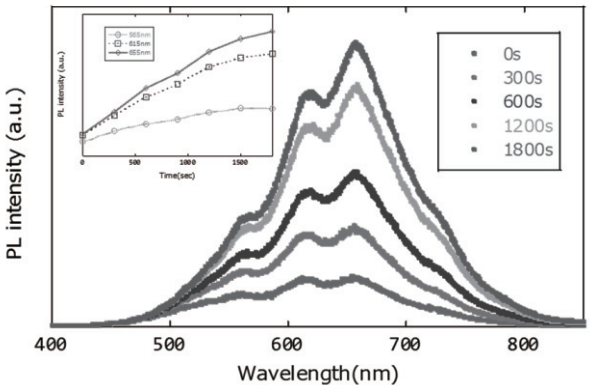

Fig.2 Fluorescence spectrum of GO autofluorescence (Inset shows increase in fluorescence over time at 565, 615, and 655 nm)

Corresponding Author: M. Sano
Tel: +81-238-26-3072,
E-mail: mass@yz.yamagata-u.ac.jp

Effects of interactions at the interface between graphene and quantum dots on their electronic properties

○Zen Inoue[1], Yasushi Ishiguro[2], Alexader Baranov[3] , Igor Nabiev[4], Kazuyuki Takai[1, 2]

[1] *Graduate school of Science and Engineering, Hosei University, Tokyo 184-8584, Japan*
[2] *Department of Chemical Science and Technology, Hosei University, Tokyo 184-8584, Japan*
[3] *ITMO Univ, 49,Kronverksky, St.Petersburg, Russia*
[4] *MEPhI Univ, 31, Kashirskoe, Moscow, Russia*

Graphene as 2-dimensional material has attractive electronic properties, such as broad spectral bandwidth, high electron mobility. However, graphene has relatively low absorbance in spite of its extremely wide-band nature, which limits its application to photodevices [1]. Semiconductor nano crystals in 0-dimension known as quantum dots (QDs) is promising for photonics applications due to their size-dependent tunable optical properties [2]. To realize a photodevices using graphene, a method of constructing hybrid structure combining graphene and QDs has been proposed. But, the mechanism of charge transfer at the interface between graphene and QDs is not yet understood [3]. In this study, we clarify the interactions at the interface between graphene and QDs.

CdSe / PbS-QDs were deposited by spin coating on single-layered (1L) graphene obtained by the mechanical exfoliation. Photoluminescence (PL) measurements were carried out by an spectrometer (LabRAM HR, Horiba) at excitation wavelength of 532 nm at room temperature. The electric conductivity was measured for a field effect transistor (FET) using 1L graphene as a channel material after annealing in vacuum chamber ($<10^{-4}$ Pa) , and after following dropping of CdSe QDs on graphene.

Fig.1 shows a comparison of optical microscope (OM) images of single-layer graphene before CdS / PbS-QDs deposition and PL intensity mapping after QDs deposition. The PL intensity was lower in the area graphene laid for both kinds of QDs, attributed to the exciton quenching caused by charge transfer or near-field interactions between graphene and QDs [4]. Fig.2 shows the transfer characteristics of a FET with CdSe-QDs deposited graphene. The charge neutral point of the FET shifted to the higher gate voltage (hole) side after deposition of CdSe QDs on graphene. Hole carrier transfer from QDs to graphene is suggested at the interface.

[1] K. Kim, et al. *Nature* **457**, 706–710 (2009). [2] Y. Sun, et al. *Scientific Reports* 8, 5107(2018)
[3] R. Li, et al. *Scientific Reports* 6 ,28224(2016). [4] R. Li, et al. *Scientific Reports* 6 ,28224(2016).

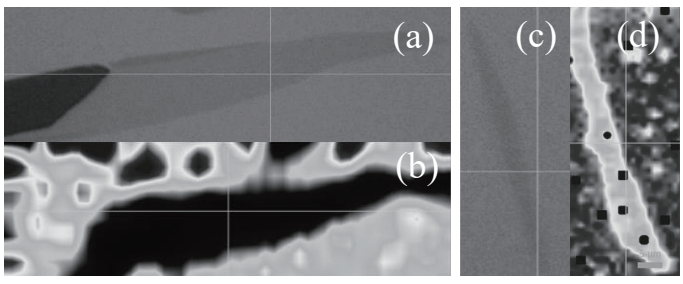

Fig.1 OM images of graphene on SiO_2 (a), (c), and PL intensity mapping of (a), (c) after coating of CdSe (b), and PbS (d), respectively

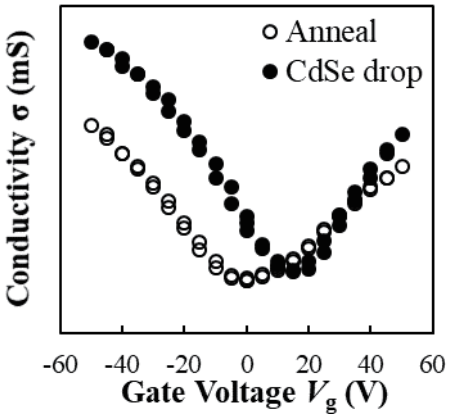

Fig.2 Effects of CdSe QDs on FET

First-principles calculation of exciton of transition metal dichalcogenide

○Pang Xiaoqi[1], Nguyen T. Hung[2], Riichiro Saito[1]

[1]*Department of Physics, Tohoku University, Sendai 980-8578, Japan*
[2]*Frontier Research Institute for Interdisciplinary Sciences, Tohoku University, Sendai 980-8578, Japan*

Coulomb interaction between a pair of electron and hole influences the optical properties of materials, which is known as excitonic effect. Usually, by measuring absorption spectroscopy, we can observe the excitonic effect on many materials, especially for 2D materials. In fact, it reflects the exciton-photon interaction. Although experimental groups report the excitonic properties, the quantitative analysis by the theoretical calculation is not possible for transition metal dichalcogenide. Therefore, the theorical analysis based on first-principles calculation which can calculate the exciton-photon interaction, is necessary to explore how excitons effect the optical absorption spectral.

In this work, we use Yambo code [1] to calculate the eigen values and eigen vectors of exciton. The optical absorption of monolayer and heterostructure transition metal dichalcogenide are discussed by the calculated results. Future by using eigen vector of exciton, we will discuss how to develop the program of Raman spectra (Fig.1).

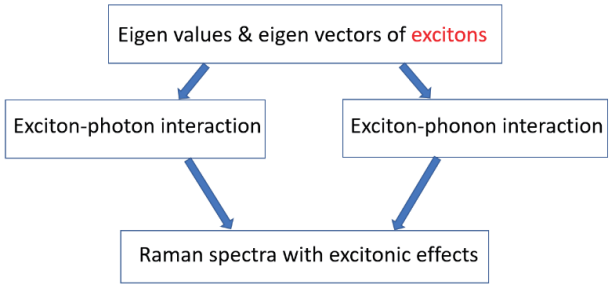

Figure 1: The flow chart to calculate resonant Raman intensity including excitonic effect

[1] Andrea Marini *et all* Comput, Phys. Commun. 180, 1392-1403 (2009)

Corresponding Author: Pang Xiaoqi
Tel: +81-22-795-6442, Fax: +81-22-795-6447,
E-mail: pang@flex.phys.tohoku.ac.jp

Theoretic Study on Raman Active Modes of SnS Thin Films

○Itsuki Yonemori[1], Sudipta Dutta[2], Kosuke Nagashio[3], Katsunori Wakabayashi[1]

[1] *School of Science and Technology, Kwansei Gakuin University, Sanda 669-1337, Japan*
[2] *Indian Institute of Science Research and Education (IISER) Tirupati, India*
[3] *Department of Materials Engineering, The University of Tokyo, Tokyo 113-8656, Japan*

Tin sulfide (SnS) is recently attracting much attention as thermoelectric material due to its low crystal density. For the application to the transparent and flexible devices, the single layer growth and control of the number of layers are demanded. In addition, it has been reported that SnS thin film has ferroelectricity depending on the number of layers. [1] In order to identify the number of layers using Raman spectroscopy, it is necessary to analyze the layer number dependence of phonon vibration mode. In this study, we investigate the phonon vibration modes of SnS thin films using first-principles calculations.

Figure 1(a) shows the crystal structure of bulk SnS crystal. It has orthorhombic structure and double layers in unit cell. The interaction between layers is van der Waals forces. In this study, we performed structure optimization and calculations of electronic states and phonon modes under Generalized Gradient Approximation (GGA-PBE)[2] using VASP[3] package. Figure 1(b) is the energy band structure for bulk SnS. Bulk SnS is an indirect transition semiconductor with a band gap about 0.64 eV. The electric states near the top of valence bands (bottom of conduction bands) are dominated S (Sn) atoms. Figure 1 (c) shows the phonon vibration modes at Γ-point for several different layer numbers. The filled circles indicate Raman active modes, and empty circles indicate Raman inactive modes. As for the Raman active modes close to 300 cm^{-1}, the frequency mode shifts lower frequency with the increase of the number of layers owing to the interlayer interaction. On the other hand, the Raman active mode near 100cm^{-1} shifts toward higher frequency with increase of the number of layers, and the Raman active mode disappears in the bulk structure. Thus, it is found that SnS thin films show the strong layer number dependence in the Raman active mode in the range 100cm^{-1} to 300cm^{-1}.

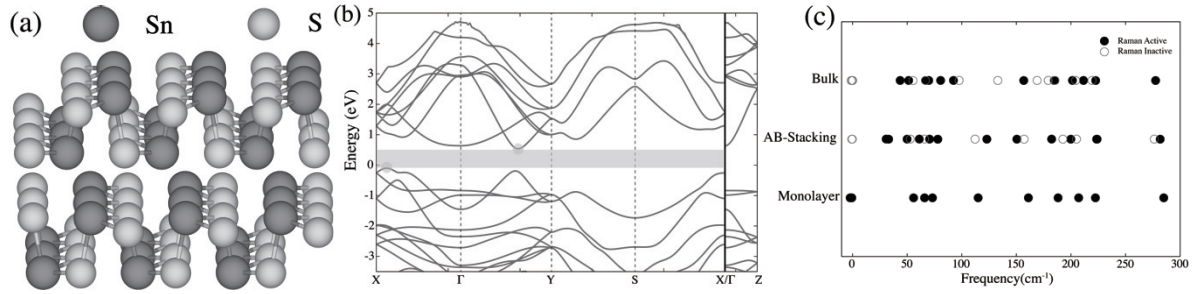

Figure (a) Crystal structure of bulk SnS. (b) Energy band structure for bulk SnS. (c) The phonon vibration mode for bulk, AB stacking bilayer and monolayer. Closed (empty) circles indicate Raman active (inactive) modes.

[1] N. Higashitarumizu *et. al*. (2019), under review.

[2] J. P. Perdew, K. Burke, M. Ernzerhof, *Phys*. *Rev*. *Lett*. 77, 3865 (1996)

[3] G. Kresse and J. Furthmüller, *Phys. Rev. B*, 54, 11169 (1996)

Corresponding Author: K. Wakabayashi, Tel: +81-79-565-9751, Fax: +81-79-565-9729, E-mail: waka@kwansei.ac.jp

Molecular adsorption effects on the electrical conduction of MoS_2 on surface-modified substrates

◯Y. Minakawa[1], T. Umehara[1], K. Takai[1,2]

[1]*Graduate school of Science and Engineering, Hosei University, Tokyo 184-8584, Japan*
[2]*Department of Chemical Science and Technology, Hosei University, Tokyo 184-8584, Japan*

The E_F of 2D-materials such as MoS_2 all of which constituent atoms lie on the surface can be easily tuned by the influence of surrounding substances[1]. Thus the surface chemical structure of the substrates also have a great influence on the electronic properties of supported 2D-materials[2]. In this study, we evaluated changes in electrical conduction caused by modifying the surface of a substrate with polymerized organic molecules such as Parylene for MoS_2. In addition, the effect of water molecules on the electrical conduction of MoS_2 was also evaluated using Parylene substrates in terms of hole doping by oxygen adsorption.

MoS_2-FET was fabricated after mechanical exfoliation on a 285 nm SiO_2/Si substrate, and the substrate deposited with Parylene. The conductivity was measured under oxygen gas or a mixed gas of oxygen and water adsorption while varying the oxygen partial pressure and adsorption time. Oxygen adsorption study was also performed while applying V_{gate}.

Fig. 1 shows the conductivity of MoS_2 under adsorption of oxygen and oxygen-water on MoS_2 on Parylene/SiO_2/Si substrate while changing the partial pressure of adsorbed oxygen. Under both conditions of oxygen adsorption and oxygen-water co-adsorption, V_{th} upshift was observed with increasing oxygen partial pressure, indicating that hole doping occurred. However, the co-adsorption of oxygen and water promotes hole doping into MoS_2, and a sharp increase in V_{th} is observed even with low-pressure oxygen. **Fig. 2** shows the adsorption time dependence of ΔV_{th} due to oxygen adsorption with the different E_F of MoS_2 modulated during gas adsorption by applying V_{gate}. V_{th} shifts rapidly when +60 V is applied during oxygen adsorption, and hole doping is promoted. Conversely, when -60 V was applied, the shift of V_{th} was small, and the hole doping was inhibited. In other words, at +60 V, the activation energy of the reaction in which MoS_2 emits electrons decreases, whereas at -60 V, the activation energy of the reaction in which MoS_2 receives electrons decreases. These results indicate that the charge transfer rate can be controlled by applying V_{gate} in MoS_2 as similar to graphene

[1] Y. Sato, K. Takai, and T. Enoki, *Nano Lett.,* **11** , 8 (2011),

[2] K.Yokota *et al., Nano Lett.* **11**, 3669 (2011),

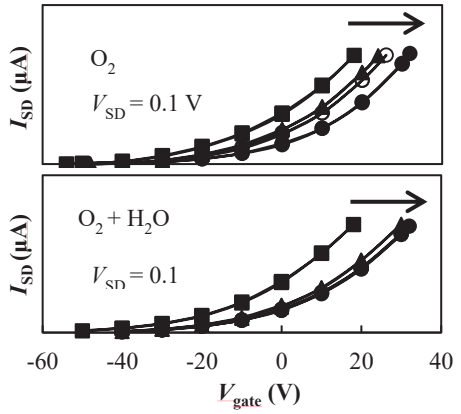

Fig. 1 Effect of gas adsorption on transfer curve

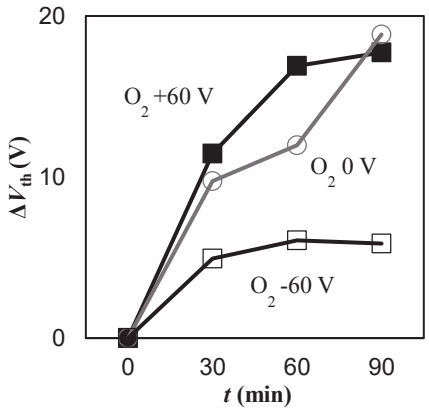

Fig. 2 Oxygen adsorption effect during V_{gate} application

Corresponding Author: Kazuyuki Takai
Tel: +81-42-387-6138, Fax: +81-42-387-7002
E-mail: takai@hosei. ac. jp

Thermal conductivity of low-cost thermoelectric Mg_3Bi_2

○ Nguyen T. Hung[1], Riichiro Saito[2]

[1]*Frontier Research Institute for Interdisciplinary Sciences, Tohoku University, Sendai 980-8578, Japan*

[2]*Department of Physics, Tohoku University, Sendai 980-8578, Japan*

Bi_2Te_3 is known as a commercial thermoelectric (TE) materials because of their highest TE performance at room temperature compared with other available TE materials. However, the expensive Te element limits the wider applications of TE devices based on Bi_2Te_3. We note that the cost of the TE materials contributes nearly one third of the total cost for the TE device. Recently, Mao et al. [1] showed experimentally that by replacing Te with Mg, a new TE material Mg_3Bi_2 can performs a figure of merit ZT ~ 0.9 at 350K, which is comparable to Bi_2Te_3 but much cheaper. Since the ZT value is inversely proportional to thermal conductivity κ, a low κ value leads to high ZT value, and then high TE performance. Thus theoretical analysis of Bi_2Te_3 is necessary.

In this work, we calculate theoretical thermal conductivity of Mg_3Bi_2 by using the density functional theory (DFT). First, to analyze the nature of chemical bonding properties, we perform COHP (crystal orbital hamilton population) analyses by using Quantum Espresso program. The COHP results show that the structure of Mg_3Bi_2 can be expressed as Mg^{2+}-$[Mg_2Bi_2]^{2-}$ as shown in Fig. 1, in which Mg1 atom is relatively more ionic while Mg2 and Bi atoms show the covalent bonds. Therefore, Mg_3Bi_2 has a structure as a crystal with glass-like, in which $\kappa = \kappa_c + \kappa_g$, where κ_c and κ_g are thermal conductivites by crystal and glass, which is called two-channel model [2]. In present work, κ_c is evaluated by the lattice anharmonicity with phonon-phonon interaction from DFT, while κ_g is calculated by using the Einstein model for glass systems. The theoretical results is well consistent with experimental data [1] with κ ~ 2 W/mK at 300K.

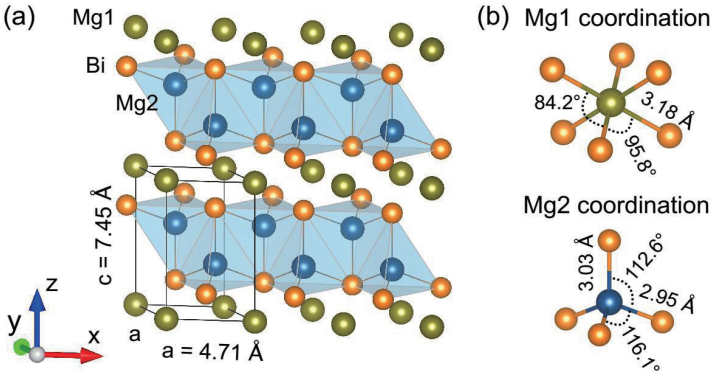

Figure 1: (a) Structure of Mg_3Bi_2. (b) Mg1 and Mg2 coordinations

[1] J. Mao et al., Science 365, 6452 (2019).

[2] S. Mukhopadhyay et al., Science 360, 1455 (2018).

Corresponding Author: Nguyen Tuan Hung

Tel: +81-22-795-6442, Fax: +81-22-795-6447, E-mail: nguyen@flex.phys.tohoku.ac.jp

発表索引
Author Index

Author Index

< A >

Abe, Naoya **2P-14**
Abe, Ryo 1P-14
Achiba, Yohji 1-12, **2C-1,** 2P-18, 2P-19, 3P-15, 3P-16
Adachi, Kento 2P-11
Ago, Hiroki 2P-12, 3P-13
Akai, Nobuyuki 1P-25
Akasaka, Takeshi 1P-18
Ando, Shusuke 1P-30, 2P-28, 2P-29
Anisimov, Anton 1P-13
Aoki, Nobuyuki 1P-1
Aoki, Yuji 1-12, 3P-15
Aoyagi, Shinobu 1-11
Aoyama, Tetsuya 1P-30, 2P-28, 2P-29
Arai, Hayato 1P-9
Araki, Tsutomu 3-9
Asaka, Koji 1-10
Asaka, Mayu 2P-23, 3P-23

< B >

Bamba, Masanori 1P-12
Bando, Yoshio 1-9
Baranov, Alexader 3P-27
Bichara, Christophe **3S-2**
Bode, Jeffery W. 3P-3

< C >

Cami, J. 2C-5
Canton, Vitoria Ruben **3P-5**
Chen, Pengfei 2P-22, **3P-21**
Cheng, Guoqing **2P-3**
Chiashi, Shohei 1P-8, 1P-9, 1P-11, 1P-12, 1P-13, 2-2, 3P-7

< D >

Das, Rasel **3P-13**
De Silva K. Kanishka H. **1P-26**
Dutta, Sudipta 3P-29

< E >

Edo, Michiko 1P-4
En, Lim Hong 1P-29
Endo, Takahiko 1P-29

< F >

Fajardo, Mario E. 2P-16
Fang, Nan **2P-5**
Fernandez, Pablo S. 2P-12
Fortner, Jacob 3-6
Fujigaya, Tsuyohiko 2P-20, 3P-18
Fujii, Yasumaru **3P-14**
Fujimoto, Yoshitaka 2-4
Fujisaki, Kotaro 2P-7
Fujita, Naoya **3P-16**
Fukuhara, Kengo 2P-8, **2P-10**
Fukumori, Kenzo 1P-3
Fukushima, Tomohiro **2-5**
Funatsu, Kimito 3-2
Furukawa, Ko 2P-19
Furukawa, Makoto 1P-18
Futaba, Don N. 1-2

< G >

Gao, Weilu 2P-10, 3P-9
Gao, Yanlin **3P-8,** 3P-10
Golberg, Dmitri 1-9
Goto, Chigusa 3-2
Goudo, Dai **1P-21,** 3P-22
Grunlan, Jaime C. **2S-1**

< H >

Haga, Taishi **2-4**
Hamano, Tsuyoshi 2P-21
Hara, Masanori 1P-5, 2P-27
Harano, Koji 1-4, **3-7,** 3P-3
Hase, Muneaki 1P-2
Hasebe, Hidetaka 2-5
Hashishin, Takahiro 1P-31
Hata, Kenji 1-2, 2P-24
Hatanaka, Miho 1P-15
Hayamizu, Yuhei 2P-30

Higashinaka, Ryuji 1-12, 3P-15
Higuchi, Mahoko 1-3
Higuchi, Shohei 3P-2
Hikage, Yurina **1P-24**
Hirai, Tadahiko 1P-1
Hirano, Atsushi 1P-2, **3P-12**
Hirao, Toshio 2P-21
Hirata, Eri 1P-6
Hiratsuka, Atsunori 1-3
Hirokawa, Sota **2P-12**
Hisama, Kaoru **1P-8**
Homma, Chishu **2P-30**
Horiuchi, Kanako 2P-10, **3P-9**
Hotta, Takato **3P-2**
Hsia, Fengchun 1-9
Hung, Nguyen T. 3-10, 3P-28, **3P-31**

< I >

Ichinose, Yota 2-1, 2P-8, 2P-10
Ideue, Toshiya 3-4
Iijima, Sumio **2C-3**
Ikuhara, Yuichi 1P-11
Inoue, Taiki 1P-9, 1P-11, 1P-12, 1P-13, 2-2, 3-6, 3P-7
Inoue, Zen **3P-27**
Isaka, Takuya 1P-25
Isayama, Miyako 2P-4
Ishida, Toshiyuki 1-10
Ishiguro, Yasushi 1P-27, 3P-27
Ishihara, Yoshiaki 1-8
Ishii, Akihiro 3-5, 3-6
Ishii, Satoshi 2P-21
Ishikawa, Takahiro 2P-21
Ishimaru, Ryoya 3P-7
Ishitsuka, Asumi **1P-16**
Isobayashi, Atsunobu 2P-30
Isobe, Hiroyuki **2C-6**
Itabashi, Yuho 1P-30, 2P-28, **2P-29**
Iwasa, Yoshihiro 3-4

< J >

Jeon, IL 1-5, 2P-2, 2P-17, 3P-1
Jeon, Sugyeong 1P-17
Jiang, Hua 1I-1
Joshi, Prerna 1P-5, **2P-27**

< K >

Kako, Masahiro 1P-18
Kameyama, Tomoya **3P-6**
Kanazawa, Katsuki **3P-26**
Kaneko, Toshiro 1-7, 3P-6
Kanzawa, Shinji 1P-18
Kasama, Yasuhiko 1-11
Kataura, Hiromichi 1-3, 2P-9, 3-1, **3-3,** 3P-12
Kato, Toshiaki 1-7, 3P-6
Kato, Yuichi **2P-24**
Kato, Yuichiro K. 2P-5, 3-5, 3-6
Kauppinen, Esko I. **1I-1,** 1P-11, 1P-13, 2-2, 2P-2
Kawachi, Kazuhiko 1-11
Kawai, Hideki 3P-9
Kawai, Tsuyoshi 3-2, 3P-19, 3P-24
Kawano, Yukio 3P-19
Kemper, F. 2C-5
Khaniya, Sharma Aliza **2P-6,** 2P-25
Kikuchi, Koichi 1-12, 2P-18, 2P-19, 3P-15, 3P-16
Kimura, Mutsumi 1P-31
Kimura, Sadahito **1P-6**
Kitabatake, Daiki 1-11
Kitamura, Nozomu 1P-15
Kitao, Takashi **1P-22**
Kitaura, Ryo 3P-2, 3P-5
Ko, Jeong Won **1P-17**
Ko, Weon Bae 1P-17
Kobashi, Kazufumi 2P-24
Kobayashi, Akari 3P-7
Kobayashi, Junei **2P-7**
Kodama, Takashi **2P-11**
Kodama, Takeshi 1-12, 2P-18, 2P-19, 3P-15, 3P-16
Kojima, Kana 1P-7, **1P-29**
Komai, Takaha 2-5
Komatsu, Naoki 2P-3
Komatsu, Natsumi 2P-10, 3P-9

Komichi, Yuma 3-9
Konishi, Teruaki 2P-21
Konno, Yui **2P-1**
Kono, Junichiro 2P-10, 3P-9
Kowashi, Satori 1-4
Koyano, Bunsho **3P-7**
Kozawa, Daichi **3-6**
Kubota, Yoshiyuki **1S-2**
Kumamoto, Akinito 1P-11
Kwon, Eunsang 1-11

< L >
Li, Kou 3P-19
Li, Qin-Yi 2P-12
Li, Yan **3S-3**
Lin, Hao-Sheng **1-5,** 2P-17, **3P-1**
Liu, Dongxin **1-4**
Liu, Ming 1P-11, **2-2**
Liu, Zheng 1P-7, 2P-15
Lungerich, Dominik 1-4

< M >
Ma, Yue **2P-17**
Machida, Tomoki 2P-4
Machiya, Hidenori **3-5**
MacLean, Michael 1P-22
Maeda, Yuta **1P-18**
Maeda, Yutaka 1P-16, 1P-18, 2P-1
Maejima, Moeno **2P-18**
Maniwa, Yutaka 1P-29, 2P-15
Maruyama, Mina 1P-8, **2-3,** 3P-10, 3P-14
Maruyama, Shigeo 1-5, 1P-8, 1P-9, 1P-11, 1P-12, 1P-13, 2-2, 2P-2, 2P-17, 3-6, 3P-1, 3P-7
Maruyama, Takahiro 1P-23, 2P-6, 2P-25, 2P-26
Masubuchi, Satoru 2P-4
Masumoto, Yui 1P-31
Matsuda, Hiroyuki **2P-21**
Matsuda, Kazunari **Tutorial,** 1P-7, 2P-1, 2P-9, 2P-15, 3-1, 3-9
Matsui, Jun 2P-1
Matsuo, Yoshiaki 1P-25
Matsuo, Yutaka 1-5, 2P-2, 2P-17, 3P-1
Matsuoka, Yuya 2P-8
Matsuura, Yuuto 2-4
Mazaki, Hitoshi 2P-22, 3P-21
Mieno, Tetsu 3P-20
Minakawa, Yuki **3P-30**
Misaizu, Fuminori 1-11
Mitsuishi, Masaya 2P-1
Miura, Yasuhiro F. 1P-30, 2P-28, 2P-29
Miyamoto, Kazunori 1P-30, **1P-31**
Miyamoto, Reona 1-13
Miyamoto, Yoshiyuki **1P-20**
Miyao, Tomoyuki 3-2
Miyata, Yasumitsu 1P-7, 1P-10, 1P-29, 2P-15
Miyauchi, Yuhei 1P-7, 2P-1, 2P-9, 2P-15, **3-1**
Momin, Md. Abdul **3P-20**
Momose, Takamasa 2P-16
Morisawa, Yusuke 1P-15
Moriya, Rai 2P-4
Mouri, Shinichiro **3-9**
Murakoshi, Kei 2-5
Muranaka, Atsuya 1P-30, 2P-28, 2P-29
Muraoka, Yoshimi **1P-3**
Murayama, Tomoko 3-2

< N >
Nabiev, Igor 3P-27
Nagashio, Kosuke 2P-5, 3P-29
Nakagawa, Rei **1P-4,** 2P-22, 3P-21
Nakahara, Kana 1P-25
Nakamura, Eiichi 1-4, 3-7, 3P-3
Nakamura, Junji **2S-2**
Nakamura, Masakazu 1P-14
Nakamuro, Takayuki 1-4, **3P-3**
Nakanishi, Yusuke 1P-29, 2P-15
Nakano, Masaki **1S-1**
Nakashima, Naotoshi **1-1**
Nakata, Kazuki 1P-22
Nakayama, Tomohito **1P-2**

Nakayasu, Takanori 1-13
Narita, Shodai 1P-31
Naritsuka, Shigeya 1P-23, 2P-6, 2P-26
Nemoto, Masaya 1P-30, **2P-28,** 2P-29
Niidome, Yoshiaki 2P-20
Nishihara, Taishi 1P-7, 2P-9, 3-1
Nishijima, Satomi 1P-24
Nishino, Akane 2P-1
Noda, Suguru 1P-4, 2P-22, 2P-23, 3P-21, 3P-23
Noguchi, Hironaga 2P-30
Nonoguchi, Yoshiyuki **3-2,** 3P-19, 3P-24
Nouchi, Ryo **1-8**

< O >
Obata, Yoshinori 1P-27
Ochiai, Masahito 1P-31
Ogawa, Shuhei 1P-26
Ogura, Noritada **1-7**
Oguri, Kanata 1-13
Ohno, Yutaka 2P-21
Ohshimo, Keijiro 1-11
Oi, Kanae **3P-19**
Okada, Daiki 1P-15
Okada, Hiroshi 1-11
Okada, Ryotaro 3P-9
Okada, Satoshi 3-7
Okada, Susumu 1P-8, 2-3, 3P-8, **3P-10,** 3P-14
Okamoto, Naofumi 1P-14
Okawa, Shuhei 1-5
Okazaki, Toshiya 3P-17
Okudaira, Saki 2P-1
Onga, Masaru 3-4
Ono, Tomoya 1-13
Onodera, Momoko **2P-4**
Ooishi, Yuya 1-13
Osawa, Ayato 1P-15
Osawa, Eiji 1P-30, **2C-4,** 2P-28, 2P-29
Osawa, Taisei 1P-31
Osawa, Toshio 2P-23, 3P-23
Otsuka, Keigo 2P-5, 3-6, 3P-7
Otsuka, Masaaki **2C-5**
Otsuki, Nao 1P-19

< P >
Pandey, Manish **1P-14**
Peeters, E. 2C-5
Pichler, Thomas 3S-4
Pratama, Fenda Rizky **1P-28,** 3-8
Pu, Jiang 2P-15

< Q >
Qian, Yang 1P-11, 2-2
Qin, Feng 3-4

< R >
Rahman Mohammad Jellur 3P-20

< S >
Saida, Takahiro 2P-6
Saito, Riichiro 1P-28, 3-8, **3-10,** 3P-25, 3P-28, 3P-31
Saito, Susumu **2C-2,** 2-4, 3P-4
Saito, Yahachi **1-10**
Sakairi, Masatoshi 1P-6
Sakurai, Shunsuke **1-2**
Sano, Masahito 3P-26
Sasaki, Ryo 1-13
Sasaoka, Kenji 2P-13, 2P-14
Sato, Akito 2P-11
Sato, Shu **1P-12**
Sawada, Tetsuro **2P-23,** 3P-23
Schipper, Derek 1-6
Schweighauser, Luca 3-7
Sei, Tomohiro 2P-23, 3P-23
Sekido, Masaru 1P-19
Sekimoto, Yuki 1P-14
Senga, Ryosuke **3S-4**
Seo, Seungju **2P-2**
Sharma, Kamal Prasad 2P-6, **2P-25**
Shawky, Ahmed 1P-13
Shiga, Takuma 3P-11
Shigehisa, Yudai **1P-27**
Shimasaki, Masafumi **1P-7**
Shinokita, Keisuke 1P-7, 3-9
Shiraki, Tomohiro **2P-20**

Smet, Jurgen 3-4
Snowdon, Monika **1-6**
Solís-Fernández, Pablo 3P-13
Suenaga, Kazu 3S-4
Sugai, Toshiki **1-13**
Sugime, Hisashi 1P-4, 2P-22, 2P-23, 3P-21, 3P-23
Sugimoto, Wataru 1-8
Sugizaki, Yoshiaki 2P-30
Sukanta, Datta 1I-1
Sun, Keyi 3P-3
Suzuki, Daichi 3P-19
Suzuki, Hal 1P-15
Suzuki, Kohei **2P-13**
Suzuki, Mitsuaki 2P-1
Suzuki, Ryuji 3-4
Suzuki, Ryutaro **1P-25**
Suzuki, Satoru 2P-21

< T >
Tachibana, Masaru 1P-1
Taguchi, Yuta **3P-4**
Tajima, Kentaro 1P-25
Takada, Sari 1P-6
Takahashi, Hiromu 2P-23, **3P-23**
Takahashi, Koji 2P-12
Takai, Kazuyuki 1P-24, 1P-25, 1P-27, 3P-27, 3P-30
Takai, Ryoya **1-12**
Takakura, Akira **2P-9,** 3-1
Takenobu, Taishi 2P-15
Tanaka, Takeshi **1-3,** 1P-2, 2P-9, 3-1, 3-3, 3P-12
Tanaka, Toshihiko **1P-30,** 2P-28, 2P-29
Tang, Dai-Ming 1-6, **1-9**
Taniguchi, Takashi 2P-4, 2P-5, 3P-2
Tenne, Reshef 3-4
Terada, Yukihiko **3P-11**
Teshima, Hideaki 2P-12
Tian, Yuan **3P-25**
Tomo, Yoko 2P-12
Tong, Wang 3-10
Tsuji, Takashi 1-2

< U >
Uchiyama, Fumiaki 1-13
Uchiyama, Masanobu 1P-30, 1P-31, 2P-28, 2P-29
Ueda, Akihiro 3P-2
Ueda, Yuki 1P-23, **2P-26**
Ueji, Kan 2-1, **2P-8**
Uemura, Takashi 1P-22
Ueno, Hiroshi **1-11**
Ueno, Keiji 3P-2
Ukhtary, M. Shoufie 1P-28, 3-8, 3P-25
Umehara, Taichi 3P-30
Utsugi, Koichi **1P-19**

< V >
Vishwanath, Pamarti 1P-26

< W >
Wada, Momoyo 3P-12
Wada, Naoki 1P-7, **2P-15**
Wakabayashi, Katsunori 3P-29
Wakabayashi, Tomonari **1P-15, 2P-16**
Wang, Guowei 3-3
Wang, Pengyingkai **1P-13**
Wang, Sake **3-8**
Wang, YuHuang **3S-1,** 3-6
Watanabe, Kenji 2P-4, 2P-5, 3P-2
Watanabe, Makoto 1P-13
Weerathunga Don Terrence Dhammika **3P-18**
Wu, Xiaojian 3-6

< X >
Xiang, Rong 1P-9, 1P-11, 1P-13, 2-2, 3-6, 3P-7
Xiaoqi, Pang 3-10, **3P-28**
Xing, Junfei 3-7
Xu, Ying **3P-17**

< Y >
Yadav, Rohit **1P-5,** 2P-27
Yagi, Takashi 2P-8
Yagi, Tomoko **3P-24**
Yamada, Jumpei **1P-23,** 2P-26
Yamada, Maho 1-2

Yamada, Michio 1P-16, 1P-18, 2P-1
Yamada, Takeo 2P-24
Yamada, Tomoyuki 2P-15
Yamagishi, Kazuki **3P-15**
Yamagiwa, Kiyofumi 1P-21, 3P-22
Yamaguchi, Nobutomo 1P-21, **3P-22**
Yamamoto, Daiki 2P-25
Yamamoto, Ryohei **1P-1**
Yamamoto, Shun 3P-7
Yamamoto, Takahiro 2P-7, 2P-13, 2P-14
Yamanouchi, Kaoru 1-4
Yanagi, Kazuhiro 1P-10, **2-1,** 2P-8, 2P-10, 3P-9
Yang, Feng 3S-3
Yang, Mei 3P-17
Yang, Meng-Ju **2P-22,** 3P-21
Yokoyama, Atsuro 1P-6
Yomogida, Yohei **1P-10,** 2-1, 2P-8, 2P-10, 3P-9
Yonemori, Itsuki **3P-29**
Yoshida, Akari 2P-8, 2P-10
Yoshida, Shun **2P-19**
Yoshimura, Masamichi 1P-5, 1P-26, 2P-27
Yotsumoto, Satoshi **1P-9,** 1P-12
Yu, Yun 2P-17
Yudasaka, Masako 1P-6, 3P-17

< Z >

Zak, Alla 3-4
Zhang, Minfang 3P-17
Zhang, Qiang 1I-1
Zhang, Wenjin 2P-15
Zhang, Yijin **3-4**
Zheng, Yongjia 1P-9, **1P-11,** 1P-13, 2-2
Zhou, Xin 1-9

2020 年 3 月 15 日発行

第 58 回フラーレン・ナノチューブ・グラフェン総合シンポジウム
講演要旨集

≪フラーレン・ナノチューブ・グラフェン学会≫
〒113-8656 東京都文京区本郷 7-3-1
東京大学大学院工学系研究科　機械工学専攻
丸山研究室内
Phone/Fax：03-3830-4848
E-mail：fntg@photon.t.u-tokyo.ac.jp
URL：http://fullerene-jp.org
印刷　/　製本　（株）創志企画

JEM-ARM200F
NEOARM*ex*

Atomic Resolution Analytical Microscope

Wide gap pole piece (WGP) unlocks the potential of NEOARM!

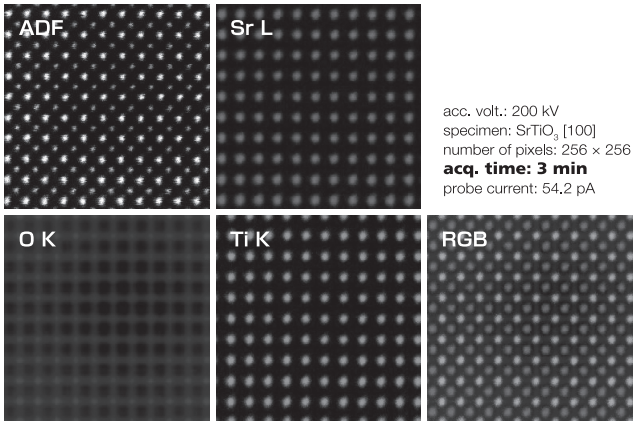

acc. volt.: 200 kV
specimen: $SrTiO_3$ [100]
number of pixels: 256 × 256
acq. time: 3 min
probe current: 54.2 pA

Damageless & high-throughput analysis!

Wide gap pole piece (WGP) integrated for

- 超高感度EDSシステムを搭載可能（Ω = 2.2 sr）
- 様々な試料ホルダーに対応
- 従来のポールピースに比べ高い試料傾斜角度
- 低加速でも高分解能観察・分析が可能

	NEOARM	**NEOARM*ex***
Pole piece + EDS sensor size	UHR or HR + 100 mm^2 × 2	**WGP** **+** **160 mm^2 × 2**

JEOL 日本電子株式会社

本社・昭島製作所　〒196-8558　東京都昭島市武蔵野3-1-2　TEL:(042)543-1111(大代表)　FAX:(042)546-3353
www.jeol.co.jp　ISO 9001・ISO 14001 認証取得

JEOLグループは、「理科学・計測機器」「産業機器」「医用機器」の3つの事業ドメインにより事業を行っております。
「理科学・計測機器事業」電子光学機器・分析機器・計測検査機器　**「産業機器事業」**半導体関連機器・産業機器　**「医用機器事業」**医用機器

ご注文品は最短で翌日納品

倉庫面積を大幅拡張。国内在庫がさらに充実し、ますます多くの製品が当日出荷可能*となりました。お客様の急なニーズにも迅速に対応いたします。

■ 当日出荷が可能な製品の一例です。

* 弊社に直接ご注文をいただいた場合の出荷予定日です。ご注文の時間帯によっては、翌営業日の出荷となる場合がございます。また出荷予定日は在庫状況に応じて変わる可能性がありますのでご了承ください。

見積・注文のご依頼はウェブサイトから

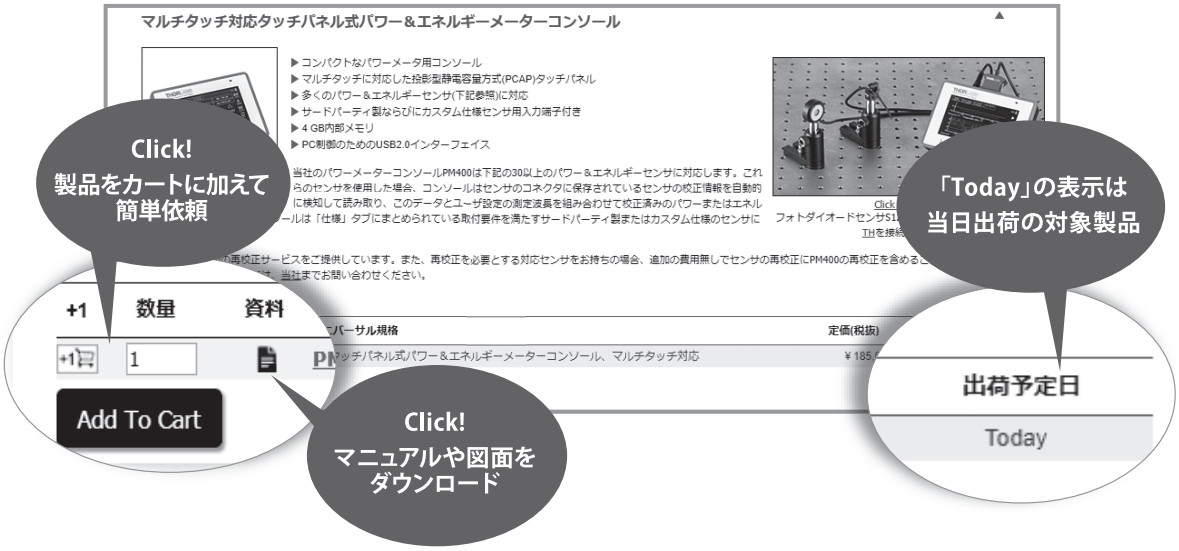

定価や出荷予定、製品仕様・図面等の詳細はウェブサイトでご確認いただけます。

www.thorlabs.co.jp E-mail: sales@thorlabs.jp

THORLABS ソーラボジャパン株式会社
〒179-0081 東京都練馬区北町3-6-3 TEL：03-6915-7701 FAX：03-6915-7716

チューナブル OPO レーザー
C-WAVE

HÜBNER

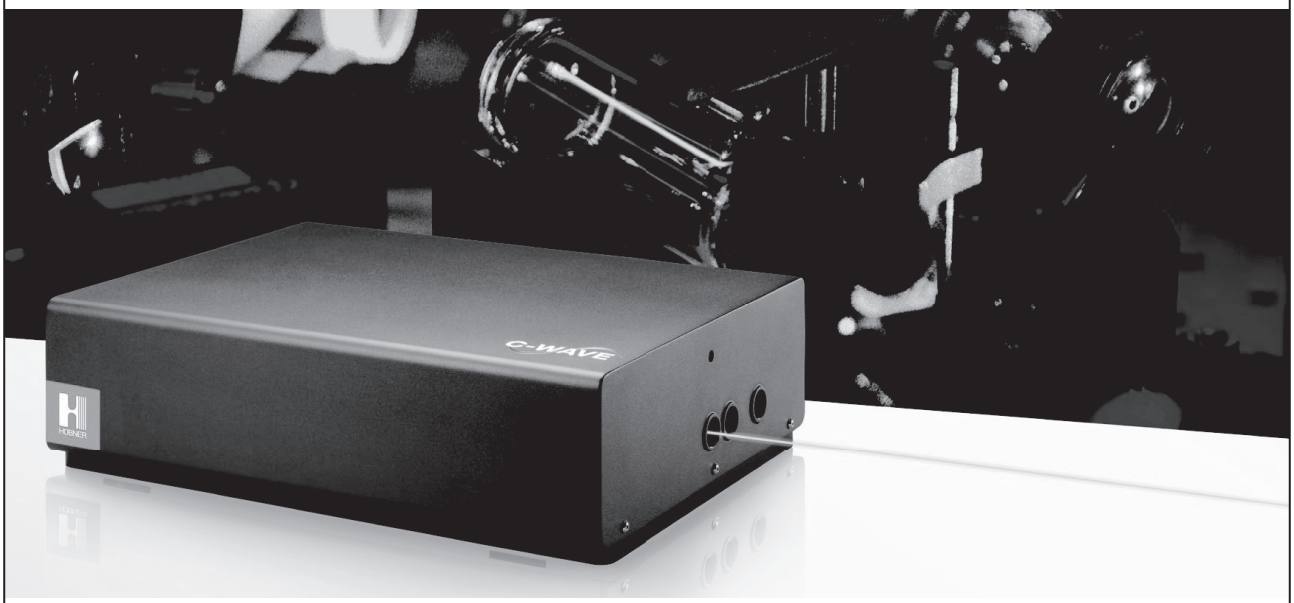

広いスペクトル可変幅と簡単な波長選択機能

- ✓ **可視域から近赤外までを完全コンピュータ制御波長チューニング**
- ✓ **パワーレベル選択可：1.5W（ポンプレーザ内蔵）、5W（外部レーザ）**
- ✓ **高精度：外部リファレンスによる周波数安定化機能**

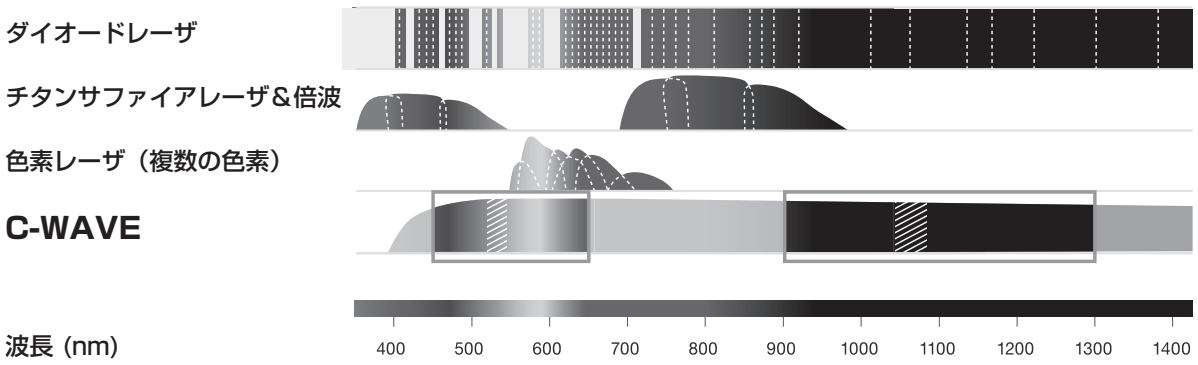

https://www.japanlaser.co.jp/ E-mail: jlc@japanlaser.co.jp

JLC JAPAN LASER 株式会社日本レーザー

東京本社 東京都新宿区西早稲田2-14-1 TEL 03-5285-0863(直)
大阪支店 大阪市東淀川区東中島1-20-12 TEL 06-6323-7286
名古屋支店 名古屋市中区錦3-1-30 TEL 052-205-9711

書籍のご案内

◈定価は本体価格＋税です。

カーボンナノチューブ・グラフェンハンドブック

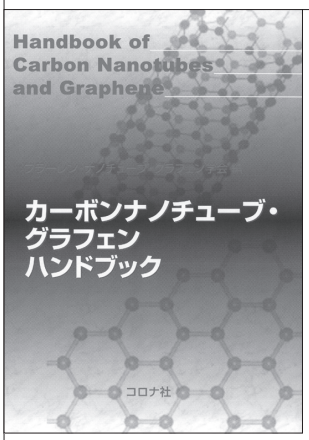

フラーレン・ナノチューブ・グラフェン学会 編
B5判／368頁
本体10,000円

本ハンドブックでは，カーボンナノチューブの基本的事項を解説しながら，エレクトロニクスへの応用，近赤外発光と吸収によるナノチューブの評価と光通信への応用の可能性を概観。最近嘱目のグラフェンやナノリスクについても触れた。

安全工学便覧（第4版）

安全工学会 編
B5判／1,192頁
本体38,000円

本改訂では，新たな科学・技術の進歩に伴う事項や社会の変化に対応するために必要な項目を更新。特に安全マネジメント，リスクアセスメント，原子力設備の安全などは多くを新たに書き起こした。安全工学関係者の総力を結集した便覧。

カーボンナノチューブの材料科学入門
齋藤弥八 編著／A5判／250頁／本体3,400円

カーボンナノチューブの基礎
齋藤弥八・坂東俊治 共著／A5判／220頁／本体2,800円

ドライプロセスによる表面処理・薄膜形成の基礎
表面技術協会 編／A5判／208頁／本体2,800円

ドライプロセスによる表面処理・薄膜形成の応用
表面技術協会 編／A5判／318頁／本体4,600円

材料マイクロ波プロセッシングの基礎
吉川 昇 著／A5判／272頁／本体3,600円

図解 傾斜機能材料の基礎と応用
上村誠一・渡辺義見 編著／A5判／304頁／本体4,200円

研究室では「ご安全に！」
―危険の把握，安全巡視とヒヤリハット―
片桐利真 著／A5判／224頁／本体2,800円

真空科学ハンドブック
日本真空学会 編／B5判／590頁／本体20,000円

航空機設計法
―軽飛行機から超音速旅客機の概念設計まで―
李家賢一 著／A5判／298頁／本体4,200円

航空機設計法 実践編
―小型ジェット旅客機からハイブリッド電動航空機の概念設計まで―
李家賢一 著／A5判／204頁／本体2,700円

科学技術と共に歩む

株式会社 コロナ社

〒112-0011 東京都文京区千石4-46-10
TEL (03)3941-3131（代），-3132，-3133（営業部直通）
https://www.coronasha.co.jp FAX (03)3941-3137
E-mail eigyo@coronasha.co.jp

モデルチェンジ　～スマートなデザインに簡単操作～

BRANSON 超音波ホモジナイザー

長くご愛顧いただいておりますBRANSON超音波ホモジナイザーで新たなモデルが誕生しました。

主な特長

1.電気エネルギーから超音波振動への変換効率が95%以上
→ 無駄なエネルギーロスが小さく、安定した振幅が得られる。

2.通常では、液体の種類によって振幅が安定し難い。
→ 条件を変えても一定の振幅を保つ機能がついている。

3.ジュール（watt×sec）による発振制御が可能
→ Total何ジュールでこの処理が完了するという情報が論文に掲載できる。

20kHz超音波ホモジナイザー
BRANSON SONIFIER SFX250,550

40kHz超音波ホモジナイザー
BRANSON SONIFIER SFX150HH

主なアプリケーション

分散

カーボンナノチューブ　有機顔料　無機顔料　セラミック　セメント　感光体　記録材料
磁性粉　粉末冶金　酸化鉄　金属酸化物　シリカ　アルミナ　カーボンブラック
ポリマー　ラテックス　製紙　ファンデーション
研磨剤　電池　フィラー　光触媒　触媒　ワクチン　体外診断薬　歯磨き粉　シャンプー
半導体　電子基盤　液晶　貴金属　金属　宝石　タイヤ　発酵菌類　その他

乳化

エマルジョン製剤　農薬　トナー　ラテックス　界面活性剤　クリーム　乳液　その他

日本国内販売総代理店　株式会社 セントラル科学貿易

東京本社: 〒136-0071 東京都江東区亀戸1-28-6 タニビル3F TEL 03-5627-8150 FAX 03-5627-8151
技術物流センター: 〒272-0146 千葉県市川市広尾2-1-9 TEL 047-701-6100 FAX 047-701-6116
大阪支店: 〒533-0031 大阪府大阪市東淀川区西淡路1-1-36 新大阪ビル TEL 06-6325-3171 FAX 03-6325-5180
福岡営業所: 〒812-0016 福岡県福岡市博多区博多駅南1-2-15 事務機ビル TEL 092-482-4000 FAX 092-482-3797
札幌出張所: 〒001-0911 北海道札幌市北区新琴似11条13-7-13-2 TEL 011-764-3611 FAX 011-764-3612
https://www.cscjp.co.jp

パフォーマンスを引き出すコードを生成

インテル® Parallel Studio XE は、マルチコアや SIMD により構成されるパフォーマンスを引き出すモダンコードを、より容易に、また短時間で開発できるように支援するツールスイートです

3 段階のエディションと主なコンポーネント

Composer Edition [ビルド]

・インテル® C++/Fortran コンパイラー

インテル ® Xeon® スケーラブル・プロセッサー向けの機能を含む SIMD 拡張命令を適用する自動ベクトル化、ループを自動的に複数スレッドで処理可能とする自動並列化などの最適化機能を提供
また C/C++、Fortran や OpenMP* の最新言語規格による高度なプログラミングのニーズに対応

・最適化された数値演算、信号・画像処理、スレッド化、データ解析用ライブラリー
・Python* 向けインテル® ディストリビューション - 高速な Python* 実行環境

Professional Edition [解析] [ビルド]

・インテル® VTune™ プロファイラー

アプリケーションの動作による CPU 使用率やメモリーアクセス状況など様々な情報を、関数やループごと、およびスレッドまたはプロセスの時系列で収集する性能解析ツール

・インテル® Inspector - スレッドエラー検出ツール
・インテル® Advisor - 並列化アドバイスツール

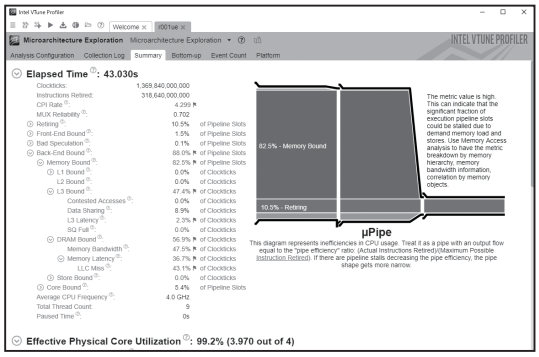

Cluster Edition [スケール] [解析] [ビルド]

・インテル® Trace Analyzer & Collector

MPI ライブラリーによる通信をトレースし、性能情報の取得および API 利用のエラー検証が可能なツール

・インテル® MPI ライブラリー
・インテル® Cluster Checker (Linux* のみ)
– クラスターシステムの診断ツール

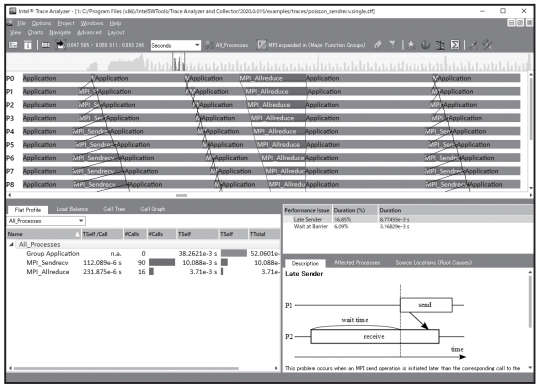

お問い合わせはこちらから >> https://xlsoft.com/jp/qa

性能の限界に挑戦する
インテル® Parallel Studio XE 2020

最新のインテル® プロセッサー向けに C/C++、Fortran、Python* アプリケーションを最適化するためのツールスイート

- インテル® Parallel Studio XE 2020 の主な新機能 -

- コンパイラーで C++20 の初期対応を含む C++ 17 をサポート、Fortran 2018 のサポートを拡張、OpenMP* 4.5/5.0 サポートを拡張
- メモリーアクセス性能解析が、最大 512 GB の不揮発性メモリーをもたらすインテル® Optane™ DC パーシステント・メモリーにも対応
- HPC クラウドをサポート – AWS* 環境で MPI アプリケーション向けに低レイテンシーと高帯域幅の通信を実現可能

インテル® Fortran コンパイラーによる優れたアプリケーション・パフォーマンス - Linux*

Polyhedron* ベンチマーク
相対 (相乗平均) パフォーマンス (数値が大きいほど高性能)

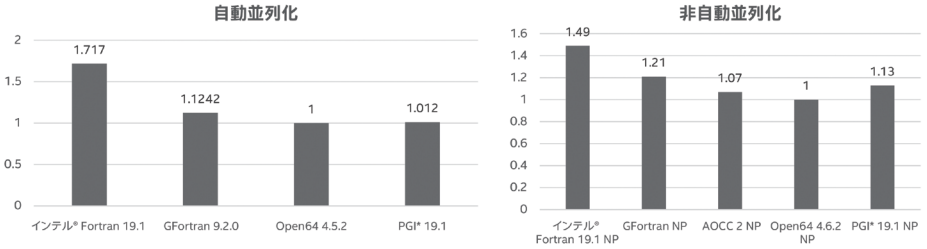

Intel technologies' features and benefits depend on system configuration and may require enabled hardware, software or service activation. Learn more at intel.com, or from the OEM or retailer. Performance results are based on testing as of **Dec. 12, 2019** and may not reflect all publicly available security updates. See configuration disclosure for details. No product can be absolutely secure.

Software and workloads used in performance tests may have been optimized for performance only on Intel microprocessors. Performance tests, such as SYSmark and MobileMark, are measured using specific computer systems, components, software, operations and functions. Any change to any of those factors may cause the results to vary. You should consult other information and performance tests to assist you in fully evaluating your contemplated purchases, including the performance of that product when combined with other products. For more complete information visit www.intel.com/benchmarks.

Configuration: Testing by Intel as of **Dec. 12, 2019**. Hardware: **Intel® Core™ I7-6700 CPU** @ 3.40GHz, HyperThreading is on. RAM 8G. Software: Intel® Fortran Compiler 19.1, PGI Fortran* 19.1, Open64* 4.6.2, gFortran* 9.2.0, Red Hat Enterprise Linux Server release 7.4 (Maipo), Kernel 3.10.0-693.11.6.el7.x86_64 Polyhedron Fortran Benchmark (www.fortran.uk), Linux compiler switches: Auto-parallel: Gfortran;gfortran -Ofast -mfpmath=sse -flto -march=skylake -funroll-loops -ftree-parallelize-loops=8. Intel Fortran compiler: -fast -parallel -xCORE-AVX2 -nostandard-realloc-lhs. PGI Fortran: pgf95 -fast -Mipa=fast,inline -Msmartalloc -Mfprelaxed -Mstack_arrays -Mconcur -mp=bind. Open64: openf95 -march=auto -Ofast -mso -apo. Non-auto parallel (NP): ifort -fast -xCORE-AVX2 -nostandard-realloc-lhs. open64:openf95 -march=auto -Ofast -mso. gcc: gfortran -Ofast -mfpmath=sse -flto -march=native -funroll-loops. pgi: pgf95 -fast -Mipa=fast,inline -Msmartalloc -Mfprelaxed -Mstack_arrays. aocc: flang -flto -Wl,-mllvm -Wl,-function-specialize -Wl,-mllvm -Wl,-region-vectorize -Wl,-mllvm -Wl,-reduce-array-computations=3 -ffast-math -Wl,-mllvm -Wl,-inline-recursion=4 -Wl,-mllvm -Wl,-lsr-in-nested-loop -Wl,-mllvm -Wl,-enable-iv-split -O3 -flto -march=znver2 -funroll-loops -Mrecursive -mllvm -vector-library=LIBMVEC -z muldefs -lamdlibm -lflang -lamdlibm -lm

Intel® s compilers may or may not optimize to the same degree for non-Intel microprocessors for optimizations that are not unique to Intel microprocessors. These optimizations include SSE2, SSE3, and SSSE3 instruction sets and other optimizations. Intel does not guarantee the availability, functionality, or effectiveness of any optimization on microprocessors not manufactured by Intel. Microprocessor-dependent optimizations in this product are intended for use with Intel microprocessors. Certain optimizations not specific to Intel microarchitecture are reserved for Intel microprocessors. Please refer to the applicable product User and Reference Guides for more information regarding the specific instruction sets covered by this notice. Notice revision #20110804

製品詳細、評価版はこちらから
www.xlsoft.com/intel/fntg58

高速化のための無料セミナー実施中!
www.xlsoft.com/intel/seminar

製品の詳細に関するお問い合わせ先：

XLSOFT エクセルソフト株式会社
〒108-0073 東京都港区三田 3-9-9 森伝ビル 6F
Tel: 03-5440-7875 Fax: 03-5440-7876 E-mail: intel@xlsoft.com

TELEDYNE
PRINCETON INSTRUMENTS
Everywhereyoulook™

Part of the Teledyne Imaging Group

高感度
高ダイナミックレンジ
高繰り返し

高感度近赤外線2次元InGaAsカメラ

NIRvana™:640

- **低暗電流ノイズ**（電子冷却：-80℃、液体窒素：-190℃）
- **110fps**（ビデオレート以上）
- **標準GigEインターフェースで50mまで延長可**
- **空冷ファンと水冷を切替可能**

アプリケーション例

・フォトニック結晶PLイメージング及びスペクトル
・一重項酸素イメージング及びスペクトル
・太陽電池PLイメージング及びスペクトル
・天体観測微弱光イメージング
・食品断面イメージング
・In-Vivoイメージング　など

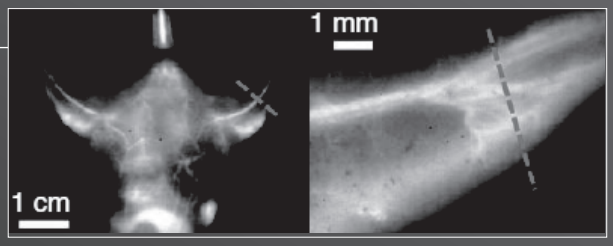

仕様

モデル	NIRvana:640ST	NIRvana:640	NIRvana:640LN
センサー	640 x 512 x InGaAs		
素子サイズ	20μm x 20μm		
波長範囲	0.9 ～ 1.7 μm		
冷却温度	-60℃	-80℃	-190℃
ダークチャージ	1500 e-/p/sec	300 e-/p/sec	<8 e-/p/sec
読み出しノイズ	<120 e-rms		15 e-rms
ダイナミックレンジ	16 Bit (>15Bit@1 素子)		
フレームレート	110 fps@10MHz		2.77 fps@250KHz
インターフェース	Gig E		
ソフトウェア	LightField, SITK-LabVIEW, WinX32		

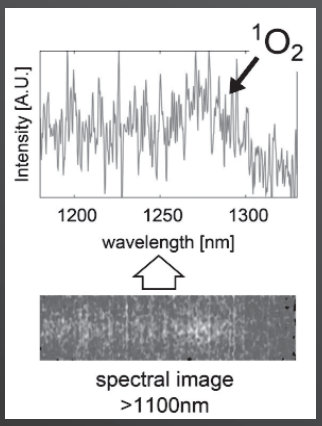

www.pi-j.jp

テレダイン・ジャパン株式会社　プリンストンインスツルメンツ

〒170-0013　東京都豊島区東池袋 3-4-3 池袋イースト13F
TEL 03-6709-0631　FAX 03-6709-0632